UNIVERSITAT DE BARCELONA

Epigenetic and Epitranscriptomic Changes during Leukemic Cell Transdifferentiation

Alberto Bueno Costa

UNIVERSITAT DE BARCELONA

UNIVERSITAT DE BARCELONA

FACULTAT DE MEDICINA

PROGRAMA DE DOCTORAT EN BIOMEDICINA

EPIGENETIC AND EPITRANSCRIPTOMIC CHANGES DURING LEUKEMIC CELL TRANSDIFFERENTIATION

ALBERTO BUENO COSTA

BARCELONA, 2023

Cover art: “*Transdifferentiating*”

Drawn by: Vanessa Ortiz (V.O.B.)

A great artist, doctor, and friend

Instituto de Investigación
CONTRA LA LEUCEMIA
Josep Carreras

IDIBELL
Institut d'Investigació Biomèdica de Bellvitge

PEBC

Cancer Epigenetics and Biology Program
Programa d'Epigenètica i Biologia del Càncer
Programa de Epigenética y Biología del Cáncer

UNIVERSITAT DE BARCELONA

UNIVERSITAT DE BARCELONA

FACULTAT DE MEDICINA

PROGRAMA DE DOCTORAT EN BIOMEDICINA

EPIGENETIC AND EPITRANSCRIPTOMIC CHANGES DURING LEUKEMIC CELL TRANSDIFFERENTIATION

ALBERTO BUENO COSTA, 2023

Memòria presentada per Alberto Bueno Costa per optar al grau de Doctor per la Universitat de Barcelona

Dr. Manel Esteller Badosa
Director i tutor

Alberto Bueno Costa
Autor

Dedicado a mis padres,
a quienes todo debo…

Y dedicado a los que ya no están,
por quienes no dejaré de luchar…

ACKNOWLEDGEMENTS

Oh dear, what a long journey this has been… A proper journey with its ups and downs, with its tears and laughs but, most importantly, a journey with a happy ending. Happy not only because of the final reward, of course, but more importantly because of the lessons that it has taught me. Indeed, I look myself at the mirror and barely recognize who this guy is: short hair, shaggy beard and a subtle ironic and cynical wrinkle in his right eye ("*oh my poor Diogenes, you did lose your innocence!*")… Pondering my soul and weighting my past and present self, I do certainly believe that I have found the answer of the most profound (at least for me) metaphysical and ethical question that a human being can raise: "*What is the meaning of life?"…* The answer is as elegant and simple as it could be: "*Love*" (yes, it really sounds *cliché*). Life is, by nature, nihilistic, but love seeds with meaningfulness everything and everyone it touches. Love for our work, love for the secrets of nature, and most importantly, love for the people that are part of our lives. And to those people I want to dedicate this chapter: to those who have accompanied me through this exciting journey. I thank you with all my heart…

To **Manel Esteller**, my thesis director, for having put his trust on me from the very first moment we met. I must confess, I've always been a little bit intimidated by you, in a professional (and not so professional) way. Your thought process has been a mystery to me for many years. But, one day, I began to understand, and by piercing through the many layers of seriousness and professional *gravitas*, I could learn extraordinary lessons: to keep it simple while never losing sight at the bigger picture; to have an always-sharpened Ockham's razor; autonomy, boldness, constancy, and quick decision making; and most importantly, to put all your energy into your passion and into the things you really love. I will always be thankful for not letting me down, just the day before starting the PhD, when my mother was diagnosed with cancer and I had to leave for almost a year. In your lab, I have achieved great things at both professional and personal levels, and I could finally find my goal in life: to contribute as much as I can to the cure of cancer. For all these reasons, thank you…

To **Fernando Setien**, our dearest lab technician; the purest man I know. If angels exist, you must be their finest representative. Your generosity is an example and a beacon we must follow to achieve personal plenitude. Thank you for all your aid and for having shared so much molecular and vital wisdom with me. You are the cornerstone of this laboratory.

To **Marta Soler**, a marvelous lab technician with a fantastic sense of humor, justice, and integrity. With you at our side, we all feel safe and protected. Thank you for all your help and for sharing with me so many funny moments.

To **Laia Coll**, one of the sweetest and kindest people I've met and will ever meet in my life. Her will to help and to comfort every person in the team has been a true inspiration for me. Your kind words, your cakes, and all those great nights with Marc, Carles, Pau and Sara have been essential for me. Thank you for turning El Prat de Llobregat into my second home.

To **Vanessa Ortiz (V.O.B.)**, artist, top-notch scientist, and one of the most beautiful human beings I've ever met. I have really enjoyed your company in the laboratory. Your intelligence, wittiness and acid (almost orange-like) sense of humor has been a real blast. Thank you (and infinite thanks for your marvelous cover art)!

To **Ignacio Campillo**, a proper *Cervantinian* man; funny, hard-worker and one of the kindest persons I've ever met. It has been a great pleasure to work hand to hand with you in our single-cell adventure. Thank you for keeping this laboratory alive with your energy.

To **Ines Oršolić**, my favourite *hravatskan* colleague. What a great sense of humor! What a joy to always see you at my right side in the office! I love jour jokes, your candor and your sincerity. For you, *dautivame na ulica*, always, whenever you want… Your favourite "*serdo*" is waiting for you... Thank you!

To **Carlos García**, the representation of Madrid in one single man: a real *chulapo*, with a sharp sense of humor and a fond passion for its work. A true inspiration for all of us. Thank you for bringing so much joy to our lab.

To **Lorea Villanueva**, our dearest "*AZA madrina*", always demethylating our best (and worst) gene promoters. My inner gipsy starts to sing whenever I see you. With you, laughs and good vibes are guaranteed. Thank you and *Goiko Nafarroa*!

To **Laura Martínez**, our favorite novelist in the *IJC*. Thank you for your kindness and your sarcastic sense of humor.

To **Yoana Veselinova**, **Eloy Santos** and **Carlos Quero**, the new generation of *Maneliers*. You three are one of the finest additions in the *IJC*, full of energy and kindness. With you, our laboratory has guaranteed a prolific future.

To **Pere Llinàs**, the one who brought me to this laboratory. My island compatriot. Through your photographer eyes, life takes shape into something beautiful and full of meaning. Thank you for all your kindness, your advice, and your contagious cheerfulness.

To **Margalida Rosselló**, my dearest *Uni* companion. You know me better than anyone and we've been through many things during this period in Barcelona. I've learnt many things with you. Your wisdom and maturity helped me in my worst moments. Thank you for all your advice and kindness.

To **Maxime Janin**, my first teacher and mentor in the laboratory. The calmest, most plentiful person one can meet. Thank you for all your patience with me. You are a true inspiration for me.

To ***Don* Andrés Gámez**, my philosophical soulmate. Only those who can maintain with you an interesting, profound, and philosophical dialogue about life can be considered friends, and you are one of them. Thank you for all the profound conversations and your always kind words. I am very lucky for having met a true *Maestro* like you.

To **Guillermo ("*Maestro*") Yoldi** and **Adrià Bernat**. You made me cry of laughter countless of times with your jokes, your lies and your "*booty-touches*". You were 4 years my senior and the way you welcomed me to the lab during the *IDIBELL* era was the best thing that could happen to me. Thank you for all the great moments!

To **Beatriz Berzosa**, **Helena Díaz** and **Martí Badal**, the greatest communication team ever. Thank you for always considering me to participate in all the *IJC* communication "*marrones*". I really had a great time with you.

To **Veronica Padial, Anna Vergés and Esperanza Marín**. Without you, nothing in this laboratory would work. Thank you for all these years of grant-writing, purchase-making and logistics-solving.

To **Sugey**, our favourite *IJC* janitor. You always kept a smile and filled our lab with joy and good vibes. Thank you for bringing so much joy.

To all my colleagues in the **Can Ruti PhD Committee**, a fantastic team of young and vibrant people, full of energy and will for helping other people. I have learnt many things with you. It's been great to share so many challenging moments with you.

To all my childhood friends in "***El consejo de sabios***" from Mallorca. Our paths have separated us, but our souls will always be bound by friendship. Thank you for all the best moments of my life.

To all the guys and gals from **Can19**. With you, I lived my "second teenage years". I enjoyed every moment of my stay with you. Thank you all!

To **Javier Vicente Herrera**, my true friend. Sea cual sea la distancia que nos separe la vida, siempre estaremos juntos. Esta amistad cruza fronteras y siempre brillará fuerte allá donde estemos. Contigo he descubierto lo que significa verdaderamente un amigo: alguien que pase lo que pase te respetará y siempre estará contigo, en lo bueno y en lo malo. Gracias por todo, compañero.

To **Sara Risco Amigó**, my soulmate and the love of my life. Como siempre te digo, eres lo mejor que me ha pasado en la vida. Gracias por entrar ese día en mi cuarto y en mi vida; gracias por ser la mejor persona del mundo, la más bondadosa y la mejor compañera de vida. Contigo desaparecen todos los miedos e inseguridades. Sin duda alguna, soy la persona más afortunada del mundo. Gracias…

To my grandparents, **Isabel Palmer Catalán** and **Juan Costa Salom**. Vosotros ya no estáis aquí. Hace 3 años, el cáncer se os llevó, a la vez. Súbita e inesperadamente, me dejó sin dos de los pilares más fundamentales en mi vida. Me privó de compartir con vosotros muchas alegrías futuras. Os desvanecisteis cuando menos nos lo esperábamos y cuando más os necesitábamos. Uno intenta no pensar, pero es inevitable. Tan solo queda recordar los mejores momentos. Tomar el recuerdo y seguir luchando. Seguir luchando por vosotros y por la vida. Por todo, os doy las gracias, abuelos.

⁂

And finally, to my parents, **Isabel Costa Palmer** and **José Antonio Bueno Reina**. A vosotros os debo todo. Juntos hemos pasado por terribles y muy numerosas dificultades. Pero juntos las hemos ido resolviendo, sin rendirnos, sin dejar de apoyarnos el uno en el otro. Y juntos lo superaremos todo. Es un orgullo teneros como padres. Todo lo que haga y diga es poco para agradeceros todo lo que habéis hecho por mí. Sé que es insignificante, pero a vosotros quiero dedicaros esta pequeña tesis que tanto trabajo ha costado. Gracias… mil y una vez gracias…

COMMENTS TO THE READERS OF THIS THESIS

Dear reader of this thesis,

Whether you are one of the members of the tribunal or just a curious person that wants to learn a little bit more about this strange and fascinating process known as “transdifferentiation”, I really want to say thank you, not just as a mere *captatio benevolentiae*, but to really express my gratitude with all my heart. This work has been a part of my life for almost five years, through which I’ve encountered many sorrows but also many joys, with some electrifying *eureka* moments and surrounded with the most marvelous and inspiring people. For all these reasons, thank you for “wasting” (or better to say “investing”) your time reading this work that means so much to me.

In order to facilitate the comprehension of all the concepts and intentions written in this thesis, we humbly propose the reader to read the next four comments and recommendations:

(1) We really suggest reading this thesis from start to finish, without any jumps or skips in between chapters or sections whatsoever. We really recommend this especially for some sections in the introduction, like “B-cell and macrophage development” (in which the reader may be already knowledgeable in this topic), since there are included key concepts that will connect to the rest of the work. For that matter, its style is fundamentally didactic, explaining the basic concepts at the beginning and increasing complexity by adding new concepts as it progresses, following a strict narrative thread. That is why we decided to include the “Materials and Methods” section at the end rather than before the “Results” section (as the University of Barcelona recommends), trying to ensure a good reading flow.

(2) The results section is divided in two major parts, each corresponding to two different but intertwined projects that have been already published in two independent scientific articles. Instead of presenting them “by papers”, we decided to describe each result step by step in a comprehensive manner, following a narrative thread. For that reason, we also recommend reading the results section orderly, from the beginning of the first project until the end of the second one.

(3) There are many results from these two projects and from many other non-related projects in which we participated that are not shown in this thesis due to space constraints and narrative reasons. Thus, in order to make it as clear and comprehensive as possible, we decided to significantly simplify the thesis, showing only those results that pinpoint the most important messages and conclusions.

(4) And of course, we recommend reading this work slowly and thoroughly in order to find as many errors, suggestions and new ideas as possible.

Yours sincerely,

Alberto Bueno Costa

INDEX

ABSTRACT

Cellular transdifferentiation is defined as the process in which a differentiated cell from one specific lineage directly differentiates into another type of cell from another different lineage without going through a common intermediate multi-/pluripotent state. This event is believed to be driven mainly by epigenetic cues that reshape the epigenome for it to take a similar configuration normally found in the new lineage. Cellular transdifferentiation is a relatively rare event that occurs in humans under both physiological and pathological conditions. In cancer, this event acts as a therapy-resistance strategy for certain types of malignancies. Specifically in hematological cancers, such as follicular lymphoma (FL) and B cell acute lymphoblastic leukemia (B-ALL), B cells can transdifferentiate into malignant macrophages that resist to conventional therapy, leading to extremely poor prognosis. Very little is known about the epigenetic and epitranscriptomic changes that occur during B-cell-to-macrophage transdifferentiation, especially during the early stages of this event. Thus, we decided to investigate the global changes in 5-methylcytosine (5mC) DNA methylation and N6-methyl-adenosine (m6A) RNA methylation at different time-points of transdifferentiation using a human pre-B-ALL-to-macrophage C/EBPα-driven transdifferentiation *in vitro* model (BLaER1).

DNA 5mC methylation array analysis revealed no global methylation changes during BLaER1 B-cell-to-macrophage transdifferentiation, but rather discrete local changes in 251 CpGs, 99.6% (250) of which were demethylated upon transdifferentiation. 15.2% of those CpGs were located at gene promoter regions, controlling key macrophage genes, while 39.4% and 43.8% of the CpGs were located at gene bodies and distant genomic regions respectively, in which distant enhancers and silencers may be acting in a methylation-dependent manner. Correlation with Hi-C and expression array data, validation with 5-aza-2'-deoxycytidine passive DNA demethylation and UMI-4C analyses indicated that these distant regulatory regions control important macrophage genes in a methylation-dependent manner.

On the other hand, m6A-seq RNA methylation analysis revealed numerous changes in the m6A epitranscriptome (6072 differential m6A peaks, corresponding to 3056 unique transcripts) upon BLaER1 B-cell-to-macrophage transdifferentiation. Gene ontology analyses revealed a strong enrichment in protein translation-related transcripts. We observed that

mRNA transcripts with an increase in m6A content at the 3'UTR region were enriched in translation-related functions. shRNA-mediated knockdown of METTL3 and treatment with STM2457 (a small molecular competitive inhibitor of METTL3) both revealed that m6A increases the decay rate of crucial ribosomal protein transcripts, fine-tuning the levels of these protein during transdifferentiation by regulating global protein synthesis. In addition, METTL3 knockdown and treatment with STM2457 also revealed a significant decrease in BLaER1 B-cell-to-macrophage transdifferentiation, highlighting the importance of m6A in this transdifferentiation process.

In conclusion, B-cell-to-macrophage transdifferentiation is an event in which both epigenetic and epitranscriptomic changes take place. While DNA 5mC methylation changes occur at discrete, local genomic regions (especially at distant regulatory regions), RNA m6A methylation changes are more drastic, both controlling key transdifferentiation processes. These findings shed some light on the vaguely studied field of cellular transdifferentiation, opening new opportunities in the diagnosis and treatment of malignant transdifferentiation events.

RESUMEN

La transdiferenciación celular se define como un proceso en el cual una célula diferenciada perteneciente a un linaje específico directamente se diferencia en otro tipo celular perteneciente a otro linaje distinto sin pasar por un estado intermedio multi-/pluripotente común. Se piensa que este evento está impulsado principalmente por señales epigenéticas que remodelan el epigenoma para que éste adquiera una configuración similar a la del nuevo linaje. La transdiferenciación celular es un evento relativamente poco común que ocurre en humanos bajo condiciones fisiológicas y patológicas. En el cáncer, este evento actúa como una estrategia de resistencia a la terapia en ciertos tipos de malignidades. Específicamente en cánceres hematológicos, como linfoma folicular (FL) y leucemia linfoblástica aguda de células B (B-ALL), las células B pueden transdiferenciar en macrófagos malignos que resisten a la terapia convencional, conduciendo a pronósticos extremadamente malos. Se sabe muy poco sobre los cambios epigenéticos y epitranscriptómicos que ocurren durante la transdiferenciación de célula-B-a-macrófago, especialmente durante las etapas tempranas de este evento. Por ello, hemos decidido investigar los cambios globales en la metilación 5-metilcitosina (5mC) en ADN y en la metilación N6-metiladenosina (m6A) en ARN a lo largo de diferentes puntos temporales de la transdiferenciación usando un modelo humano de transdiferenciación *in vitro* pre-B-ALL-a-macrófago estimulado por C/EBPa (BLaER1).

El análisis mediante array de la metilación 5mC en ADN no revela cambios globales de metilación durante la transdiferenciación de célula-B-a-macrófago en BLaER1, sino que muestra cambios discretos locales en 251 CpGs, 99,6% (250) de las cuales se desmetilan a lo largo de la transdiferenciación. 15,2% de estas CpGs están localizadas en promotores génicos, controlando genes clave para el macrófago, mientras que un 39.4% y un 43.8% de las CpGs están respectivamente localizadas en cuerpos de genes y en regiones genómicas distantes, donde regiones potenciadoras y silenciadoras distantes pueden estar actuando de forma dependiente a la metilación. La correlación con Hi-C y arrays de expresión y la validación con la desmetilación pasiva del ADN mediada por 5-aza-2'-deoxycytidine y análisis mediante UMI-4C muestran que estas regiones distantes reguladoras controlan genes importantes para macrófago de forma dependiente a la metilación.

Por otra parte, el análisis de metilación del ARN mediante m6A-seq revela numerosos cambios en el epitranscriptoma de m6A (6072 picos de m6A diferenciales, correspondiéndose con 3056 transcritos únicos) tras la transdiferenciación de célula-B-a-macrófago en BLaER1. Análisis de ontología génica muestran un fuerte enriquecimiento en transcritos relacionados con la traducción proteica. Hemos observado que aquellos transcritos con un aumento en m6A en la región 3'UTR están enriquecidos en transcritos relacionados con la traducción. La depleción de METTL3 mediada por shRNA así como el tratamiento con STM2457 (un inhibidor molecular pequeño competitivo contra METTL3) han revelado que m6A aumenta la velocidad de decaimiento de transcritos de proteínas ribosomales cruciales, controlando de forma precisa los niveles de estas proteínas durante la transdiferenciación mediante la regulación de síntesis proteica global. Además, la depleción de METTL3 o el tratamiento con STM2457 también reveló una disminución significativa en la transdiferenciación de célula-B-a-macrófago en BLaER1, destacando la importancia de m6A en este proceso de transdiferenciación.

En conclusión, la transdiferenciación de célula-B-a-macrófago es un evento en el que ocurren cambios epigenéticos y epitranscriptómicos. Mientras que la metilación 5mC en ADN ocurren en regiones discretas, locales del genoma (especialmente en regiones reguladoras distantes), los cambios de metilación m6A en ARN son más drásticos, ambos controlando procesos clave de la transdiferenciación. Estos hallazgos arrojan algo de luz sobre el vagamente estudiado campo de la transdiferenciación celular, abriendo nuevas oportunidades en el diagnóstico y tratamiento de eventos de transdiferenciación maligna.

INTRODUCTION

INTRODUCTION

Cellular differentiation: a straight road for cell specialization

From the very first moment in which the sperm meets the egg, a perfectly orchestrated symphony begins. The totipotent zygote gradually divides, generating more and more differentiated and specialized cells, adjusting their epigenomes to the taste and needs of each forming tissue and organ, and giving rise to an extremely complex, rational and emotional autonomous entity composed of approximately 37.2 trillion cells: the human being [1]. This chain of events, termed embryonic development, allowed us to lay the foundations for a key process which we still do not fully comprehend: the cellular differentiation. Cellular differentiation is defined as the process in which a cell specializes by adopting a specific phenotype to fulfill a particular function in the organism [2]. As this definition suggests, these specialized cells come from an unspecialized cell, known as a stem cell, which has a certain plasticity to not only replicate itself, but also to give rise to specific differentiated cells when the organism requires it. These stem cells are not only found in the embryo; in the adult organism, different tissues harbor thousands of stem cells that, although they are not capable of forming an organism *de novo* as the zygote does (totipotency) nor to generate any type of cell in the body as embryonic cells do (pluripotency), they can differentiate to give specific specialized cells for a particular type of tissue (multipotency).

These multipotent stem cells allow the adult organism to develop over the years and ensures the regeneration of certain tissues that suffer constant damage (skin, intestine, blood, etc.) throughout the whole lifespan of an individual [3]. However, this binary hierarchy described here (multipotential stem cells giving rise to differentiated cells) is extremely simplistic. In fact, between the multipotent stem cell and the fully differentiated cell, there are many "shades of grey": intermediate cells with variable potential that, although they are still not fully specialized, they act as progenitor cells, committed to differentiate into a more specific cell type. The perfect example of this scenario is the hematopoietic system (figure I-1). The hematopoietic system originates from multipotent hematopoietic stem cells (HSCs) that reside in the bone marrow (BM) [4, 5]. These self-renewable cells are rare (1 HSC per 100.000 cells in the adult BM), but they give rise to the entire blood and immune systems throughout the lifetime of an individual. These HSCs differentiate into myeloid-committed or lymphoid-

committed oligopotent progenitor cells, which will further differentiate into specialized myeloid cells (granulocytes, monocytes, erythrocytes or megakaryocytes) and lymphoid cells (natural killer cells, B-cells and T-cells) respectively. The precise mechanisms by which an HSC decides its fate (myeloid versus lymphoid) is still under research due to the enormous complexity of the signals that co-occur inside the BM. Nevertheless, it is now accepted that this decision is driven by a combination of both microenvironmental stimuli (inductive model, driven by cell-to-cell crosstalk) and intrinsic stochastic signals (stochastic model, driven by fluctuations in the expression and activity of various transcription factors) [5, 6]. Thus, depending on the external and internal signals, HSCs will differentiate into oligopotent myeloid or lymphoid progenitor cells.

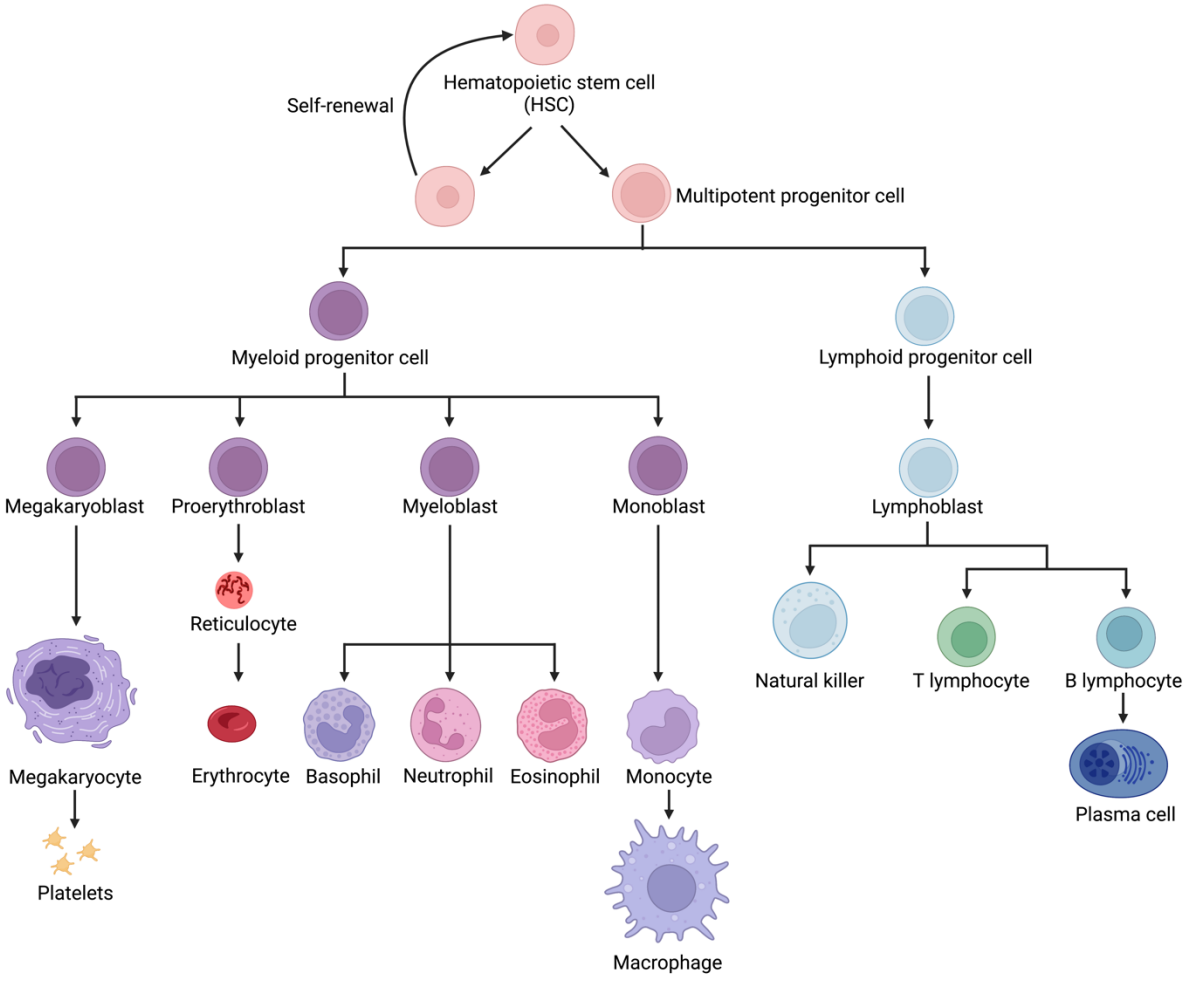

Figure I-1. Oversimplified view of the hematopoietic system.

These progenitor cells still hold certain plasticity, but only applied into their corresponding lineages. Driven by different external and internal stimuli, the progenitor cells will undergo several rounds of cellular differentiation, giving rise to more and more committed progenitor cells, until they generate a fully differentiated and specialized cellular type. To illustrate this gradual differentiation process (HSCs → Progenitor 1 → Progenitor 2 → ⋯ → Specialized cell), we are going to describe in detail the differentiation steps taken in B-cell (lymphoid cells) and macrophage (myeloid cells) development, since both cells will be the main focus of this doctoral thesis.

⁂

B-cell development

B-cell development can be divided in 2 distinct phases: (1) early B-cell development, which takes place in the bone marrow (BM) and (2) late/peripheral B-cell development, which takes place in secondary lymphoid organs such as the spleen and the lymph nodes [7–10]. Both stages are summarized in figure I-2.

(1) Early B-cell development

First, a bone marrow (BM) resident HSC experiences several rounds of differentiation, going through different multipotential stages. Starting from late-term HSC (LT-HSC, with high self-renewal capacity), the HSC differentiates into a short-term HSC (ST-HSC, with reduced self-renewal potential) and then to a multipotent progenitor cell (MPP). In humans, ST-HSC and MPP are difficult to distinguish, due to the similarities in the pattern of cell surface markers. The MPP cell still has the potential to go through either myeloid or lymphoid differentiation fates. The most important factors that drive MPP into the lymphoid lineage is the co-expression and co-operation of 2 transcription factors: PU.1 and Ikaros. PU.1 activity is necessary to promote both myeloid and lymphoid differentiation processes, but its interaction with Ikaros pushes the differentiation of MPP cells exclusively into the lymphoid lineage, first differentiating into lymphoid-myeloid primed progenitor (LMPP) cells and then to common lymphoid progenitor (CLP) cells.

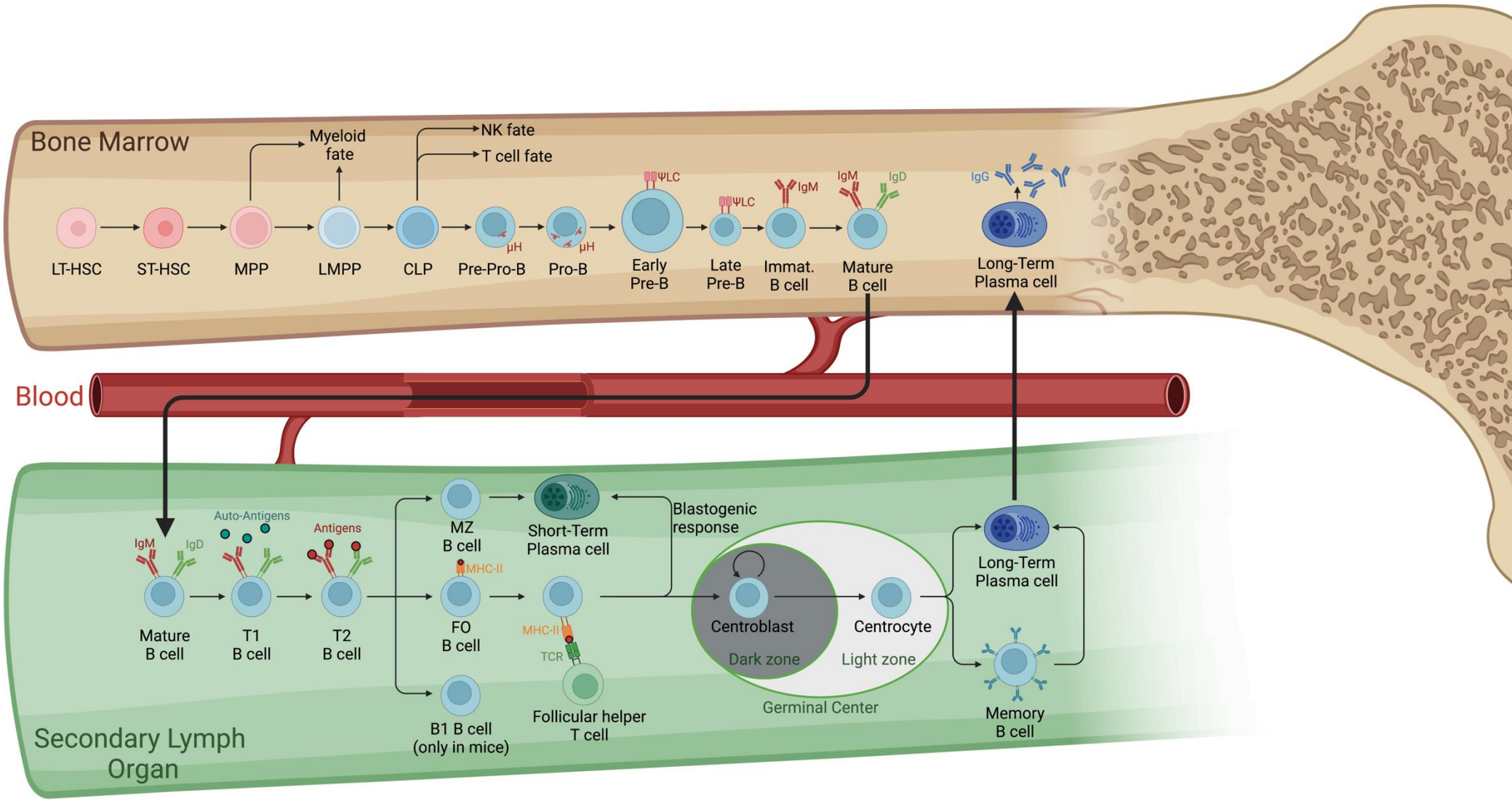

Figure I-2. B cell development; schematic view. Secondary lymph organ architecture is oversimplified, depicting only one cortex node. Germinal center's mantle zone is not shown for space reasons. **Abbreviations**: LT-HSC: Long-term hematopoietic stem cell (HSC); ST-HSC: Short-term HSC; MPP: Multipotent progenitor cell; LMPP: lymphoid-myeloid primed progenitor; CLP: common lymphoid progenitor; NK: Natural killer; T1/T2: Transitional 1/2 B cell; MZ: Marginal Zone B cell; FO: Follicular B cell. Figure designed by the thesis author using BioRender licensed software.

These CLP cells are oligopotent progenitors that are fully committed to the lymphoid differentiation program, with the potential of generating B-cells, T-cells, and natural killer (NK) cells. At this point, an increase in the expression of 2 key lymphoid transcription factors, E2A and EBF1, drives the CLP cells to differentiate into Pre-Pro-B-cells, which are the first fully committed B-cell precursors. Afterwards, RAG1 and RAG2 proteins are activated, which foster the VDJ rearrangement of the heavy chain immunoglobulin genomic locus (VDJ regions) of Pre-Pro-B-cells, differentiating into Pro-B-cells that express the μ heavy immunoglobulin chain (μH). At this stage, μH is only located inside the endoplasmic reticulum of the Pro-B-cells.

Next, the Pro-B-cells display an increase in the expression of a key lymphoid transcription factor: PAX5. This protein is crucial for the Pro-B → Pre-B transition and locks these progenitor B-cells in the B-cell lymphoid lineage, avoiding the transitioning of these B-cell progenitors to other lymphoid lineages, such as T-cells [11]. PAX5 increases the expression of CD19 (a key B-cell membrane protein that co-stimulates B-cell antigenic response), Igα/Igβ (both BCR signal transducers), and VpreB/λ_5 (both forming the scavenger pre-BCR light chain, ΨLC). In addition, the μH is liberated from the endoplasmic reticulum into the cytoplasm. This marks the differentiation of Pro-B-cells into early-Pre-B cells.

Early-Pre-B cells (also known as large-Pre-B cells) go through a 2-step quality control checkpoint. First, the μH chain scaffolds with the Igα/Igβ and the ΨLC to form the pre-BCR complex on the cell membrane; if the assembly is ineffective, the cells enter in apoptosis. Secondly, the VpreB protein from the ΨLC complex acts as a pseudo-antigen that must be recognized by this pre-BCR scaffold to confirm the proper functionality of the early-Pre-B-cells. This marks the transition of early-Pre-B-cells into late-Pre-B-cells (also known as small-Pre-B cells).

Once the pre-BCR scaffold is correctly assembled, RAG1 and RAG2 are re-activated in the late-Pre-B-cells, which stimulate the VJ rearrangement of the λ and κ immunoglobulin light chains and the subsequent generation of a membrane-bound IgM-BCR, marking the differentiation of late-Pre-B-cells into IgM+ immature B-cells. These IgM+ immature B-cells go through repeated rounds of light chain VJ rearrangement to further lessen immunoglobulin self-specificity. In addition, the constant δ (Cδ) immunoglobulin locus is also transcribed, generating membrane-bound IgD-BCRs, which marks the transition of IgM+ immature B-

cells into IgM+/IgD+ mature B-cells. These mature B-cells leave the BM into the bloodstream to reach the secondary lymphoid organs (spleen and lymph nodes) to continue with their development.

(2) Late/peripheral B-cell development

Once the IgM+/IgD+ mature B-cells arrive to the secondary lymphoid organ (either the spleen or a lymph node), they undergo a series of differentiation steps that will prepare these B-cells to execute proper antigenic response. First, as the IgM+/IgD+ mature B-cells arrive to the secondary lymphoid organ, the soluble B-cell activating factor (BAFF) present in this new microenvironment interacts with the B-cell's BAFF-receptor, which triggers the first transitional stage 1 (T1) of the B-cells. T1 B-cells undergo negative selection to detect if their BCR is reactive to auto-antigens. T1 B-cells that recognize auto-antigens are eliminated by apoptosis induction. Afterwards, T1 B-cells that pass negative selection differentiate into transitional stage 2 (T2) B-cells, which undergo a positive selection to confirm that their BCR recognize foreign antigens. Once T2 B-cells successfully pass positive selection, they can differentiate into 2 distinct types of Naïve B-cells: (1) Marginal Zone (MZ) B-cells and (2) Follicular (FO) B-cells, also known as B2 B-cells. In addition, and only in mice, there is a third type of Naïve B-cell: the B1 B-cells, which are functionally similar to MZ B-cells, although their existence in humans is currently under debate.

MZ B-cells are a type of Naïve B-cells located in the follicular marginal zone of the cortical regions of the spleen and the lymph nodes (though difficult to visualize by microscopic techniques in the latter tissue). They are originated from T2 B-cells after NOTCH2 and canonical-NFκB stimulation. MZ B-cells preferentially recognize T-cell independent antigens (polymeric antigens with repetitive epitopes, like LPS), directly differentiating into short-living plasma cells (PCs) that secrete low-affinity IgM, acting as a rapid initial B-cell-mediated innate immune response against bacterial pathogens.

On the other hand, FO B-cells are Naïve B-cells that accumulate in the cortical region of secondary lymphoid organs, forming clumps of FO B-cells which will constitute a primary follicle. FO B-cells are originated from T2 B-cells after BAFF and non-canonical-NFκB stimulation. In addition, the BCR signaling generated in FO B-cells is much stronger than in MZ B-cells, which potentiates T2 → FO differentiation. FO B-cells preferentially recognize T-cell

dependent antigens. First, a FO B-cell recognizes a soluble antigen by its BCR, but instead of generating a rapid response, the FO B-cell uptakes the antigen by endocytosis, lyses the antigen and presents it through the MHC-II. Secondly, the TCR of a specific Follicular Helper T-cell (T_{fh} cell) clone that surrounds the primary follicle in the cortical space binds to that MHC-II-presented antigen, activating the FO B-cell.

This T-cell mediated activation of FO B-cells stimulate the conversion of the primary follicle into a secondary follicle, which is divided in 3 parts, each one corresponding with the 3 distinct differentiation fates an activated FO B-cell can undertake: (1) the mantle zone that surrounds the germinal center of the secondary follicle, composed by FO B-cell-derived blastogenic response mantle B-cells, (2) the dark zone of the germinal center, composed by FO B-cell-derived centroblasts and (3) the light zone of the germinal center, composed by FO B-cell-derived centrocytes.

Blastogenic response mantle B-cells are short-living plasma cells (PCs) originated from the differentiation of a subset of activated FO B-cells which immediately maturate to PCs. These PCs secrete low-affinity IgM (similarly to MZ B-cells) to provide a rapid innate initial response to an infection.

Centroblasts are germinal center (GC) B-cells also originated from the differentiation of a subset of activated FO B-cells. They accumulate in the dark zone of the secondary follicle and they continuously keep cycling to expand the activated B-cell clone.

Centrocytes are also germinal center (GC) B-cells directly differentiated from FO B-cells or from centroblasts that ceased proliferation. Centrocytes are located in the light zone of the secondary follicle and undergo the final step of B-cell development: the germinal center response. After the initial blastogenic low-affinity IgM antigenic response, these GC B-cells undergo a 3-step germinal center response: (1) immunoglobulin heavy chain class switching, by which B-cells will express γ_1, γ_{2a}, γ_{2b}, γ_3, ε or α high-affinity immunoglobulins, (2) light chain receptor editing by RAG1 and RAG2, to further increase immunoglobulin affinity to the reactive antigen and (3) somatic hypermutation, in which activation-induced cytidine deaminase enzyme (AID) generate single nucleotide exchanges and mutations in the antigen-binding region of the immunoglobulins to further increase their affinity.

Finally, centrocytes that successfully underwent germinal center response will differentiate into long-living PCs, which will migrate into the BM and will mediate a very strong adaptive

immunological response by secreting high-affinity immunoglobulins, while the other fraction of centrocytes will differentiate into memory B-cells, which are the responsible of rapid high-affinity adaptive responses against the same pathogens in future infections.

Every progenitor and specialized cell described here has been catalogued to a great extent thanks to the differential surface markers that each of these cells express throughout the different stages of differentiation. Annexed table A-1 (page 155) depicts the distinct internal and surface markers that characterize each type of cell during B-cell development.

Macrophage development

Relatively recently, the field of macrophage biology has undergone a paradigm shift in relation to the origin of macrophages in the adult organism. Classically, researchers thought that tissue macrophages were originated exclusively via bone marrow HSC-derived monocytes. Nevertheless, since the 2010s, we know that most of the tissue-resident macrophages in the adult organism have an HSC-independent embryonic origin, completely independent of monocytic differentiation [12–14]. Thus, to fully understand macrophage development, we need to take into consideration both cell origins (figure I-3).

(1) Embryonic-origin macrophages

During embryonic development, macrophages are generated in the yolk sack endothelium, way before the emergence of the aorta-gonad-mesonephros system responsible for the generation of HSCs. Thus, instead of having a monocytic origin, these embryonic-derived macrophages come from HSC-independent TIE2+/CSF1R+ erythro-myeloid progenitors (EMPs) already present in the yolk sack. Once generated, embryonic macrophages leave the yolk sack into the bloodstream to spread and seed the whole embryo (figure I-3, left). These macrophages persist in the adult organism throughout the whole lifetime of the individual, self-maintaining themselves independently of the adult hematopoietic system. Tissues that are mostly composed of embryonic-derived macrophages include the liver (Kupffer cells), kidney (marginal zone macrophages and red pulp macrophages), brain (microglia), peritoneum (peritoneal macrophages) and lung (alveolar macrophages). Nevertheless, most of these tissues can harbor both embryonic-derived and adult HSC-monocytic-derived macrophages.

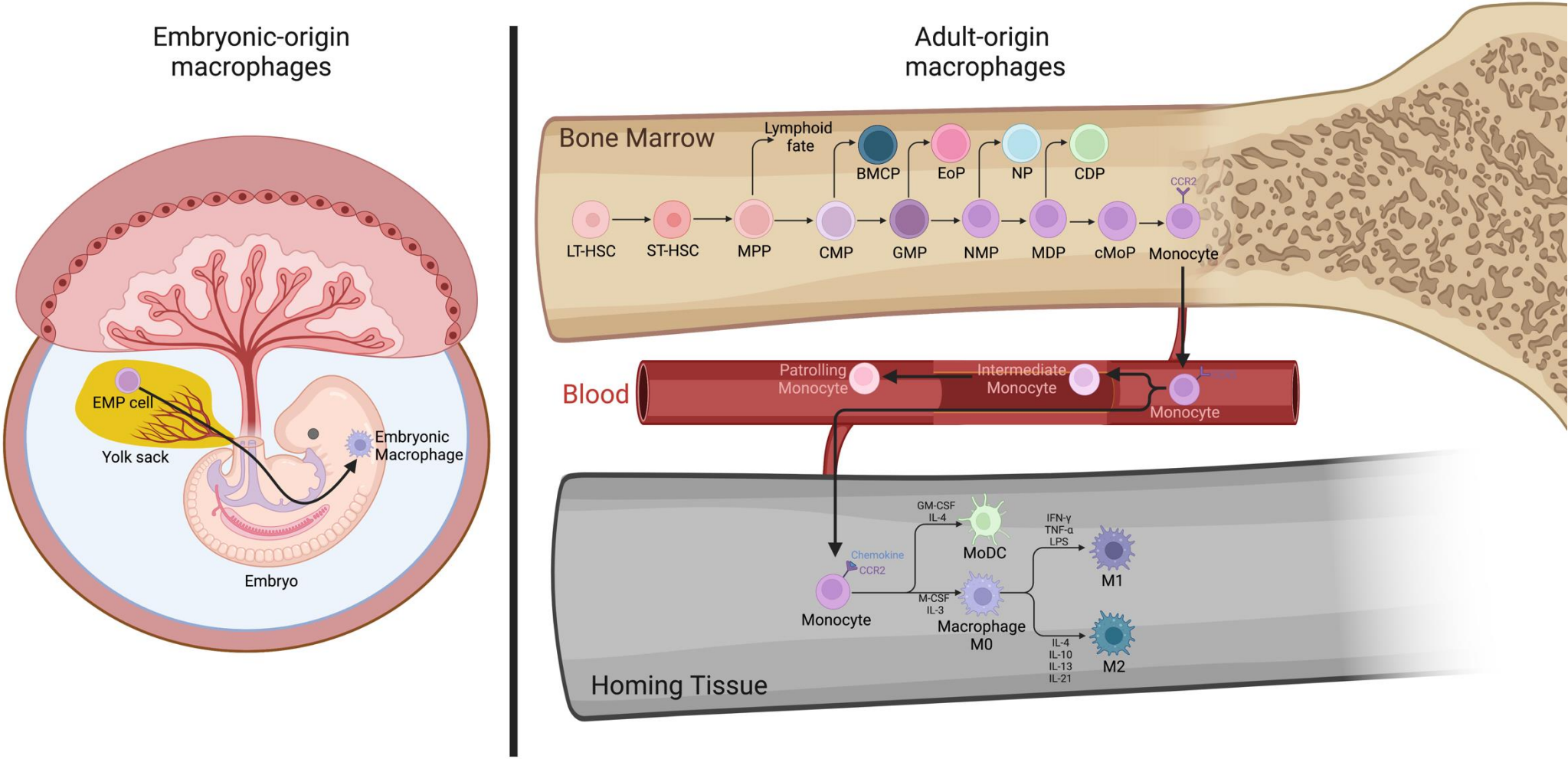

Figure I-3. (Left) Embryonic-origin macrophage development in humans. (Right) Adult-origin macrophage development in humans. **Abbreviations**: EMP: Erythro-Myeloid Progenitor cells; LT-HSC: Long-term hematopoietic stem cell (HSC); ST-HSC: Short-term HSC; MPP: Multipotent Progenitor; CMP: Common Myeloid Progenitor; BMCP: Basophil/Mast-Cell Progenitor; GMP: Granulocyte/Monocyte Progenitor; EoP: Eosinophil Progenitor; NMP: Neutrophil/Monocyte Progenitor; NP: Neutrophil Progenitor; MDP: Monocyte/Dendritic-cell Progenitor; CDP: Common Dendritic-cell Progenitors; cMoP: Common Monocyte Progenitor; MoDC: Monocyte-derived Dendritic Cells; M1/M2: Macrophages M1/M2. Figure designed by the thesis author using BioRender licensed software.

However, the function of embryonic-macrophages differs from HSC-monocytic-derived macrophages, in which the former are dedicated to the homeostatic support and clearance of the tissues they reside in, while the latter usually act in response to tissue inflammation.

(2) Adult monocyte-derived macrophages

The origin of monocyte-derived macrophages is much better studied than in their embryonic-derived counterparts. Essentially, the generation of monocyte-derived macrophages can be divided in 2 stages: (1) the generation of CD14+/CD16- monocytes in the adult BM and (2) the extravasation and tissue-homing of monocytes and their differentiation into functional macrophages [12–20]. These differentiation stages are summarized in figure I-3 (right).

(2.1) Generation of monocytes in the bone marrow

First, as already seen in B-cell development, a BM resident HSC experiences several rounds of differentiation. An LT-HSC differentiates into a ST-HSC and then to an MPP cell. MPP cells still have the potential to go through either myeloid or lymphoid differentiation fates. The most important factors that drive MPP cells into the myeloid lineage is the co-expression of PU.1 and C/EBPα (or C/EBPβ in certain conditions) transcription factors. As previously explained, PU.1 activity promotes both myeloid and lymphoid differentiation processes, but its co-expression with C/EBPα (a crucial myeloid-priming transcription factor) pushes the differentiation of MPP cells exclusively into the myeloid lineage. In addition, although ubiquitously expressed in all hematological cell lineages, RUNX1 transcription factor seems to be also necessary for myeloid differentiation at this stage, since myeloid committed progenitor cells express significantly higher amounts of this protein in comparison to lymphoid committed progenitors. Thus, MPP cells can directly differentiate into common myeloid progenitor (CMP) cells, also known as CFU-GEMM cells (CFU-GEMM stands for “Colony Forming Unit – Granulocyte/Erythrocyte/Monocyte/ Megakaryocyte”).

The fate of CMP cells can take different roads depending on the timing-based interplay of two transcription factors: GATA2 and C/EBPα. GATA2+ CMP cells differentiate into basophil/mast-cell progenitor (BMCP) cells, while C/EBPα+ CMP cells differentiate into granulocyte/monocyte progenitor (GMP) cells. Needless to say, this picture is oversimplified, since other additional transcription factors and cytokines present in the BM microenvironment also play a role in deciding the fate of CMP cells. The activity of c-Myb transcription factor and

the interaction with the cytokine GM-CSF are both crucial factors for CMP → GMP differentiation.

Once GMP cells are formed, they can undergo 2 distinct differentiation paths. If C/EBPα expression is maintained, GMP cells can further differentiate in neutrophil/monocyte progenitor (NMP) cells, but if C/EBPα expression is downregulated and GATA2 expression increases, then these GMP cells differentiate into eosinophil progenitor (EoP) cells. NMP cells can further differentiate into neutrophil progenitor (NP) cells or monocyte/dendritic-cell progenitor (MDP) cells. An upregulation in IRF8 transcription factor is crucial for NMP → MDP transition.

MDP cells can differentiate either into common dendritic cell progenitors (CDP, which will generate classical dendritic cells) or common monocyte progenitor (cMoP) cells. M-CSF stimulation and the expression of KLF4 transcription factor drives MDP → cMoP differentiation. Finally, cMoP cells differentiate into CD14+/CD16- "classical" monocytes (also known as $Ly6C^{Hi}$ monocytes in mice) upon C/EBPα and C/EBPβ re-activation, among other key transcription factors.

(2.2) Monocyte tissue homing and differentiation into macrophages

CD14+/CD16- "classical" monocytes abandon the BM, entering in the bloodstream. Classical monocytes express CCR2, an important chemokine receptor that allow these cells to extravasate into inflamed tissues. Nevertheless, some classical monocytes circulating in the bloodstream overexpress NR4A1 and CX3CR1, which allow them to differentiate into $CD14+/CD16^{Low}$ "intermediate" monocytes, which in turn they differentiate into $CD14+/CD16^{Hi}$ "patrolling" monocytes (also known as $Ly6C^{Low}$ monocytes in mice). The role of these patrolling monocytes is not clear, though judging by their similarities to differentiated macrophages, some researchers classify them as "blood-resident macrophages".

Circulating classical monocytes sense inflamed tissues through CCR2. When stimulated, this homing chemokine receptor triggers the extravasation of the circulating classical monocytes into the inflamed tissue. Depending on the cell and cytokine composition of the tissue microenvironment, homed classical monocytes can undergo different roads of differentiation. If they are stimulated with GM-CSF and IL-4, they differentiate into monocyte-derived

dendritic cells (MoDCs). On the other hand, if homed classical monocytes are stimulated with M-CSF and IL-3, they differentiate into non-polarized M0 macrophages.

Depending on the composition of the tissue microenvironment, M0 macrophages can be polarized either to pro-inflammatory M1 macrophages (also known as classically activated macrophages) or anti-inflammatory M2 macrophages (also known as alternatively activated macrophages). M0 → M1 polarization is stimulated by IFN-γ, TNF-α and/or LPS, while M0 → M2 polarization is stimulated by IL-4, IL-10, IL-13 and IL-21. M1 macrophages act as pro-inflammatory phagocytic cells that foster T-cell activation in the homed tissue, while M2 macrophages (which can be further subdivided into M2a, M2b, M2c and M2d macrophages, depending on the type of cytokine stimulation) are anti-inflammatory cells that stimulate wound healing, tissue fibrosis and angiogenesis. The balance between M1/M2 macrophage content is being continuously fine-tuned by the dynamically-changing cytokine composition in the homed tissue through the entire course of the inflammation.

As also seen in B-cell development, every progenitor and specialized myeloid cell described here has been catalogued mostly thanks to the differential surface markers that each of these cells express throughout the different stages of differentiation. Annexed table A-2 (page 156) depicts the distinct surface markers that characterize each type of cell during macrophage development.

***

It is very important to remember that the previously described pictures of B-cell and macrophage development constitute only a consensual and simplified model that may be very far from explaining the real events these cells undergo upon hematopoietic differentiation. There is a myriad of non-described transcription factors, soluble cytokines and cell-to-cell interactions involved in all the various steps of differentiation, each one of them acting in a precisely controlled time-and-space-dependent manner. Detailing every one of these fluctuations would be virtually impossible and is completely out of the scope of this doctoral thesis. Moreover, it is expected that many undetected progenitor cells and differentiation intermediates lie hidden due to our current technical limitations. Hopefully, with the advance of single-cell sequencing technologies, new progenitors and differentiation intermediates will be discovered, expanding our still little knowledge on this immeasurably complex field of biology.

Cellular de-differentiation and re-differentiation: the back-and-forths of cell specialization

Now that we have taken an overall view on how cellular differentiation works during B-cell and macrophage development, we might picture the differentiation process as a straight and vertical “no-return” road in which progenitor stem cells become more and more committed to a specific lineage. Thus, committed cells are “sentenced” to be locked in their corresponding lineages. For many years, that statement was believed to be true. Nonetheless, in 2006, a ground-breaking discovery made by Kazutoshi Takahashi and Shinya Yamanaka completely shifted our paradigm about cell differentiation. By retrovirally transducing 4 embryonic-related transcription factors (known as the OSKM gene “cocktail”: Oct-4, Sox-2, Klf-4 and c-Myc) into fully differentiated somatic mice fibroblasts cultured *in vitro*, they managed to de-differentiate these cells into embryonic-like induced pluripotent stem cells (iPSCs). These iPSCs can then be re-differentiated into completely different cell types, unrelated to the original cell [21]. Thus, not only they proved that fully differentiated cells can de-differentiate and re-differentiate when applying the correct inputs, but also discovered a very promising technique with potential clinical applications in tissue regeneration. Nowadays, iPSCs are still under study, being the source of valuable discoveries in both basic and clinical research. Since then, new ways of de-differentiating cells *in vitro* have been found. In the case of hematological cells, one of the most well-known cases of de-differentiation and re-differentiation was discovered by Cobaleda et al in 2007, in which they conditionally deleted Pax5 gene in mice, *in vivo*, allowing mature B-cells that reside in secondary lymphoid organs to de-differentiate into common immature progenitors that later re-differentiate into T-cells [11].

Cellular de-differentiation and later re-differentiation is also a naturally occurring event observed in adult healthy organisms, especially in the regeneration of damaged tissues. In this scenario, quiescent differentiated cells may de-differentiate into replicating progenitor cells to then re-differentiate and repopulate the lost pool of cells. Although mammals have a very limited tissue regeneration potential, especially when compared to other vertebrate species, we still display important de-differentiation/re-differentiation processes that allow some form of tissue repair. For example, upon nerve injury, mature quiescent Schwann cells re-express molecules associated with immature states (p75NTR, NCAM and L1), allowing them to de-

differentiate into progenitor cells that divide and re-differentiate again to replenish the lost pool of Schwann cells [22, 23]. Additionally, astrocytes can de-differentiate into cycling neural stem/progenitor cells (NSPCs), which will later re-differentiate to regenerate the lost cells [24–26]. Moreover, myocardial infarction induces de-differentiation of cardiomyocytes into a more immature state, allowing them to survive and to proliferate in order to recover their functions after re-differentiation [27, 28]. Other tissues in which cell de-differentiation is also used in tissue-repair include the intestines, liver, skeletal muscle and skin [29].

The rarity of physiological de-differentiation events in mammalian organisms may be explained through an evolutionary point of view, in which there is a trade-off between maximizing tissue repair and minimizing the risk of malignant cell transformation [30]. Supporting this hypothesis, researchers have found that cell de-differentiation events are usually triggered by the inactivation of pRB and ARF, both crucial tumor suppressors that are regularly silenced in pro-tumorigenic processes [29]. In fact, one major drawback of using iPSCs in clinical tissue regeneration is their high risk of malignant transformation and emergence of teratomas, due to the ectopically-induced expression of the cancer-related OSKM gene "cocktail" [31]. Thus, cell de-differentiation may act as an important malignant initiating event in various types of cancer, as seen in glioma and intestinal cancer [32]. Additionally, recent studies suggest that some cancer cells can de-differentiate into cancer stem-cells (CSCs), which are self-renewable cells that are resistant to routinely used antineoplastic agents and can indefinitely differentiate into tumor cells [33].

Cellular transdifferentiation: when mature cells behave like "chameleons"

Summarizing what we have seen so far, stem cells can differentiate into committed mature cells and, in certain especial occasions, the latter can de-differentiate into earlier progenitors in order to proliferate and re-differentiate in response to tissue damage. But, at this point, a new fundamental question emerges: is it possible for a fully committed differentiated cell to directly differentiate into another type of cell from a completely different lineage, without de-differentiating into a common pluri/multipotent progenitor stage? This direct mature-to-mature cell conversion is coined "transdifferentiation", and for many years its existence has been subject of many speculations. Similar to a chameleon instantly changing its skin color

to adapt to changes in its surroundings, a committed cell may directly transdifferentiate into another type of lineage-committed mature cell in response to microenvironmental stimuli, without needing to perform any asymmetrical division whatsoever. Since transdifferentiation is the central subject of this doctoral thesis, we will extensively describe this process in the present chapter.

(1) Transdifferentiation under experimental conditions

Cellular transdifferentiation was believed to be biologically impossible, but researchers throughout the years have found ways in which mature cells can bypass de-differentiation into pluri/multipotent progenitor states, taking a direct detour into a new cellular lineage without the need of previously generating a common cell intermediate [34]. The first *in vitro* demonstration of this process was performed in 1987 by Davis et al, by transfecting MyoD cDNA into mature mice fibroblasts cultured *in vitro*, which transdifferentiated into contracting myocytes (cells from a completely different lineage) in less than 24 hours [35]. MyoD act as a transdifferentiation pioneering factor, whose actions reshape the epigenome of the original cell to take the configuration of the new lineage. Since 1987, new transdifferentiation pioneering factors have been discovered, and fibroblasts have been transdifferentiated *in vitro* into many different types of cells from completely different lineages (figure I-4). Genetic lineage tracing experiments have proven that these transdifferentiating cells do not require a de-differentiation step, bypassing canonical progenitor states. Additionally, the absence of cellular divisions and the lack of expression in progenitor markers during transdifferentiation have been taken as measures of conversion directness. Other types of mature cells that have been transdifferentiated *in vitro* are catalogued in table I-1.

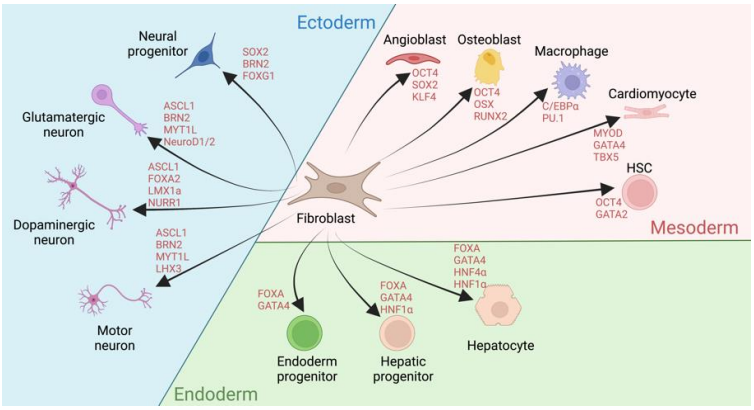

Figure I-4. Experimental *in vitro* transdifferentiation of fibroblasts and associated transcription factors [36–55].

Table I-1. Examples of experimental *in vitro* transdifferentiation.

Cell type	Transdifferentiated to	Associated transcription factors	Ref.
B cell	Macrophages	C/EBPα, C/EBPβ	[56–58]
T cell	NK cells	BCL11B deletion	[59]
Pancreatic duct cells	Beta cells	PDX1	[60]
Pancreatic exocrine cells	Beta cells	NGN3, MAFA, PDX1	[61]
Hepatocytes	Beta cells	Exendin-1, PDX1	[62]
Astrocytes	Neurons	PAX6, Neurogenin2, ASCL2	[63]
Fibroblasts	Multiple (see figure I-4)	Multiple (see figure I-4)	[36–55]

(2) Transdifferentiation in physiological conditions

In physiological conditions, transdifferentiation also takes place in the context of tissue repair. Instead of de-differentiating to a common progenitor that cycles and proliferates in order to then re-differentiate and regenerate the tissue (process coined as epimorphosis), transdifferentiating cells are directly converted into the different mature cells that are lost during tissue damage, without involving cell proliferation (process coined as morphyllaxis) [64]. The best examples of physiological transdifferentiation are the pancreas, the liver and the thymus. Upon pancreatic damage and loss of insulin-producing β-cells, glucagon-producing α-cells can directly transdifferentiate into β-cells without previously de-differentiating into a common progenitor [65]. On the other hand, liver hepatocytes can directly transdifferentiate into biliary epithelial cells in response of tissue damage by overexpressing NOTCH family of proteins [66]. Finally, in the thymus, it has been found that early lymphoid T-cell progenitors can naturally transdifferentiate into myeloid monocytic/granulocytic cells [67].

(3) Transdifferentiation in cancer

The most common pathological scenario in which transdifferentiation can be involved is cancer. The process known as metaplasia, defined as the changes in a tissue involving the replacement of one cell type into another, is a common feature that manifests upon tissue damage and usually involves cellular transdifferentiation [64]. The most well-known scenario is Barret's oesophagus, in which stratified squamous epithelial cells in the oesophagus transdifferentiate into intestinal-like columnar epithelial cells as an adaptation to chronic acid exposure and inflammation from reflux esophagitis [68]. This transdifferentiation event is considered to be a premalignant condition, acting as a cancer initiating event associated with high-risk oesophageal adenocarcinoma. There are many other metaplastic transdifferentiation events associated with an increased risk of cancer, all of them summarized in table I-2.

Table I-2. Examples of metaplastic transdifferentiation in human cancer.

Cancer type	Tissue	Metaplastic cells	Ref.
Intrahepatic cholangiocarcinoma	Liver	Hepatocytes to biliary cells	[69, 70]
Pancreatic ductal adenocarcinoma	Pancreas	Exocrine cells to ductal cells	[71, 72]
Barret metaplasia and oesophageal adenocarcinoma	Oesophagous	Oesophageal cells to intestinal-like cells	[68]
Bladder squamous cell carcinoma	Bladder	Transitional epithelium to squamous cells	[73]
Intestinal metaplasia and gastric cancer	Stomach	Gastric squamous cells to intestinal cells	[74]
Cervical cancer	Cervix	Metaplasia to squamous cells	[75]
Non-small-cell lung cancer	Lung	Metaplasia to squamous cells	[76]

On the other hand, epithelial-to-mesenchymal transition (EMT) is a well-known metastasis-initiating event, featuring in many types of solid cancers. This process is characterized by the conversion of a cancer cell with epithelial phenotype into a mesenchymal type of cell, manifesting a significant higher mobility that allows it to migrate into the bloodstream and to invade distant tissues. Once homed in the new tissue, the mesenchymal cell will perform a mesenchymal-to-epithelial transition (MET) to return to its former phenotype and adapt to this new distant niche. Both EMT and MET are transdifferentiation processes, fostered by a combination of genetic and epigenetic events modulated by microenvironmental signals found in both the primary and the secondary cancer sites [77, 78].

Nonetheless, what is considered nowadays as the “gold standard” of cancer-related trans-differentiation events is the direct conversion of androgen receptor positive (AR+) prostatic cancer cells into neuroendocrine-like AR- cancer cells upon androgen inhibition therapy [79]. Thus, transdifferentiation acts in this case as a drug-resistance mechanism. These new neu-roendocrine-like cancer cells stop expressing androgen receptors and they do not require their signaling to keep proliferating as in classic prostatic cancer cells. The combination of genetic mutations in key tumor-suppressors (RB1, TP53 and PTEN) and microenvironmen-tal fluctuations induced by the treatment allow a reconfiguration in the epigenome of prostate cancer cells, forcing their transdifferentiation into resistant cells. Consequently, these new transdifferentiated cells eventually lead to the development of castration-resistant prostate cancer (CRPC), a very high-risk metastatic and incurable disease.

Although all this evidence clearly demonstrates that cellular transdifferentiation can play a significant role in cancer at many different levels (as a cancer initiating event, as a pro-metastatic process, or even as a mechanism of therapy resistance), this process is not as extensively studied as other topics in the cancer literature. This is probably due to the difficulty to detect clinical cases in which transdifferentiation has occurred, since there are no intermediates detected and thus, an undetermined number of different types of cancer that are considered as independent entities might be generated from a previously undetected transdifferentiation process [80].

Since our research laboratory focuses on epigenetic changes that occur in hematological malignancies, we asked ourselves if transdifferentiation may act as a key process in the development or evolution of some types of leukemia/lymphoma.

Cellular transdifferentiation in hematological malignancies

In order to find as much published literature as possible relating transdifferentiation with cancer (especially with hematological malignancies), we performed extensive bibliographic research in PubMed by exclusively using the keyword “transdifferentiation”. The bibliographic research flow chart can be seen in figure I-5.

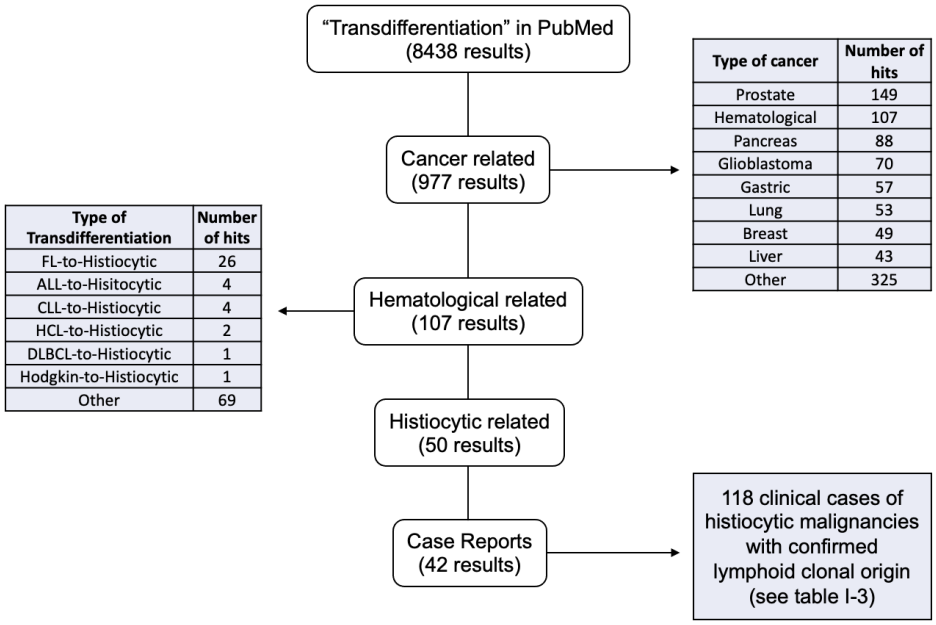

Type of cancer	Number of hits
Prostate	149
Hematological	107
Pancreas	88
Glioblastoma	70
Gastric	57
Lung	53
Breast	49
Liver	43
Other	325

Type of Transdifferentiation	Number of hits
FL-to-Histiocytic	26
ALL-to-Hisitocytic	4
CLL-to-Histiocytic	4
HCL-to-Histiocytic	2
DLBCL-to-Histiocytic	1
Hodgkin-to-Histiocytic	1
Other	69

Figure I-5. Flow chart representing the PubMed search strategy for transdifferentiation clinical reports on B-cell-to-macrophage transdifferentiation (as of July 28th 2022).

There are only 8438 scientific articles (including research articles, reviews, short letters, and case reports) that address, to a greater or lesser extent, the concept of transdifferentiation. This small number of articles indicates how little explored is this concept in the literature. Next, we selected those articles that are related with any type of cancer, finding up to 977 articles that explore transdifferentiation in some type of malignancy. As expected, most of these articles (149) are related with prostate cancer cells transdifferentiating into therapy-resistant neuroendocrine-like cells, which is the “gold standard” transdifferentiation event occurring in cancer, as we described in the previous section. But the second most studied malignancy in relation to cellular transdifferentiation are hematological malignancies (107 articles). The most recurrent transdifferentiation event found in these hematological malignancies-related articles is the conversion of a B-cell lymphoid malignancy into a histiocytic-derived cancer. “Histiocyte” is a morphological term referring to tissue-resident macrophages and dendritic cells, both myeloid cells that are part of the mononuclear phagocytic system [81]. These articles state that these B-cell-derived leukemias and lymphomas (lymphoid malignancies), whether they are derived from progenitor/early development B-cells (B-ALL) or mature/late B-cells (FL, CLL/SLL, DLBCL, HCL and others), they can transdifferentiate into cancerous sarcomatoid macrophages after the initial treatment, as a therapy-resistance strategy, leading to the development of histiocytic sarcoma (HS) and other types of histiocytic-derived myeloid malignancies. This malignant transdifferentiation event is rare (e.g., histiocytic sarcoma presents an incidence of 0.17/million individuals worldwide, in which 25% are confirmed cases of transdifferentiation with a history of a pre-existing lymphoproliferative disorder), but the mortality rate in patients suffering these types of malignancies is close to 100% [82]. Thus, we focused solely on articles describing this malignant lymphoid-cell-to-macrophage transdifferentiation, finding only 50 articles, 42 of which were clinical case reports describing this cell conversion in different types of early/late lymphoid malignancies, which transdifferentiate into macrophages sometime after the initial therapy.

In table I-3, we classified these transdifferentiation cases depending on the pre-existing lymphoid malignancy. Nevertheless, it is very possible that many more reported cases of B-cell-to-histiocyte malignant transdifferentiation remain undisclosed due to the bibliographic search strategy, but also due to the fact that many cases of malignant transdifferentiation are incorrectly catalogued as pure/sporadic cases of histiocytic malignancies.

Table I-3. Clinical cases (n = 118) of lymphoid-cell-to-histiocyte malignant transdifferentiation found in the bibliographic PubMed search depicted in figure I-5. References for each clinical case are annexed in table A-3 (page 157).

Lymphoid malignancy of origin		Transdifferentiated histiocytic malignancy							
		HS	**LCS**	**IDCT**	**IDCS**	**LCH**	**XTG**	**AHL**	**Total**
Precursor (early) lymphoid neoplasms	**B-ALL**	6	1	4	0	0	3	0	**14**
	T-ALL	8	1	5	0	1	0	0	**15**
Mature (late) lymphoid neoplasms	**FL**	22	4	0	1	1	0	1	**29**
	CLL/SLL	6	2	1	6	1	0	0	**16**
	DLBCL	4	0	0	0	0	0	0	**4**
	MZL	3	1	0	0	0	0	0	**4**
	MCL	1	0	0	0	0	0	0	**1**
	HCL	0	1	0	0	0	0	0	**1**
	AITL	0	0	0	1	0	0	0	**1**
	HL	0	0	0	0	1	0	0	**1**
Ig/TCR rearrangements without detected lymphoid pre-malignancies	**Rearranged IGH**	11	0	0	1	4	0	0	**16**
	Rearranged IGK	2	0	0	0	5	0	0	**7**
	Rearranged TCRγ	0	0	0	0	9	0	0	**9**

Abbreviations: B-ALL: B-cell Acute Lymphoblastic Leukemia; T-ALL: T-cell Acute Lymphoblastic Leukemia; FL: Follicular Lymphoma; CLL/SLL: Chronic Lymphocytic Leukemia/Small Lymphocytic Leukemia; DLBCL: Diffuse Large B-Cell Lymphoma; MZL: Marginal Zone Lymphoma; MCL: Mantle Cell Lymphoma; HCL: Hairy Cell Leukemia; AITL: Angioimmunoblastic T-cell Lymphoma; HL: Hodgkin Lymphoma; HS: Histiocytic Sarcoma; LCS: Langerhans Cell Sarcoma; IDCT: Indetermined Dendritic Cell Tumor; IDCS: Interdigitating Dendritic Cell Sarcoma; LCH: Langerhans Cell Histiocytosis; XTG: Xanthogranuloma; AHL: Acute Histiocytic Leukemia.

We can observe that the most common B-cell malignancies that transdifferentiate into a histiocytic cancer are follicular lymphoma (FL) and B-cell acute lymphoblastic leukemia (B-ALL), which mostly transdifferentiate into a poor-prognosis histiocytic sarcoma (HS), as a mechanism of therapy resistance after the initial treatment. Nevertheless, there are other significant cases of malignant transdifferentiation involving other B-cell malignancies. For example, an interesting case of therapy-resistant B-cell-to-macrophage transdifferentiation is reported by Qiang Zhang et al [83], describing a mantle cell lymphoma (MCL) patient that evolved into a clonal-related histiocytic sarcoma (HS) after immunotherapy with autologous chimeric-antigen receptor T-cells targeting CD19 (CAR-T-19). Another interesting clinical report written by Bryan Steussy et al [84], describes the case of a 52-year-old woman with stage IV follicular lymphoma (FL, a late/mature B-cell-derived lymphoid malignancy) who

was treated with bendamuxine and rituximab. After treatment, computed tomography scans revealed no evidence of this disease. Unfortunately, after 2 years of apparent remission, she returned to the clinic with the typical symptoms found in acute leukemia patients. Bone marrow biopsy revealed 100% cellular marrow entirely replaced by tumoral cells with histiocytic features and, strikingly, with the same IgH and light-chain immunoglobulin rearrangements as the ones found in the B-cells originated from the previous follicular lymphoma.

Since macrophages do not rearrange their immunoglobulin chain genes (only B-cells do, remember the “B-cell development” chapter), the detection of Ig rearrangements (or TCR rearrangements in T-cell-to-histiocyte transdifferentiation cases) clearly indicate a clonal relationship between the previous lymphoid malignancy and the new myeloid cancer, suggesting the occurrence of B-cell-to-macrophage transdifferentiation as a therapy-resistance mechanism [80]. Thus, the detection of clonally-related heavy (H) and light (K) chain immunoglobulin rearrangements is a common hallmark of B-cell-to-histiocyte transdifferentiation.

***

After carefully observing these data, a very important question arises: Why is this malignant B-cell-to-macrophage conversion considered a transdifferentiation event? Is it not possible that we are looking instead at a de-differentiation event, generating common progenitors that later re-differentiate into malignant histiocytes? Indeed, from the clinical perspective and outside the controlled settings found in a laboratory, it is very difficult to distinguish transdifferentiation from an alternative de-differentiation/re-differentiation process or even from the differentiation of a very immature cancer stem cell (CSC) with both lymphoid and myeloid differentiation potentials (see figure I-6) [80]. To answer this question, clinicians usually use 2 standard criteria to determine if these cases are real transdifferentiation events: (1) the absence of detectable common neoplastic progenitor cells indicate that probably there is no de-differentiation event, since some form of maturation arrest in the secondary neoplasm would be detectable; (2) on the other hand, if the lineage conversion is explained by a common immature progenitor (like a CSC with both lymphoid and myeloid differentiation potential), the new neoplasm should retain a genealogically-linked genotypic signature similar to the immature progenitor (e.g. without heavy/light chain immunoglobulin rearrangements)

and different from the original neoplasm. In all the clinical cases previously documented, there are no detectable common neoplastic progenitors (criterion 1) and every new neoplastic cell shares the same exact heavy/light chain immunoglobulin rearrangements as in the original neoplasm (criterion 2), thus indicating that transdifferentiation was truly the event that drove this B-cell-to-macrophage lineage conversion [80, 85, 86].

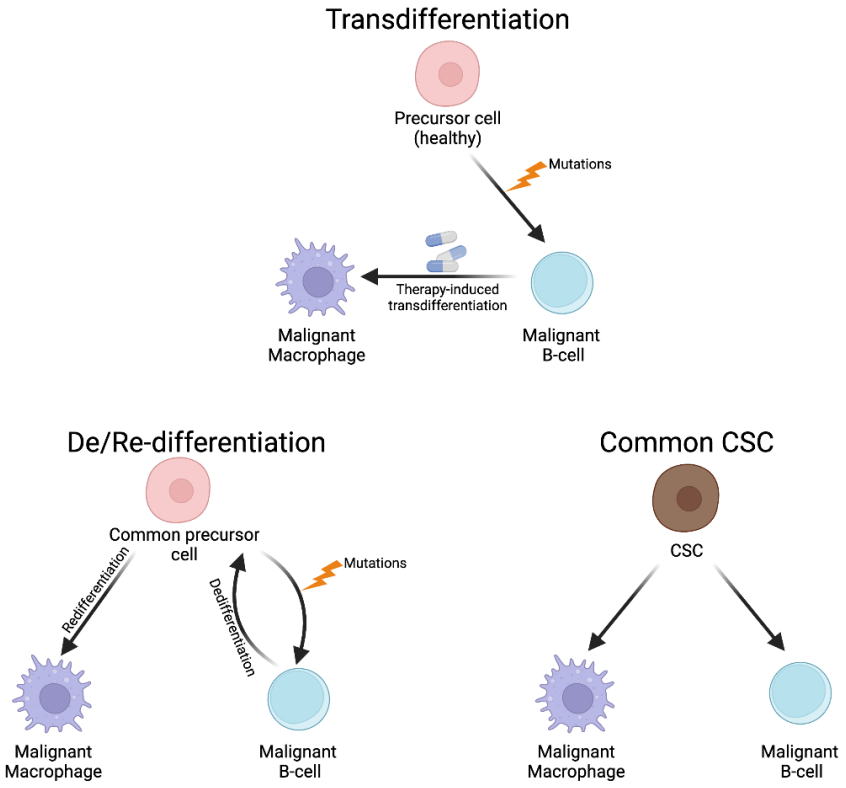

Figure I-6. The three possible scenarios of lineage switch during malignant course. **Abbreviations**: CSC: Cancer Stem Cell.

At the molecular level, cases of B-cell-to-macrophage transdifferentiation are characterized by a downregulation in the expression of PAX5 (crucial B-cell lineage-commitment transcription factor, remember “B-cell development” chapter) and the upregulation in PU.1 (common lymphoid/myeloid transcription factor) and C/EBPα or C/EBPβ (key macrophage lineage-commitment transcription factors, remember “Macrophage development” chapter) [87–91]. As a matter of fact, C/EBPα will play a central role in the present doctoral thesis, as a key

regulator of B-cell-to-macrophage *in vitro* transdifferentiation. But that information will be explained in the final chapter of the *Introduction*.

*
**

In short, to allow transdifferentiation to occur, the cell requires a combination of multiple factors (genetic alterations, expression of pioneer transcription factors like C/EBPα, and microenvironmental inputs) that, at the end, will have an impact on its epigenetic background, reshaping its epigenome to a similar configuration found in the cells from the new lineage. That is why transdifferentiation is considered, at the utmost fundamental level, an epigenetic-driven event [80, 92]. Consequently, our laboratory became very interested in studying the epigenetic basis of B-cell-to-macrophage transdifferentiation, specifically how the epigenome changes in the early phases of this process. But before addressing this matter, we need to explain the fundamental concepts of epigenetics and its newest addition in the field: epitranscriptomics.

Epigenetics: the fundamentals

The term “epigenetics” (“epi-“ meaning “above” or “on top of” in ancient Greek) was first coined in 1942 by the biologist Conrad Hal Waddington in his article entitled “*The epigenotype*” [93]. He defined epigenetics (or epigenotype) as the changes in the phenotype that occur without changes in the genotype, after investigating the development of the wings in *Drosophila melanogaster*. Eighty years later, our definition has been reshaped to our far better understanding of cellular biology. We now define epigenetics as the cellular mechanisms that modulate gene expression without altering the underlying DNA sequence [94].

Epigenetic mechanisms can be classified in 5 groups: (1) DNA methylation, (2) Histone modifications, (3) chromatin accessibility and histone deposition, (4) chromatin tridimensional architecture, and (5) non-coding RNA-mediated interference. We will summarize these epigenetic mechanisms in the next pages.

(1) DNA methylation

DNA can be chemically modified by the addition of a methyl group (-CH_3) in the 5th carbon of the cytosines (C) that are followed by a guanine (G, forming a 5'-to-3' CpG pair), generating 5-methylcytosine (5mC, see figure I-7A/B) [94, 95]. The generation of 5mC is mediated by DNA methyltransferases. These methyltransferases are classified in two distinct groups: (1) maintenance DNA methyltransferase (DNMT1), which is the responsible of copying the same methylation pattern from the parental DNA strand into the nascent DNA strand during DNA replication, ensuring the transmission of the epigenetic methylation marks to the progeny cells; and (2) *de novo* DNA methylatransferases (DNMT3A and DNMT3B), which mediate the addition of 5mC in previously unmethylated positions [96]. Conversely, DNA methylation can be dynamically removed by the action of the TET family of DNA dioxygenases (TET1, TET2 and TET3), which catalyze the hydroxymethylation of 5mC into 5-hydroxymethylcytosine (5hmC), which will spontaneously convert into 5-formylcytosine (5fC) and then into 5-carboxylcytosine (5caC), until the cytosine is completely demethylated [97]. The role of DNA methylation highly depends on the relative gene position in which the 5mC modification is deposited (figure I-7C).

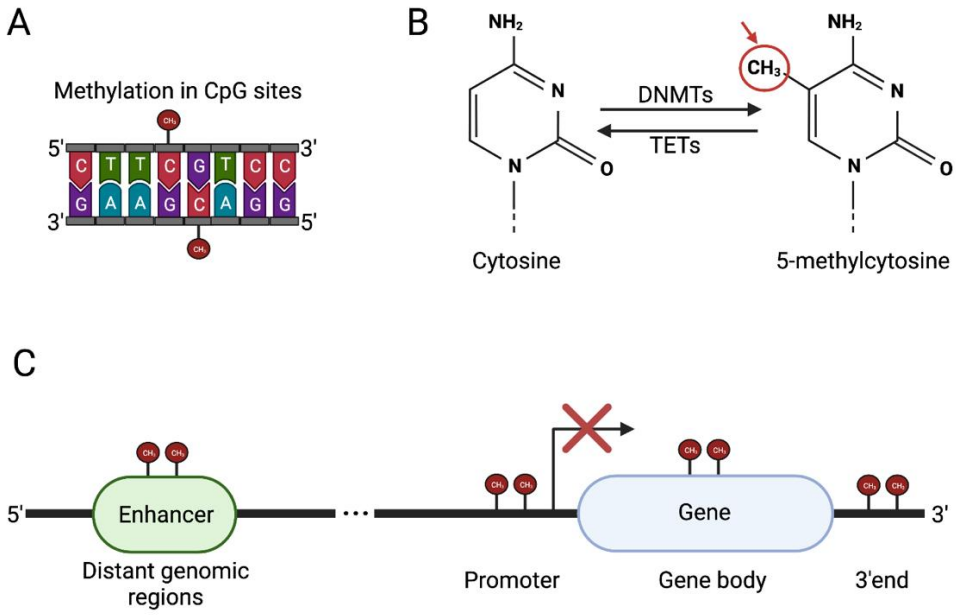

Figure I-7. DNA 5mC methylation. (A) Methylation mostly 0occurs at genomic CpG sites. (B) Molecular structure of cytosine and 5-methylcytosine. (C) Genomic regions susceptible to methylation.

- **Gene promoter methylation:** When 5mC is deposited in the promoter region (approximately 1-to-1500 base pairs upstream to the transcription start site down to the 5'UTR of the gene), DNA methylation negatively correlates with the expression of the methylated gene (the more methylated is the gene promoter, the less will be expressed). This negative correlation is found in 70.5% of all the human genes [95, 98]. Nevertheless, there is still a 29.5% of the human genome that does show a positive correlation, or no correlation at all. The negative correlation is enriched in genes with CpG islands in their promoters. CpG islands are clusters of multiple CpGs (usually spanning 1000 base pairs long) that are very susceptible of methylation. 70% of all the human genes harbor CpG islands in their promoter regions and hypermethylated promoter CpG islands are associated with gene repression [99]. DNA methylation readers, such as MeCP2, are recruited to hypermethylated gene promoters, which deacetylate nearby histones, further decreasing gene expression by fostering gene compaction and ensuring the heritability of this gene silencing to the cell progeny after cellular division.
- **Gene body methylation:** The body of a gene spans from the 1st exon up to its 3' end. Contrary to promoter methylation, gene body methylation does not show a clear negative nor positive correlation with gene expression [99]. Nevertheless, gene body methylation is evolutionary well conserved, so its function is still under research. Some gene bodies harbor *cis* regulatory regions (e.g. enhancers and silencers) that regulate other distant genes by establishing tridimensional DNA contacts [100]. Methylation in these regions may have an important impact in the expression of those distant genes.
- **3' downstream methylation:** Downstream the transcription ending site, DNA is also methylated. Nevertheless, as also seen in gene body regions, the function of 3' methylation is not well understood [98].
- **Distant regulatory region methylation:** Finally, distant genomic regions that are >10kb apart from any gene may harbor distant *cis* regulatory elements (enhancers and silencers) that can interact with or insulate other distant genes by interacting with specific transcription factors that will tridimensionally reconfigure the chromatin, bringing physically together genomic regions that are hundreds of kilobases apart, which will have an impact in gene expression [101]. DNA methylation in these regions is not well-understood, although some transcription factors that bind to these regions (e.g. CTCF) are sensible to DNA methylation, affecting their function [102, 103].

(2) Histone modifications

Histones are a family of proteins (H1, H2A, H2B, H3 and H4) responsible for the packaging of the DNA (a 2-meter-long molecule) inside the cell nucleus. Histones are positively charged proteins that form octameric complexes (two H2A, two H2B, two H3 and two H4) which strongly interact with the negatively charged DNA, forming 147 base pair DNA-histone interactions that are stabilized by histone H1 (figure I-8) [104, 105]. This DNA-protein complex is known as nucleosome, which is defined as the basic unit of the chromatin. Depending on the nucleosome density found in a genomic region, we can find heterochromatin regions (densely pack with nucleosomes, associated with gene repression) and euchromatin regions (low density regions, associated with active gene expression).

Histones are susceptible of being chemically modified, especially at their histone tails that protrude from the octameric complex. At least 28 different types of histone modifications have been discovered, each one having its own distinct function [104]. It is not in the scope of this thesis to define every one of these modifications. Instead, we will briefly describe the 2 most well characterized histone modifications, which are methylation and acetylation.

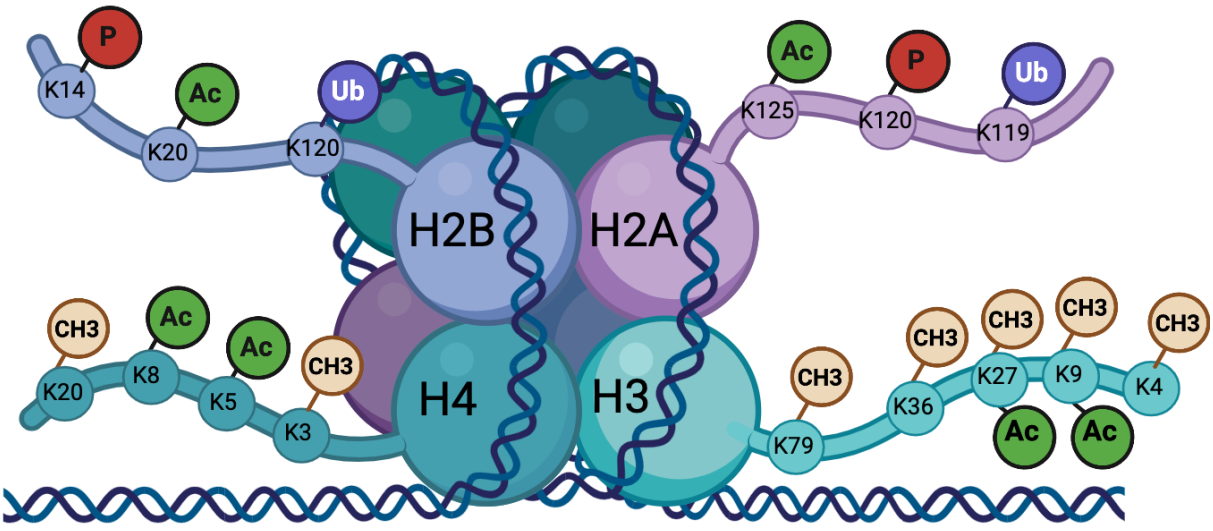

Figure I-8. Some of the most commonly studied histone modifications found in humans.

- **Histone methylation:** Histones H3 and H4 can be enzymatically methylated (by histone methyltransferases: HMTs) at different lysines (K) found in their histone tails. These lysines can be mono-, di- or tri-methylated, having completely different effects in gene expression [104, 106, 107]. For example, H3K27 mono-methylation (H3K27me1) in promoter and distant enhancer regions is associated with gene activation, but H3K27me3 is associated with gene repression, while H3K27me2 represents “poised” genes and enhancers (ready to be activated). On the other hand, H3K9me3 is mostly found in silenced heterochromatic regions, while H3K4me3 and H3K4me1 are enriched in activated genes and enhancers, respectively.

- **Histone acetylation**: Histones H3 and H4 can also be acetylated (by histone acetylases: HATs) or deacetylated (by histones deacetylases: HDACs). Acetylation reduces the positive charge of the histones, allowing the DNA to loosen and thus this modification is usually considered as gene activation mark [108]. H3K27ac is the most common histone acetylation and is found in active gene promoters and enhancers.

(3) Chromatin accessibility and histone deposition

As previously mentioned, the nucleosomal density found in a particular chromatin region will have a local impact in gene expression. Genes inside dense heterochromatic regions will be silenced, while genes in euchromatic remain more accessible to transcription factors and thus more active. Nucleosomal density is highly dynamic, since chromatin structures are being constantly remodeled in response to multiple intrinsic and external inputs. Chromatin remodeling is conducted by ATP-dependent chromatin remodeling complexes that hydrolyze ATP to foster or disrupt DNA-histone interactions, locally packing/unpacking a chromatin region and silencing/activating gene expression (figure I-9) [109]. There are 4 families of chromatin remodeling complexes: SWI/SNF, ISWI, CHD, and INO80. In addition to this mechanism, canonical histones can be replaced by special histone variants like H2A.Z (deposited in the +1 position of transcription start sites, fostering gene expression), H3.3 (found in active gene promoters and enhancers) and H2A.X (deposited in DNA damaged regions during DNA repair), among many other variants, also participating in chromatin remodeling (figure I-9) [110, 111].

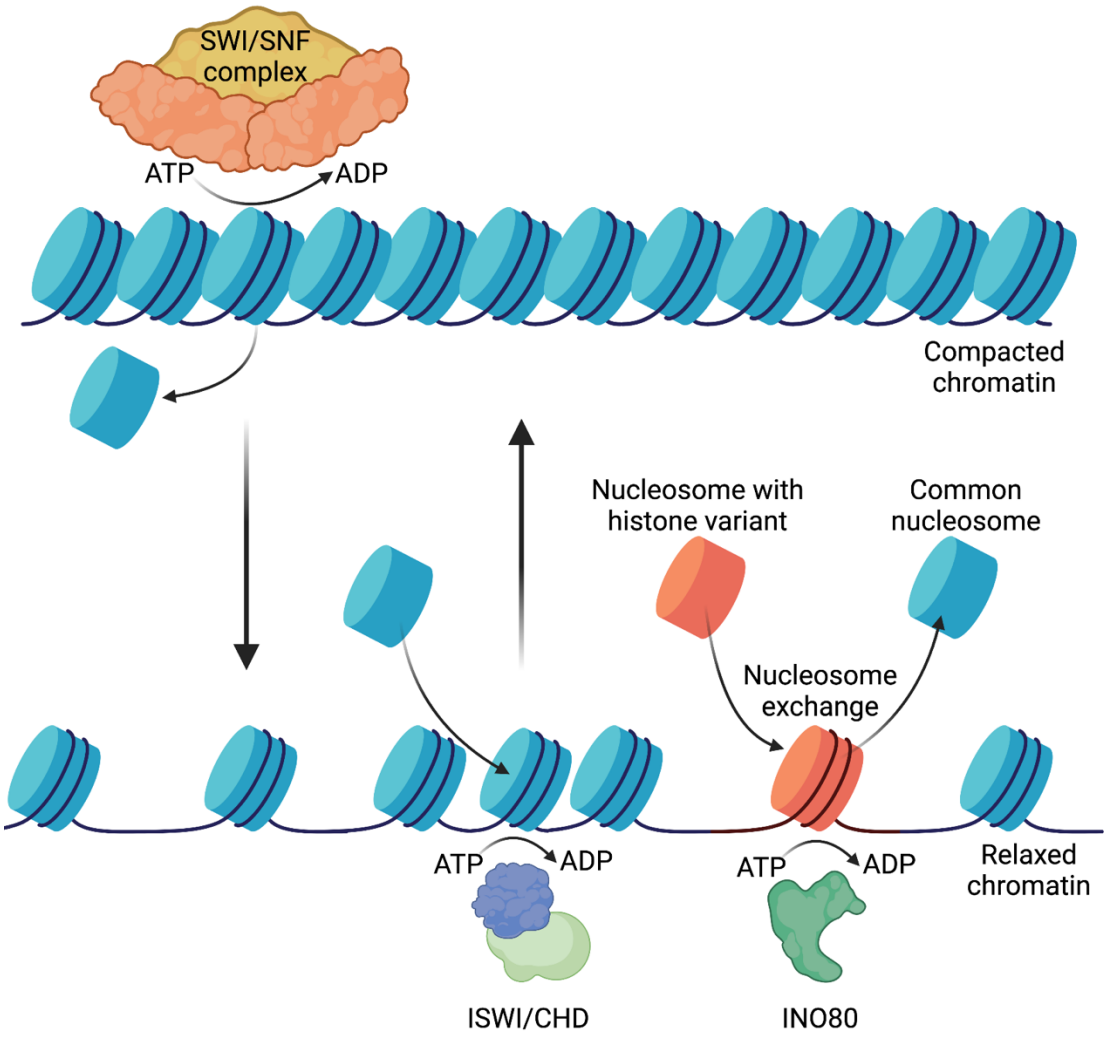

Figure I-9. Chromatin remodeling by ATP-dependent remodeling complexes.

(4) Chromatin tridimensional architecture

DNA is not randomly packed inside the nucleus. Instead, it follows a very well-defined architecture, organized in highly structured domains. Each chromosome occupies a certain predefined territory inside the nucleus, with minimal interactions in between territories. Inside each chromosome territory, chromatin can be subdivided in 2 major compartments: (1) the "Compartment A" (chromatin clustered near nuclear speckles, enriched with transcriptionally active regions); and (2) the "Compartment B" (chromatin usually associated with nuclear lamina, enriched with silenced genes) [112–114]. Compartment B is enriched with lamin-

associated domains (LADs) that harbor silenced or low-expressed genes. These LADs are rich in repressive histone modifications (H3K9me3, a key heterochromatin mark) and are usually bound to the internal nuclear envelope by interacting with inner nuclear membrane (INM) proteins [113]. On the other hand, inside the Compartment A, there is an enrichment in topologically associated domains (TADs), which are self-interacting looped regions containing a variable number of co-regulated genes with similar expression patterns, insulated from other TADs by the action of CTCF (a crucial TAD insulator) [112]. Inside each TAD, cohesin complexes form tridimensional chromatin loops that physically connect genes and other distant regulatory regions (e.g., enhancers or silencers), allowing a fine-tuned control in gene expression. TAD and LAD architecture significantly varies depending on the cellular type and on the intrinsic and extrinsic signals that affect the cell in real time. Figure I-10 summarizes this hierarchical chromatin architecture.

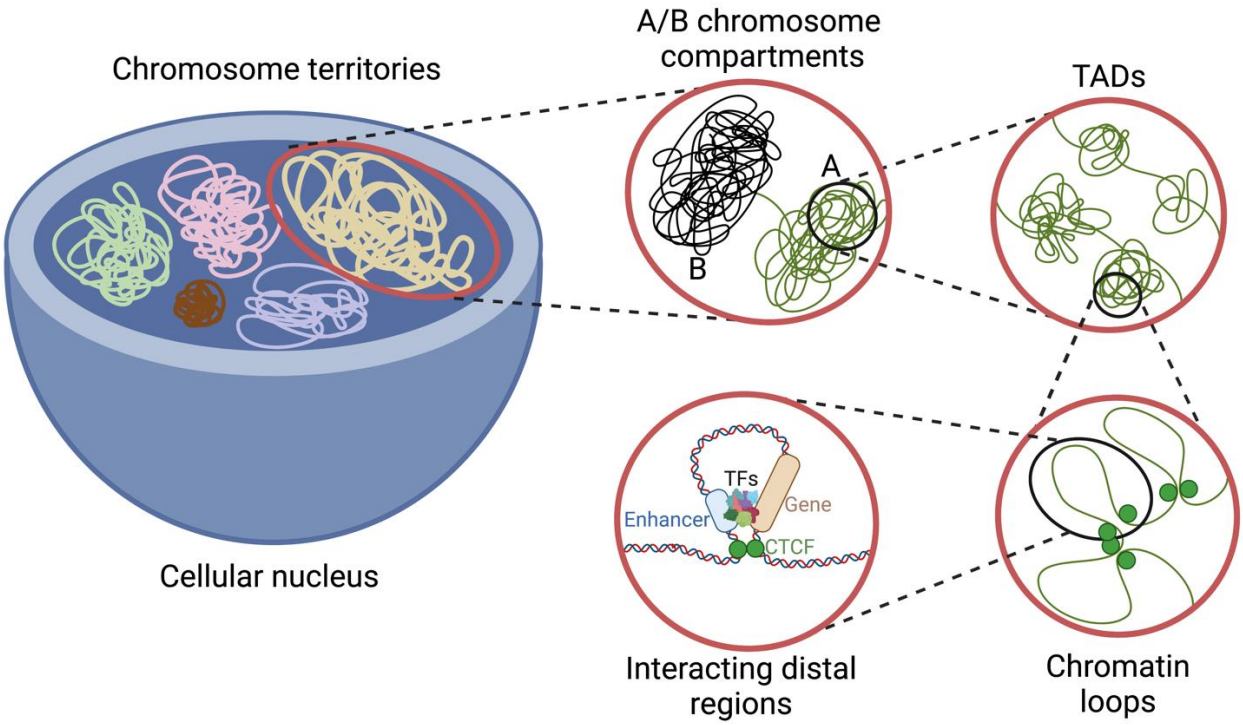

Figure I-10. Hierarchical tridimensional chromatin interactions in the cellular nucleus. **Abbreviations:** TADs: Topological Associated Domains; TFs: Transcription factors.

(5) Non-coding RNA-mediated interference

RNA molecules can be divided in 2 great groups: (1) coding RNA (cRNA), also known as messenger RNA (mRNA), which are recognized by the ribosomes to be translated into proteins; and (2) non-coding RNA (ncRNA), which are not translated into proteins but perform crucial functions for the cell [115]. The ncRNAs can be further divided in 2 groups: (1) housekeeping ncRNAs, which play fundamental roles in the cell, like transfer RNA (tRNA) and ribosomal RNA (rRNA) in protein translation, among others; and (2) regulatory ncRNAs. Depending on their size (figure I-11A), regulatory ncRNAs can be divided in short-chain (19-24 nucleotides long) regulatory ncRNAs (miRNAs, siRNAs and piRNAs) and long non-coding RNAs (lncRNAs). miRNAs (micro RNAs), which are the most well-known short-chain regulatory ncRNAs, complementary bind to specific endogenous mRNAs, inhibiting its translation by blocking ribosome assembly and inducing its degradation by recruiting the RISC protein complex (figure I-11B) [115, 116]. On the other hand, the regulatory mechanisms of lncRNAs are less understood (figure I-11C); some of them (e.g. H19 lncRNA) can interact with mRNAs and degrade them through a siRNA-like mechanism, while other lncRNAs act as miRNA sponges (blocking their action against mRNA) or even interacting directly with the chromatin, silencing gene expression (e.g. *Xist* lncRNA during X chromosome inactivation) [115, 117]. Both types of regulatory ncRNAs modulate gene expression, quickly fine-tuning the expression in response to intrinsic and extrinsic cues.

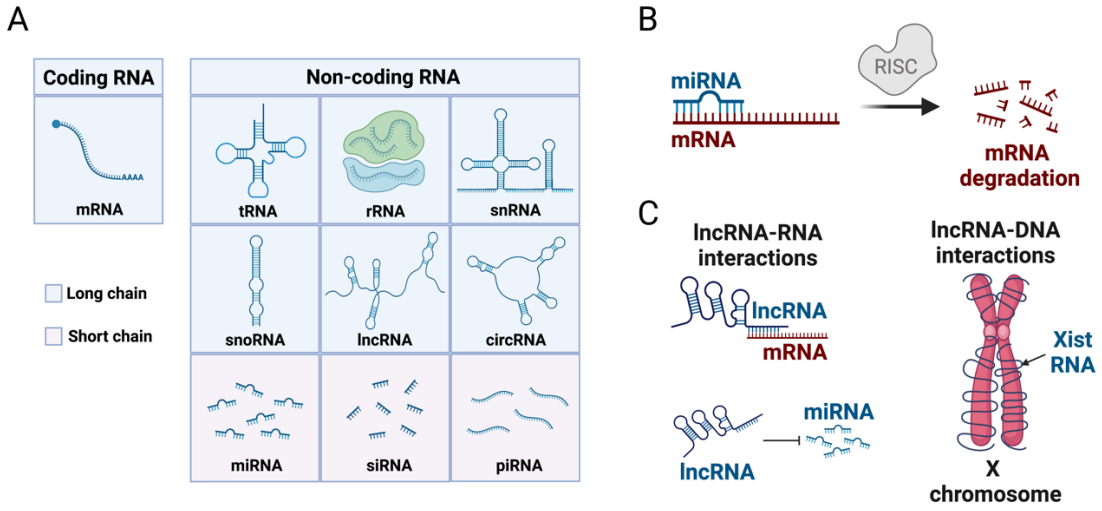

Figure I-11. (A) Types of coding and non-coding RNA. (B) Mechanism of action of miRNA-mediated mRNA degradation. (C) Various mechanisms of interaction between lncRNA and RNA/DNA.

⁂

Every one of these epigenetic mechanisms are in continuous crosstalk, allowing a cell to quickly adapt to every kind of internal and external input. Cellular differentiation requires precise and coordinated adjustments in the epigenetic machinery across all the different stages of cell specialization. This also true for cellular transdifferentiation, but the implications of these changes and how do they work in a malignant transdifferentiation context are practically unknown. Almost no experimental research has been conducted to understand the epigenetic changes that occur during transdifferentiation, not to mention in the context of malignant B-cell-to-macrophage transdifferentiation. For that reason, in our first thesis project we decided to focus on the DNA 5mC methylation changes that occur during the early stages of a human *in* vitro B-cell-to-macrophage transdifferentiation model.

Nevertheless, before starting with the results, we still need to introduce one last concept that will be the focus of our second thesis project: In addition to the changes in DNA methylation, we investigated how RNA methylation is altered during B-cell-to-macrophage transdifferentiation. RNA methylation is part of a vast collection of RNA chemical modifications that together constitute the central goal of one of the newest fields in biology: epitranscriptomics.

Epitranscriptomics: fundamentals and molecular functions of m6A

Epitranscriptomics is the field of biology that studies the RNA chemical modifications found in a cell. The epitranscriptome comprises more than 170 different types of RNA modifications, each having its own unique function (figure I-12) [118]. RNA modifications have been found in almost every type of coding and non-coding RNA. The first epitranscriptomic modification ever discovered was pseudouridine (Ψ), in 1951, which is the most abundant modification found in tRNA and rRNA, having a role in RNA folding, stability and translation [119, 120]. Another well-known epitranscriptomic modification is inosine (I), product of the deamination of adenosines (process known as A-to-I editing), changing the encoded information in mRNAs (I is recognized as a C, instead of as an A) and altering the secondary structure of several ncRNAs [121, 122]. Unfortunately, it is out of our scope to describe every different RNA modification. Instead, we are going to focus only in the one we are studying in our second thesis project: N6-methyladenosine.

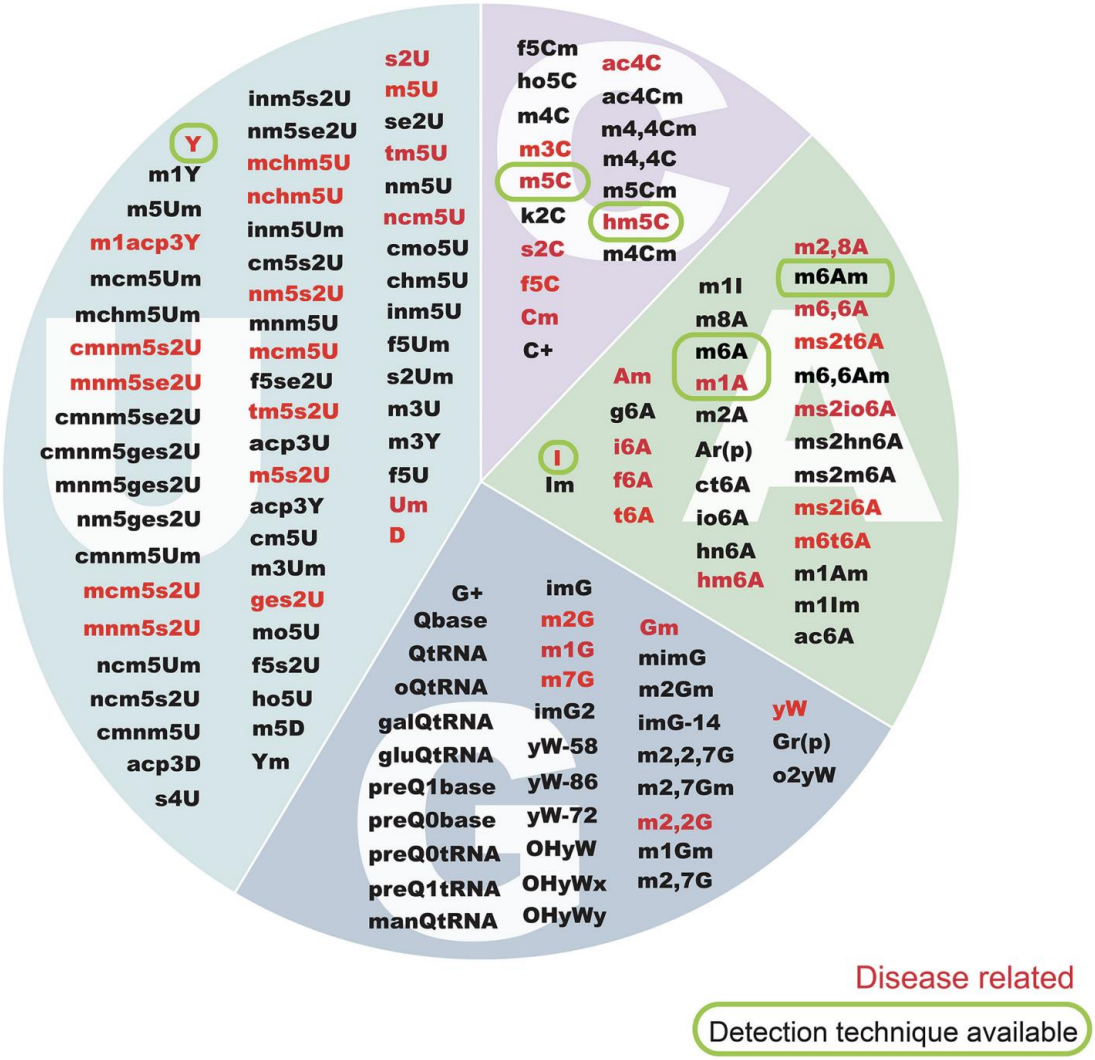

Figure I-12. RNA epitranscriptomic modifications (>100). Figure retrieved from the article "*The RNA modification landscape in human disease*", from Nicky Jonkhout et al (*RNA*, 2017) [118].

N6-methyladenosine (m^6A) is the most abundant mRNA modification found in humans. Although it was discovered in 1974 [123], it was not until the development of next generation sequencing-based m6A detection technologies, like m^6A-seq (also known as MeRIP-seq), that this RNA modification became the main focus of attention [124–126]. Although it is mostly deposited in mRNA, m6A can also be found in tRNA, rRNA, snRNA, miRNA, lncRNA and circRNA. m6A is a highly dynamic RNA modification due to the coordinated action of proteins that deposit ("writers"), eliminate ("erasers") and interpret ("readers") this modification (figure I-13) [127–129].

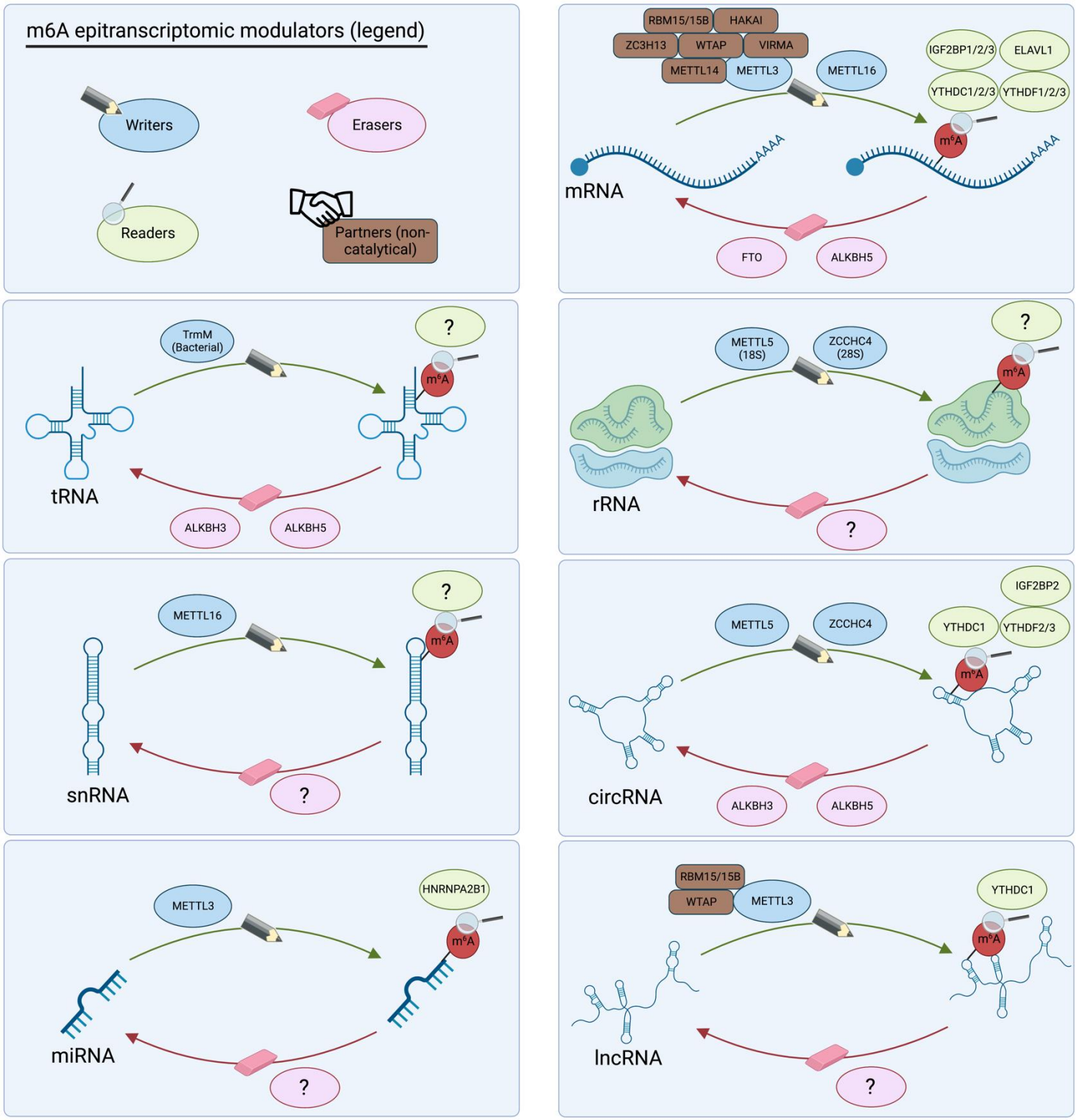

Figure I-13. Writers, readers, erasers and non-catalytical protein partners that modulate the m6A epi-transcriptome in various types of human RNA.

The enzyme METTL3, together with its non-catalytical partners METTL14 and WTAP, form the WMM complex (WTAP-METTL3-METTL14), which is the main m6A writer complex that modifies human mRNAs [127–129]. The WMM complex can also interact with additional non-catalytical proteins (RBM15, RBM15B, VIRMA, HAKAI, and ZC3H13) depending on the targeted RNAs. METTL5, ZCCHC4, METTL4 and METTL16 are other m6A catalytical writers, methylating 18S rRNA, 28S rRNA, miRNAs and U6 spliceosomal small nuclear RNA (snRNA), respectively. On the other hand, FTO and ALKBH15 are two dioxygenase enzymes that catalyze the removal of m6A and constitute the two only known erasers of this RNA modification. Finally, there are a variety of proteins that recognize and bind to m6A in order to promote different molecular functions, such as mRNA splicing (YTHDC1, HNRNPG and HNRNPC), mRNA nuclear translocation (YTHDC1), mRNA stability (YHTDF1/2/3 and IGF2BP1/2/3) and mRNA translation (YTHDF1/3 and YTHDC2). m6A-seq analysis have confirmed that m6A in mRNA is enriched in 5'-RRACH-3' motif sequences (R = G/A, H = A/U/C), although a significant fraction of m6A peaks can be detected outside this consensus motif (non-canonical m6A sites), hinting that there are other *cis*-independent drivers of m6A deposition that remain undisclosed [125]. Approximately there are 1-to-3 m6A residues per molecule of mature mRNA (or ~1 m6A residue per 2000 nucleotides), although additional m6A residues that are deposited co-transcriptionally in intronic regions may remain undetected due to the elimination of introns after splicing [125].

m6A deposition in mRNA occur co-transcriptionally inside the nucleus, specifically within nuclear speckles, in which active mRNA transcription and splicing takes place [130, 131]. The WMM complex inside the nucleus interacts with the transcriptional machinery, modifying different regions of nascent mRNAs. Approximately 70% of the mRNA-deposited m6A is located in the 3'UTR region and near the STOP codon [125, 132]. Other regions in which m6A can be found are exons, introns and, less frequently, in 5'UTR. Depending on the relative location of an m6A residue in an mRNA molecule and its interaction with the different m6A readers, this epitranscriptomic modification can exert different functions, many of which remain unclear to this day (figure I-14):

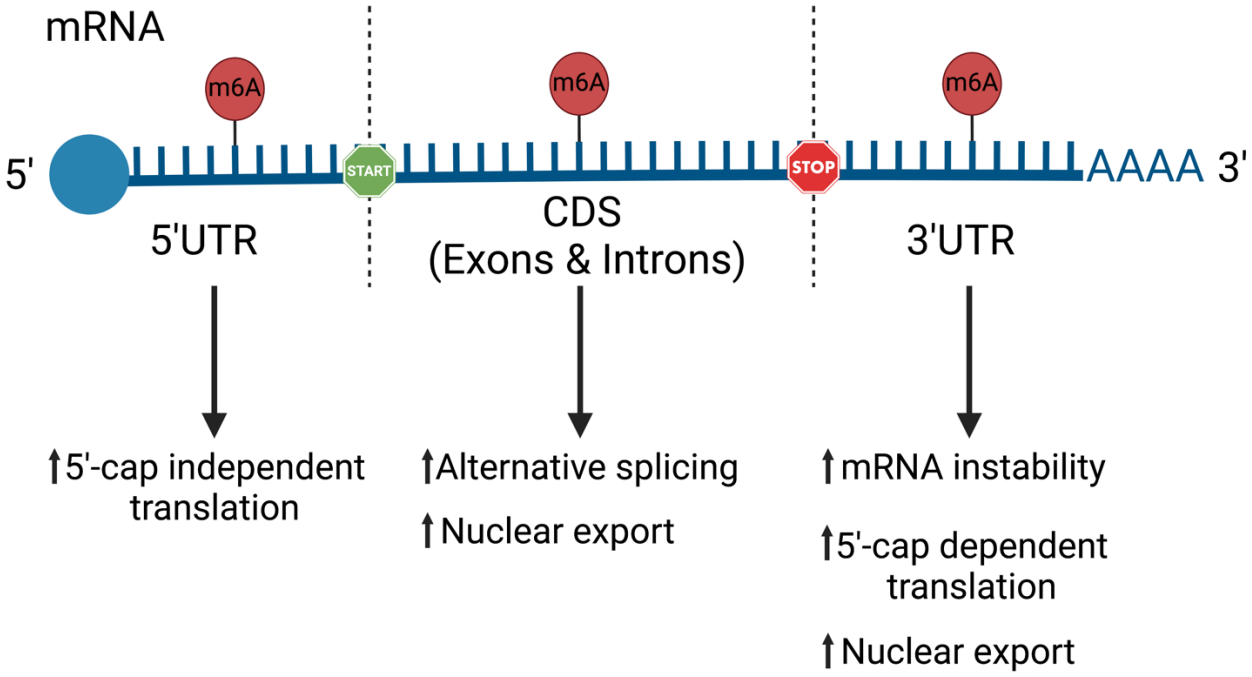

Figure I-14. Different biological effects of m6A on human mRNA depending on the relative m6A position.

(1) m6A and mRNA instability

The most well-established function of m6A is to increase the instability of mRNA. The m6A cytosolic readers YTHDF1, YTHDF3 and especially YHTDF2 can bind to 3'UTR-associated m6A, relocating the mRNA into the processing bodies (P-bodies), in which deadenylation and endonuclease-driven cleavage of the transcripts take place [133, 134]. Knockout of YTHDF2 increases ~40% the stability of many 3'UTR-methylated transcripts, indicating that m6A is a crucial factor for rapid degradation of transcripts [135]. On the other hand, IGF2BP1/2/3 proteins bind preferentially to 3'UTR-m6A methylated transcripts, promoting their stability by protecting the methylated mRNA from P-body-mediated degradation [136].

(2) m6A and mRNA translation

Another well-known function of m6A is to enhance translation of the modified mRNA. The reader YTHDF1 can also bind to 3'UTR-methylated transcripts in order to recruit eIF3, enhancing translation [137]. Additionally, METTL3 (the catalytical enzyme of the WMM complex) is also found in the cytosol, not exerting its methyltransferase activity, but binding to

3’UTR-m6A and enhancing translation by interacting with eIF3 through the creation of a 3’UTR-5’Cap mRNA loop [138]. Finally, if 5’UTR is methylated instead, eIF3 can directly bind to m6A, fostering a cap-independent translation of the transcript, without needing the presence of eIF4E (a crucial cap-dependent translation initiation factor) [139].

(3) m6A and mRNA splicing

The role of m6A and mRNA splicing was proven by the depletion of several writers, readers and erasers of m6A, all of them leading to changes in alternative splicing [140, 141]. The m6A reader HNRNPG co-transcriptionally binds to m6A deposited in exon-intron junctions, slowing down the transcriptional activity of RNA polymerase II and giving time for the spliceosome to splice the region [142]. On the other hand, the m6A reader YTHDC1 also binds to m6A deposited near exon-intron junctions, recruiting SRSF3 into the nuclear speckles (favoring exon inclusion) while excluding SRSF10 (a factor that promotes exon skipping) [143]. Additionally, the presence of m6A in introns (far from exon-intron boundaries) has a direct effect on pre-mRNA splicing kinetics, allowing the regulation of alternative splicing events in slowly processed introns, and avoiding intron retention [144].

(4) m6A and mRNA cellular localization

After mRNA nuclear processing has finished, the m6A reader YTHDC1, together with SRSF3, binds to m6A-modified transcripts as a cytosolic export signal in a TREX:NXF1-dependent nuclear export pathway [145]. In addition, WMM complex also recruits the TREX:NXF1-exporting complex after transcription completion. This has been demonstrated by depletion of ALKBH5 (an m6A eraser), in which higher m6A content prematurely accelerated mRNA nuclear export [146]. Nevertheless, many mRNA molecules lack m6A and they are still exported to the cytosol, making the need of m6A ambiguous for nuclear export [147].

***

m6A in hematopoiesis and hematological malignancies

m6A RNA modification plays a crucial role in many aspects of cellular biology, including early fetal development of the brain, the formation of germ cells and the development and maintenance of hematopoietic cells [148–150]. Specifically, METTL3 depletion inhibits the formation of HSCs (inhibiting the endothelial-to-hematopoietic transition that occur in the fetal aorta-gonad-mesonephros region) during zebrafish and mouse embryogenesis due to m6A hypomethylation of NOTCH1A mRNA, increasing its stability and leading to hematopoietic failure and perinatal lethality [151]. Conversely, overexpression of human METTL3 inhibits HSC differentiation and increases cell proliferation *in vitro* [152]. In fact, murine Mettl3-mediated m6A methylation of Myc mRNA controls the differentiation potential of bone marrow HSCs [153]. On the other hand, knockout of murine Ythdf2 increases the self-renewal capacity of human HSCs [154] while Igf2bp2 deficiency accelerates Bmi1 mRNA decay, a key gene in HSC self-renewal, inducing quiescence loss and impairing HSC function by increasing mitochondrial activity [155].

The implications of m6A in B-cell development are very little known. Recently, a group discovered that deleting Mettl14 in murine models impairs IL7-induced proliferation of pro-B cells and early-to-late-Pre-B cell transition, due to Ikzf3 mRNA m6A hypomethylation [156]. On the other hand, during germinal center positive selection of murine naïve B cells, Mettl14-dependent m6A deposition on negative immune regulators such as Tipe2 and Lax1 mRNAs promote their decay in a Ythdf2-dependent manner, and thus upregulating genes that are required for germinal center positive selection [157].

Neither is there much information about the implications of m6A in macrophage development. A study claims that m6A deposition in STAT1 mRNA by METTL3 induces M0-to-M1 polarization, while METTL3 depletion stimulated M0-to-M2 polarization [158]. Conversely, depletion of IGF2BP2 exhibit enhanced M1 polarization, indicating that IGF2BP2 stimulates M2 polarization by targeting TSC1 mRNA in an m6A-dependent manner [159]. On the other hand, FTO depletion blocks both M1 and M2 polarization [160]. Additionally, METTL3 depletion impairs m6A deposition on IRAKM mRNA, impeding IRAKM-mediated TLR4 negative regulation, which is crucial for macrophage activation [161].

The relation between m6A and cancer has been extensively studied since the last decade, being linked with many types of malignancies including lung, liver, breast, colon, pancreas, kidney, and hematological cancers, among many other types of malignancies [128]. Depending on the cancer cell type, alterations in m6A levels may suppress or promote cancer progression [162]. Focusing on hematological cancers, the most studied blood malignancy in relation to m6A is acute myeloid leukemia (AML). In this case, AML patient samples exhibit higher content of m6A and higher METTL3 expression levels [163, 164]. METTL3 promotes AML proliferation contributing to the translation of c-MYC, BCL2, and PTEN, contributing to the bone marrow differentiation blockade and the expansion of leukemic stem cells in this tissue [152]. Additionally, WMM components METTL14 and WTAP also promote AML progression [165, 166]. As a matter of fact, the development of STM2457, a new small molecular competitive inhibitor of METTL3's catalytical function has shown promising results in the treatment of AML, significatively reducing cancer growth in murine AML models [167]. On the other hand (and somewhat paradoxically), the m6A eraser FTO is highly expressed in some subtypes of AML, especially in AML with MLL rearrangements [168]. This FTO overexpression can lead higher stability and expression of ASB2 and RARA oncogenes promoting leukemic growth *in vivo*, highlighting the ambiguous role of m6A as a dual effector, acting as a tumor suppressor or as a cancer promoter depending on the subtype of leukemia. In addition to AML, METTL3 is also overexpressed in diffuse large B cell lymphoma (DLBCL), increasing the levels of m6A in PEDF mRNA, promoting cancer proliferation [169]. Moreover, WTAP upregulation induced by piRNA-30473 increases the m6A levels in HK2 transcript, promoting DLBCL progression [170].

All this evidence clearly indicates that m6A plays a crucial role in both physiological and malignant hematopoiesis, acting on key differentiation steps. Nevertheless, there is no research whatsoever relating m6A with cellular transdifferentiation. Thus, unveiling the link between m6A and transdifferentiation will be the focus of our second project in this thesis. Finally, before showing the results of both projects, we will explain what type of model we used to investigate the implications of both DNA and RNA methylation in B-cell-to-macrophage transdifferentiation.

⁂

BLaER1: the human pre-B-ALL-to-macrophage *in vitro* transdifferentiation model

The main problem of studying human cellular transdifferentiation lies in the difficulty to detect the transitional states between the original cell and the newly transdifferentiated cell, since there are no intermediate cells that can be pinpointed between the two states. Thus, it is practically impossible to examine transdifferentiation in malignant clinical cases such as FL-to-histiocytic sarcomas or B-ALL-to-histiocytic leukemias by solely using biopsied patient samples, especially when we want to understand the early events that drive this transdifferentiation process. Therefore, we need a cellular transdifferentiation model that permit us to temporally pinpoint each early epigenetic and epitranscriptomic event between the two differentiation states. The only human B-cell-to-macrophage transdifferentiation model available at present is BLaER1, a human pre-B-ALL-to-macrophage *in vitro* transdifferentiation cellular model (figure I-15), developed by Francesca Rapino and colleagues in 2013 at Thomas Graf's laboratory (Centre for Genomic Regulation, CRG, Barcelona) [58].

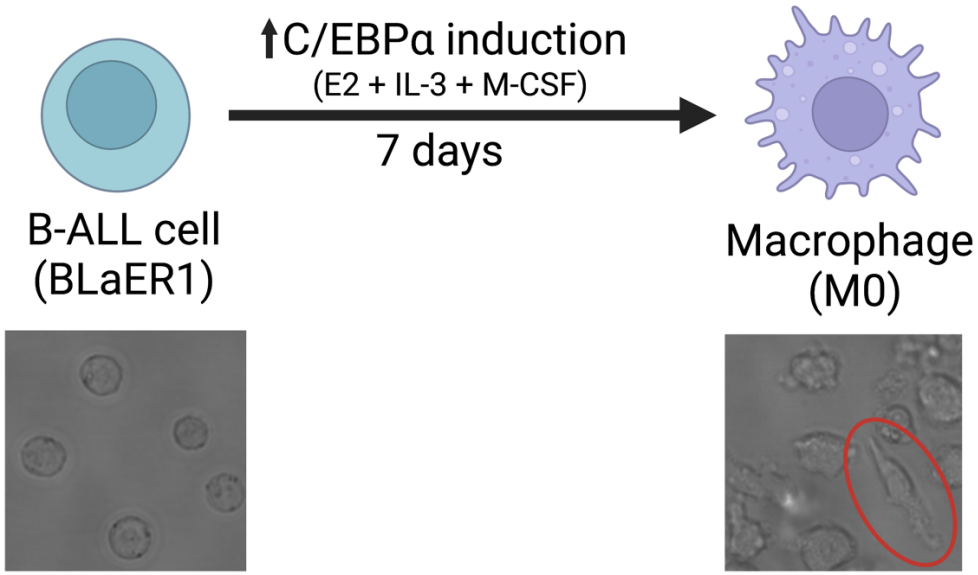

Figure I-15. BLaER1 human *in vitro* B-ALL-cell-to-macrophage transdifferentiation model. A transdifferentiated macrophage is highlighted in red.

By retrovirally transducing a genetic construct containing the fusion of C/EBPα gene with the estrogen receptor hormone binding domain (C/EBPαER) into a human pre-B-ALL cancer cell line (RCH-ACV), almost 100% of the B-cells directly transdifferentiate into fully functional non-tumorigenic quiescent macrophages in just 7 days after *in vitro* treatment with a single dose of estradiol (E2, which induces the translocation of the C/EBPαER fusion protein from the cytosol into the cell nucleus) and two key macrophage differentiation cytokines (IL-3 and M-CSF), without any intermediate asymmetrical divisions whatsoever [171]. As already seen in previous chapters of the introduction, C/EBPα is a crucial myeloid differentiation transcription factor that fosters early differentiation of progenitor cells into the myeloid lineage and, if sustained, into the monocyte lineage. Adding IL-3 and M-CSF (two crucial macrophage differentiation cytokines) pushes transdifferentiation directly into non-activated (M0) macrophages.

Thus, BLaER1 model is a good candidate to examine the early epigenetic and epitranscriptomic events that occur during B-cell-to-macrophage transdifferentiation, permitting to extrapolate the results to possible cases of malignant B-cell-to-macrophage transdifferentiation (such as FL-to-histiocytic sarcoma or B-ALL-to-histiocytic leukemia) in which C/EBPα upregulation plays a crucial role.

Having finished with the introduction, we will now proceed to establish the hypothesis and objectives of this thesis.

⁂

HYPOTHESIS

- During B-cell-to-macrophage transdifferentiation, changes in 5mC and m6A methylation content in DNA and RNA respectively may occur.

- These epigenetic and epitranscriptomic changes that occur during B-cell-to-macrophage transdifferentiation may be crucial for making this conversion possible.

- Studying the relation of B-cell-to-macrophage transdifferentiation and these epigenetic/epitranscriptomic changes will reveal valuable information that may lead to the discovery of new potential diagnostic and/or therapeutic targets.

OBJECTIVES

- To analyze the global DNA (5mC) and RNA (m6A) methylation changes that occur at different time-points of BLaER1 B-cell-to-macrophage *in vitro* transdifferentiation.

- To detect targets that are differentially methylated upon this B-cell-to-macrophage transdifferentiation.

- To study the implications of these targets on B-cell-to-macrophage transdifferentiation and how DNA/RNA methylation modulate their activity.

- To finally establish a causative link between DNA/RNA methylation and B-cell-to-macrophage transdifferentiation.

RESULTS

FIRST PROJECT RESULTS

DNA 5mC methylation changes in leukemic transdifferentiation

DNA methylation changes upon BLaER1 transdifferentiation occur locally rather than globally across the genome

To detect the changes in DNA 5mC methylation that occur during BLaER1 B-cell-to-macrophage transdifferentiation, we purified DNA samples at different timepoints of transdifferentiation (0h, 3h, 12h, 24h, 48h, 72h and 168h) and used the Illumina Methylation EPIC-850k array, which interrogates the methylation status of approximately 850.000 CpGs across the entire genome (figure R-1). Complementary, we analyzed the changes in RNA expression during this process using an RNA expression array at the same timepoints of BLaER1 transdifferentiation (0h, 3h, 12h, 24h, 48h, 72h and 168h).

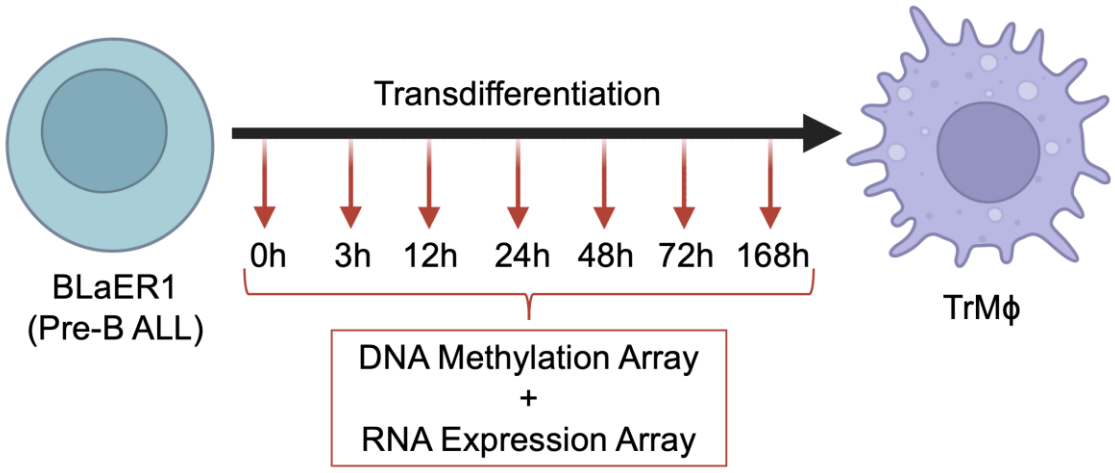

Figure R-1. Experimental design of the first project. **Abbreviations**: TrMϕ: transdifferentiated macrophage.

First, to see global DNA methylation changes across the genome, we analyzed the beta value differences (Δβ) between "BLaER1-168h vs BLaER1-0h" (figure R-2A) samples. Beta values (β) for each CpG span from 0 to 1 (0 being completely unmethylated and 1 completely methylated). For a specific CpG, an absolute Δβ of > 0.66 between two conditions is considered a significant methylation change [172]. In addition, we also analyzed the Δβ between "donor-derived macrophages vs leukemic pre-B cells (RCH-ACV)" samples (figure R-2B).

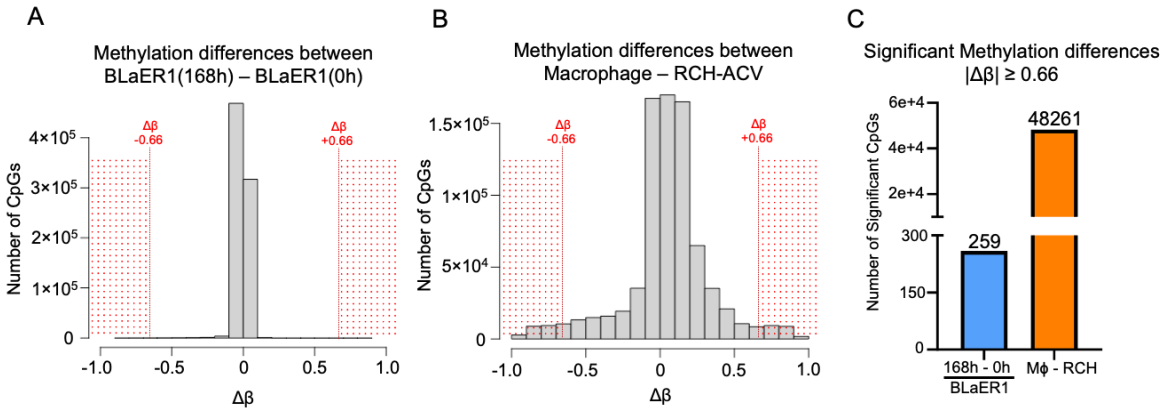

Figure R-2. (A and B) Histograms depicting the global methylation beta value difference (Δβ) between (A) BLaER1(168h) – BlaER1(0h) and (B) donor-derived macrophages – RCH-ACV. (C) Number of significant differentially methylated CpGs (with an absolute Δβ ≥ 0.66) when comparing BLaER1(168h) – BlaER1(0h) and donor-derived macrophages – RCH-ACV. **Abbreviations**: Mϕ: macrophage; RCH: RCH-ACV (pre-B-ALL cell line, same as BLaER1 but without the estradiol-inducible C/EBPα construct).

By looking at these results, we can see that transdifferentiated BLaER1 cells did not show significant global methylation differences in comparison with non-transdifferentiated BLaER1 cells (Figure R-2A), but only 259 differentially significant CpGs (figure R-2C). When comparing donor-derived macrophages with RCH-ACV cells (pre-B-ALL), there were substantially many more significant global methylation changes (figure R-2B), which suggests that transdifferentiated BLaER1 cells did not require, at least at a global genomic scale, to acquire the same methylomic patterns as a natural macrophage.

This fact can be better seen in figure R-3. These heatmaps show that most of BLaER1 DNA methylation levels across different promoter regions (TSS1500, TSS200, 5'UTR, and 1stExon) did not change after 168 hours of transdifferentiation, resembling more a pre-B-ALL cell rather than a natural macrophage at a global DNA methylomic scale (figure R-3).

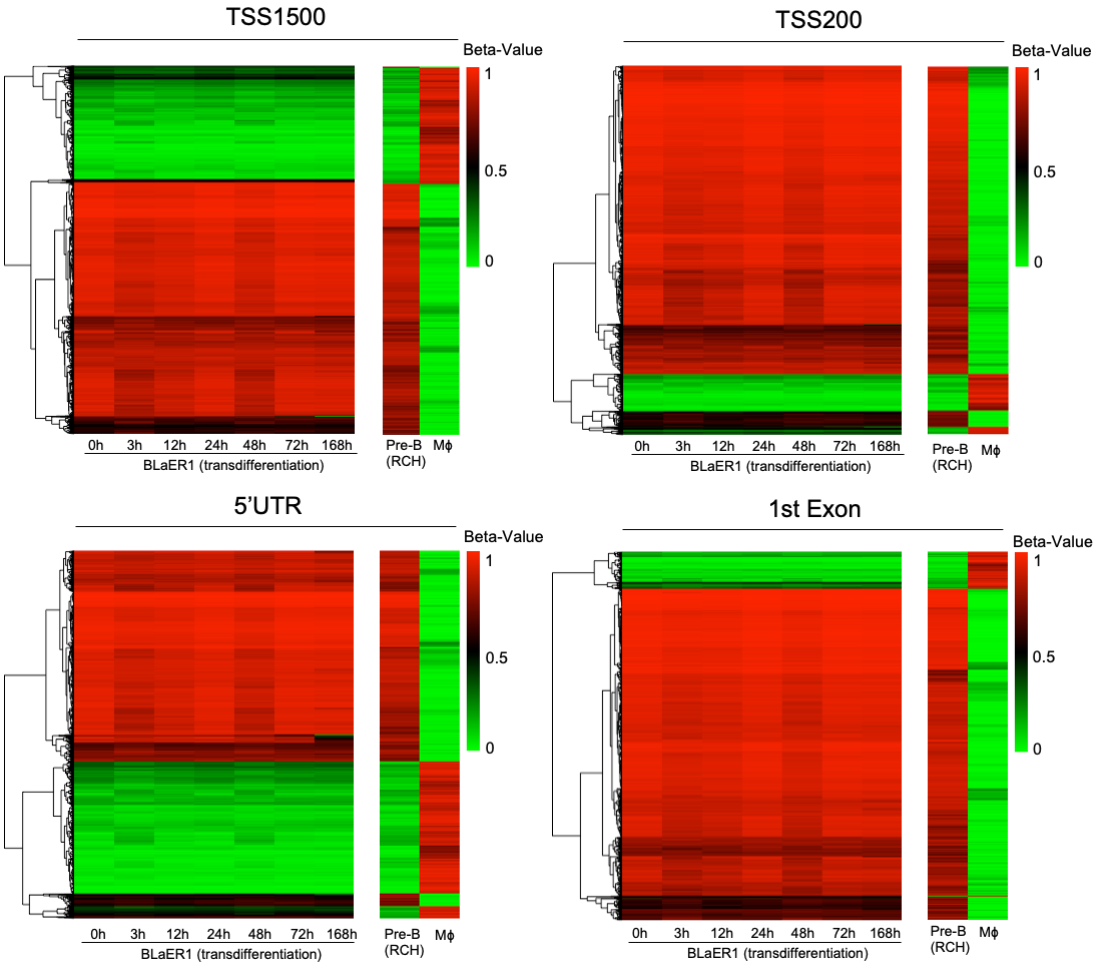

Figure R-3. DNA Methylation heatmaps depicting the unsupervised clustering of CpGs that show an absolute Δβ ≥ 0.66 between donor-derived macrophages (Mϕ) and Pre-B RCH-ACV cells (RCH).

In addition, when analyzing the top 200 downregulated genes and the top 200 upregulated genes upon BLaER1 transdifferentiation by using an RNA expression array and comparing these results with the methylation state of the promoter regions of these genes, we observed no clear global association between RNA expression changes and gene promoter DNA methylation fluctuations during B-cell-to-Macrophage transdifferentiation (figure R-4). There are no apparent global DNA hyper-/hypomethylation changes that respectively lead to down-/upregulation of gene expression patterns. Thus, at the global genomic scale, the acquisition of new gene expression patterns during transdifferentiation is independent of (or at least precedes) global DNA methylation changes.

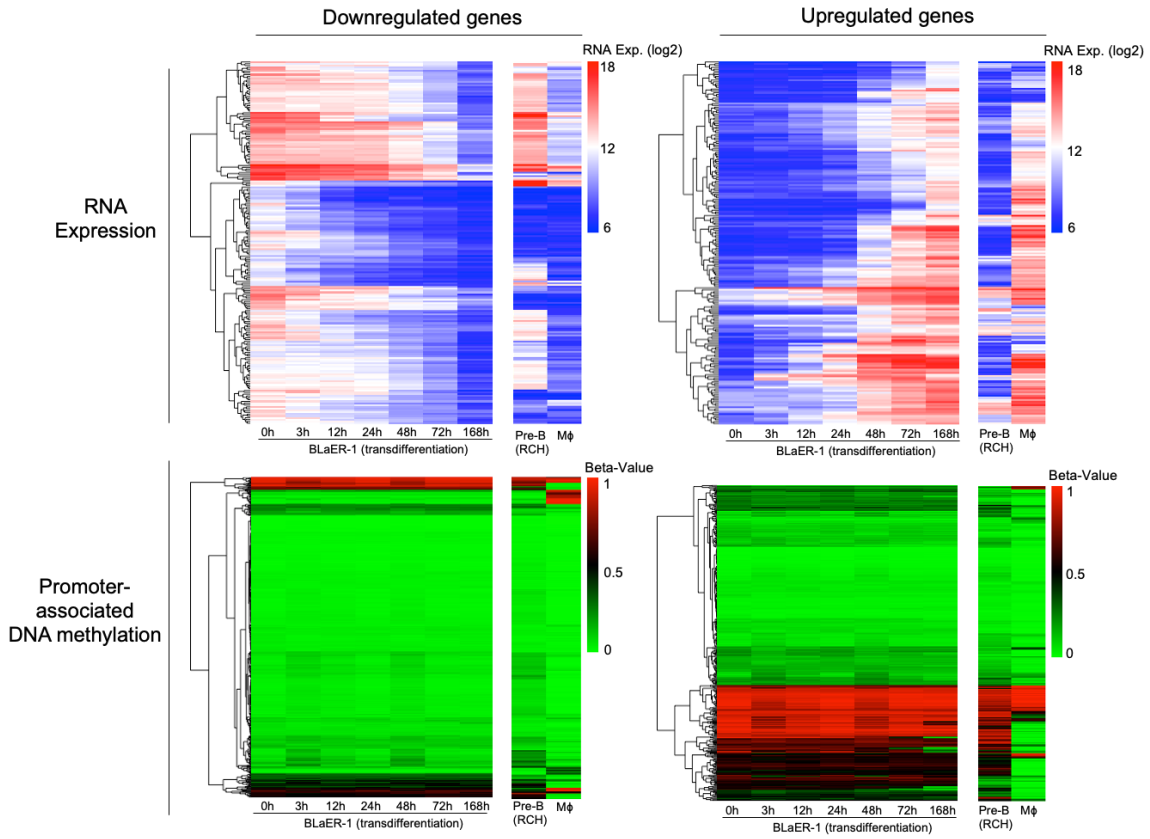

Figure R-4. (Top) RNA expression array heatmaps depicting the unsupervised clustering of the top 200 downregulated genes and the top 200 upregulated genes upon BLaER1 trans-differentiation. (Bottom) DNA methylation heatmaps showing the unsupervised clustering of the TSS200-centered CpGs localized in the promoter of these top genes. Similar results were obtained with TSS1500/5'UTR/1stExon-centered CpGs (data not shown).

Regardless of these results, the fact that there were no apparent global changes in DNA methylation levels upon transdifferentiation does not mean that there could not be local, site-specific fluctuations that may be important for this B-cell-to-Macrophage switch to happen. To investigate more site-specific DNA methylation changes, we retrieved those 259 CpGs that showed an absolute $\Delta\beta \geq 0.66$ between BLaER1-168h and BlaER1-0h (figure R-2C) and performed a linear time regression analysis to find the CpGs in which the methylation changes are more strongly associated to treatment duration, thus avoiding "elbow-joint" cases that may not reflect real treatment-associated fluctuations (figure R-5).

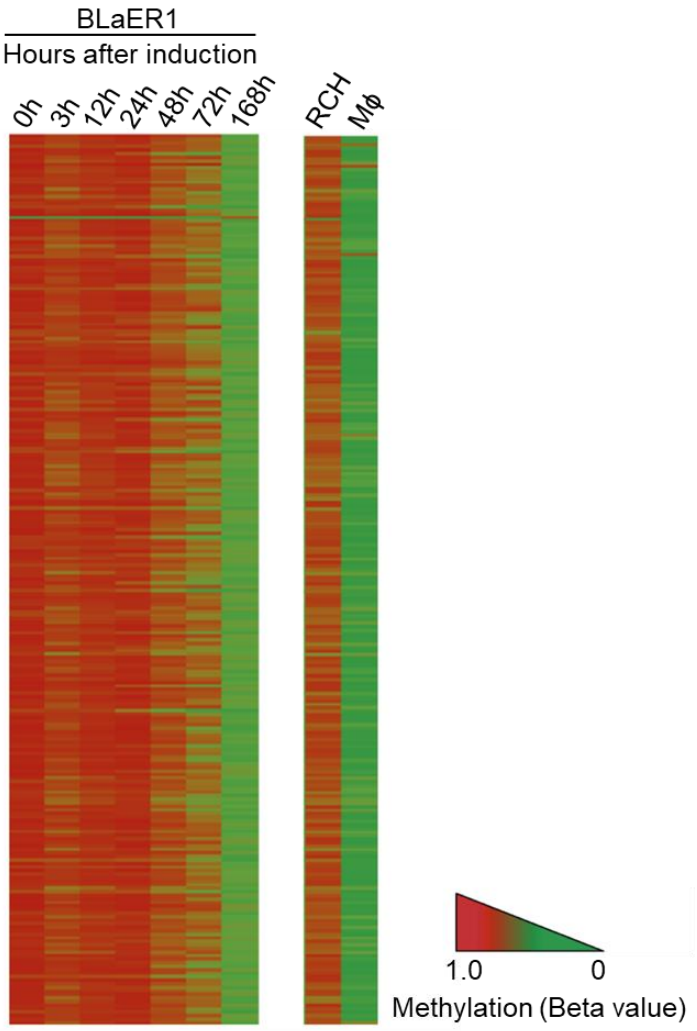

Figure R-5. DNA Methylation heatmap depicting the significant 251 CpGs that fitted the BLaER1 "methylation ~ treatment duration" linear regression model. Only 1 hypermethylated CpG upon transdifferentiation was to be found (99.4% hypomethylated CpGs after 168h).

This linear time regression analysis showed that only 251 CpGs with an absolute $\Delta\beta \geq 0.66$ between "BLaER1-168h vs BLaER1-0h" fit significantly with the "methylation ~ treatment duration" regression model, thus manifesting a gradual change in the methylation status upon transdifferentiation. Interestingly, 99.4% (250) of these 251 CpGs become hypomethylated upon B-cell-to-Macrophage lineage switch, with only 1 significant CpG becoming hypermethylated (figure R-5). This almost exclusive prevalence of significant hypomethylated CpGs may be partly explained by the gradual downregulation in the protein levels of DNMT1 and DNMT3B (maintenance and *de novo* methyltransferases, respectively) and a significant

upregulation in TET2 (demethylase) at 72h of transdifferentiation treatment (figure R-6). Nevertheless, it is surprising that even with these significant changes in DNMT1, DNMT3B and TET2 protein levels, only 250 CpGs become hypomethylated upon treatment. This may reinforce the fact that global DNA methylation fluctuations upon transdifferentiation are independent (or precede) global gene expression changes, but may be important within local, loci-specific regions that could be crucial for B-cell-to-macrophage lineage switch to occur.

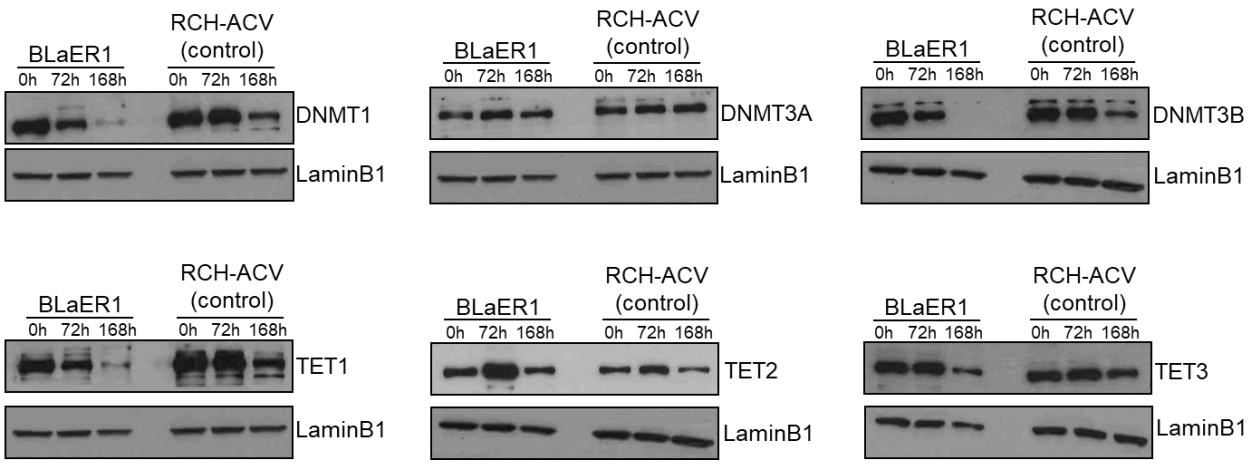

Figure R-6. Western blot analysis depicting the protein levels of 3 DNA methyltransferases (DNMT1, DNMT3A and DNMT3B) and 3 DNA demethylases (TET1, TET2 and TET3) at different time-points after transdifferentiation induction (0h, 72h and 168h) in BLaER1 and RCH-ACV cells.

We then mapped these 251 CpGs onto the human genome (hg19 version) and classified their relative position to their nearest gene (figure R-7). Interestingly, only 15.2% (38) of these CpGs are localized in promoter-related regions (TSS1500, TSS200, 5'UTR and 1stExon).

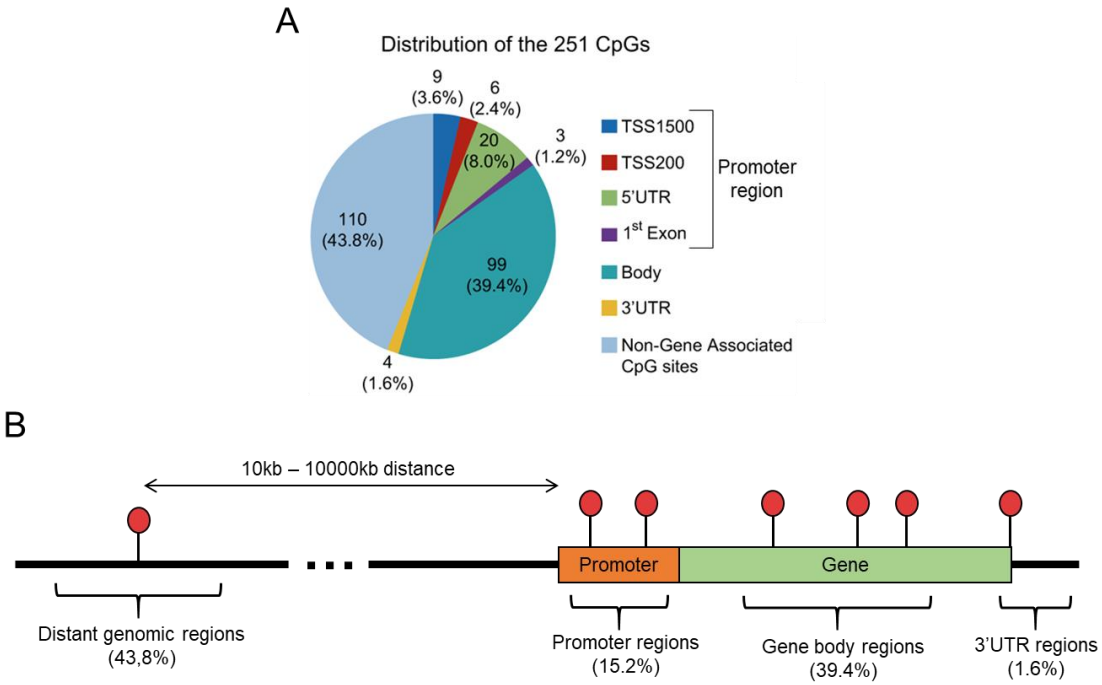

Figure R-7. (A) Relative position of the 251 significant CpGs across the genome in relation to their nearest gene. (B) Graphical representation of (A). Red lollipops represent a methylated CpG.

Differential methylation in promoter regions of crucial macrophage-related genes

First, we focused only on the promoter-related CpGs and their impact in gene expression. We performed a linear time regression analysis for "DNA methylation ~ gene expression" in order to find those CpGs in which the methylation fluctuations are strongly associated to treatment duration and correlate with gene expression changes, comparing the DNA methylation array data with a RNA expression array at the same time-points of transdifferentiation (0h, 3h, 12h, 24h, 48h, 72h and 168h). We found a total of 13 CpGs whose downmethylation upon transdifferentiation correlated with a significant change in the RNA expression of 11 unique genes (table R-1). Most of them (11 CpGs) correlated negatively as expected, showing an expression upregulation upon loss of promoter DNA methylation, while only 2 CpGs correlated positively with gene expression. Gene ontology analyses for cell type gene classifiers indicated that these 11 genes are related to important macrophage functions (EnrichR, FDR-corrected Q-value: 0.014).

Table R-1. Significant hits retrieved from the "DNA methylation ~ gene expression" linear time regression analysis performed on significantly downmethylated promoter-related CpGs.

Genes	Downmethylated promoter CpGs	Relative Position	Adj. R^2	Adj. P-Value	Effect in RNA Expression
CFLAR	cg06885857	5'UTR	0.88	0.0011	Upregulation
TTLL4	cg03487391	5'UTR	0.83	0.0026	Upregulation
ITGAX	cg20851120	TSS200	0.83	0.0027	Upregulation
IL1RN	cg02543462	TSS200	0.82	0.0030	Upregulation
SNX27	cg00387445	TSS1500	0.73	0.0091	Upregulation
ITGAX	cg04742550	TSS200	0.72	0.0094	Upregulation
RBM47	cg03283282	5'UTR	0.72	0.0098	Upregulation
CFLAR	cg04843710	5'UTR	0.68	0.0140	Upregulation
RNASE1	cg12940993	TSS200	0.67	0.0147	Upregulation
CD300E	cg27084498	TSS200	0.61	0.0229	Upregulation
FGR	cg23561791	1stExon	0.57	0.0311	Upregulation
ARHGAP15	cg00506704	5'UTR	0.84	0.0024	Repression
C12orf10	cg08525575	TSS1500	0.50	0.0459	Repression

We orthogonally validated the methylation state of IL1RN and ITGAX promoters (both genes highly expressed in macrophages) by bisulfite Sanger sequencing (BSP) and by pyrosequencing (figure R-8). Both techniques successfully validated the results already seen in the Illumina DNA methylation array. Next, we validated by RT-qPCR, Western blot and flow cytometry the RNA and protein expression levels of both IL1RN and ITGAX at 0h and 168h of BLaER1 transdifferentiation (figure R-9).

Additionally, to test whether DNA demethylation is functionally associated with a gain in expression of IL1RN and ITGAX, we treated non-transdifferentiated BLaER1 cells with 5-aza-2'-deoxycytidine (5-Aza), a passive demethylating agent, for 72h and performed RT-qPCR to detect both transcripts (figure R-10). As expected, RNA expression of both genes increased upon 5-Aza induction without the need of inducing transdifferentiation.

A

CpG	Gene	Relative Position	BLaER1 Methylation Beta-Value after Induction						
			0h	3h	12h	24h	48h	72h	168h
cg02543462	IL1RN	TSS200	0,894	0,853	0,879	0,831	0,663	0,448	0,193
cg20851120	ITGAX	TSS200	0,753	0,809	0,771	0,729	0,548	0,282	0,071
cg04742550	ITGAX	TSS200	0,928	0,919	0,913	0,877	0,767	0,406	0,077

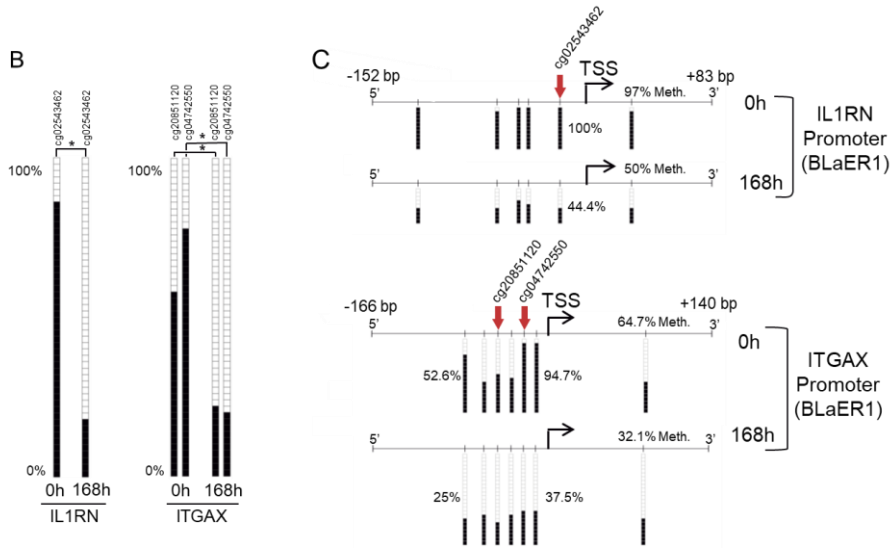

Figure R-8. (A) Beta values of the promoter-related demethylated CpGs found in IL1RN and ITGAX, retrieved from the Illumina 850K Methylation array at different time-points of trans-differentiation. (B) Pyrosequencing and (C) BSP DNA methylation orthogonal validation of both IL1RN and ITGAX promoters. Percentages depict the methylation levels of the detected CpGs (0%: no methylation; 100%: full methylation).

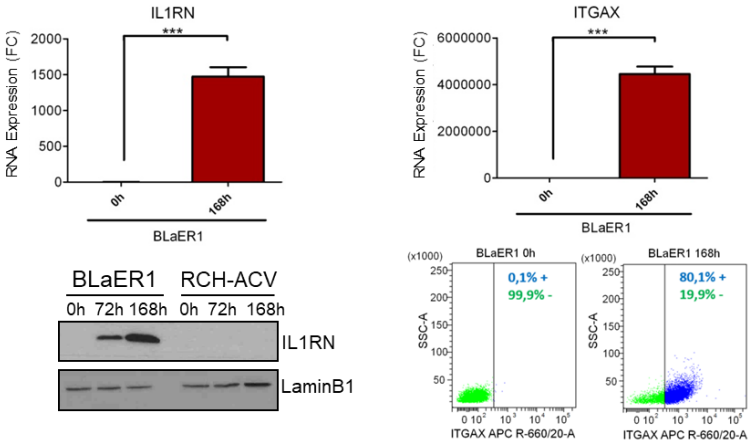

Figure R-9. RNA and protein expression validation of IL1RN and ITGAX by RT-qPCR (top) and by Western blot/flow cytometry (bottom) in BLaER1 cells upon transdifferentiation. T-Student test (P-Value Significances: * < 0.05, ** < 0.001, *** < 0.0001)

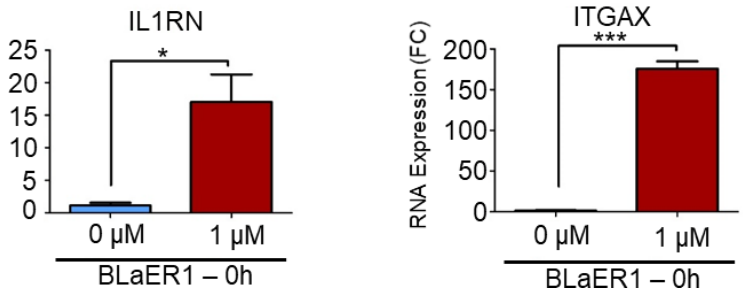

Figure R-10. RT-qPCR of IL1RN and ITGAX on untreated (0 µM for 72h) and 5-Aza treated (1 µM for 72h) untransdifferentiated (0h) BLaER1 cells. T-Student test (P-Value Significances: * < 0.05, ** < 0.001, *** < 0.0001)

To see if there is a DNA motif enrichment in the regions where these 13 promoter-associated CpGs are located, we performed a motif enrichment analysis to detect putative transcription factors that may bind to these demethylated regions (figure R-11). Interestingly, we detected an enrichment in GMEB2 binding motif (a CpG-rich DNA motif). GMEB2 is a ubiquitous transcription factor that has been seen to be sensitive to CpG methylation (the more methylated is the motif, the less binding affinity GMEB2 manifests to its target sequence) [173].

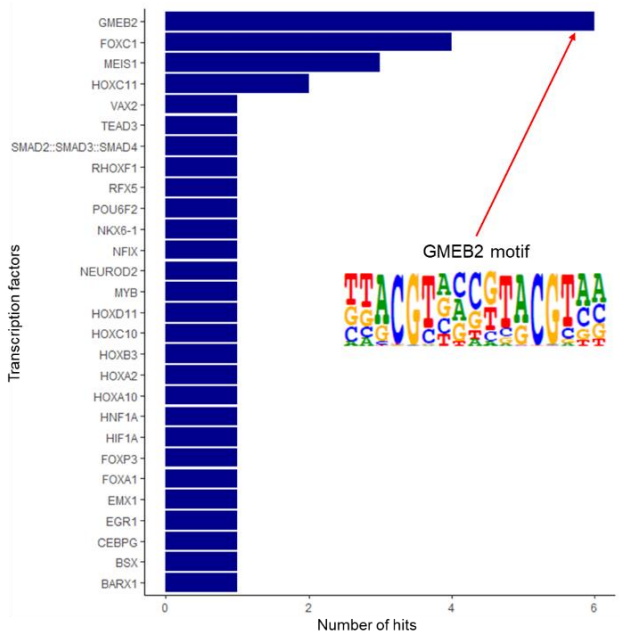

Figure R-11. Enriched transcription factor motifs found within the identified 13 significantly demethylated promoter CpG sites (-19/+20 base pairs centered around the CpG) with correlated methylation/expression values. All the detected hits are shown.

Differential DNA methylation in distal genomic regions have an impact in distant genes during transdifferentiation

Although these demethylated promoter CpGs are located in important genes for macrophage functions, they only represent 15.2% (38) of all the 251 CpGs with significant transdifferentiation-dependent methylation changes. Up to 39.4% CpGs (99) are in gene bodies, 1.6% (4) in 3'UTR regions and 43.8% (110) are located in distant genomic regions, with no proximal genes. The functional role of DNA methylation in these non-promoter regions are not well understood. Methylation in gene bodies do not show a clear negative nor positive correlation with gene expression. On the other hand, the significance of CpG methylation in distal genomic sites remains enigmatic. One logical possibility is that these differentially methylated CpGs are located in intra/intergenic regulatory elements (enhancers or silencers) that may interact with other distant genes, regulating their expression by modulating tridimensional chromatin interactions. The methylation of these regulatory elements may have an impact on how these chromatin interactions are established (figure R-12). Thus, we analyzed the already published Promoter Capture Hi-C (PC-HiC) data from Biola Javierre *et al* [174], by which they studied all the distant chromatin interactions between distal regulatory elements and gene promoters that are present in human M0 macrophages. By projecting the position of our 251 significant CpGs to the PC-HiC data, we obtained all the putative interactions between these CpG sites and other potential DNA regulatory regions.

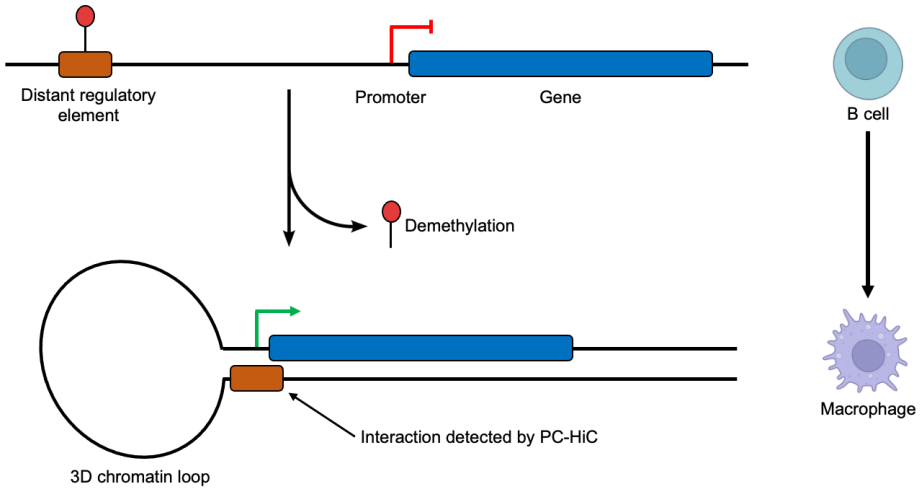

Figure R-12. Schematic representation of a tridimensional chromatin interaction between a gene promoter and a distant regulatory element. The methylation state of these distant elements might have an impact in the formation (or destruction) of these distal interactions.

From this analysis, we retrieved 72 unique CpGs sites (all of them hypomethylated upon transdifferentiation) that putatively interact with 233 unique genes. We then correlated DNA methylation fluctuations of the 72 CpGs versus the RNA expression changes of these genes upon transdifferentiation by applying a linear time regression analysis. These analyses revealed that up to 59 genes, which interact with up to 34 unique CpG sites, manifest expression changes upon transdifferentiation that correlate significantly with the DNA methylation fluctuations. From these 59 genes, 38 increase their gene expression upon transdifferentiation (enhancer interactions), while 21 decrease their expression (silencer interactions). A flow diagram of these triple *in silico* analyses is summarized in figure R-13.

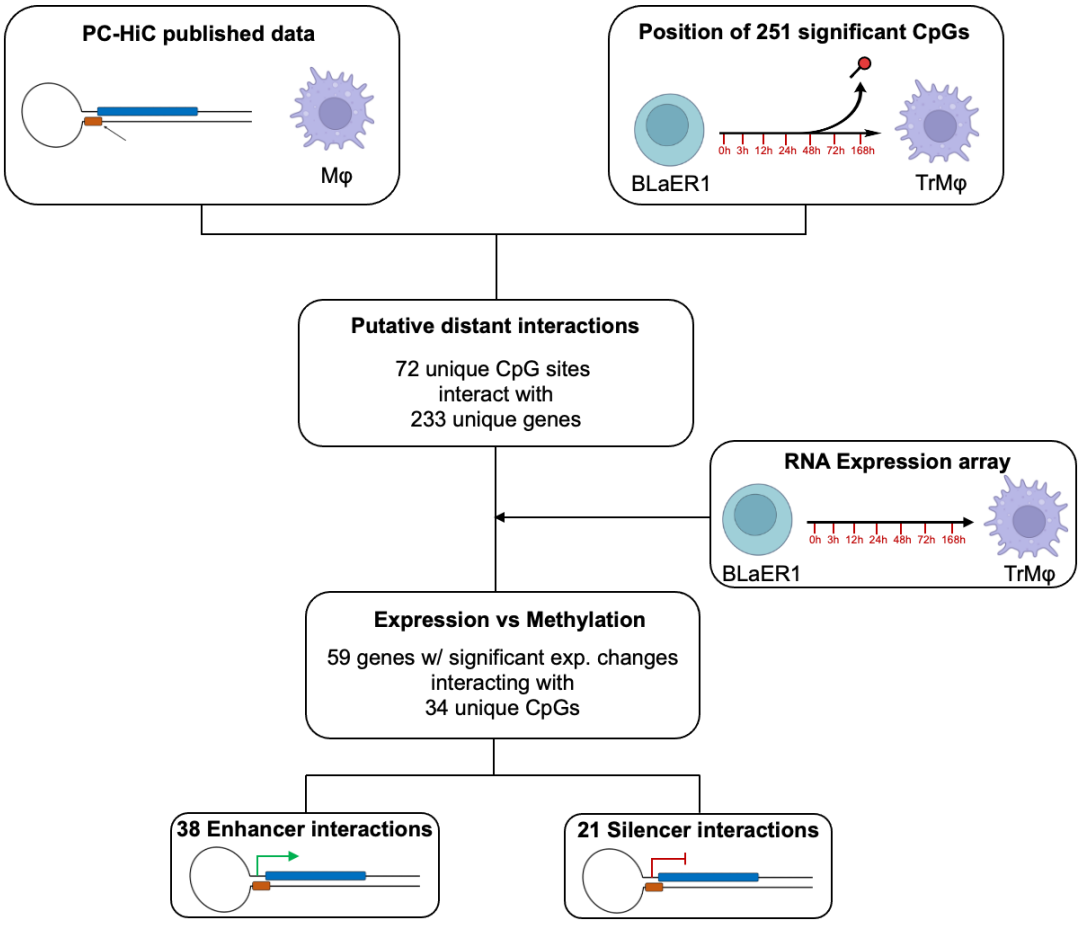

Figure R-13. Flow diagram of the "PC-HiC" ~ "DNA methylation" ~ "RNA expression" triple analysis pipeline, depicting those differentially methylated CpG sites upon transdifferentiation which putatively interact with gene promoters and correlate with RNA expression changes.

Gene ontology analyses for cell type gene classifiers indicated that the enhancer-interacting genes (38 interactions) are related to important macrophage functions (EnrichR, FDR-corrected Q-value: 0.009). Conversely, the silencer-interacting genes (21 interactions) are related to B-lymphoblast cell functions (EnrichR, FDR-corrected Q-value: 0.033). Interestingly, from the 34 unique CpGs interacting with the 59 differentially expressed genes, most of these CpG sites putatively interacted with only 1 gene, but we can find individual CpG sites that may potentially interact with 2-to-5 genes (figure R-14A). As expected, most of these CpG sites are either located in distant genomic regions (intergenic enhancers/silencers, 52.9%, 18 CpGs), but they are also present in gene bodies (intragenic enhancers/silencers, 29.4%, 10 CpGs), while the rest are located either in promoter regions or in 3'UTR (figure R-14B).

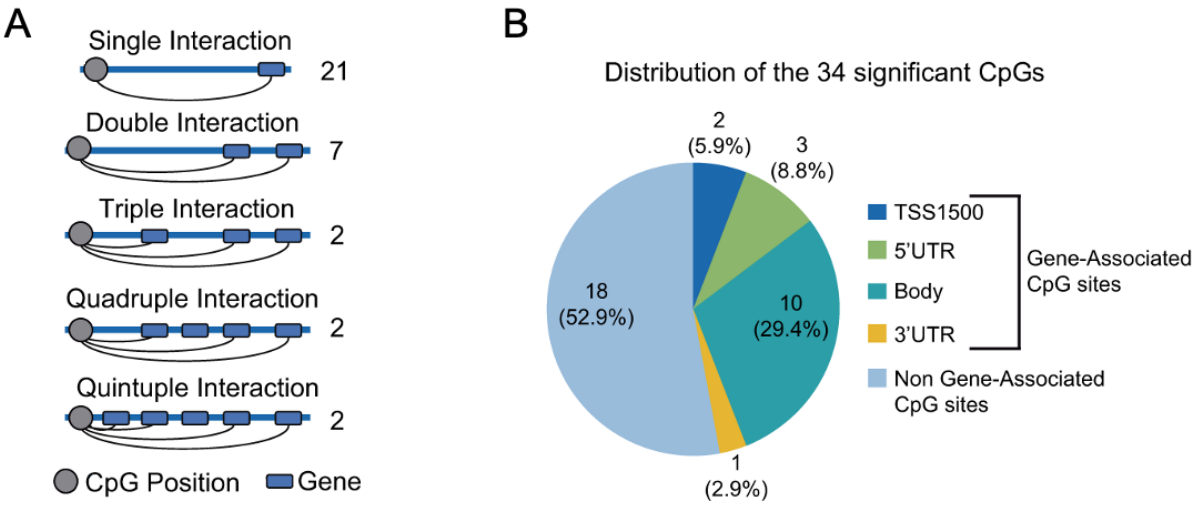

Figure R-14. (A) Number of putative interactions detected between a single significant CpG site and a different number of genes. (B) Relative position of the 34 significant unique CpG sites in relation to their nearest gene.

Then, we orthogonally analyzed the methylation state of 5 CpG sites (3 putative enhancer sites and 2 putative silencer sites), located at distant genomic regions, by bisulfite Sanger sequencing (BSP) and by pyrosequencing (figure R-15), demonstrating that these CpG sites were indeed demethylated upon transdifferentiation and thus validating the results already seen in the Illumina DNA methylation array. Next, we validated by RT-qPCR the changes in RNA expression of the 3 putative enhancer-interacting genes (RHOG, CCR1 and CXCL8) and the 2 putative silencer-interacting genes (CHML and DBF4), depicted in figure R-16.

A

CpG	Interacting Gene	BLaER1 Methylation Beta-Value after Induction						
		0h	3h	12h	24h	48h	72h	168h
cg21880051	RHOG	0,786	0,845	0,844	0,769	0,590	0,369	0,091
cg21655255	CCR1	0,867	0,873	0,879	0,848	0,751	0,474	0,137
cg05146536	CXCL8	0,921	0,906	0,903	0,860	0,731	0,521	0,218
cg00250658	CHML	0,803	0,842	0,869	0,869	0,762	0,388	0,059
cg06297012	DBF4	0,895	0,906	0,918	0,885	0,800	0,448	0,148

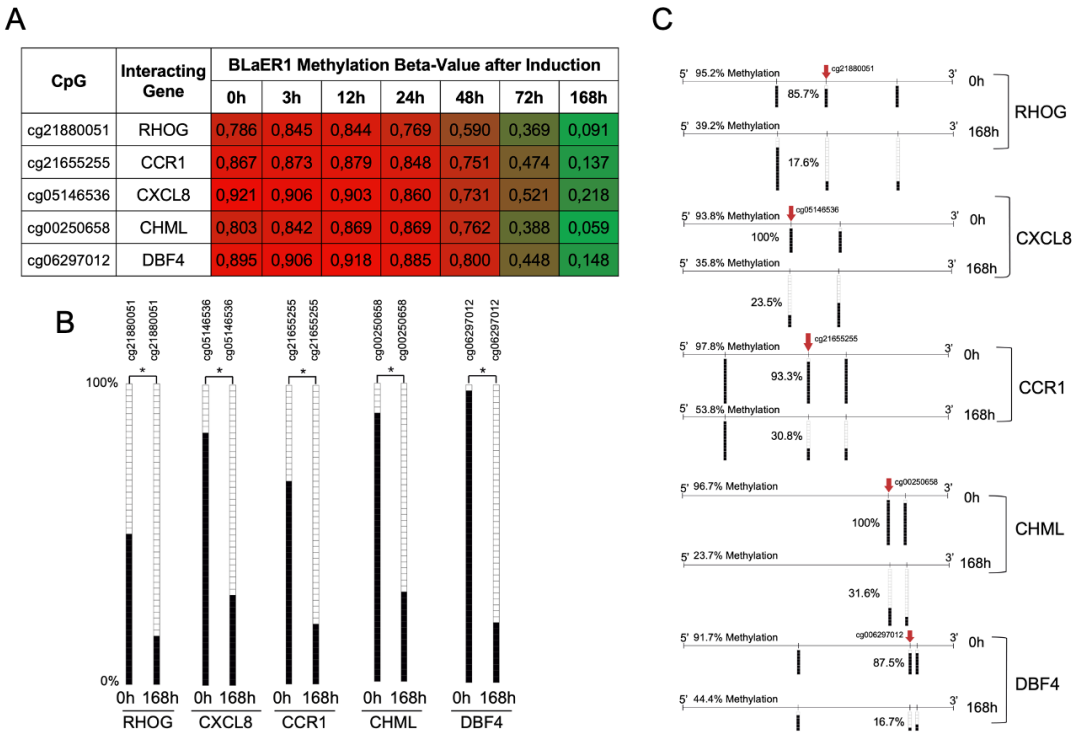

Figure R-15. (A) Beta values of the 5 distant genomic demethylated CpG sites that putatively interact with 5 distant genes (RHOG, CXCL8, CCR1, CHML and DBF4), retrieved from the Illumina 850K Methylation array at different time-points of transdifferentiation. (B) Pyrosequencing and (C) BSP DNA methylation orthogonal validation of the 5 distant genomic demethylated CpG sites. Percentages depict the methylation levels of the detected CpGs (0%: no methylation; 100%: full methylation).

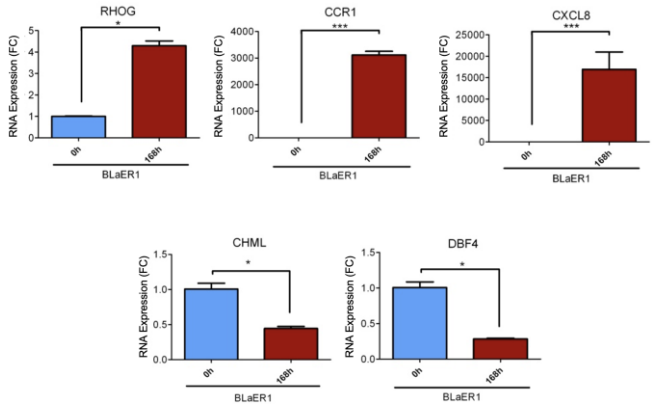

Figure R-16. RT-qPCR of (top) 3 putative enhancer-regulated genes and (bottom) 2 putative silencer-regulated genes. T-Student test (P-Value Significances: * < 0.05, ** < 0.001, *** < 0.0001)

In addition, we also treated non-transdifferentiated BLaER1 cells with 5-Aza for 72h to test whether DNA demethylation is functionally associated with a gain in expression of some of these putative interacting genes (figure R-17). Indeed, RNA expression of the 3 enhancer-regulated genes was significantly increased upon 5-Aza treatment while, conversely, the expression of the 2 silencer-regulated genes is significantly downregulated. These results strengthen the fact that DNA methylation has a functional role in these distant-regulated genes.

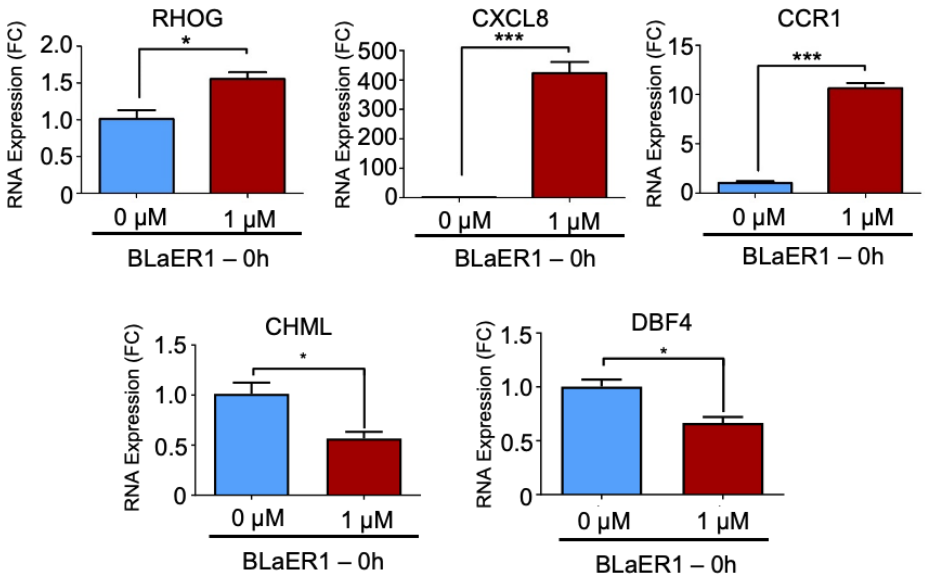

Figure R-17. RT-qPCR of the 3 enhancer-regulated genes (RHOG, CXCL8 and CCR1) and the 2 silencer-regulated genes (CHML and DBF4) on untreated (0 µM for 72h) and 5-Aza treated (1 µM for 72h) untransdifferentiated (0h) BLaER1 cells. T-Student test (P-Value Significances: * < 0.05, ** < 0.001, *** < 0.0001)

To validate the putative distant chromatin contacts, we performed an UMI-4C analysis in BLaER1 at 0h and 168h of transdifferentiation (figure R-18). This technique allows for the detection of all possible contacts between 1 specific locus (the putative demethylated enhancer/silencer of our interest, named “bait region”) and any DNA region in the same chromosome that directly contacts with that specific locus (“one-vs-all” approach). One drawback of this technique is that it only detects contacts that are less than 2 megabases distant to the bait region. Thus, the only significant gene that fulfills this condition is CCR1 (figure R-18).

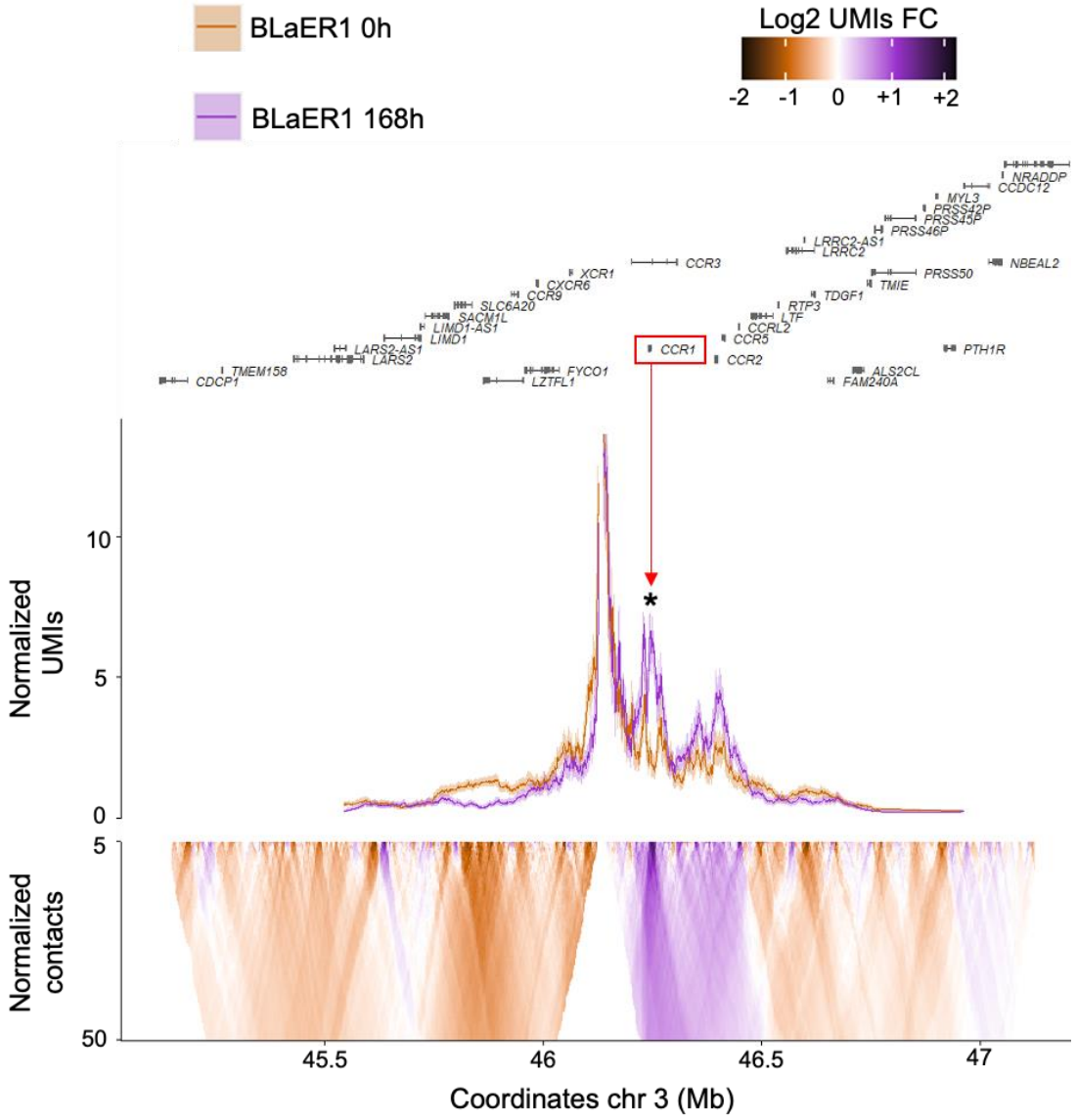

Figure R-18. UMI-4C representation of all the chromatin contacts spanning ± 2 megabases of distance between the putative enhancer demethylated region (center of the graph, bait region) and other distant DNA regions. On the top, the genes present in these coordinates are represented by horizontal lines; CCR1 gene is highlighted in a red box. In the middle, the trends line plot indicates the normalized UMIs detected for each region. On the bottom, the domainogram represents the differential contacts between BLaER1 0h (orange) and BLaER1 168h (purple). The chromatin contact intensity for the CCR1 promoter region was very high for the hypomethylated distant regulatory CpG site at time 168h of transdifferentiation (* Chi-square adjusted P-value < 0.0001).

This UMI-4C analysis showed that the putative demethylated enhancer region (represented in the center of the graph, figure R-18) interacted with CCR1 promoter with a significant higher affinity upon transdifferentiation. This reinforces the correlation between the demethylation at the distant CpG site, the newly generated distant chromatin interactions and gene expression.

In addition, we performed a transcription factor motif analysis on the 34 significant unique CpGs that putatively interact with distant genes (figure R-19). The most enriched DNA-binding motif was MEIS1, which is a well-known transcription factor that binds to actively-demethylated enhancers, regulating specific cell fates [175].

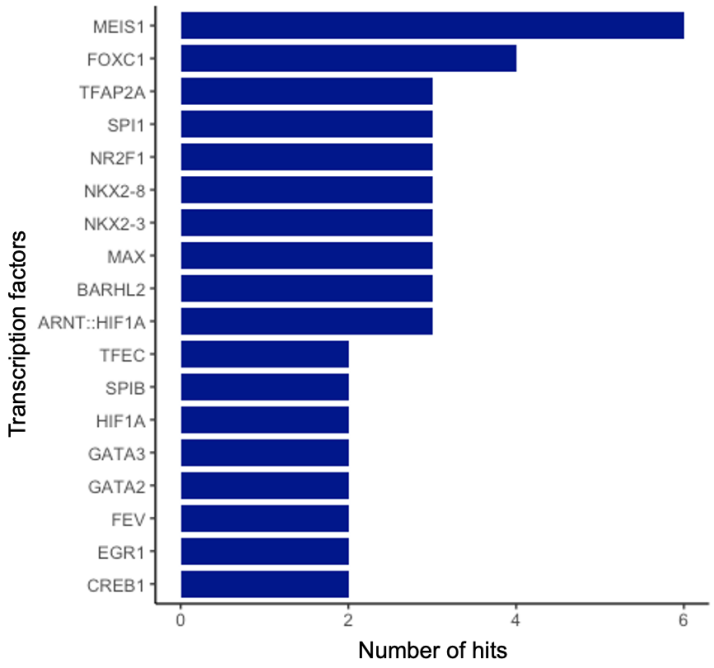

Figure R-19. Enriched transcription factor motifs found within the identified 34 significantly demethylated distant CpG sites (-19/+20 base pairs centered around the CpG) that putatively interact with 59 distant genes. Only those motifs with ≥ 2 hits are shown.

We also performed an analysis for finding specific CTCF binding sites on these 34 differentially methylated distant CpG sites using the CTCFBSDB2.0 prediction tool. Only 4 of these 34 CpG sites were potential CTCF sites, two of them found in distant genomic regions (cg05146536 and cg08505032) and two found in gene-related regions (cg22541962 and cg25941751).

All these results indicate that changes in DNA methylation during B-cell-to-macrophage transdifferentiation do not occur at a global genomic scale, but rather at discrete, local positions that can affect the expression of key genes for macrophage functions which may be essential for this transdifferentiation to occur. Specifically, these local DNA methylation changes occur not only at gene promoters, but take place more abundantly at potential enhancers and silencers that regulate gene expression by generating long-range chromatin interactions between these distal regulatory regions and gene promoters. DNA methylation fluctuations at these distant regions may have an important causative effect in the establishment of tridimensional chromatin loops during transdifferentiation. These results may help to improve our knowledge of the critical determinant for cell type specification and to understand what goes awry in hematological malignancies that, in response to pharmacological or cellular therapies, undergo lineage switching to develop resistance to the applied treatment.

This first work was published in the journal *Leukemia*, under the title "*B-cell leukemia transdifferentiation to macrophage involves reconfiguration of DNA methylation for long-range regulation*" [176].

SECOND PROJECT RESULTS

RNA m6A methylation changes in leukemic transdifferentiation

RNA m6A methylation changes upon BLaER1 transdifferentiation were enriched in translation-related transcripts

To detect the changes in RNA m6A methylation that occur during BLaER1 B-cell-to-macrophage transdifferentiation, we purified total RNA samples (~ 500 μg) at 3 timepoints of transdifferentiation (0h, 72h and 168h) and performed an m6A-Seq (also known as MeRIP-Seq) in collaboration with Gideon Rechavi's laboratory (figure R-20). This technique immunoprecipitates m6A-modified RNA by using an m6A-specific antibody and performs an RNA-Seq of these immunoprecipitated transcripts in comparison with a non-precipitated input.

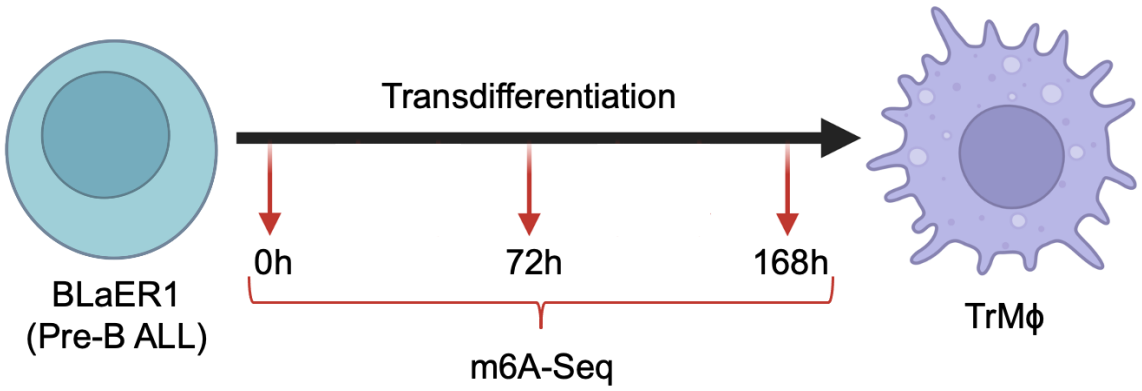

Figure R-20. Experimental design of the second project.

We observed up to 6072 differential m6A peaks upon BLaER1 transdifferentiation, corresponding to 3056 unique RNA transcripts (figure R-21A). Interestingly, as seen in figure R-21B, most of these peaks were located at internal exons (31%) and introns (32%), in comparison with 3'UTR (18%) and 5'UTR (19%). The presence of m6A peaks in intronic regions is explained by the fact that m6A is abundantly deposited in introns during RNA polymerization, but they are usually lost after splicing. Since m6A-Seq is able to detect nascent RNA and transcripts with intron retention, m6A peaks in these regions are traceable.

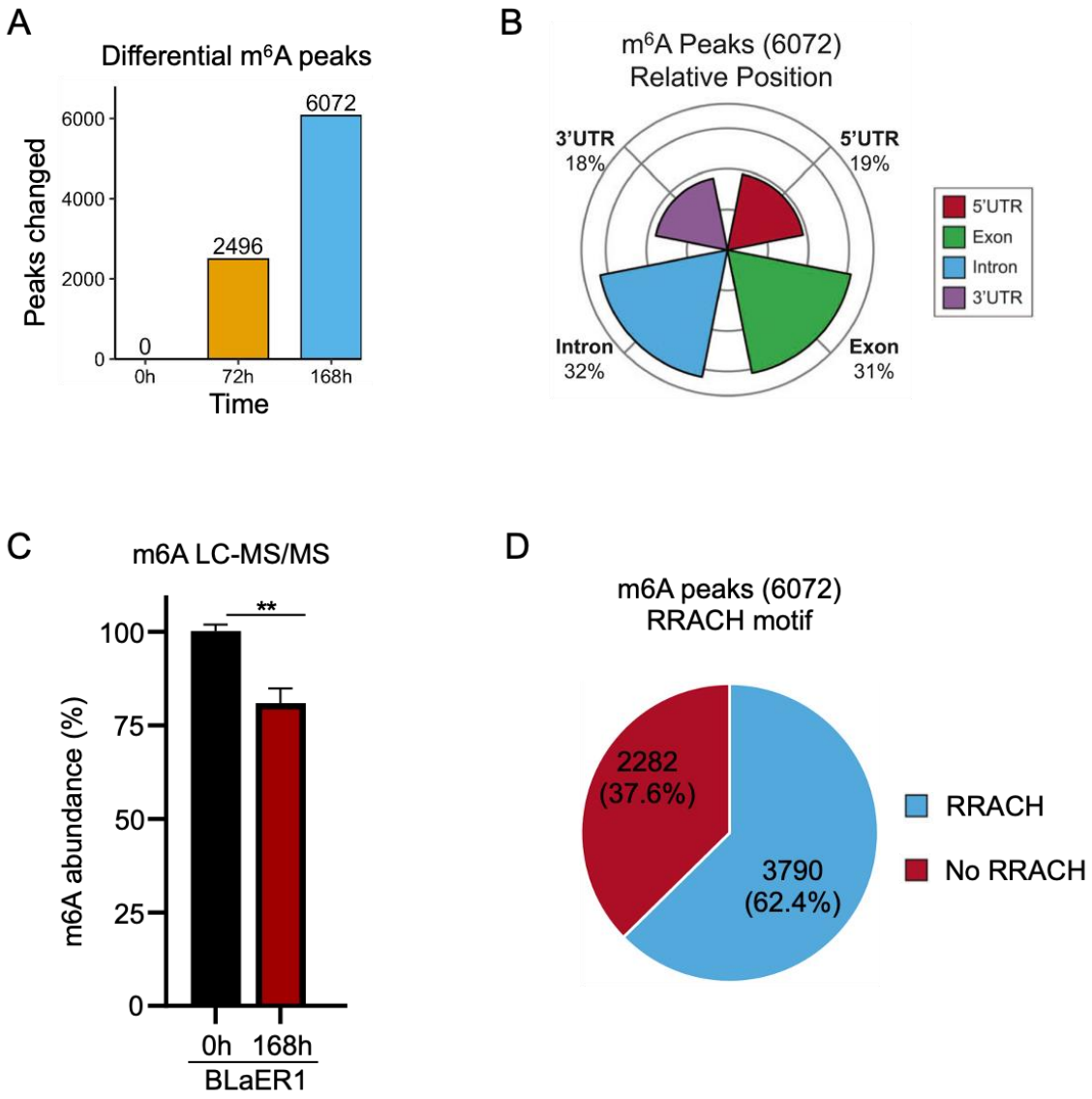

Figure R-21. (A) Differential m6A RNA peaks at 0h, 72h and 168h of BLaER1 transdifferentiation detected by m6A-Seq. (B) Radar plot depicting the proportion of differentially methylated m6A peaks at 168h of BLaER1 transdifferentiation based on their relative transcriptomic position. (C) m6A abundancy of BLaER1 before (0h) and after (168h) transdifferentiation, quantified by LC-MS/MS. T-Student test (P-Value Significances: * < 0.05, ** < 0.001, *** < 0.0001) (D) Presence of the RRACH motif on the 6072 differential m6A peaks.

Mass spectrometry analyses confirmed a subtle but significant decrease of total m6A cell content upon BLaER1 transdifferentiation, of around < 25% (figure R-21C). In addition, up to 62.4% of the differential m6A peaks harbored a RRACH motif, as expected in this type of analysis (figure R-21D).

To determine if the expression of some of the most important writers, readers and erasers of m6A changes upon BLaER1 transdifferentiation, we performed a western blot analysis of METTL3 (writer); METTL14 and WTAP (non-catalytical partners of METTL3); YTHDF2 (one reader); ALKBH5 and FTO (two erasers).

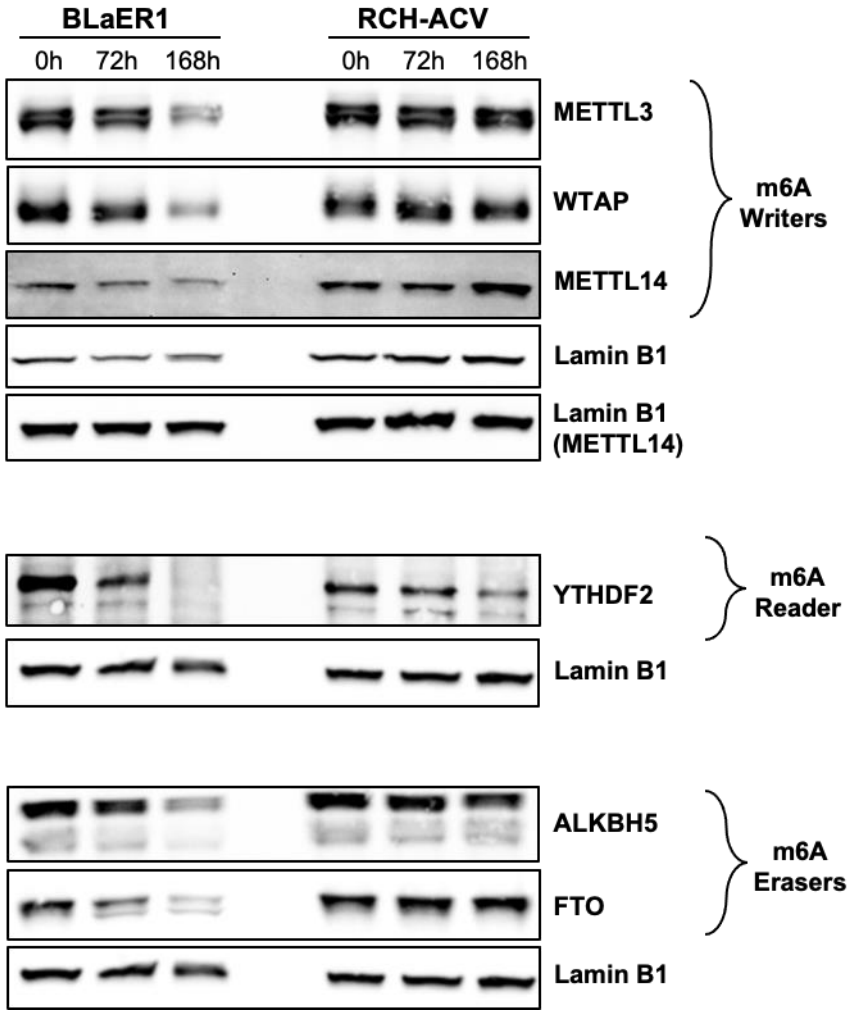

Figure R-22. Western Blot analysis of some important m6A writers, readers and erasers upon BLaER1 transdifferentiation. RCH-ACV was used as a negative transdifferentiation control.

It seems that all the writers, readers and erasers studied by Western Blot were downregulated upon BLaER1 transdifferentiation (figure R-22). This would explain why m6A cell content was decreased by only < 25% upon BLaER1 transdifferentiation (figure R-21C), although the mechanisms of compensation between these proteins cannot be explained in such simplistic forms.

To shed some light in the biological role of the detected m6A peaks, we performed a gene ontology and pathway analyses on the 3056 unique transcripts differentially methylated upon 168h of transdifferentiation (figure R-23). Both gene ontology and pathway analyses showed a significant enrichment in protein translation pathways (figure R-23, highlighted in green).

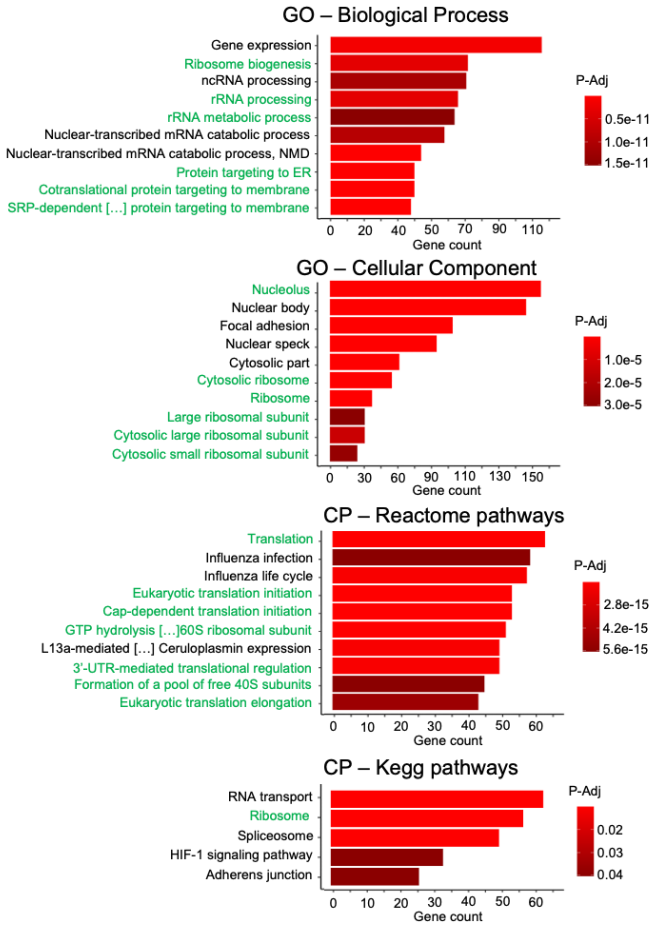

Figure R-23. Gene ontology and pathway analysis of all the 3056 unique transcripts that correspond to the 6072 differentially methylated m6A peaks upon BLaER1 transdifferentiation. Ontologies related to protein translation are highlighted in green.

To further characterize the role of these m6A modified transcripts, we divided them into m6A-upmethylated (m6A-Up) transcripts and m6A-downmethylated (m6A-Down) transcripts. Figure R-24 shows the relative position of each up/down-methylated m6A peak after 168h of BLaER1 transdifferentiation. From the 6072 significant m6A peaks, 2880 peaks (corresponding to 1664 transcripts) were upmethylated, while 3192 peaks (corresponding to 1560 transcripts) were downmethylated upon BLaER1 transdifferentiation (figure R-24). Very interestingly, m6A-Up peaks were enriched in exonic regions, while m6A-Down peaks were very enriched in intronic regions.

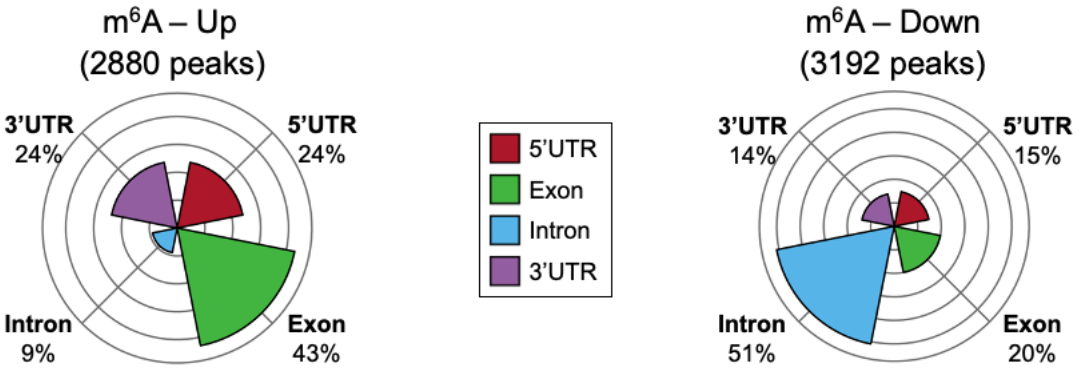

Figure R-24. Radar plots depicting the proportion of differentially methylated up/down-methylated m6A peaks at 168h of BLaER1 transdifferentiation based on their relative transcriptomic position.

To further characterize the biological role of these up/down-methylated transcripts, we performed again gene ontology and pathway analyses, this time separating m6A-Up transcripts from m6A-Down transcripts (figure R-25). Interestingly, m6A-Up transcripts were the ones enriched in translation-related ontologies, while m6A-Down transcripts did not appear to show a clear enrichment in any particular ontology, although they seemed to be more related to transcriptional and splicing regulation.

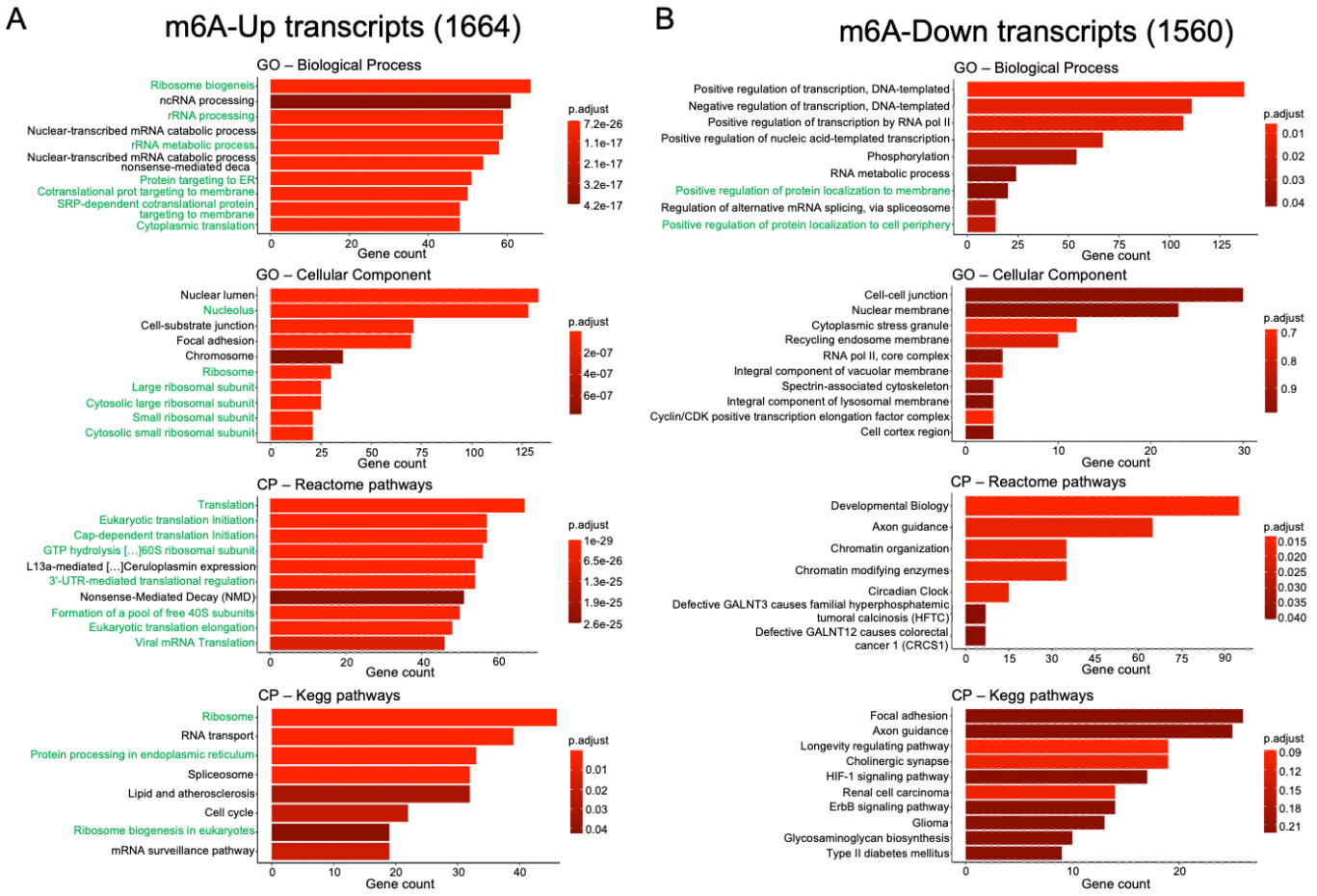

Figure R-25. Gene ontology and pathway analysis of the m6A-upmethylated (A) and m6A-downmethylated (B) transcripts that correspond to the 6072 differentially methylated m6A peaks upon BLaER1 transdifferentiation. Ontologies related to protein translation are highlighted in green.

Since most of the m6A-Up transcripts were related to translation pathways, we wondered if m6A deposition in these transcripts might have an impact in BLaER1 transdifferentiation by regulating the expression of these translation-related transcripts. To test this hypothesis, we correlated the m6A up/down-methylated transcripts with an RNA expression array (the same as in the first project) at different timepoints of transdifferentiation. A flow diagram summarizing the results of this analysis is depicted in figure R-26.

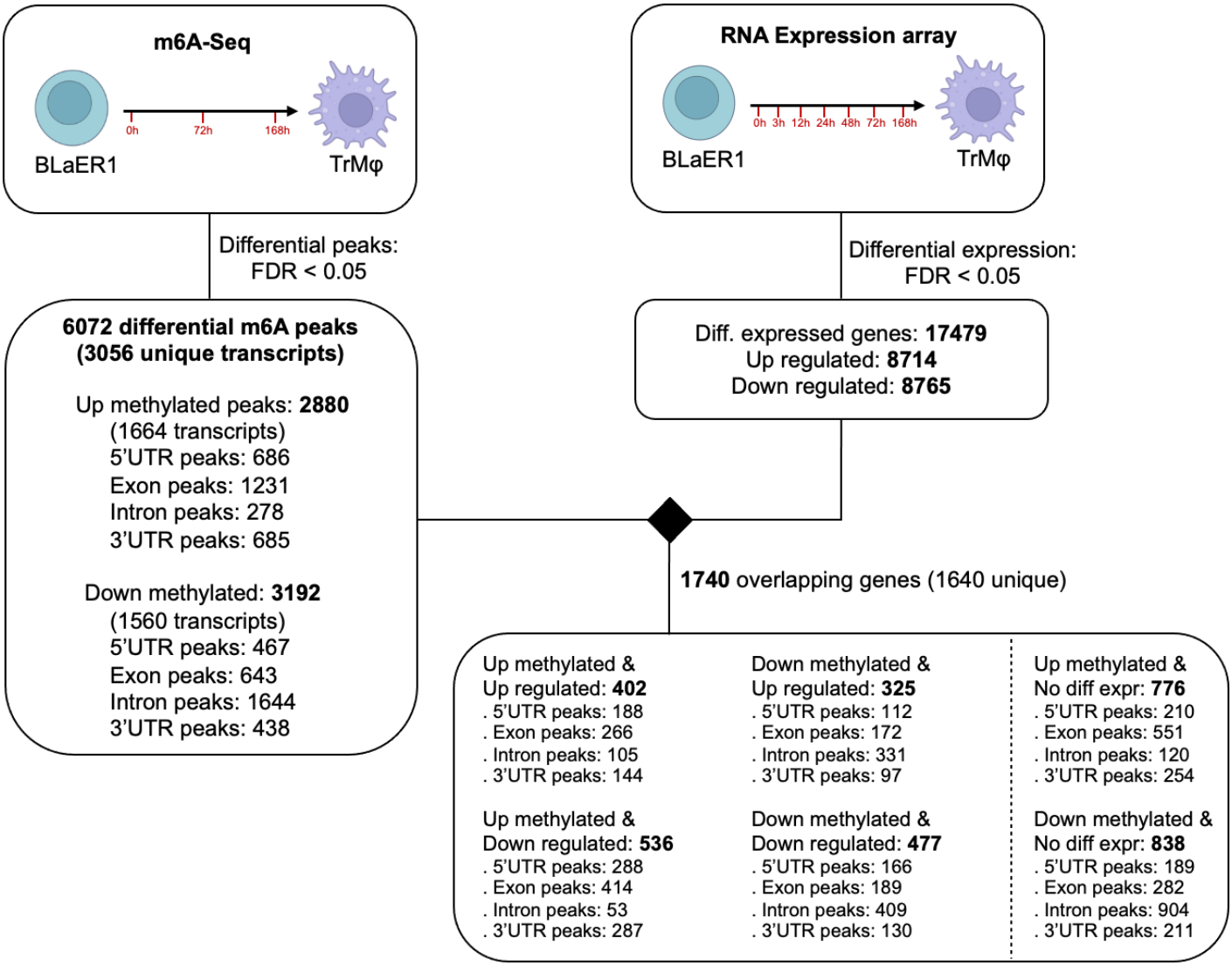

Figure R-26. Flow diagram of the correlation between m6A-Seq and RNA expression array upon BLaER1 transdifferentiation. The sum of the number of transcripts between m6A-Up and m6A-Down being greater than 3056 is explained by the fact that some transcripts lose and/or gain multiple m6A simultaneously at different molecular locations.

As seen in figure R-26, we catalogued all the combinations based on the direction of m6A methylation (Up-methylated and Down-methylated) and mRNA expression (Up-regulated and Down-regulated). Since the function of m6A depends on its relative location in the mRNA molecule, we further catalogued each m6A peak based their relative transcriptomic location (5'UTR, Exon, Intron and 3'UTR-located m6A peaks).

To ensure that losses and gains in m6A methylation were not explained by overall changes in mRNA transcription (due to possible technical limitations because of the m6A-Seq immunoprecipitation step) but by m6A deposition *per se*, we performed a 2-tailed Fisher's exact test comparing transcripts that are Up-/Down-methylated with their Up-/Down-regulation. We did not observe any overall association between the presence of m6A peaks and expression levels (P-value = 0.78), even when stratified for losses and gains of m6A vs upregulation or downregulation of the corresponding transcripts (P-value = 0.29). Thus, the integration of m6A-seq and RNA expression array data was able to correctly differentiate between loss and gain of m6A marks in existing transcripts due to controlled m6A modification versus gene expression.

Next, we determined which group of transcripts (catalogued in figure R-26) are the most enriched in translation-related functions, according to the results depicted in figure R-23 and figure R-25. In agreement with those results, we found an enrichment in down-regulated genes related to protein translation whose transcripts are m6A up-methylated at their 3'UTR upon BLaER1 transdifferentiation (Fisher's exact test, 2-tailed, P-value = 1.2 × 10e−13). In fact, in agreement with previously published literature, an increase in 3′-UTR-associated m6A was associated with transcript downregulation, taking into consideration the 742 m6A peaks that exhibited a corresponding transcript in the expression microarray (Fisher's exact test, 2-tailed, P-value=0.017).

By looking at these "3'UTR-m6A-Up & Expression-Down" transcripts, we detected up to 47 unique translation-related genes. The most abundant were ribosomal proteins (RPs): up to 29 different RP transcripts with 3'UTR-m6A up-methylation were downregulated upon BLaER1 transdifferentiation (table R-2).

We then validated by RT-qPCR the changes in gene expression of 7 of these RPs upon BLaER1 transdifferentiation (figure R-27). As expected, all these RPs were downregulated gradually after 72h and 168h of B-cell-to-macrophage conversion, correlating with the stepwise increase of 3'UTR m6A in these transcripts through time.

To further confirm that 3'UTR-m6A up-methylation was related to expression downregulation by fostering transcript instability, we performed an actinomycin chase assay to assess the time-dependent decay of RPS25 mRNA, which was the top RP with the highest m6A-up-methylation upon BLaER1 transdifferentiation (figure R-28).

Table R-2. Table depicting the 29 downregulated ribosomal protein (RP) unique transcripts with 3'UTR-m6A up-methylation upon BLaER1 transdifferentiation. RPs validated by RT-qPCR are highlighted in green. RPs with an m6A-upmethylation log2 fold change > 1.5 are highlighted in orange.

Transcript	Chromosome (hg38)	Peak Position	m6A Log2(FC)	m6A Adj.p.val	Expression Adj.p.val	Expression direction
RPS25	chr11	119015739	3.90	1.0E-05	0.013	Down
RPS23	chr5	82276164	3.39	5.7E-28	0.000	Down
MRPS23	chr17	57840967	3.31	8.3E-04	0.000	Down
RPL27	chr17	43002891	2.65	2.1E-05	0.000	Down
RPS7	chr2	3580832	2.61	7.6E-07	0.005	Down
RPL23	chr17	38850431	2.50	2.1E-19	0.030	Down
RPL23A	chr17	28723886	2.39	5.5E-05	0.000	Down
RPS12	chr6	132817499	2.39	1.9E-08	0.000	Down
RPL15	chr3	23919729	2.18	9.3E-04	0.003	Down
RPL31	chr2	101006369	2.07	9.0E-06	0.000	Down
RPS3	chr11	75405633	2.06	4.6E-10	0.000	Down
RPL36A	chrX	101395747	2.05	5.9E-03	0.000	Down
RPL24	chr3	101681188	1.83	9.2E-05	0.000	Down
RPL17	chr18	49488543	1.81	4.1E-05	0.000	Down
RPS21	chr20	62388476	1.79	1.7E-03	0.008	Down
RPL3	chr22	39312965	1.77	2.0E-09	0.000	Down
RPS6	chr9	19376369	1.75	4.2E-07	0.000	Down
RPL14	chr3	40461959	1.74	1.9E-10	0.005	Down
RPLP1	chr15	69455447	1.73	7.1E-07	0.000	Down
RPS27	chr1	153992094	1.68	3.8E-05	0.013	Down
RPL14	chr3	40461487	1.64	1.6E-11	0.005	Down
RPS14	chr5	150444333	1.64	8.9E-05	0.000	Down
RPL35A	chr3	197954087	1.64	2.8E-05	0.000	Down
RPS17	chr15	82538352	1.61	3.2E-05	0.028	Down
RPS3	chr11	75402407	1.52	3.4E-08	0.000	Down
RPL35A	chr3	197955769	1.47	9.4E-03	0.000	Down
RPL19	chr17	39203056	1.47	1.2E-10	0.000	Down
RPLP2	chr11	812779	1.43	1.7E-04	0.000	Down
RPL14	chr3	40461639	1.38	1.6E-07	0.005	Down
RPL11	chr1	23696363	1.36	7.0E-04	0.009	Down
RPS9	chr19	54207527	1.30	5.7E-05	0.039	Down
RPS27A	chr2	55235469	1.12	5.2E-04	0.043	Down
RPS24	chr10	78040634	1.01	2.4E-04	0.001	Down
RPS24	chr10	78037241	0.83	2.5E-06	0.001	Down

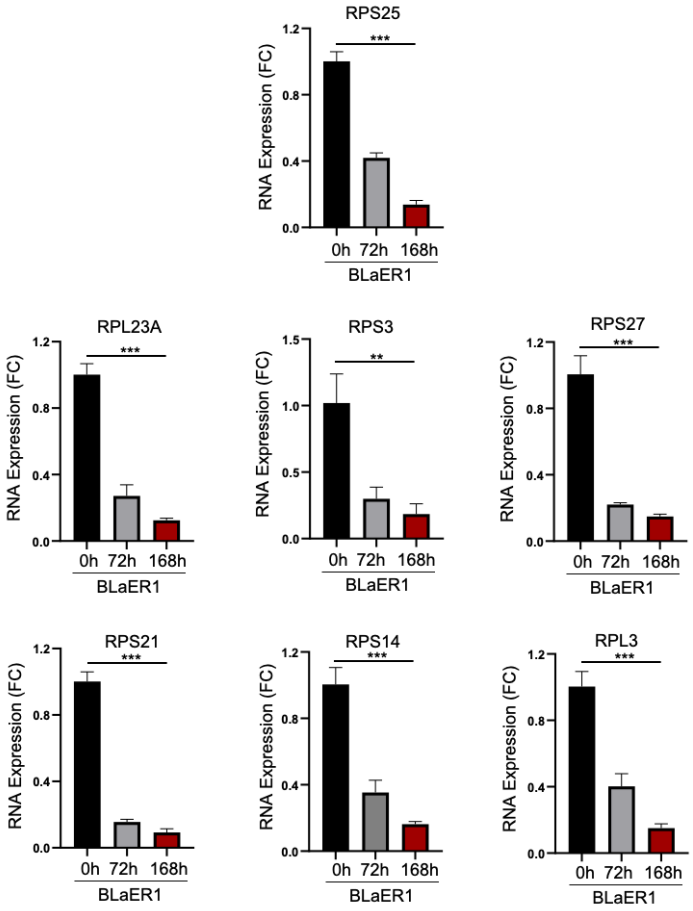

Figure R-27. RT-qPCR expression validation of the 7 selected downregulated ribosomal proteins (RPs) with 3'UTR-m6A up-methylation upon BLaER1 transdifferentiation. T-Student test (P-Value Significances: * < 0.05, ** < 0.001, *** < 0.0001)

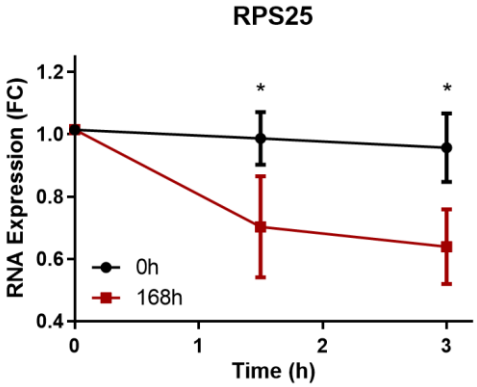

Figure R-28. Actinomycin chase assay on RPS25 mRNA at 0h and 168h of BLaER1 transdifferentiation. T-Student test (P-Value Significances: * < 0.05)

By looking at figure R-28, we can observe that RPS25 mRNA decay was faster at 168h of BLaER1 transdifferentiation, which correlated with an increase in 3'UTR-m6A methylation at this transcript. All these results indicated that the m6A epitranscriptome drastically changed upon BLaER1 transdifferentiation. Specifically, there is a significant enrichment in ribosomal protein (RP) transcripts that were m6A-upmethylated at their 3'UTRs, correlating with an increased RP mRNA decay.

METTL3 depletion impairs BLaER1 transdifferentiation by stochastically blocking B-cell-to-macrophage conversion

To determine if m6A regulates B-cell-to-macrophage transdifferentiation, we generated a constitutive METTL3 knockdown (KD) model (shRNA-based) on BLaER1 cells (figure R-29).

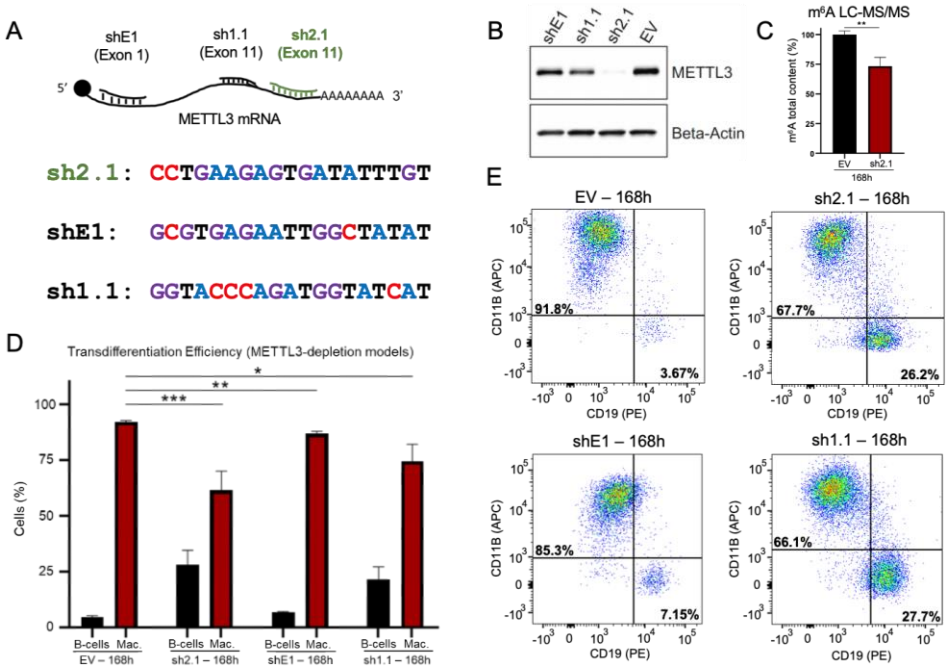

Figure R-29. (A) Design of 3 shRNA against METTL3. The final selected shRNA is highlighted in green. (B) Western Blot of METTL3 on METTL3-KD untransdifferentiated BLaER1 selected clones. (C) m6A abundancy of EV and sh2.1 METTL3-depletion BLaER1 model at 168h of transdifferentiation, quantified by LC-MS/MS. T-Student test (P-Value Significances: * < 0.05, ** < 0.001) (D) Transdifferentiation efficiency of BLaER1 METTL3-depletion models. (E) Flow cytometry of some biological replicates of METTL3-KD models. CD19: B-cell surface marker; CD11b: Macrophage surface marker.

The shRNA-mediated knockdown (KD) of METTL3 (figure R-29A) successfully depleted METTL3 protein levels, especially with the sh2.1 shRNA (figure R-29B). We confirmed by LC-MS/MS that METTL3 depletion led to a significant decrease in m6A cell content (figure R-29C). Much to our surprise, METTL3-KD impaired transdifferentiation efficiency upon BLaER1 transdifferentiation (figures R-29D/E). Intriguingly, sh1.1-mediated protein depletion of METTL3 was less efficient than sh2.1 (figure R-29B), but the impairment in the efficiency of BLaER1 transdifferentiation was very similar for both shRNAs, although with higher variability for sh1.1 (figures R29-D/E). This could be explained by the fact that, even though protein levels were more depleted in sh2.1 model, the effect of METTL3 depletion on transdifferentiation efficiency reached a plateau that was independent on METTL3 protein levels. Nevertheless, we selected sh2.1 depletion model to perform the next set of experiments, since sh2.1 shRNA is the most efficient in depleting METTL3 protein levels (figure 29-B).

To further confirm that METTL3 depletion impaired transdifferentiation efficiency (and was not due to possible shRNA off-targets), we performed a recovery assay by overexpressing an sh2.1-insensitive version of METTL3 (without the 3'UTR region targeted by the sh2.1 shRNA) on the sh2.1 METTL3-depletion BLaER1 model, to test if the transdifferentiation efficiency returned to normal (figure R-30). We selected 2 METTL3 recovery BLaER1 models ("low" and "high" expression METTL3 recovery clones) and an empty vector control (figure R-30A), all of them expressing tdTomato as an intensity selection marker (figure R-30B). As expected, METTL3 overexpression in the METTL3-depletion BLaER1 model recovered transdifferentiation efficiency in a dose-dependent manner (figures R-30C/D), confirming the role of METTL3 in regulating BLaER1 B-cell-to-macrophage transdifferentiation.

In addition, we interrogated the RNA expression of other additional B-cell and macrophage differentiation markers by RT-qPCR and flow cytometry to fully confirm the impairment in transdifferentiation efficiency mediated by METTL3 depletion (figure R-31A/B). As expected, sh2.1 METTL3-depletion BLaER1 model displayed a deregulated expression in differentiation markers when compared to EV (lower expression on macrophage markers and higher expression in B-cell markers upon transdifferentiation).

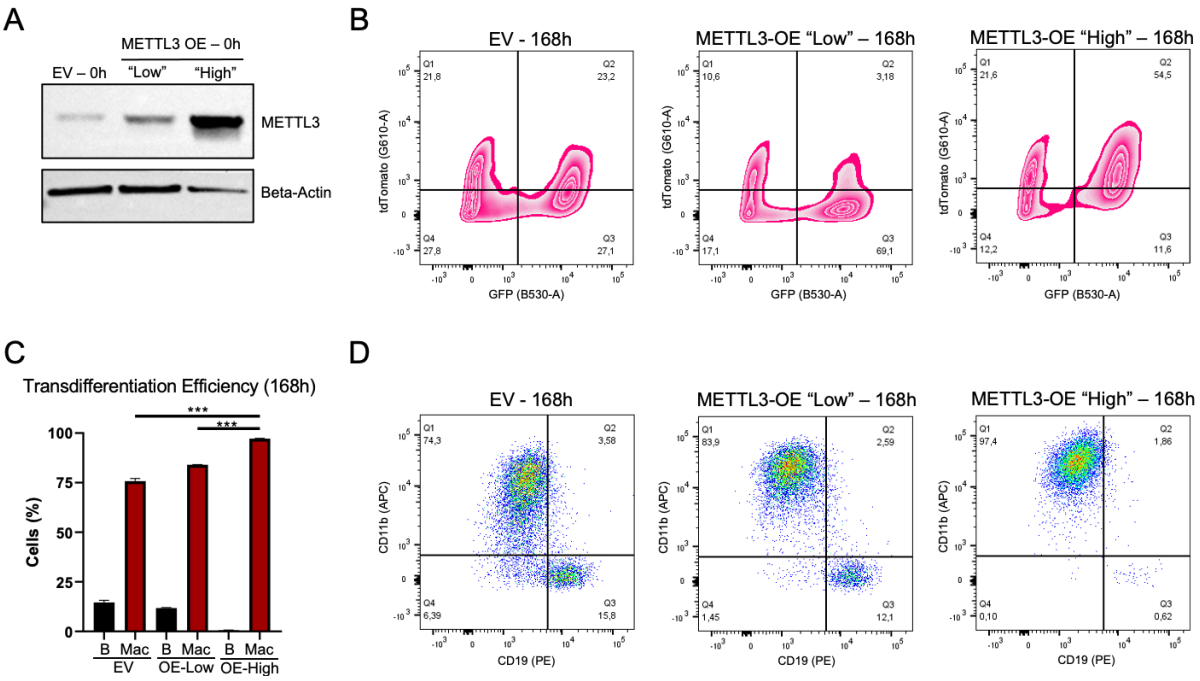

Figure R-30. (A) Western blot of METTL3 on untransdifferentiated METTL3-recovery sh2.1 BLaER1 model. Two different sh2.1-BLaER1 clones of METTL3-recovery were selected, based on their recovered METTL3 expression (low expression and high expression), plus one empty vector (EV) sh2.1 BLaER1 clone. (B) tdTomato-GFP flow cytometry assay on empty vector (EV) and METTL3-recovery BLaER1 models. Quadrant Q2 indicates tdTomato+/GFP+ double positives, with the associated percentage of double positive cells. All the BLaER1 cells were GFP+, so GFP acted as a survival marker. tdTomato intensity correlated with METTL3-recovery expression (the more intense was tdTomato signal, the more METTL3 it expressed). (C) Transdifferentiation efficiencies of the EV and the 2 METTL3-recovery BLaER1 clones. B: B-cells; Mac: Macrophages. T-Student test (P-Value Significances: * < 0.05, ** < 0.001, *** < 0.0001) (D) Flow cytometry of some biological replicates of EV and METTL3-recovery BLaER1 models. CD19: B-cell surface marker; CD11b: Macrophage surface marker.

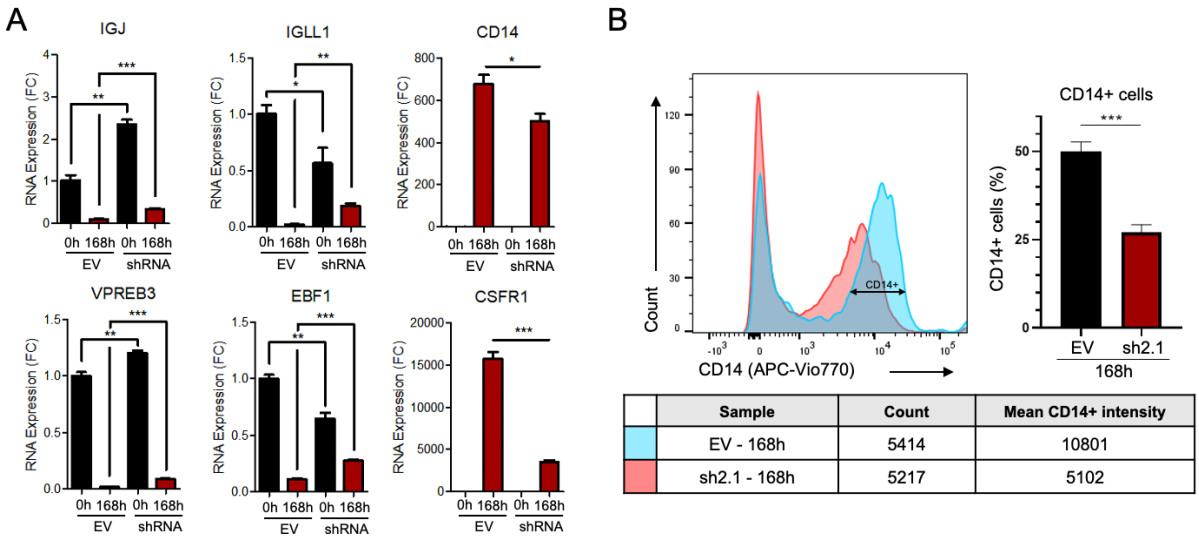

	Sample	Count	Mean CD14+ intensity
	EV - 168h	5414	10801
	sh2.1 - 168h	5217	5102

Figure R-31. (A) RT-qPCR analysis of various B-cell (IGJ, IGLL1, VPREB3 and EBF1) and macrophage (CD14 and CSFR1) differentiation markers at 0h and 168h of transdifferentiation in EV and sh2.1 METTL3-depletion BLaER1 models. (B) Flow cytometry analysis of CD14 (macrophage marker) on EV and sh2.1 METTL3-depletion BLaER1 models upon 168h of transdifferentiation. T-Student test (P-Value Significances: * < 0.05, ** < 0.001, *** < 0.0001)

To further characterize the phenotype of the METTL3-depletion model upon B-cell-to-macrophage conversion, we performed growth, cell cycle and apoptosis assays on EV vs sh2.1 METTL3-depletion BLaER1 models (figure R-32). Contrary to our expectations, METTL3-depleted sh2.1 BLaER1 cells displayed increased growth upon cell transdifferentiation in comparison to wildtype and EV BLaER1 (figure R-32A). In fact, METTL3-depleted sh2.1 cells manifested increased cellular division, with more cells in S phase (figure R-32B) and a decrease in cell apoptosis (figure R-32C/D), as shown by annexin-V assay and by caspases immunoblot analyses.

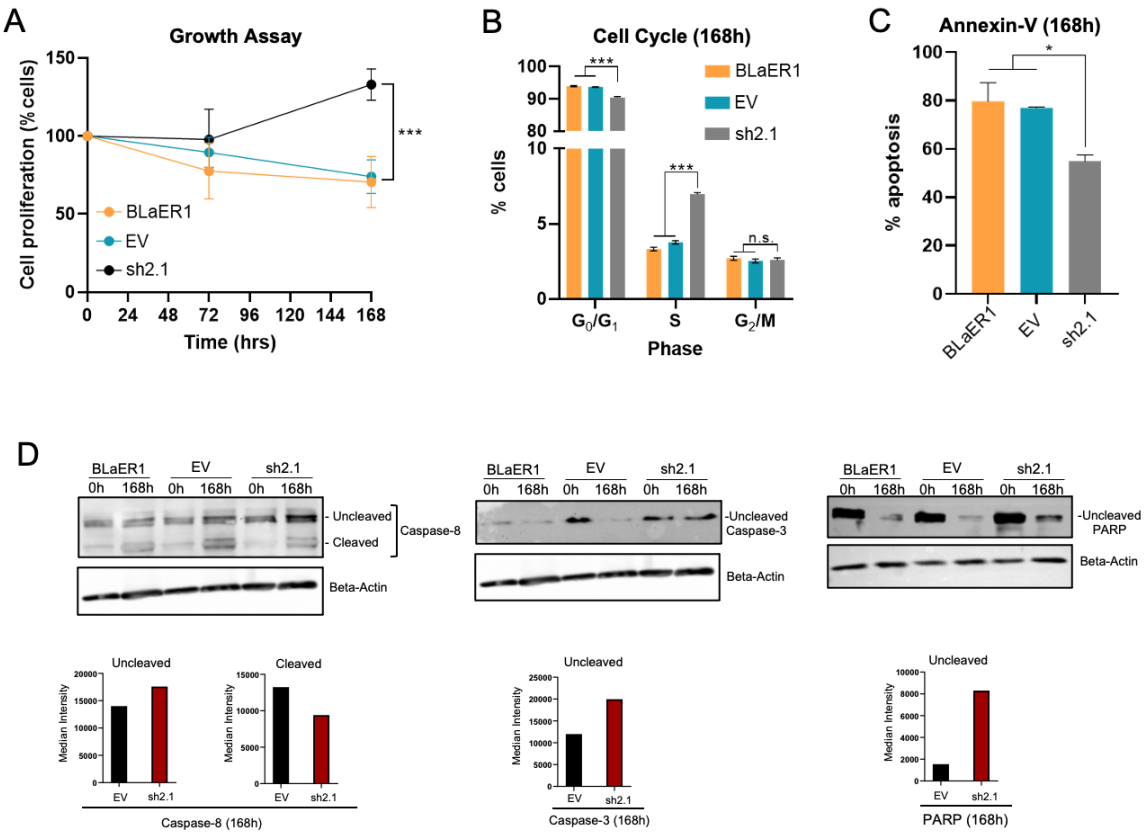

Figure R-32. (A) Trypan blue-assisted growth assay of wildtype BLaER1, empty vector BLaER1 (EV) and sh2.1 shRNA-METTL3 depletion BLaER1 model (sh2.1) at 0h, 72h and 168h of transdifferentiation. (B) Propidium iodide-assisted cell cycle assay of BLaER1, EV and sh2.1. (C) Annexin-V flow cytometric apoptosis assay (biological triplicates) of BLaER1, EV and sh2.1 cells at 168 hours of transdifferentiation. (D) Top, Western Blot analysis of apoptosis markers of BLaER1, EV and sh2.1 cells at 0 and 168 hours of transdifferentiation. Below, densitometric quantification of the Western Blot analysis. T-Student test (P-Value Significances: * < 0.05, ** < 0.001, *** < 0.0001).

Wildtype and EV BLaER1 cells stopped growing upon transdifferentiation (figure R-32A), considering that the newly generated macrophages stopped dividing (macrophages enter in a quiescent state). Thus, there were 2 possible hypothesis that could explain the increase in cell growth displayed by the sh2.1 METTL3-depletion model: (1) METTL3 depletion led to an stochastic transdifferentiation blockade, in which some leukemic B-cells in culture could not be converted to macrophages and, thus, they kept dividing; (2) METTL3-depletion did

not lead to a transdifferentiation blockade, but rather made transdifferentiation slower, thus needing more than 168h to completely transdifferentiate every cultured leukemic B-cell. To decide which hypothesis fits the best, we transdifferentiated sh2.1 METTL3-depleted BLaER1 cells for 240h (10 days) instead of only 168h (7 days), to test whether the leukemic B-cells completely transdifferentiate or they keep dividing. Flow cytometry analysis of CD19 (B-cell marker) and CD11b (macrophage marker) at 168h and 240h showed that leukemic B-cells that did not transdifferentiate at 168h kept dividing, thus confirming the first hypothesis: METTL3 depletion led to an stochastic transdifferentiation blockade (figure R-33).

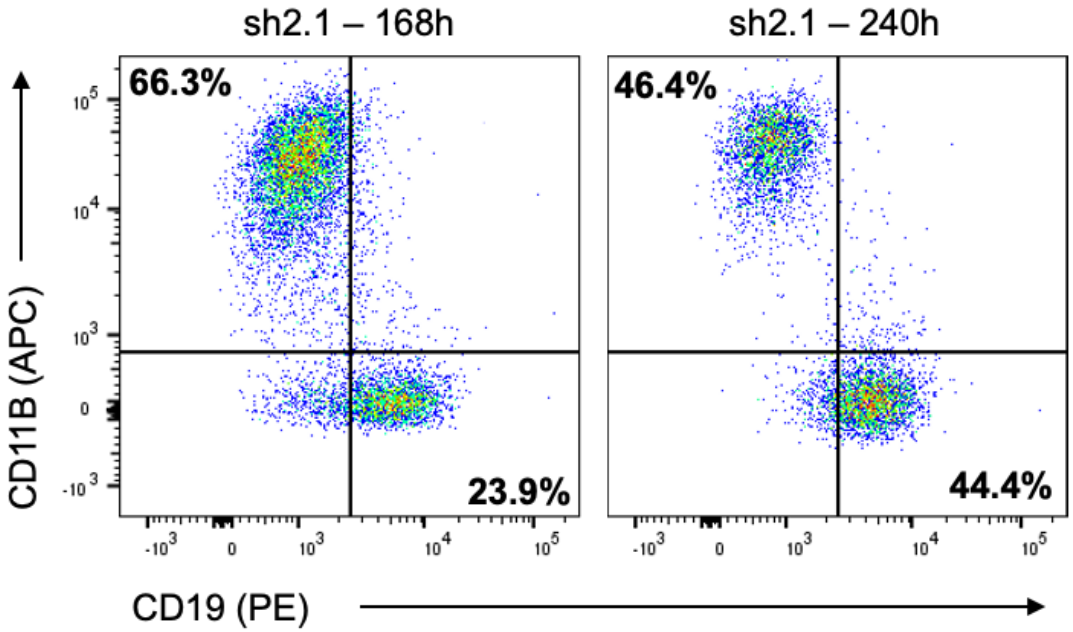

Figure R-33. Flow cytometry assay of CD19 (B-cell marker) and CD11b (macrophage marker) at 168h and 240h on sh2.1 METTL3-depletion BLaER1 model, showing a percentage increase in leukemic B-cells and a percentage decrease in macrophages after 240h of transdifferentiation, indicating that METTL3 depletion led to a stochastic transdifferentiation blockade and, thus, leukemic B-cells that didn't transdifferentiate kept dividing.

METTL3 depletion led to ribosomal protein deregulation in BLaER1 transdifferentiation model

Since wildtype BLaER1 transdifferentiation led to an increase in 3'UTR-m6A methylation on ribosomal protein (RP) transcripts and this upmethylation was correlated with a decrease in transcript stability and a lower expression, we wanted to analyze the effects of METTL3 depletion on these RPs during B-cell-to-macrophage conversion. As expected, METTL3 depletion led to an upregulation of the previously analyzed 7 RPs (figure R-34). Concordantly, actinomycin assay of RPS25 (the top RP with the highest m6A-upmethylation upon BLaER1 transdifferentiation) on sh2.1 METTL3-depletion model revealed that METTL3 depletion led to an increased RPS25 mRNA stability, as expected (figure R-35).

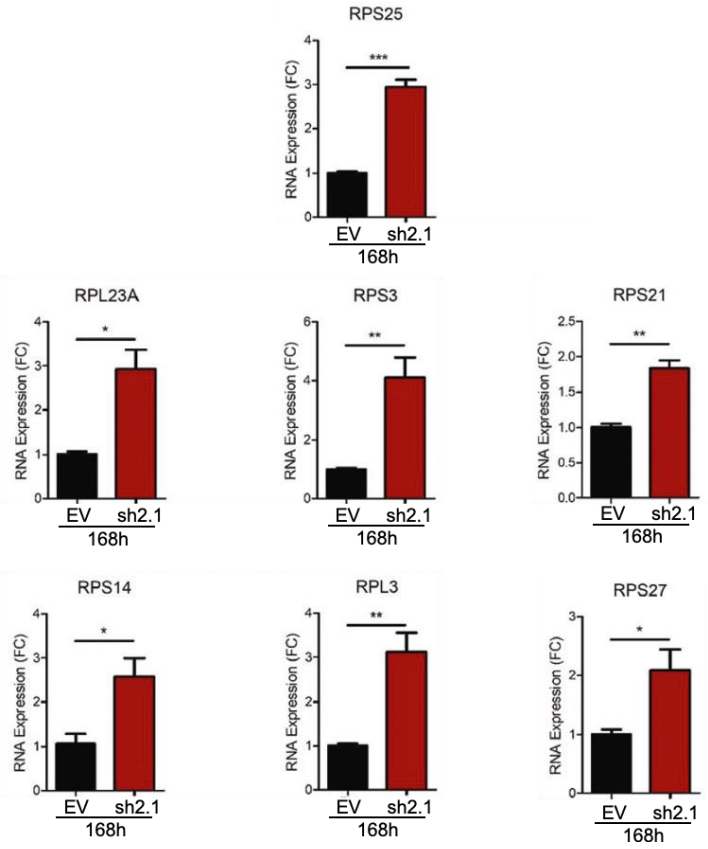

Figure R-34. RT-qPCR expression validation of the 7 selected downregulated ribosomal proteins (RPs) with 3'UTR-m6A up-methylation upon EV and sh2.1 METTL3-depletion BLaER1 model transdifferentiation. T-Student test (P-Value Significances: * < 0.05, ** < 0.001, *** < 0.0001).

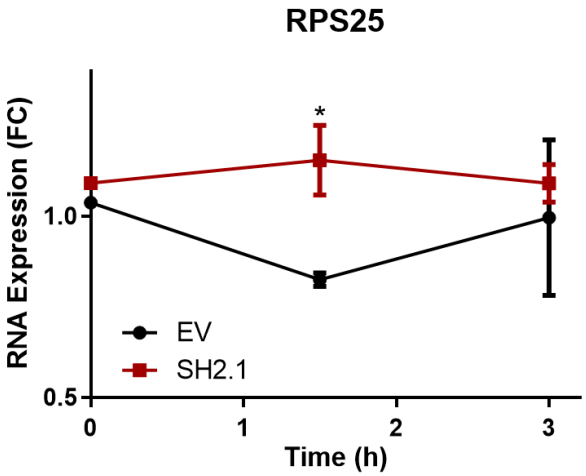

Figure R-35. Actinomycin chase assay on RPS25 mRNA at 168h of EV and sh2.1 METTL3-depletion model transdifferentiation. T-Student test (P-Value Significances: * < 0.05)

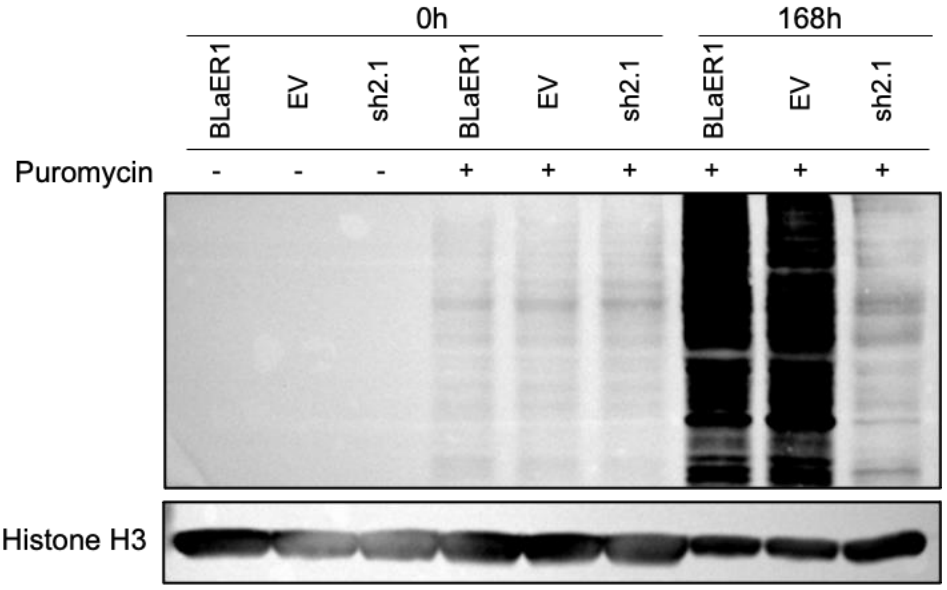

Figure R-36. Puromycin immunoblot of assay of wildtype BLaER1 (BLaER1), pLKO.1-TRC empty vector BLaER1 (EV) and shRNA-METTL3 BLaER1 (sh2.1) at 0 and 168 hours of transdifferentiation, showing great global translational impairment in METTL3 knockdown cells (sh2.1), which could be explained by deregulation in various ribosomal proteins levels upon METTL3 depletion.

To understand the implications of METTL3 depletion on global protein synthesis, we performed a puromycin assay, which allowed to quantify global protein synthesis after the addition of puromycin to cells in culture (figure R-36). We observed a very significant impairment in global protein synthesis on the sh2.1 METTL3-depletion BLaER1 model at 168h of transdifferentiation. This global protein synthesis impairment correlated with the deregulation of RP transcript expression and stability upon METTL3 depletion (figures R-34 and R-35). At first sight, these results may seem contradictory, since one might expect an increase in global protein synthesis after the METTL3 knockdown-mediated upregulation of RP transcript expression. Nevertheless, to ensure a correct global protein synthesis, it is necessary to maintain the correct proportions of RPs (neither over- nor under-expressed) to allow the proper assembly and function of ribosomes [177].

Since sh2.1 METTL3-depleted BLaER1 cells were a mixture of macrophages and leukemic B-cell in culture after 168h of transdifferentiation (~25% B-cells and ~75% macrophages), we wanted to confirm that RP expression deregulation really occurs in macrophages and is not a “shielding effect” produced by the untransdifferentiated leukemic B-cells in the cell mixture. Thus, we sorted EV and sh2.1 168h-transdifferentiated macrophages (CD19-/CD11b+ cells) by flow cytometry and performed an RT-qPCR of the 7 significant RPs (figure R-37) and of some B-cell and macrophage differentiation markers (figure R-38). We observed that sorted sh2.1 macrophages after 168h of transdifferentiation also exhibited a higher expression of 4 of the 7 RPs (RPS25, RPS21, RPS14 and RPL3) when compared to sorted EV macrophages, although the 3 non-significant RPs (RPL23A, RPS3 and RPS27) showed a clear tendency towards upregulation in sh2.1 macrophages (figure R-37). In addition, both B-cell markers (IGJ and VPREB3) were significantly more expressed in sorted sh2.1 macrophages, while the macrophage marker (CD14) was less expressed in these sh2.1 macrophages when compared to the sorted EV macrophages, indicating that sh2.1 METTL3-depleted BLaER1 cells were not properly differentiated towards the macrophage lineage after 168h of transdifferentiation (figure R-38).

This global protein synthesis and RP deregulation may have an impact not only in the transdifferentiation efficiency but also in the function of the converted macrophages. Thus, we performed a dsRed^{+} *E.coli* phagocytosis assay on EV and sh2.1 METTL3-depletion BLaER1 models (figure R-39A). The phagocytosis efficiency of METTL3-depleted macrophages (sh2.1) was significantly impaired in comparison to EV macrophages (figure R-39B/C).

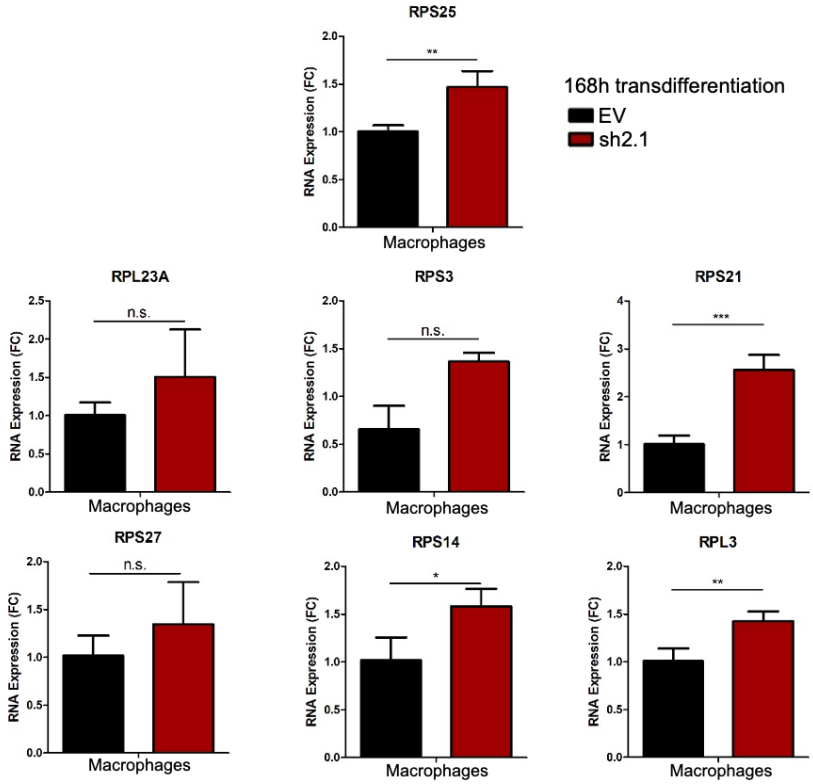

Figure R-37. RT-qPCR expression of the 7 selected downregulated ribosomal proteins (RPs) with 3'UTR-m6A up-methylation on sorted EV macrophages and sorted sh2.1 macrophages upon 168h of transdifferentiation. T-Student test (P-Value: * < 0.05, ** < 0.001, *** < 0.0001).

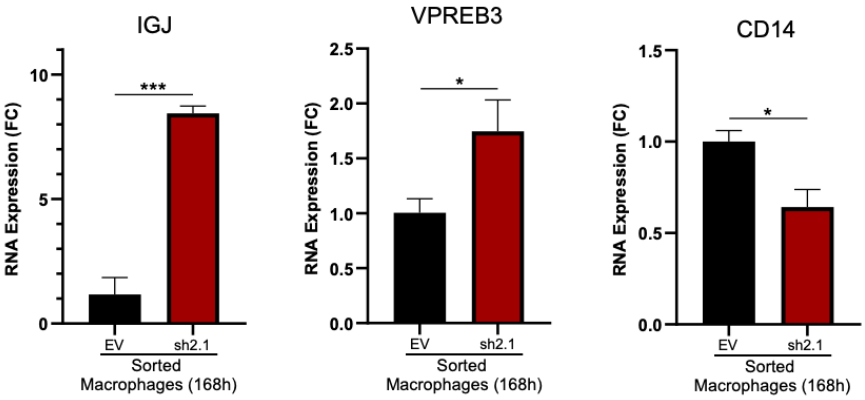

Figure R-38. RT-qPCR expression of 2 B-cell markers (IGJ and VPREB3) and 1 macrophage marker (CD14) on sorted EV macrophages and sorted sh2.1 macrophages upon 168h of transdifferentiation. T-Student test (P-Value: * < 0.05, ** < 0.001, *** < 0.0001).

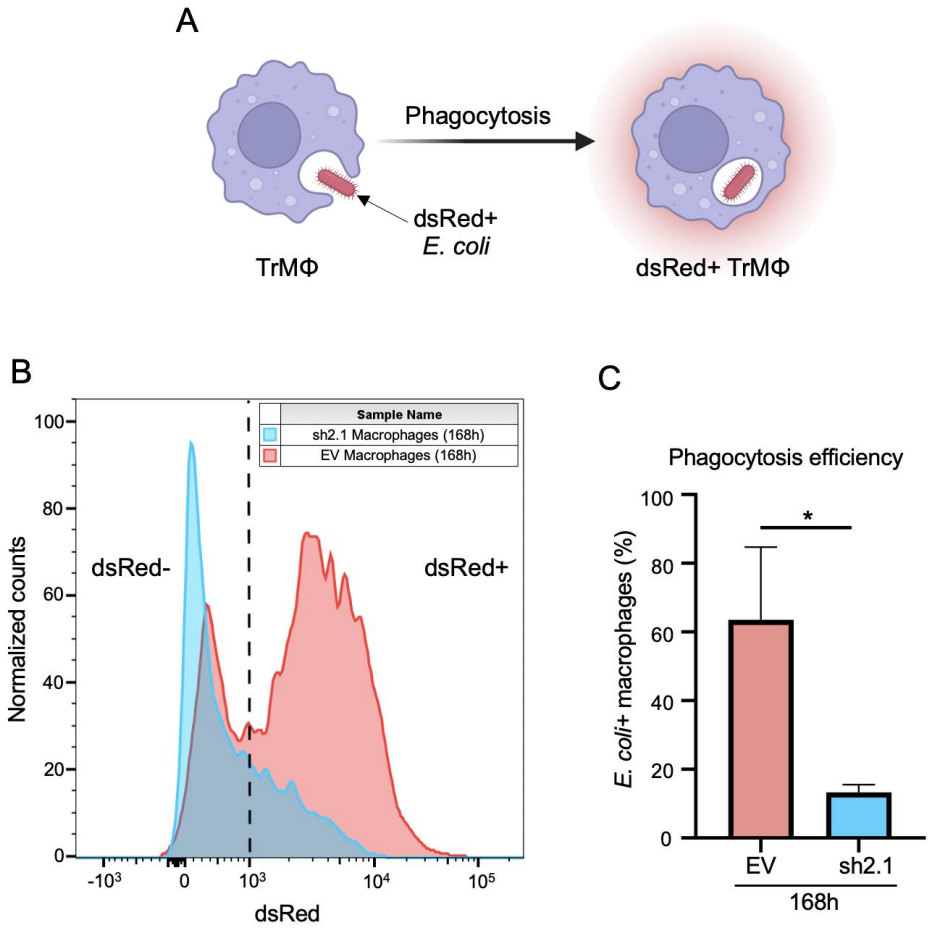

Figure R-39. dsRed+ *E. coli* phagocytosis assay on METTL3-depletion BLaER1 model. (A) Phagocytosis assay experimental design. (B) Representative flow cytometry histogram of 168h-transdifferentiated macrophages ($CD19^-/CD11b^+$) on sh2.1 shRNA-METTL3 and EV BLaER1 models. dsRed intensity positively correlates with the phagocytic competence of the transdifferentiated macrophages. (C) Barplot depicting the phagocytosis efficiency of EV and sh2.1 BLaER1 transdifferentiated macrophages. T-Student test (P-Value: * < 0.05).

All these results indicated that METTL3 depletion led to RP deregulation and global protein synthesis impairment, which may not only explain the impairment on BLaER1 transdifferentiation efficiency (~25% efficiency reduction), but also the commitment and function of those macrophages that did transdifferentiate, demonstrating that METTL3 (an m6A writer) was crucial for B-cell-to-macrophage transdifferentiation.

METTL3 inhibitor (STM2457) impaired transdifferentiation efficiency and deregulated ribosomal protein RNA expression

To further prove that m6A is important for B-cell-to-macrophage transdifferentiation and to add a potential clinical/translational value to our work, we used the small molecular METTL3 inhibitor named STM2457 (STM), developed by Storm Therapeutics LTD (Cambridge, UK) in 2021 (figure R-40A) [167]. STM is highly specific for METTL3, competitively binding to its SAM-binding site and thus inhibiting its catalytical methyltransferase activity (figure R-40B). We tested STM on untransdifferentiated BLaER1 cells for 72h at different concentrations to assess the half-maximal inhibitory concentration (IC50) of the compound (figure R-40C). In addition, to confirm that STM inhibits m6A deposition by METTL3, we performed an LC-MS/MS of m6A on transdifferentiated BLaER1 cells (168h) treated 12 hours with a non-lethal dose (5 μM, >90% viability) of STM (figure R-40D). As expected, a significant drop in m6A content was observed upon STM treatment (figure R-40D).

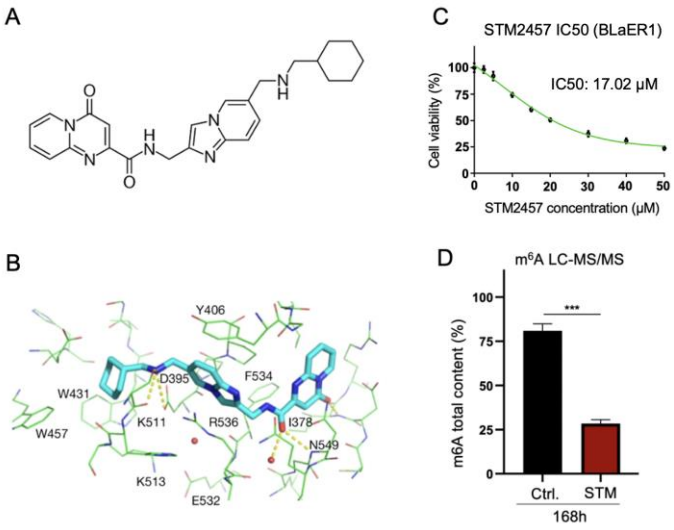

Figure R-40. Molecular characterization of STM2457. (A) STM2457 (STM) chemical structure. (B) Crystal structure of STM (blue) bound to METTL3 SAM-binding site (green). Hydrogen bonds (yellow lines) and water molecules (red spheres) are shown (Protein Data Bank (PDB) ID: 7O2I). Figure retrieved from Yankova E. et al (Nature, 2021) [167]. (C) IC50 assay of STM on untransdifferentiated BLaER1 cells. IC50: 17.02 μM (D) LC-MS/MS of m6A on BLaER1 untreated (BLaER1) and treated (STM) with a non-lethal dose (5 μM, >90% viability) of STM for 12h after 168h of transdifferentiation.

Then, we treated BLaER1 cells with a non-lethal dose of STM (5 μM, >90% viability) at the start of transdifferentiation induction (0h) to determine if B-cell-to-macrophage conversion is impaired as seen with the shRNA-METTL3 depletion model (figure R-41). STM was able to impair transdifferentiation efficiency (figure R-41B) and to deregulate the expression of 2 key macrophage differentiation markers (figure R-41C).

In addition, we transdifferentiated BLaER1 cells (without adding an initial 0h STM dose) and added a single non-lethal dose of STM (5 μM, >90% viability) at 168h of transdifferentiation for 12 hours to determine if m6A depletion in macrophages would affect the mRNA expression of the ribosomal proteins (RPs) that increase 3'UTR-associated m6A upon BLaER1 transdifferentiation. As expected, STM induced a significant increase in expression on most of the studied RPs (figure R-42).

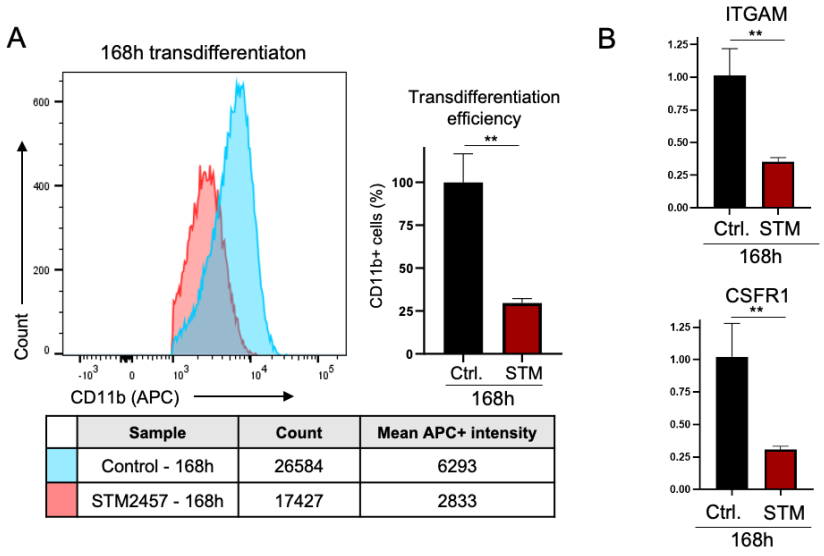

	Sample	Count	Mean APC+ intensity
	Control - 168h	26584	6293
	STM2457 - 168h	17427	2833

Figure R-41. STM2457 effects on BLaER1 transdifferentiation (A) Quantification of m6A by LC-MS/MS on BLaER1 cells untreated (Ctrl.) and treated (STM) with STM2457 (STM) for 168h of transdifferentiation. Percentage of m6A total content is relative to untransdifferentiated (0h) BLaER1 (100%). (B) Flow cytometry analysis of $CD19^{-}$/CD11b+ cells after 168h of transdifferentiation on treated (STM) and untreated (control) BLaER1 cells. The efficiency of transdifferentiation is represented in the barplot next to the cytogram. (C) RT-qPCR RNA expression analysis on 2 macrophage differentiation markers (ITGAM and CSFR1) after 168h of transdifferentiation in untreated (Ctrl.) and treated (STM) BLaER1 cells.

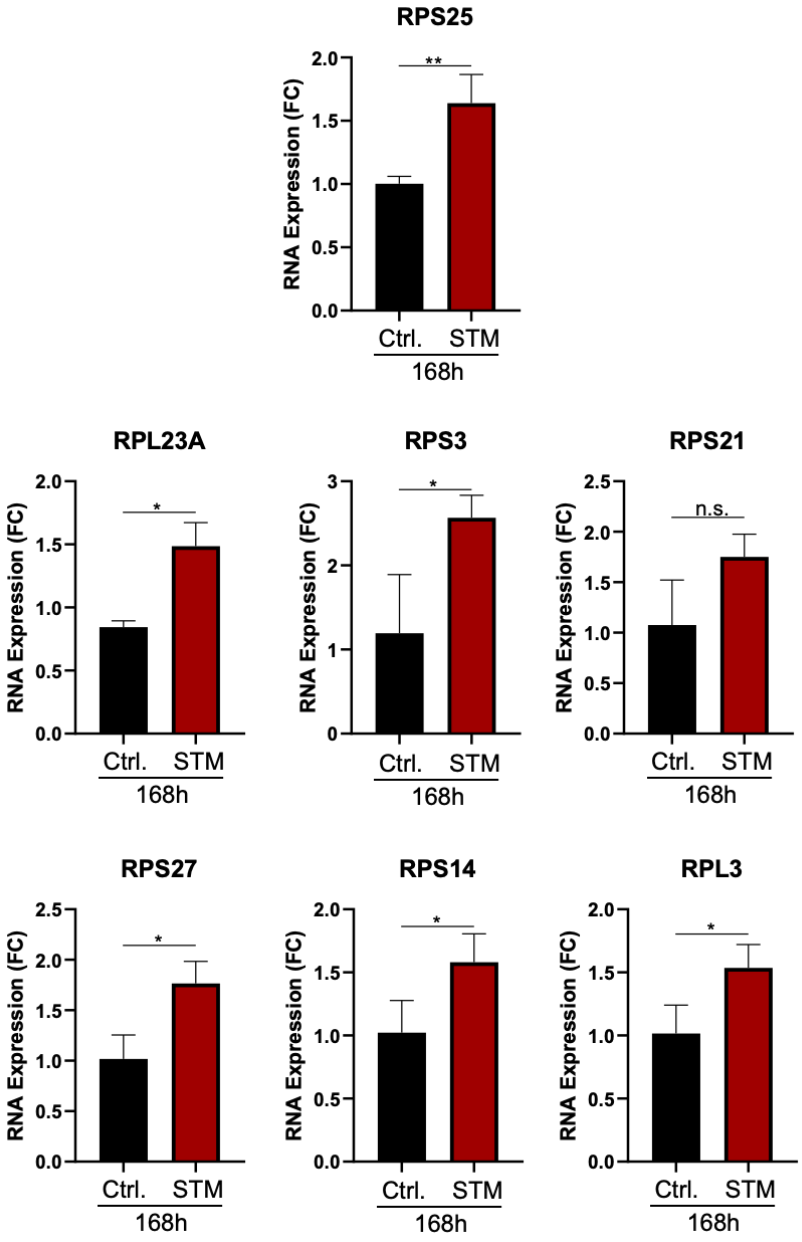

Figure R-42. RT-qPCR expression validation of the 7 selected downregulated ribosomal proteins (RPs) with 3'UTR-m6A up-methylation upon EV and sh2.1 METTL3-depletion BLaER1 model transdifferentiation. T-Student test (P-Value Significances: * < 0.05, ** < 0.001).

The results obtained with STM2457 (STM) confirmed that m6A has an important role in B-cell-to-macrophage transdifferentiation and in regulating the mRNA expression of important ribosomal proteins. Thus, STM could be considered as an interesting candidate in the treatment of clinical cases with malignant transdifferentiation.

***

The results of this second project confirm that m6A epitranscriptome drastically changes upon B-cell-to-macrophage transdifferentiation. Throughout this process, many different types of transcripts lose and gain m6A at different molecular positions (5'UTR, Intron, Exon or 3'UTR). mRNA molecules with m6A upmethylation at 3'UTR are enriched in ribosomal protein transcripts, resulting in an increased transcript instability. On the other hand, METTL3 depletion increases the stability of those transcripts, dysregulating global protein synthesis and provoking a stochastic transdifferentiation blockade.

This second work was published in the journal *Leukemia*, under the title "*Remodeling of the m6A RNA landscape in the conversion of acute lymphoblastic leukemia cells to macrophages*" [178].

DISCUSSION

FIRST PROJECT DISCUSSION

DNA 5mC methylation changes in leukemic transdifferentiation

Local rather than global changes in DNA methylation occur during B-cell-to-macrophage transdifferentiation

Cells that undergo transdifferentiation must overcome important epigenetic barriers in a relative short period of time to successfully achieve lineage reprogramming [179–181]. An important question arising from this issue is whether (1) the reprogrammed cells need to entirely change their epigenome at a global, genome-wide scale to completely switch lineages (acquiring an epigenetic background as close as possible to the parental cell of the new lineage) or (2) they just need to reshape their epigenome at specific, discrete genomic positions, which will be sufficient to trigger and settle the lineage switch, without the need of mimicking the whole epigenome of the new parental cell lineage. Thus, to analyze the DNA methylation fluctuations upon pre-B-ALL-cell-to-macrophage transdifferentiation at a genome-wide scale, we interrogated the DNA methylation state of ~ 850,000 CpGs at different time-points of BLaER1 transdifferentiation (0h, 3h, 12h, 24h, 48h, 72h, and 168h) using the 850k-EPIC Illumina DNA methylation array. We have only detected 251 significant differentially methylated CpGs (absolute $\Delta\beta \geq 0.66$, lineal time regression adjusted P-Value < 0.05), 250 of which were demethylated upon this process (figure R-5). This small number of differentially methylated CpGs indicate that changes in DNA methylation during B-cell-to-macrophage transdifferentiation occur at local, discrete positions, rather than at a global scale (figures R-2, R-3 and R-5). Furthermore, the lack of global changes in DNA methylation heavily contrasts with the substantial fluctuations in gene expression upon transdifferentiation, indicating that, at a global perspective, changes in gene expression precede the changes in DNA methylation upon B-cell-to-macrophage transdifferentiaton (figure R-4).

Although there is a significant scarcity of scientific works addressing the relationship between DNA methylation and transdifferentiation, most of them seem to be in accordance with our findings: in hepatocyte-to-pancreatic-cell *in vitro* transdifferentiation (induced by forcing ectopic expression of several pancreatic transcription factors), only 201 CpGs are found to be differentially methylated upon transdifferentiation (detected by using the 450k Illumina DNA methylation array), where the majority of them are demethylated and located

at important pancreatic-specific genes [182]. In addition, a murine B-cell-to-macrophage *in vitro* transdifferentiation model did not show global changes in DNA methylation upon conversion, but rather specific local demethylation at key differentiation and macrophage-specific genes [183]. In contrast, fibroblast-to-neuron *in vitro* transdifferentiation has shown 10,000-to-15,000 differentially methylated CpGs upon 22 days of transdifferentiation [184]; this higher number of differentially methylated CpGs could be explained by the fact that fibroblasts and neurons have a different germ layer origin (medoserm and ectoderm, respectively), while the other two transdifferentiation cases share the same germ layer origin (e.g. B-cell and macrophages are both mesodermic), since most of the DNA methylation patterns are already established during the establishment of the 3 germ layers [185].

Additionally, it might be possible that, if the experiment had lasted longer (much more than only 168 hours), we would have observed more significant changes in 5mC DNA methylation, which would act not as an early driver of gene expression changes, but rather as a *posteriori* maintenance mechanism that ensures the perpetuation of the new global gene expression pattern. The role of 5mC DNA methylation as a gene expression maintenance mechanism has been very well established in previous works, especially in cellular differentiation, acting as a mechanism that ensures lineage commitment [186–188]. On the contrary, the 251 CpGs that did change their methylation state upon BLaER1 transdifferentiation are early events of this process, indicating that these particular changes may precede and modulate gene expression in discrete, specific patterns. In fact, the detected promoter-related CpGs seem to regulate important macrophage-related genes (table R-1) and treatment with 5-aza (a passive DNA demethylating agent) on non-transdifferentiated BLaER1 cells induce the expression of these genes (figure R-10), reinforcing the causative role of these specific methylation changes in modulating gene expression during early B-cell-to-macrophage transdifferentiation.

Nevertheless, it is very difficult to precisely pinpoint the timing in the sequence of events and we would need to perform a more fine-tuned, time-dependent simultaneous analysis on both RNA expression and DNA methylation in order to confirm if 5mC DNA methylation changes are cause or consequence of gene expression fluctuations, even during the early stages of transdifferentiation. An interesting experiment that would solve this question is to perform a Smart-RRBS analysis, which would allow to simultaneously sequence DNA methylation and RNA expression at the single cell level, at different time-points of transdifferentiation [189].

As a matter of fact, I personally went 2 months to Dan Landau's laboratory (one of the creators of Smart-RRBS) at New York to learn this technique and to establish it in our laboratory. Unfortunately, at the moment we are applying this technique into another different line of research ("Simultaneous epigenetic and transcriptomic single-cell analysis of myelodysplastic syndrome patients before and after azacytidine treatment"), completely unrelated to our B-cell-to-macrophage transdifferentiation research. Despite this, our results confirm that transdifferentiating B-cells do not need to endure drastic global changes in their DNA methylome in order to acquire a macrophage phenotype, but rather experience localized DNA methylation changes in important key macrophage-related genes. Additional depletion experiments on these genes would be required to test whether they are crucial for the transdifferentiation process to occur or are just early DNA-methylation driven events.

DNA methylation changes in distant regulatory regions predominate over changes in gene promoter regions during B-cell-to-macrophage transdifferentiation

When mapping these 251 differentially methylated CpGs to their relative genomic positions, we can observe an enrichment in distant genomic regions (110 CpGs, 43.8%) and gene bodies (99 CpGs, 39.4%), whereas only 38 CpGs (15.2%) are located in promoter regions. As previously described in the introduction, gene promoter methylation is classically related with gene silencing [99], which we properly confirmed in our BLaER1 transdifferentiation experiments, having a role in regulating the expression of crucial macrophage genes. On the other hand, the function of DNA methylation in gene bodies and distant genomic regions is not so clearly established [100, 101]. Gene body methylation does not clearly correlate neither positively nor negatively with the expression of its associated gene. Previous works claim that intragenic DNA methylation protects the gene body from spurious RNA polymerase II entry and cryptic transcription initiation [190]. However, about half of all annotated enhancers are intragenic, which could also be under the regulation of DNA methylation [100]. On the other hand, distant genomic regions can harbor distant regulatory elements (e.g. enhancers, silencers and CTCF binding sites) which may also be regulated by DNA methylation. Published methyl-SELEX assays, which interrogated the binding affinity of more than 500 transcription factors (TFs) to their respective methylated and unmethylated motifs, showed that >30% TFs increase their affinity to their motifs when these are methylated, while >20% TFs displayed a lower affinity to their motifs when these are unmethylated

[102]. Thus, enhancer and silencer methylation could directly affect the binding of key TFs that mediate B-cell-to-macrophage transdifferentiation. Furthermore, CTCF is a well-known insulator protein that blocks the distant interaction between gene promoters and other distant regulatory regions, and it is extremely sensible to the methylation of its DNA binding motif, only binding to DNA when this motif is unmethylated [102, 103].

This predominance of DNA demethylation at distant regulatory regions upon BLaER1 transdifferentiation can also be observed during normal hematopoietic differentiation. Demethylation of intra-/intergenic enhancers has been observed in various steps of hematopoiesis, such as in the differentiation of naïve B cells into memory B cells, or during the generation of the different types of T cells (cytotoxic T cells, helper T cells, etc.), which acquire distinct DNA methylation patterns at multiple enhancers [191]. In addition, various *in vitro* transdifferentiation experiments have shown a similar predominance of DNA demethylation at distant regulatory regions [182, 184, 188, 192]. By looking at our western blot data in figure R-6, which depicts the protein levels of three DNA methyltransferases (DNMT1, DNMT3A and DNMT3B) and three DNA demethylases (TET1, TET2 and TET3), the demethylation of these regions could be explained not only by a passive mechanism of demethylation (due to the loss of DNMT1 and DNMT3B expression upon transdifferentiation), but also by an active demethylation mechanism mediated by TET2, which increases its protein expression at 72 hours of BLaER1 transdifferentiation, time-point at which we can start to observe a clear demethylation on the 250 detected CpGs (figure R-5).

Of the three TET enzymes discovered to this date, TET2 seems to be the most important family member for somatic cell reprogramming [193]. A previous study discovered that the depletion of Tet2 in a murine C/EBPα-driven pre-B-cell-to-macrophage transdifferentiation model downregulated the expression of a small subset of myeloid genes, although barely affecting transdifferentiation efficiency [192]. In addition, another recent study discovered that Tet2 mediates site-specific demethylation in a murine two-step B-cell-to-iPSCs C/EBPα/OSKM-driven de-differentiation model, being recruited by C/EBPα onto highly methylated myeloid and pluripotency enhancers, stimulating hydroxymethylation-driven demethylation of these distant regulatory regions [193]. Thus, it is very likely that TET2, being recruited by C/EBPα (since TET2 lacks a DNA binding domain) to specific genomic sites, mediates the observed selective demethylation during the early stages of BLaER1 B-cell-

to-macrophage transdifferentiation. To confirm this, we would need to perform a chromatin immunoprecipitation DNA sequencing (ChIP-seq) for both TET2 and C/EBPα to confirm if they overlap with the genomic positions of our 250 demethylated CpGs. Furthermore, generating a TET2 knockdown/knockout BLaER1 model would confirm if changes in DNA methylation are dispensable or not for transdifferentiation to occur. In addition, although the Illumina 850k-EPIC DNA methylation array used in our experiments interrogates 333,265 CpGs located at distant regulatory regions (including 58% of FANTOM5 enhancers) [194], they only represent a 7% of all the distal regulatory elements catalogued by the ENCODE project [195]. This is an important limitation of our analyses, and thus it would be necessary to apply other more-in-depth techniques, such as whole genome bisulfite sequencing (WGBS), to detect more CpG sites which could also be involved in B-cell-to-macrophage transdifferentiation but remain undetectable under the Illumina DNA methylation array. Additionally, since 5hmC (an intermediate of demethylation) is undistinguishable from 5mC when using the Illumina 850k-EPIC DNA methylation array, we may be detecting methylated CpGs that are actually in the course of demethylation. To distinguish 5hmC from 5mC, we would need to perform specific 5hmC sequencing techniques such as Aba-seq (DNA modification-dependent restriction endonuclease AbaSI coupled with sequencing) or hMeDIP-seq (hydroxymethylation DNA immunoprecipitation sequencing). In addition, as seen in previous works [184], many DNA methylation events that occur during differentiation and transdifferentiation take place at non-CpG sites (CpH sites; H: A,T,G), and these seem to have an important role in gene repression [196]; unfortunately, the 850k-Illumina methylation array only interrogates CpGs and, thus, other genome-wide experiments (like RRBS or WGBS) are needed.

DNA methylation at distant regulatory regions may impact gene expression by regulating distant chromatin interactions

At the present time, the relationship between changes in DNA methylation at distal regulatory regions and how this modulates chromatin tridimensional conformation to regulate the expression of distant genes is poorly understood, with almost no scientific articles interrogating this triple “DNA methylation – chromatin conformation – gene expression” relation. In 2018, it was demonstrated that both global methylation and demethylation in early murine embryonic development correlated with the formation of distinct tridimensional chromatin

compartments, modulating gene expression, although the causality between DNA methylation and chromatin conformation fluctuations was not established [197]. Nevertheless, the mere existence of methylation-sensitive transcription factors and other methylation-sensitive DNA binding proteins (like GMEB2 and CTCF) is a major clue indicating that DNA methylation can directly modulate the tridimensional conformation of chromatin, thus regulating enhancer-promoter interactions. By analyzing published promoter capture Hi-C (PC-HiC) data performed on M0 macrophages [174], we putatively inferred the long-range interactions in which our 251 CpG sites are involved during B-cell-to-macrophage transdifferentiation, finding 34 demethylated unique CpGs that putatively interact with 59 genes (figure R-13), 38 of them increasing their expression (we named coined these interactions as “enhancer interactions”) whereas 21 of them decreasing their expression (“silencer interactions”). The 38 enhanced genes are related with macrophage functions, while the 21 silenced genes are related with B cell functions. Validation of some interactions was performed with UMI-4C, although due to the limitations of this technique (it provides reliable contact quantifications only between DNA sequences located within a ~0.5 Kb to ~1 Mb interval), only one enhancer interaction could be validated: the CpG “chr3:46136952” (hg19) interacting with CCR1 gene (figure R-18), which is a crucial receptor for the detection of the chemokine MIP1α (macrophage inflammatory protein 1α) [198]. The small UMI-4C detection interval is an important limitation that could be solved if we had performed a genome-wide Hi-C experiment at different time-points of transdifferentiation, although the resolution in Hi-C experiments is way lower than in UMI-4C, which is a more site-specific technique [199]. In addition, the newly discovered single-cell Methyl-Hi-C technique would allow us to simultaneously interrogate the DNA methylation and the tridimensional chromatin interactions from a single cell, which would really help correlating these two events in a time-dependent manner, although extreme low coverage per cell must be expected [200].

On the other hand, passive DNA demethylation assay with 5-aza followed by RT-qPCR of various enhancer/silencer-interactive genes in non-transdifferentiated BLaER1 (figure R-17) demonstrated that DNA demethylation has indeed a direct functional role, in which 3 enhancer-interacting genes increase their expression while 2 silencer-interacting genes decrease their expression upon 5-aza treatment, following the same trend as observed in our previous triple correlation “DNA methylation – PC-HiC – Expression array” analysis upon BLaER1 transdifferentiation. In addition, motif finding analysis of the 34 demethylated CpGs

that putatively interact with distant genes (figure R-19) revealed binding sites for important transdifferentiation factors involved in various differentiation processes, such as MEIS1, TFAP2A, NR2F1 and MAX, which are known to differentially bind to methylated/unmethylated DNA sequences [173, 175, 201–203]. These results reinforce the fact that DNA demethylation at specific distant regulatory regions has an impact on gene expression by altering chromatin distal interactions during B-cell-to-macrophage transdifferentiation. Nevertheless, one limitation of this experiment is the non-specificity of 5-aza, which passively demethylates the entire genome. Instead, to strengthen this connection, we would need to perform other more specific experiments, such as CRISPR Cas9-mediated deletion of the demethylated enhancers and silencers, or site-specific demethylation of these enhancers and silencers using a deactivated Cas9 coupled to TET2 enzyme (dCas9-TET2) on non-transdifferentiated BLaER1 cells [204], or even site-specific hypermethylation of these distal regions by using a deactivated Cas9 coupled to DNMT3A (dCas9-DNMT3A), maintaining those regions hypermethylated throughout B-cell-to-macrophage transdifferentiation [205].

Although there is still much work to do, this descriptive project provided us with crucial information about how specific DNA demethylation at distant regulatory regions can impact gene expression through chromatin remodeling during the early stages of B-cell-to-macrophage transdifferentiation.

Linking DNA methylation with malignant B-cell-to-macrophage transdifferentiation

As previously mentioned, C/EBPα is the cornerstone of B-cell-to-macrophage transdifferentiation cases found in the clinics. In B-cell precursor acute lymphoblastic leukemias (BCP-ALL), up to 5% of patients develop monocytosis with clonal relation with leukemic B lymphoblasts (detected by the presence of share immunoreceptor gene rearrangements) after therapy administration [206]. These switching BCP-ALL (swALL) cells exhibit a significant upregulation in C/EBPα expression and demethylation of its gene promoter before and after the treatment, correlating with a coordinated upregulation of PU.1 and GM-CSF and downregulation of PAX5 and EBF1, indicating a switch from the B cell to the myeloid program [206]. Patients with swALL respond much slower to initial ALL therapy when compared to non-swALL cases. Thus, this B-cell-to-macrophage switch is an important warning sign,

opening new questions about which are the optimal treatment strategies to be used in these cases.

Additionally, another subset of ALL patients manifest 11q23 translocations associated with MLL gene fusions [207]. B-cell-to-macrophage clonally related switch is a common characteristic of MLL-positive ALL cases [208]. Although there are no scientific research tackling the relation between C/EBPα and the propensity of MLL-positive ALL cases to transdifferentiate into the myeloid lineage, C/EBPα is a crucial collaborator in MLL-rearranged acute myeloid leukemia (AML) as an indispensable factor that drives transformation in this subset of AML patients, highlighting the role of C/EBPα in establishing myeloid malignancies in cases with MLL-rearrangements [209].

In more mature lymphoid neoplasms, like follicular lymphoma (FL), chronic lymphocytic leukemia (CLL) or diffuse large B cell lymphoma (DLBCL), treatment-induced B-cell-to-macrophage transdifferentiation also seems to be dependent on C/EBPα or even on C/EBPβ (whose role in B-cell-to-macrophage transdifferentiation seems to be interchangeable with C/EBPα, as demonstrated in various *in vitro* experiments) [56, 210, 211].

The link between C/EBPα and DNA methylation has been observed in various types of hematological malignancies. In AML, inactivating mutations in C/EBPα are found in a subset of patients manifesting global hypermethylation levels in malignant cells [212]. Similarly, other AML cases with epigenetically silenced C/EBPα (due to hypermethylation of its gene promoter, instead of genetic mutations) also exhibit a global hypermethylation phenotype, associated with poor prognosis [212–214]. This could be explained by the fact that, as previously explained, C/EBPα directly recruits TET2 to stimulate site-specific demethylation [193]. Furthermore, it has been recently discovered that C/EBPα can also negatively interact with the N-terminus of DNMT3A methyltransferase, blocking its access to DNA and avoiding aberrant hypermethylation, which would explain why leukemic cells with C/EBPα inactivating mutations are hypersensitive to hypomethylating agents [215]. Additionally, C/EBPα directly upregulates PU.1 expression, which also binds to TET2, inducing site-specific demethylation [216, 217].

All this evidence demonstrates that BLaER1, a C/EBPα-driven B-cell-to-macrophage transdifferentiation model, is a good option to explore the epigenetic changes that occur during

the early stages of this event and to extrapolate the results to actual malignant transdifferentiation processes. Our results prove that, upon BLaER1 transdifferentiation, DNA is demethylated locally (rather than globally) at specific CpG sites, especially at distant regulatory regions, controlling many important macrophage-related genes, such as RHOG (crucial for macrophage phagocytosis) [218], CXCL8 (an important macrophage-derived chemotactic cytokine) [219], and CCR1 (an important MIP1α receptor) [220], among others. To further test the importance of these new genes, we would need to develop depletion and overexpression models of these genes on BLaER1 cells to evaluate whether they have a direct role by regulating B-cell-to-macrophage transdifferentiation or are just the final products of this process. In addition, it is necessary to develop new additional *in vitro* and *in vivo* B-cell-to-macrophage transdifferentiation models to orthogonally validate these results. Although there is still much work to do, this project has given new insights about the epigenetic mechanisms of physiological and malignant transdifferentiation, finding new potential targets that could be applied in the development of new diagnosis, prognosis, and therapeutic strategies against this process.

***

SECOND PROJECT DISCUSSION

RNA m6A methylation changes in leukemic transdifferentiation

m6A epitranscriptome drastically changes upon B-cell-to-macrophage transdifferentiation

Our m6A-seq RNA methylation analysis revealed drastic changes in the m6A epitranscriptome upon BLaER1 B-cell-to-macrophage transdifferentiation (figure R-26). Up to 6072 m6A peaks were differentially methylated (corresponding to 3056 unique transcripts), with 2880 upmethylated peaks and 3192 downmethylated peaks, corresponding respectively to 1664 and 1560 unique transcripts. Intersecting these results with an expression array at multiple time-points of transdifferentiation allowed us to correlate changes in expression with changes in m6A methylation, cataloguing each transcript by the relative position of the m6A peak (5'UTR, Exon, Intron, 3'UTR). This considerable number of changes is a clear indicative that epitranscriptomic fluctuations may be playing a crucial role during this process, but since there are no published scientific articles (other than our work) that explore the relation between cellular transdifferentiation and epitranscriptomics, we do not have a reference point to which compare our results. Fortunately, there are other excellent works that explore the epitranscriptomic changes occurring in hematopoietic differentiation and hematological malignancies. The importance of m6A in these two processes has been very well established and we have already summarized its most important implications in pages 54 to 60 of the introduction. Each type of hematopoietic cell has a dynamic but well-defined pattern of m6A marks decorating specific transcripts, fine-tuning their stability, splicing, cellular localization and translation [221, 222]. Thus, the drastic changes in m6A content observed upon BLaER1 transdifferentiation is a consequence of the original B-cell modulating and adapting its epitranscriptome to acquire similar m6A patterns to those found in a normal macrophage. During this adaptation, one would expect that some of these changes in m6A are required for the B-cell-to-macrophage transition, while other m6A changes are just the final product of this conversion. When compared to the previous project, changes in DNA 5mC methylation are much slower and localized in comparison to the fast and highly dynamic m6A epitranscriptome, which quickly adapts to any intra-/extracellular inputs. One limitation of our m6A-seq experiment when compared with the DNA methylation project is the lack of human pre-B and macrophage cells as controls, which would have been very

valuable as reference points between the initial and ending time-points of B-cell-to-macrophage transdifferentiation. Unfortunately, an extremely large amount of material (donor-derived pre-B and macrophage cells) was needed to perform m6A-seq, which was not technically feasible at the time. Nevertheless, since our focus is to see the changes in m6A during transdifferentiation, we finally decided to prescind from these controls. Another limitation of the m6A-seq experiment is the lack of biological replicates for each time-point of BLaER1 transdifferentiation. This again was due to the technical limitations in the BLaER1 transdifferentiation experiment, which requires specific volumes and cell concentrations that cannot be scaled, forcing us to pool more than 30 independent transdifferentiation reactions per time-point in order to obtain the desired amount of total RNA (>500 micrograms per time-point) to perform the m6A-seq experiment. Fortunately, the bioinformatic analysis tool "m6A-Viewer" allowed us to determine the significantly enriched m6A peaks for each replicate individually using Fisher's exact test between the immunoprecipitated (IP) and the input fractions. Additionally, motif analysis revealed an enrichment in the typical RRACH m6A motif (figure R-21D), indicating that the m6A-experiment worked correctly.

The changes in m6A content tend to progressively increase upon BLaER1 transdifferentiation (figure R-21A), depicting how the m6A epitranscriptome of the original pre-B cell is quickly reconfigured and adapted upon transdifferentiation in a time-dependent manner, highlighting the great dynamism of m6A in response to internal and external stimuli. In total, the balance of down-/upmethylated m6A peaks upon transdifferentiation tilts slightly towards downmethylation (52.6% downmethylated peaks *versus* 47.4% upmethylated peaks). This trend is also observed in the m6A-LC-MS/MS experiment, where we detected a loss of ~ 25% total m6A content upon BLaER1 transdifferentiation (figure R-21C). It is difficult to assess the mechanisms of this subtle demethylation, since western blot results show a downregulation in all the analyzed m6A writers, readers, and erasers upon transdifferentiation (figure R-22), indicating that these changes in methylation are well-orchestrated site-specific events, and not a result of massive unspecific waves of down-/upmethylation. Finally, when we look at the distribution of m6A across the length of the transcripts, we can see a clear enrichment in both exonic and intronic m6A (figure R-21B). Unexpectedly, downmethylated transcripts are enriched in m6A peaks at intronic regions (51%), while upmethylated transcripts are enriched at exonic regions (43%), as seen in figure R-24. Very interestingly, this difference in m6A position (intronic vs exonic) seems to be independent of changes in the

expression of the associated transcripts, which indicates that these changes in m6A may have a role either in splicing, intron retention, or translation. This last detail will be addressed in later sections of the discussion.

m6A controls the stability of ribosomal protein transcripts, regulating global translation upon B-cell-to-macrophage transdifferentiation

Gene ontology analyses of all the differentially methylated transcripts upon BLaER1 transdifferentiation (3056) revealed a strong enrichment in translation and ribosomal protein ontologies (figure R-23), and subgrouping each transcript by m6A direction (upmethylated *versus* downmethylated transcripts) revealed that upmethylated transcripts are the ones richer in these translation-related ontologies (figure R-25). Thus, we decided to focus on upmethylated transcripts, finding that transcripts that were upmethylated at 3'UTR position were enriched in important translation-related proteins, including 29 ribosomal proteins (table R-2). It is well known that ribosomal proteins (RPs) play a key role in controlling gene expression at the translational level to determine the differentiation fate of cells [223]. Different classes of RPs interact together to generate different types of ribosomes, each one recognizing specific subsets of mRNAs (something known as "ribosomal heterogeneity") [177, 224]. Therefore, RPs must keep a very delicate balance between them in terms of quantity and quality to ensure a correct differentiation process. As previously explained in the introduction, m6A upmethylation at 3'UTR is classically related with increased mRNA decay and instability, by the action of YTHDF family of m6A readers (especially YTHDF2), which recognize the modified mRNAs and relocate them into P-bodies, where deadenylation and endonucleolytic cleavage takes place [133, 134]. To interrogate if 3'UTR m6A upmethylation in RPs is associated with increased mRNA decay upon BLaER1 transdifferentiation, we performed RT-qPCR of 7 out of 29 RPs and detected a progressive downregulation in their mRNA content coupled with transdifferentiation, as expected (figure R-27). Actinomycin chase assay with RPS25 (the most upmethylated transcript) confirmed that the increase in 3'UTR m6A is associated with increased mRNA decay (figure R-28). To further confirm this, we would need to perform a transcript-specific orthogonal validation technique to assess the m6A upmethylation in the 3'UTR of RPS25 mRNA upon transdifferentiation. To do so, and with the help of several team members of Storm Therapeutics (our collaborators from Tony

Kouzarides' laboratory in Cambridge), we are now trying to establish the SELECT method, a new RT-qPCR-based site-specific m6A detection technique that exploits the ability of m6A to hinder the activity of the ligase after the m6A-centered nick repair [225]. In addition, to test if RPS25 mRNA decay is mediated by YTHDF2, we would need to perform a cross-linking immunoprecipitation RNA sequencing (CLIP-seq) to confirm the differential interaction between RPS25 mRNA and YTHDF2 protein at 0 and 168 hours of BLaER1 transdifferentiation.

Despite these two limitations, we validated the effects of m6A on RP's mRNAs by establishing an shRNA-mediated METTL3 depletion BLaER1 model and by using STM2457 (a small molecular specific inhibitor of METTL3's catalytical activity) upon BLaER1 transdifferentiation. Both depletion methods significantly decreased the m6A cell content (figures R-29C and R-40D) and both lead to a significant increase in RP mRNA content (figures R-34 and R-42), indicating that loss of m6A probably stabilizes RP transcripts. To confirm this, we performed an actinomycin chase assay on RPS25 mRNA using the shRNA-mediated METTL3 depletion model, showing increased stability when METTL3 is depleted (figure R35). Although RP mRNA content is increased upon m6A depletion, it does not mean that protein synthesis will be upregulated. On the contrary, as we previously described, RP content must be strictly kept in balance in terms of quantity and quality to maintain a correct global protein synthesis. The effects of RP imbalance on global translation can be observed in figure R-36, in which a puromycin assay shows that METTL3 depleted BLaER1 cells display a completely dysfunctional global protein synthesis upon B-cell-to-macrophage transdifferentiation, in comparison to the wild-type and empty-vector cells. These results confirm the role of m6A as a crucial regulator of global protein synthesis by fine-tuning RP mRNA content upon BLaER1 B-cell-to-macrophage transdifferentiation.

m6A is crucial for the correct functioning of transdifferentiated macrophages and METTL3 depletion leads to a stochastic transdifferentiation blockade

To explore if the dysregulation on global protein synthesis observed upon METTL3 depletion has an impact on B-cell-to-macrophage transdifferentiation, we performed flow cytometry and RT-qPCR assays on several B cell and macrophage differentiation markers. We can observe a significant impairment of BLaER1 transdifferentiation efficiency in both shRNA-mediated (sh2.1) and STM2457-mediated depletion of METTL3 (figures R-29 and R-41).

Around 25% - 30% of the cells do not transdifferentiate after 168 hours of induction. Growth assay, cell cycle and apoptosis assays indicate that cells in the sh2.1 METTL3 depletion model continue actively proliferating (figure R-32), possibly due to untransdifferentiated leukemic pre-B cells that continue dividing as a consequence of a transdifferentiation blockade. To discard the possibility that METTL3 depletion leads to a slower B-cell-to-macrophage transdifferentiation instead of a transdifferentiation blockade, we induced transdifferentiation on METTL3 depleted BLaER1 cells and waited 240 hours (instead of only 168 hours). The leukemic $CD19^{+}/CD11b^{-}$ pre-B cells that still remained untransdifferentiated at 168 hours didn't complete transdifferentiation even after 240 hours (figure R-33); instead, they continued dividing, indicating that there is indeed a B-cell-to-macrophage transdifferentiation blockade. This rises a very intriguing question: Why METTL3 depletion only impairs 25% – 30% of B-cell-to-macrophage transdifferentiation efficiency? To answer this question, we propose a model of "stochastic transdifferentiation blockade", in which METTL3 (the most important m6A writer) reduces the activation energy required for B-cell-to-macrophage transdifferentiation, but when METTL3 is depleted, this activation energy significantly rises, making it more difficult for the cells to transdifferentiate (figure D-1). Nevertheless, the increase in the activation energy upon METTL3 depletion is not enough to completely block transdifferentiation, allowing for some cells that did achieve the necessary energy to cross the "go/no-go line". Thus, when METTL3 is depleted, some cells will still transdifferentiate while other cells will not, in a stochastic fashion.

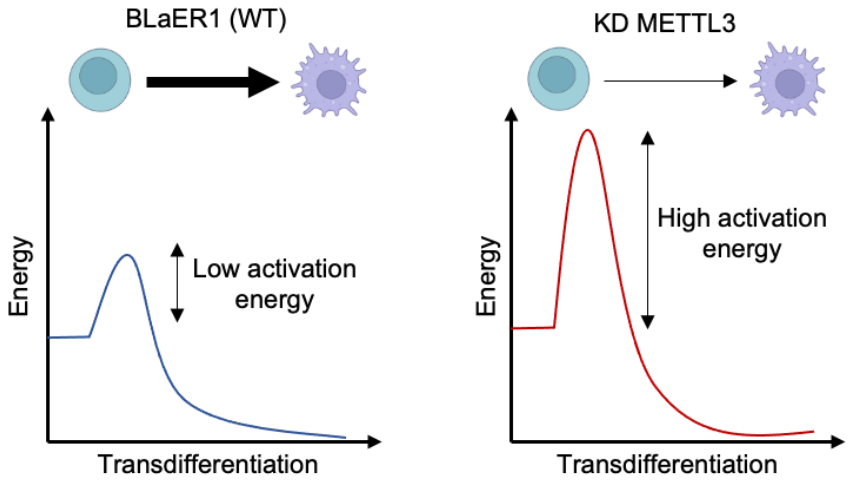

Figure D-1. Proposed model of stochastic B-cell-to-macrophage transdifferentiation blockade upon METTL3 depletion. **Abbreviations:** WT: Wildtype; KD: Knockdown.

Additionally, these results rise another question about the cells that did achieve to transdifferentiate in the METTL3 depletion model: Are these transdifferentiated macrophages functional when compared to the empty-vector control? To answer this question, we sorted empty-vector and sh2.1 METTL3-depleted transdifferentiated macrophages (after 168 hours of induction) and performed RT-qPCR of several RPs and differentiation markers (figures R-37 and R-38). We still see an upregulation in RPs mRNA content and a dysregulation in some differentiation markers, indicating that METTL3-depleted macrophages may have not differentiated correctly. To fully confirm this, the best way to assess macrophage functionality is analyzing its phagocytic activity. Thus, we performed a dsRed^{+} *Escherichia coli* phagocytosis assay, confirming that METTL3-depleted transdifferentiated macrophages do not phagocyte correctly (figure R-39). In conclusion, these results indicate that m6A depletion impairs B-cell-to-macrophage transdifferentiation, possibly due to RP dysregulation, leading to a stochastic transdifferentiation blockade and macrophage dysfunction.

m6A in other relative mRNA positions may harbor important consequences for B-cell-to-macrophage transdifferentiation.

As we previously described, the m6A epitranscriptome drastically changes upon BLaER1 B-cell-to-macrophage transdifferentiation. Only a small subset of transcripts (11%) exhibits 3'UTR-associated m6A upmethylation, contrasting with other more affected regions such as exons and introns. 51% of downmethylated transcripts are enriched in intronic m6A peaks, while 43% of upmethylated transcripts are enriched in exon m6A peaks (figure R-24). Thus, despite our results, we might be missing other m6A-dependent mechanisms that also contribute to transdifferentiation.

The function of intronic m6A is not currently well understood. Some researchers claim that intronic m6A can affect splicing in 3 different ways: (1) regulating the interactions between small nuclear RNA (snRNA) and the nascent pre-mRNA; (2) regulating the binding of RNA-binding proteins (RBPs); (3) rearranging splicing sites by altering the secondary structure of RNA [144]. Mechanistically, the deposition of intronic m6A restrains the movement of RNA polymerase II, slowing it down and allowing the correct performance of the splicing machinery. In fact, depletion of intronic m6A is associated with increased intron retention and aberrant accumulation of unprocessed pre-mRNA [226]. On the other hand, exonic m6A can also

affect splicing in a similar fashion. Exonic m6A can be deposited near 5' exonic boundaries, regulating splicing events. In order to detect possible m6A-dependent splicing events, we would need to perform an RNA-seq of wild-type, empty-vector and shRNA-METTL3 BLaER1 cells at different time-points of transdifferentiation and perform an alternative splicing bioinformatic analysis by generating "*spline*" intersecting curves between gene isoforms to detect possible splicing shifts upon transdifferentiation among the 3 conditions. In addition, intron retention could also be quantified by RNA-seq. These results can be then intersected with our m6A-seq data to detect possible dependencies between m6A and differential splicing events.

Last but not least, m6A deposited in the 5'UTR region of mRNA has its own unique functions. Although the frequency of m6A deposition in 5'UTR is low, it can foster 5'-cap independent translation by directly recruiting eIF3 [137]. To inspect this, we could use 4EGI-1, a small molecule specific inhibitor of 5'-cap dependent translation, to test the importance of 5'-cap independent translation on BLaER1 transdifferentiation [227]. In addition, we would need to perform proteomic and ribosome profiling analysis on wild-type, empty-vector and shRNA-METTL3 BLaER1 cells to interrogate how m6A really affects global translation during transdifferentiation.

⁂

As we can see, m6A is a never-ending source of knowledge, with many functions and mechanisms waiting to be discovered. Regarding our project, the results clearly indicate that m6A has an important role in the regulation of B-cell-to-macrophage transdifferentiation, fine-tuning the stability of several RPs and ensuring a correct global protein synthesis upon cell conversion. Moreover, the fact that STM2457 (a specific inhibitor of METTL3 that is currently under clinical trial as a novel AML treatment) can inhibit B-cell-to-macrophage transdifferentiation opens a new promising door for treating cases of malignant transdifferentiation. Hopefully, this work will serve as a starting point to strengthen the relationship between the fields of epitranscriptomics and cellular transdifferentiation.

CONCLUSIONS

Conclusions of the first project

- During BLaER1 B-cell-to-macrophage transdifferentiation, DNA becomes demethylated at only a few specific CpG sites.

- Most of the DNA demethylation events occur at distant regulatory regions.

- DNA demethylation at gene promoters and distant regulatory regions regulates the expression of important genes for macrophage function.

- DNA demethylation at distant regulatory regions may regulate gene expression by modulating long-range chromatin interactions.

Conclusions of the second project

- m6A epitranscriptome drastically changes upon BLaER1 B-cell-to-macrophage transdifferentiation.

- mRNA molecules with m6A upmethylation at 3'UTR are enriched in ribosomal protein (RP) transcripts, resulting in increased transcript instability.

- METTL3 depletion is associated with increased RP transcript stability and dysregulation of global protein synthesis upon BLaER1 transdifferentiation.

- METTL3 depletion triggers a stochastic transdifferentiation blockade.

- STM2457 blocks B-cell-to-macrophage transdifferentiation, opening new opportunities for treating clinical cases of malignant transdifferentiation.

MATERIALS AND METHODS

MATERIALS AND METHODS

Cell lines and donor-derived macrophages

BLaER1 and RCH-ACV cell lines were provided by Thomas Graf group [58]. These cells were cultured at 5% CO2, 37°C with RPMI-1640 GlutaMAX (Gibco, Ref: 61870-044), 10% FBS (Gibco, Ref: 16000-044), 1X Penicillin/Streptomycin (BioWest, Ref: L0022-100). All cell lines were authenticated by short tandem repeat profiling (LGS Standards SLU) and tested for the absence of mycoplasma.

Macrophages were obtained from Macrophage colony-stimulating factor (M-CSF) induced differentiation of donor-derived monocytes as previously described [228, 229]. Briefly, an initial buffy coat with peripheral blood of an anonymous donor was obtained through the Catalan Blood and Tissue Bank (CBTB). The CBTB follows the principles of the Declaration of Helsinki (World Medical Association, WMA). Before providing the first blood sample, the donor received detailed oral and written information and signed a consent form at the CBTB. Pure monocytes were isolated from PBMCs using positive selection with MACS CD14 beads (Miltenyi Biotec, Bergisch Gladbach, Germany, Ref: 130-050-201). 5 x 10^6 monocytes were then plated in 10 mL of serum-free RPMI-1640 GlutaMAX medium and incubated at 5% CO2, 37°C. After 2 hours of incubation, medium was replaced with 10 mL RPMI-1640 GlutaMAX, 10% FBS, 1X Penicillin/Streptomycin and 25 ng/mL of M-CSF (Peprotech, 300-25-50UG). Cells were cultured at 5% CO2, 37°C and harvested after 3 days of culture.

Transdifferentiation of BLaER1 cells

In order to induce B-cell-to-Macrophage transdifferentiation, 5 x 10^6 BLaER1 cells were cultured in 10 mL RPMI-1640 GlutaMAX medium supplemented with 10% FBS, 1X Penicillin/Streptomycin, and one single dose of 100 nM of 17β-estradiol (Sigma, Ref: E8875), 10 ng/mL of IL3 (Peprotech, Ref: 200-03-50UG) and 10 ng/mL of M-CSF. BLaER1 cells were harvested at seven different time-points of transdifferentiation (0, 3, 12, 24, 48, 72, and 168 hours) and pellets were frozen at -80°C.

DNA from each time-point was purified as previously described. Briefly, cell pellets were lysed with 600 µL of lysis buffer (10 mM Tris-HCl, pH=7.4; 10 mM EDTA; 200 mM NaCl), 75

µL of 10% SDS and 15 µL of Proteinase K (20 mg/mL), incubated for 3 hours at 55 ºC. Proteinase K was inactivated by simple incubation at 75 ºC, 15 minutes. 2 µL of RNase A 10 mg/mL were added to each sample and incubated for 1 hour at 37 ºC. 300 µL of NaCl 5M were added to the samples and then were centrifuged for 5 minutes at 14000 g (25 ºC), collecting the supernatant. 0.1 volumes of AcNH4 10 mM, 1 µL of GlycoBlue 15 mg/mL (Ambion, Ref: AM9515) and 1 volume of isopropanol 100% were added and centrifuged for 15 minutes at 4 ºC (maximum speed). The supernatant was discarded, the pellet was re-suspended with 500 µL of Ethanol 70% and centrifuged 15 minutes at 4 ºC (maximum speed). The pellet was air-dried, resuspended in DNase-free water for 10 minutes at 55 ºC and stored at -20 ºC.

DNA Methylation analysis

The DNA methylation array used was the MethylationEPIC BeadChip 850K microarray [194]. Genomic location of the CpGs under study are depicted in the table below. The term “Beta-value”, as included in the text, refers to the estimate of methylation level using the ratio of intensities between methylated and unmethylated alleles in the Illumina DNA methylation microarray. It does not refer to the statistical term. B-values for each CpG are between 0 and 1 with 0 being unmethylated and 1 fully methylated. Validation of the methylation state of promoters and distant regulatory regions was determined by bisulfite genomic sequencing (BSP), using EZ DNA Methylation Gold kit (Zymo Research, Orange, CA, USA, Ref: D5006) for DNA conversion and specific primers to amplify the regions of interest (see table below). Amplicons were cloned into the pGEM-T Easy Vector System I (Promega, Ref: A1360). Competent E. coli (DH5α strain) were transformed in LB-agar plates treated with ampicillin, X-Gal and IPTG. A minimum of six clones were selected to calculate the methylation frequency. Plasmid purification for each clone was performed using the NucleoSpin 96 plasmid kit (Macherey-Nagel, Ref: 740625.24). Amplicon sequencing was performed using the 3730 DNA analyzer (Applied Biosystems, Ref: 3730S) and methylation state for each clone was represented using BSmapR software. DNA methylation was also studied by pyrosequencing using the PyroMark Q48 Advanced Reagents kit (PyroMark Q48 Autoprep Pyrosequencer, Qiagen, Ref: 974002). T-Test for unpaired samples was used to perform

statistical analysis. Normality and homogeneity in variance are assumed for Pyrosequencing experiments with biological triplicates. Primers are listed in the table below.

Illumina Infinium HumanMethylation 850k-EPIC raw data (.idat files) were loaded into R statistical language, to perform all the analyses [230]. QC and pre-processing steps were performed using *minfi* package [231, 232]. Briefly, raw data was normalized using *ssNoob* algorithm. Then, probes with low detection p-value (< 0.01), probes with a known SNP (Single Nucleotide Polymorphism) at the CpG site and known cross-reactive probes, were removed [233]. For the resulting CpGs, Beta- and M-values were calculated using *minfi* functions. Beta-value for an *i*th interrogated CpG site is defined as:

$$Beta_i = \frac{max(methy_i, 0)}{max(unmethy_i, 0) + max(methy_i, 0) + \alpha}$$

where $methy_i$ and $unmethy_i$ are the intensities measured by the $_i$th methylated and unmethylated probes, respectively. Illumina recommends using a regularization parameter (α = 100) to avoid dividing by small numbers. However, in practice this is not necessary as most of the probes have intensities ($methy_i$ + $unmethy_i$) larger than 1000 [234]. Therefore, this regularization parameter is not used by default (α = 0). The name “Beta-values” was chosen because they should follow approximately a Beta distribution, assuming that probe intensities are normally distributed.

M-value for an *i*th interrogated CpG site is defined as:

$$M_i = log_2\left(\frac{max(methy_i, 0)}{max(unmethy_i, 0)}\right)$$

The relationship between Beta- and M-values can be derived by substitution as follows:

$$Beta_i = \frac{2^{M_i}}{2^{M_i} + 1}; M_i = log_2\left(\frac{Beta_i}{1 - Beta_i}\right)$$

It is known that Beta-values suffer from significant heteroscedasticity at both sides of their distribution. This problem is effectively solved after transforming Beta-values to M-values, making them more appropriated for subsequent statistical analysis, as the linear models explained below.

DNA methylation changes upon differentiation treatment.

M-values were used to fit time linear regression models in order to find the more "methylation ~ treatment duration" correlated CpGs. Using R statistical language, the following linear model was implemented:

$$M_{pred} = \beta_0 + \beta_1 X + \varepsilon$$

where Mpred is the predicted methylation M-value (response or dependent variable), X is the treatment time in hours (predictor or explanatory variable), β1 is the estimated coefficient for the time variable, β0 is the intercept and ε is the error term. In order to find the CpGs in which its methylation is more strongly associated to treatment duration, we filter out CpGs based on the following criteria:

1) The t-test p-value for the β1 coefficient estimate should be below 0.05. This test provides a good notion of how far this coefficient is from 0 and therefore if the treatment is significantly affecting the methylation.

2) As a goodness of fit indication, the R-squared (coefficient of determination) was also required to be above 0.5. This statistic represents the proportion of the variability explained by the model.

3) To make sure that the magnitude of the methylation changes is biologically significant and far above the expected measuring error, a difference of 0.66 in Beta-value between the beginning and the end of the treatment was also required.

DNA Methylation data (GEO-GSE132845):

https://www.ncbi.nlm.nih.gov/geo/query/acc.cgi?acc=GSE132845

DNA methylation ~ gene expression correlation.

In order to investigate whether methylation changes found affected gene expression, we took advantage of previous gene expression data from the same model (Gene Expression Omnibus accession: GSE44700) [58]. Thus, a methodological limitation of the study is that

DNA methylation and microarray expression were not evaluated in the same biological samples. Gene expression microarray raw data were processed using *agilp* package [235]. From the 251 selected CpGs, 141 had an associated gene, i.e. were located in the gene or nearby the TSS (Transcription Start Site). Using this 141 CpGs subset and the aforementioned gene expression data, we then fit linear regression models to find significant "methylation ~ gene expression" correlations along the differentiation treatment.

Using R statistical language, a linear model similar to the previous one was implemented:

$$M_{pred} = \beta_0 + \beta_1 X + \varepsilon$$

where Mpred is the predicted methylation M-value (response or dependent variable), X is now the log2 gene expression value (predictor or explanatory variable), β1 is the estimated coefficient for the gene expression variable, β0 is the intercept and ε is the error term. In order to find the CpGs in which its methylation is more strongly associated to expression, we filter out CpGs based on a similar criterion as previously:

1) The t-test p-value for the β1 coefficient estimate should be below 0.05. This test provides a good notion of how far this coefficient is from 0 and therefore if the treatment is significantly affecting the methylation.

2) As a goodness of fit indication, the R-squared (coefficient of determination) was also required to be above 0.5. This statistic represents the proportion of the variability explained by the model.

DNA methylation in distant regulatory regions.

From the 251 CpGs found responding to the differentiation treatment and, taking advantage of the available PC-HiC data from a relevant macrophage-0 (M0) model [174], we investigated how many of those CpGs were located in enhancer/silencing active regions. We first selected 72 out of 251 CpGs located in putative distant regulatory regions found in the PC-HiC experiment. For this 72 CpGs subset, we investigated the correlation between methylation and expression of the distant genes found in contact by PC-HiC data, by fitting linear regression models using the same formulation as previously described (see the previous

section: “DNA methylation ~ gene expression correlation” from supplementary methods). In this case, the X parameter (the log2 gene expression value) corresponds to distant genes found in contact by PC-HiC.

As a result, a total of 34 CpGs for which methylation and gene expression values were significantly correlated throughout the differentiation treatment. These 34 CpGs were located in 34 different distant regulatory regions and, as some of them were found in contact with more than a single promoter region, we found a total of 59 enhancer/silencing – promoter significant interactions: 38 putative enhancers, as methylation anti-correlated with gene expression; and 21 putative silencers, as methylation directly correlated with gene expression.

Validation of the Gene Expression changes

RT-qPCR, PCR, Western Blot and Flow Cytometry analysis were performed to confirm mRNA and protein expression changes of some of the most significant genes. For RT-qPCR, biological triplicates were harvested at different timepoints (0 hours vs 168 hours). RNA extraction was carried out using the RNAeasy mini kit (Qiagen) according to the manufacture guidelines. Retrotranscription of 2 µg of total RNA was performed using RevertAid RT kit (Thermo Scientific, Ref: 00719361). RT-qPCR was performed using the QuantStudio 5 system (Applied Biosystems, Ref: A28140) with the conditions listed in the table below. PGK was used as housekeeping gene as previously described [58]. T-Test for unpaired samples was used to perform statistical analysis (T-Test, *$p<0.05$). Normality and homogeneity in variance are assumed for RT-qPCR experiments with biological triplicates. Primer sequences are listed in the tables below.

Western blot was performed as previously described [236]. Briefly, total protein extract was obtained from frozen cell pellets using RIPA 1X lysis buffer (PBS 1X, deoxycholate 0.5%, NP-40 1%, SDS 0.5% and 1 pill of protease/phosphatase inhibitor from Roche, Ref: 04 693 132 001), sonicated for 5 seconds and denatured for 5 minutes at 95 °C. Protein concentration was determined using the BCA assay (Pierce BCA Protein Assay Kit, Thermo Scientific, Ref: 23225). 40 µg of each protein sample was separated on 12-15% SDS-polyacrilamide gels by SDS-electrophoresis and transferred onto a 0.2 µm-porus nitrocellulose membrane

(Amersham Protran 0.2 µm NC, GE Healthcare, Ref: 10600001) by wet electroblotting (Mini Trans-Blot Cell, Bio-Rad, Ref: 1703930) for 1 hour at 100 V. The membrane was blocked with 5% non-fat dry milk in PBS Tween-20 0.1% for 1 hour at room temperature. Primary antibodies were used overnight at 4 °C (dilution conditions are listed in the table below). Membranes were washed thrice for 7 minutes in PBS Tween-20 0.1% and incubated with secondary antibodies conjugated to horseradish peroxidase for 1 hour at room temperature. Finally, the reaction was detected with Classico and Crescendo Immobilon Western HRP Substrate kits (Millipore, Ref: WBLUC0100 and WBLUR0100). Film images were obtained using Ortho CP-G Plus (Agfa, Ref: EASUF) and Amersham Hyperfilm ECL (GE Healthcare, Ref: 28906837) films developed in an Amersham Hypercassette (GE Healthcare, Ref: RPN11643) and a Curix60 film developer (Agfa, Ref: 9462-1064095). Two biological replicates were performed. All used antibodies are listed in the tables below.

Flow cytometry was performed as previously described [237]. Briefly, 500,000 cells were resuspended in 200 µL PBS with BSA 0.5% (FC-Solution). 0.5 µL of FcR Blocking Reagent (Miltenyi Biotech, Ref: 130-059-901) was added and cells were incubated 10 minutes in ice. Then, 0.5 µL anti-ITGAX antibody conjugated to APC (see reference in table below) was added and cells were incubated 30 minutes in ice. Cells were washed once with 1 mL of FC-Solution, centrifuged 1000 g for 5 minutes and resuspended in 400 µL of FC-Solution. Finally, flow cytometry experiment was performed in a BD FACSCanto II (Becton Dickinson, Ref: 338962). Three biological replicates were performed. Antibodies are listed in the table below.

5-aza-2'-deoxycytidine treatment of BLaER1 cells and qRT-PCR of validated genes

BLaER1 cells were treated with 5-aza-2'-deoxycytidine (5-Aza) as previously described [238]. Briefly, 2 x 10^6 BLaER1 cells were cultured in 10 mL RPMI-1640 GlutaMAX, 10% FBS, 1X Penicillin/Streptomycin and two different concentrations of 5-Aza (0 µM and 1 µM). Cells were plated in 25 cm^2 flasks in triplicate for each 5-Aza condition, incubated at 5% CO2, 37°C and harvested after 3 days of culture. Total RNA from frozen pellets was extracted, retrotranscribed and RT-qPCR was performed as described in the previous section "Validation of the Gene Expression changes".

Chromosome capture with unique molecular identifiers (UMI-4C).

UMI-4C was performed on ~4M cells before and after the transdifferentiation protocol. Cells were fixed with Formaldehyde 1%. Then, nuclei were digested with Csp6I and processed as previously described [239]. Each library was obtained by nested PCRs and its molecular complexity was ensured by pooling 6 independent PCRs using the following primers: Downstream primer: GTTGTCCTTGGGTTTAGCTGC; Upstream primer: AGAAAGAGGAAGTCCTGGCAAT. Libraries were sequenced to a depth of >1M, 75bp long paired-end reads using either NextSeq or HiSeq 2500 platforms. UMI-4C sequencing reads were analyzed using the UMI4Cats package [240]. A Chi-squared test comparing UMIs chromatin contacts in a 4Kb windows centered on the transcriptional start site of the up-regulated genes annotated in the locus, was computed to identify differential chromatin contacts in cells that underwent, or not, the differentiation protocol.

UMI-4C data (SRA-PRJNA548887):

https://www.ncbi.nlm.nih.gov/bioproject/PRJNA548887

Transcription Factor Binding Site (TFBS) search in candidate CpG positions.

In order to investigate the possibility that CpG methylation in our candidate positions could affect Transcription Factor (TF) binding, we performed an exhaustive search for putative TFBSs in the location of our candidate CpGs. We collect the -19/+20 bp sequences from the genomic positions of each of our 251 candidate CpGs (GCA_000001405.1, hg19 genome assembly) using bedtools (v2.28.0) [241]. Then, we use TFBSTools R package [242] to search for motifs from JASPAR database [243] in our collection of sequences. This tool performs the alignment of each of the input sequences (as well as their complementary reverse) with the position weight matrix (PWM) of each of the TFs in the selected database. Each alignment is scored with a percentage value representing the quantile between the minimal and the maximal possible value from the PWM. If present, we selected up to 5 alignments with a score over 90% as a potential TFBSs in our sequences.

In addition, a more specific search for CTCF binding sites was also conducting using CTCFBSDB2.0 prediction tool available at http://insulatordb.uthsc.edu/storm_new.php [244].This tool uses the STORM program [245] and six selected PWM for CTCF binding sites to report the single best hit in the sequence. The PWM score corresponds to the log-odds of the observed sequence being generated by the motif versus being generated by the background. We selected sequences with a PWM score > 3.0, as suggested in the tool's documentation, thus finding a total of 33 CpG sites with a putative CTCF binding site.

m6A-Seq

Up to 500 µg of total RNA of each time-point was purified using the RNeasy Mini Kit (Qiagen, Ref: 74106). All the samples were sent to Gideon Rechavi's laboratory (Sheba Cancer Research Center, Israel), where m6A-Seq was performed as previously described [125, 126]. Briefly, multiple biological replicates of total RNA for each time-point were pooled and RNA was chemically fragmented using a ZnCl2 mixture. An input aliquot of total RNA was stored for each time-point. Then, m6A-modified RNA was immunoprecipitated using antibodies against m6A-RNA (Synaptic Systems, Ref: 202 111). cDNA library was prepared using TruSeq sample preparation kits (Illumina, Refs: 1004814, 15013136, 15013676, 15019749). Next generation sequencing was performed using the Illumina GAIIx platform via 36-cycle module. Raw data was stored in the NCBI SRA (PRJNA734010). RRACH motif analysis was performed with a custom alignment R script.

m6A-Seq data (SRA-PRJNA734010):

https://www.ncbi.nlm.nih.gov/bioproject/PRJNA734010

m6A-seq bioinformatic analysis

Raw data quality was assessed using FASTQC tool (v0.11.8; https://www.bioinformatics.babraham.ac.uk/projects/fastqc/) and pre-processed (adapter and quality trimming) using Trimmomatic (v0.39) [246]. Surviving reads were mapped to the human genome (GRCh38) using STAR (v2.7.3a) [247]. Alignment sam and bam files were further processed

using samtools (v1.9) [248]. Next, alignment bam files were deduplicated using picard MarkDuplicates tool (v2.23.4) [249]. m6aViewer tool (v1.6.1) [250] was used to identify m6A peaks and to perform differential m6A analysis. Peaks were considered differentially methylated at FDR < 0.05. Found peaks were further annotated using annotatePeaks.pl script from the Homer suite (v4.10) [251], using annotations from Gencode (v.28 https://www.gencodegenes.org/). Graphical representation of the peaks was performed using R (v.3.6.3) and Gviz (v1.36.0) package [252].

Gene Set Enrichment analyses

Gene set enrichment analyses were conducted using Enrichr (https://maayanlab.cloud/Enrichr/) by performing hypergeometrical tests, using different gene sets: Gene Ontology Biological Process, Gene Ontology Molecular Function, Gene Ontology Cellular Component, Reactome and KEGG pathways. Enrichments were considered significant at FDR < 0.05. Graphical representations were performed using R (v.3.6.3) and ggplot2 (v3.3.0) package [253].

Integration m6A-seq gene expression

Microarray expression array data was collected from GEO (GSE44700) [58] and differential expression analysis was conducted using limma R package (v3.42.2) [254], using FDR < 0.05 as significance threshold. Integration analysis between m6A-seq results and gene expression data were performed using custom python scripts.

METTL3-shRNA Knockdown model generation

For the generation of METTL3 knockdown models, we performed lentiviral infection of BLaER1 cells with pLKO.1-TRC (Addgene, Ref: 10878). Briefly, we designed two sets of shRNA (sh-1 and sh-2, see supplementary methods table) following Addgene's instructions, in order to ensure maximum target complementarity and Argonaut-mediated strand-specific RNA decay. pLKO.1-TRC-shRNA and pLKO.1-TRC-Empty Vector (EV) plasmids were packed in lentiviral particles using HEK-293T jetPRIME-transfected cells (Polyplus, Ref: 114-15). After 48 hours of incubation, 1 mL of lentiviral supernatant was added to 1 x 10^6 BLaER1 cells cultured in a 6-well plate and spinoculation was performed (1000g, 90min,

36°C). After incubating for 24 hours, cells were selected with 2 µg/mL of puromycin for 24 more hours. Afterwards, clones were generated by cell sorting (BD FACSAria II). Viable clones were selected, and METTL3-knockdown was validated by Western Blot (see antibodies in supplementary methods table).

Recovery overexpression BLaER1 model for METTL3

METTL3 cDNA without the 3'UTR region complementary to sh2.1 was obtained from wild-type BLaER1 cells using two custom primers (Forward: TTTTTTTTTTCGAAGCCGCCAC-CATGTCGGACACGTGGAGCTCTATCCAGG; Reverse: TTTTTTTTTCTAGAC-TATAAATTCTTAGGTTTAGAGATGATACCATCTGGGTACCTTTGCTTGAACCG) and cloned into a custom pLVX-tdTomato expression plasmid. Lentiviral infection by spinoculation was performed in sh2.1 BLaER1 cells, following the same procedure as described in "METTL3-shRNA Knockdown model generation". Positive clones for tdTomato were single-cell sorted by FACS and cultured in 96 well plates with 100 RPMI-1640 GlutaMAX, 10% FBS, 1X Penicillin/Streptomycin per well. Positive clones were grown and METTL3 content was validated by western blot. Then, transdifferentiation was performed for low and high-METTL3 expressing clones as described in "Transdifferentiation of BLaER1 cells". Empty vector sh2.1, low-METTL3 sh2.1 and high-METTL3 sh2.1 BLaER1 transdifferentiated cells (168 hours) were analyzed stained with αCD19-PE and αCD11b-APC antibodies to calculate transdifferentiation efficiency and tdTomato expression.

Flow cytometry analysis of transdifferentiation efficiency and cell sorting

For assessing transdifferentiation efficiency, we performed flow cytometry as previously described [237]. CD19-PE and CD11b-APC or CD14-APC-Vio770 fluorescent antibodies (see supplementary methods table) were used to detect B-cell and Macrophage cells, respectively. To calculate transdifferentiation efficiencies, cells were quantified using CountBright Plus Absolute Counting Beads (Invitrogen, C36995). CD Flow cytometry was performed in a BD FACSCanto II (Becton Dickinson, Ref: 338962) and results were analyzed with BD FlowJo Software.

RT-qPCR of differentiation markers and ribosomal protein-related mRNAs

For wild-type BLaER1 qRT-PCR, biological triplicates were harvested at different time-points of transdifferentiation (0 hours vs 168 hours). For shRNA-METTL3 knockdown RT-qPCR, biological triplicates at 168h of transdifferentiation were harvested. RNA extraction was carried out using the RNAeasy mini kit (Qiagen) according to the manufacture guidelines. Retrotranscription of 2 µg of total RNA was performed using RevertAid RT kit (Thermo Scientific, Ref: 00719361). qRT-PCR was performed using the QuantStudio 5 system (Applied Biosystems, Ref: A28140) with the conditions listed in the table below. PGK was used as housekeeping gene as previously described [58]. T-Test for unpaired samples was used to perform statistical analysis (T-Test, *p<0.05). Normality and homogeneity in variance are assumed for RT-qPCR experiments with biological triplicates. Primer sequences are listed in the supplementary methods table.

IC50 cell viability assay for STM2457 in BLaER1 wild-type cells

10,000 wild-type untreated BLaER1 cells per well were seeded in a 96-well plate (100 µL/well). Lyophilized STM2457 (Storm Therapeutics) was dissolved in 100% DMSO at a final concentration of 10 mM. Cells were treated with different concentrations of STM2457 (biological sextuplicates). DMSO 1% was used as untreated control. After 72 hours, 10 µL of 5 mg/mL MTT (Thiazolyl Blue Tetrazolium Bromide, Sigma, Ref: M2128-10G) dis-solved in PBS pH 7.2 1X (Gibco, Ref: 20012-019) were added to each well. After 3 hours of incubation at 37 ºC, 100 µL of lysis buffer (54% N,N-Dimethylformamide dissolved in H2O, 216 mg/L SDS, 2.7% acetic acid glacial, pH 4.6 adjusted with HCl) were added to each well and incubated 37 ºC overnight. Plates were analyzed in a ThermoScientific Multiskan Sky spectrophotometer (λ = 630 nm). Two-tailed unpaired Student T-test was applied for statistical analysis (* $p < 0.05$; ** $p < 0.001$, *** $p < 0.0001$).

STM2457 m6A inhibitor treatment of BLaER1 cells

Lyophilized STM2457 (Storm Therapeutics) was dissolved in 100% DMSO at a final concentration of 10 mM. 5 x 10^6 BLaER1 cells cells (biological triplicates) were cultured in 10 mL of RPMI-1640 GlutaMAX, 10% FBS, 1X Penicillin/Streptomycin and transdifferentiation was induced as aforementioned. To test the effects of STM2457 on transdifferentiation efficiency, 5 µM of STM2457 was added at 0 hours of induction. CD19 and CD11b expression was analyzed by flow cytometry and RNA was purified in order to quantify the expression of ITGAM and CSFR1 macrophage differentiation markers. To test the effects of STM2457 on the levels of ribosomal protein mRNA, 5 µM of STM2457 was added at 168 hours of induction. Cells were harvested, RNA purified, retrotranscribed and analyzed by RT-qPCR as previously described.

Measurement of m6A on polyA RNA by LC-MS/MS

A fraction of RNA with a polyA tail (polyA RNA, which is mostly mRNA) was separated from total RNA using a dynabeads-based kit (Thermo). This polyA RNA was digested to component nucleosides with an enzyme cocktail of benzonase, phosphodiesterase and alkaline phosphatase (Merck), all used as according to the manufacturer's instructions. Nucleosides were separated by reverse phase liquid chromatography (Agilent) - eluent A was 0.1% v/v formic acid in water, and eluent B was 0.1% v/v formic acid in acetonitrile, and a non-linear gradient of 2-15% B resolved nucleosides on a Acquity HSS T3 C18 column (Waters). The eluent was sprayed into a 4500 triple quadrupole mass spectrometer (Sciex) and characterised by tandem mass spectrometry using a multiple reaction monitoring approach. Injection amounts were assessed by internal calibration with isotopically-labelled uridine and quantification (in ng) was extrapolated from external calibration of a range of nucleoside standards using Multiquant software (Sciex). The final expression of the data was the ng of modified nucleoside (m6A) divided by the ng of total canonical nucleoside (A, C, G and U) expressed as a percentage.

Actinomycin-D chase assay (RPS25 mRNA decay analysis)

For RPS25 mRNA decay analysis, 2.5 x 10^6 BLaER1, EV and sh2.1 cells were plated (in biological quadruplicates) in 5 mL of RPMI-1640 GlutaMAX, 10% FBS, 1X Penicillin/Streptomycin and transdifferentiation was induced as aforementioned. At 0 hours and at 168 hours of transdifferentiation, 10 µg/mL of Actinomycin-D (Sigma, A4262) is added for 1.5 hours and 3 hours in separate biological quadruplicates. After each time has passed, cells are harvested and RNA is extracted, retrotranscribed and analyzed by qRT-PCR as aforementioned in section “qRT-PCR of ribosomal protein-related mRNAs”. T-Test for each time point was used to perform statistical analysis (T-Test, *p<0.05).

Growth assay

5 x 10^6 BLaER1, EV and sh2.1 cells (biological triplicates) were cultured in 10 mL of RPMI-1640 GlutaMAX, 10% FBS, 1X Penicillin/Streptomycin and transdifferentiation was induced as aforementioned. Cells were counted at 0h, 72h and 168h after transdifferentiation induction (in triplicate) by centrifuging the cells (200 g, 5 minutes, room temperature), resuspending them in 10 mL PBS 1X (Gibco, 20012050), diluting 10 µL of the cell suspension in 10 µL Trypan Blue (Gibco, 15250061) and introducing 10 µL of this dilution in a cell counting Neubauer hemocytometer chamber. Count was performed manually with the help of a visible light inverted microscope. T-Test for each time point was used to perform statistical analysis (* $p < 0.05$; ** $p < 0.001$, *** $p < 0.0001$).

Cell cycle assay

5 x 10^6 BLaER1, EV and sh2.1 cells (biological triplicates) were cultured in 10 mL of RPMI-1640 GlutaMAX, 10% FBS, 1X Penicillin/Streptomycin and transdifferentiation was induced as aforementioned. After 168 hours of transdifferentiation, cells were harvested and concentration was calculated by Trypan Blue hemocytometer counting. 1 x 106 cells were centrifuged and resuspended in 1 mL of Propidium Iodide (Sigma-Aldrich, P4864-10ML) previously mixed with Triton-X100 (0.1% v/v final concentration, in PBS 1X) and 0.2 mg/mL of RNase A. After 15 minutes of incubation at 37 °C, cells were analyzed by flow cytometry in a BD FACSCanto II (Becton Dickinson, Ref: 338962) and results were analyzed with BD FlowJo Software. T-Test for each time point was used to perform statistical analysis (* $p < 0.05$; ** $p < 0.001$, *** $p < 0.0001$).

Annexin-V apoptosis assay

5 x 10^6 BLaER1, EV and sh2.1 cells (biological triplicates) were cultured in 10 mL of RPMI-1640 GlutaMAX, 10% FBS, 1X Penicillin/Streptomycin and transdifferentiation was induced as aforementioned. After 168 hours of transdifferentiation, cells were harvested and concentration was calculated by Trypan Blue hemocytometer counting. 200,000 cells were centrifuged and resuspended in 150 µL of Annexin-V binding buffer 1X (50 mL PBS pH 7.2 1X, 2.5 mM CaCl2, 140 mM NaCl, 10 mM HEPES) freshly supplemented with 0.01 µg/mL of Annexin-V-APC (BioLegend, Ref: 640930). Cells were immediately analyzed in a BD FACSCanto II flow cytometer. Two-tailed unpaired Student T-test was applied for statistical analysis (* $p < 0.05$; ** $p < 0.001$, *** $p < 0.0001$).

Puromycin assay for assessing global protein synthesis

5 x 10^6 wild-type, EV and sh2.1 BLaER1 cells in 10 mL RPMI-1640 GlutaMAX, 10% FBS, 1X Penicillin/Streptomycin at 0 and 168 hours of transdifferentiation were treated with 20 µg/mL of puromycin for 2 hours (cells incubated at 37 ºC, 5% CO_2). Cells were harvested, proteins were extracted with RIPA 1X lysis buffer and western blot was performed (as we previously described) using an anti-puromycin antibody (Sigma-Aldrich, Ref: MABE343).

Phagocytosis Assay

1 x 10^6 EV and sh2.1 BLaER1 cells were seeded into 6-well plates (in biological triplicates) in 2 mL of RPMI-1640 GlutaMAX, 10% FBS, 1X Penicillin/Streptomycin and transdifferentiated for 168 hours as previously described. Then, 100 x 10^6 dsRed+ *Escherichia coli* (100 *E. coli* per 1 cell) were added in each well and plates were immediately centrifuged at 800g for 5 minutes. Afterwards, 400 µg/ml gentamycin was added in each well for 3 hours at 37°C to eliminate extracellular *E. coli*. To remove excess bacteria and, cells were washed three times with PBS, trypsinized and collected. αCD19-PE and αCD11b-APC antibodies (reference in table below) were used to stain cells and dsRed+ *versus* dsRed- macrophages were quantified by flow cytometry. dsRed+ *E. coli* were provided by Thomas Graf, in behalf of Dr. R. Copin.

Figure drawings and statistical analysis software

Otherwise specified, all the drawings in this PhD thesis have been created using BioRender online licensed software. Statistical tests and graphics were performed with GraphPad Prism licensed software.

Primers used for Real-Time Quantitative PCR (RT-qPCR)

Primers qRT-PCR	Forward (5' to 3')	Reverse (5' to 3')
RPS25	GAAGATTCGAGGCTCCTTGG	CTCGAGCATCTCCACCCTTG
RPL23A	TTTCACAAGATGGCGCCGAA	TGGCTGTGGACACCTTTCAA
RPS3	TGCGAGTTACACCAACCAGG	TTGGGTTCCACAATGCTCTAC
RPS21	CGCTAGCAATCGCATCATCG	CTCTGCCTGTACCTTCACCC
RPS27	CGAGAACATGCCTCTCGCAA	ACTACCGTTTGTGCATGGCT
RPS14	TGGAGACGACGTGCAGAAAT	TTCATCCCACCAGTCACACG
RPL3	CAGTGATGAATGCAAGAGGCG	GACACGGATGACTTGGCAGT
PGK	CTGGGCAAGGATGTTCTGTT	CACATGAAAGCGGAGGTTCT
IGJ	TGTTCATGTGAAAGCCCAAG	TCGGATGTTTCTCTCCACAA
IGLL1	GGCAGGTTCCTGCTCCAG	CCAAACACATGCGTCACTG
CD14	GATTACATAAACTGTCAGAGGC	TCCATGGTCGATAAGTCTTC
VPREB3	GGGGACCTTCCTGTCAGTTT	ACCGTAGTCCCTGATGGTGA
EBF1	TGCTACTCCCTGTATCAAAG	ATGGTACCGAATATGACCTG
CSFR1	TCCAAAACACGGGGACCTATC	CGGGCAGGGTCTTTGACATA
ITGAM	GGGGTCTCCACTAAATATCTC	CTGACCTGATATTGATGCTG
IL1RN	TGAGGACCAGCCATTG	AGACCATTCTGGAGGCAG
ITGAX	CGTTCGACACATCCGTGTA	TTTGCCTCCTCCATCATTTC
RHOG	CTCTCACTTCCTTCTCGAGCC	GTTGCTGTAGTGGAGGCAGT
CCR1	GCATGAACTCTCTGCTGGGT	CCCCAGGCCACCATTACATT
CXCL8	TGGACCCCAAGGAAAACTGG	TGGCATCTTCACTGATTCTTGGA
CHML	GCAGGAGGTTTAATATTGATTTG	AAGACATCTGCTCTGGAACA
DBF4	TACCTTCTGTCACCATATCTGAA	TCGACCCAAGGTTTGTG

shRNA METTL3 sequences

shRNA primer sequences	Sense (5' to 3')	Antisense (5' to 3')
sh1	CCGGAAGGTACCCAGATGGTATCA TCTCGAGATGATACCATCTGGGTAC CTTTTTTTG	AATTCAAAAAAAGGTACCCAGATGGT ATCATCTCGAGATGATACCATCTGGG TACCTT

sh2	CCGGAACCTGAAGAGTGATATTTGTCTCGAGACAAATATCACTCTTCAGGTTTTTTTG	AATTCAAAAAAACCTGAAGAGTGATATTTGTCTCGAGACAAATATCACTCTTCAGGTT
shE1	CCGGCCGCGTGAGAATTGGCTATATCTCGAGATATAGCCAATTCTCACGCGGTTTTTG	AATTCAAAAACCGCGTGAGAATTGGCTATATCTCGAGATATAGCCAATTCTCACGCGG

Bisulfite sequencing (BSP) primers

Primers BSP	Forward (5' to 3')	Reverse (5' to 3')
ITGAX promoter	TTAAGGGTGAGTTTGGGA	CTACCCTAATCCTAATCATAACTAAAA
IL1RN promoter	AGGGGAGGGAATTAGTTATAAT	AAAACCTCTACAAATTTCCATTC
RHOG related distant region	GGGGGTTTGATGAGATAAGG	AAACCACCACACCTAACCTAAA
CCR1 related distant region	TTTGTAAGTTAGGAAGGGGGATA	CATCAAAACAAAACTCCATCTCA
CXCL8 related distant region	TAGAAGTAAATGAAGTTTGGGTTGG	CCAAATATCTTCTCCCCACCA
CHML related distant region	TGAGGGTAATTTTGGGGATTT	AAAATCACACTCCCTCAACACA
DBF4 related distant region	TTTTAAAATTTGTTGAAAGGGATG	TTCAAAACAATATATTATCCCAAAACC

Pyrosequencing primers

Primers PCR Pyrosequencing	Forward (5’ to 3’)	Reverse (5’ to 3’)	Sequencing (5’ to 3’)
ITGAX promoter	AGGGTATTAAGTTAAGTTATTTGATGAGA	Biotin(5’)-ACCCTAATCCTAATCATAACTAAAAAATC	AGTGGGGTTGAAAGTGATAAT
IL1RN promoter	Biotin(5’)-AGTGGGGTTGAAAGTGATAAT	AAAACCTCTACAAATTTCCATTCTA	CACTCACCCAAACTAA
RHOG related distant region	TGTAAATGGTGGTTTTTATTAAAAGTGAAG	Biotin(5’)-CACCTCAACCTCCCAAAAT	AGGTATTTATTTTATGTAGAA
CCR1 related distant region	Biotin(5’)-AGTTAGGAAGGGGGATATTATTAG	TACCAAAACTTCCTCTTTCTTCAC	CCTCTTTCTTCACCTAC
CXCL8 related distant region	Biotin(5’)-GGTTGGGTTTAAATTTATTGTGGTAAAG	ACAACTTCTCCCCATAAAACACATCATT	AAAACACATCATTAAAAATAACTA

CHML related distant region	GGGGATTGTTTATTTAGATTTAGTAGT	Biotin(5')-ACTCCCTCAACACAATACTT	AGAAAAGAGGAATAGGTTAT
DBF4 related distant region	GTTTTAAAATTTGTTGAAAGGGATGTT	Biotin(5')-ATTCAAAACAATATATTATCCCAAAACC	TGTTAATTGTAGTGGTTAATTTT

UMI-4C primers

Primers UMI-4C	Upstream Primer	Downstream Primer
CCR1	GTTGTCCTTGGGTTTAGCTGC	AGAAAGAGGAAGTCCTGGCAAT

Antibodies for Western Blot and Flow Cytometry

Antibodies	Company	Reference	Source	Dilution
IL1RN	R&D Systems	AF-280-NA	Goat	1:400
ITGAX-APC	BD Pharmingen	559877	Mouse	1:400
DNMT1	Boster	CI1105	Rabbit	1:500
DNMT3A	Abcam	ab2850	Rabbit	1:500
DNMT3B	Sigma-Aldrich	HPA001595	Rabbit	1:500
TET1	Novus Biologicals	NBP2-19290	Rabbit	1:1000
TET2	Cell Signaling	12/2017	Rabbit	1:1000
TET3	Abcam	ab139311	Rabbit	1:1000
Lamin B1	Abcam	ab16048	Rabbit	1:5000
Anti-Rabbit HRP	Sigma-Aldrich	A0545	Goat	1:10000
Anti-Goat HRP	Dako	P0449	Rabbit	1:5000
METTL3	Cell Signaling	86132S	Rabbit	1:1000
WTAP	Cell Signaling	41934S	Rabbit	1:1000
METTL14	Cell Signaling	51104S	Rabbit	1:1000
YTHDF2	Cell Signaling	80014S	Rabbit	1:1000
FTO	Cell Signaling	45980S	Rabbit	1:1000
ALKBH5	Novus	NBP1-82188	Rabbit	1:1000
Caspase-8	Cell Signaling	9746S	Mouse	1:1000
Caspase-3	Cell Signaling	9668S	Mouse	1:1000
PARP	Cell Signaling	9542T	Rabbit	1:1000
β-Actin-HRP	Sigma	A3854	Mouse	1:10000
Lamin-B1	Abcam	ab16048	Rabbit	1:5000

Anti-Rabbit-HRP	Sigma-Aldrich	A0545	Goat	1:10000
Anti-Mouse-HRP	Sigma	A9044	Rat	1:10000
CD19-PE	MACS	130-091-247	Mouse	1:400
CD11B-APC	BioLegend	101212	Rat	1:400
CD14-APCVio770	Miltenyi Biotec	130-113-144	Mouse	1:400

Genomic regions of the demethylated CpGs under study. Genomic nucleotidic position correspond to the hg19 human genome version.

CpG Regions	**CpG code**	**Genomic Position**
IL1RN promoter	cg02543462	chr2:113885116
ITGAX promoter	cg20851120	chr16:31366406
	cg04742550	chr16:31366429
RHOG related distant region	cg21880051	chr11:9661734
CCR1 related distant region	cg21655255	chr3:46136952
CXCL8 related distant region	cg05146536	chr4:77140678
CHML related distant region	cg00250658	chr1:223349112
DBF4 related distant region	cg06297012	chr7:90929852
BSP Regions	**From (5' to 3')**	**To (5' to 3')**
IL1RN promoter	chr2:113884986	chr2:113885222
ITGAX promoter	chr16:31366289	chr16:31366594
RHOG related distant region	chr11:9661553	chr11:9661894
CCR1 related distant region	chr3:46136807	chr3:46137151
CXCL8 related distant region	chr4:77140560	chr4:77140859
CHML related distant region	chr1:223348914	chr1:223349150
DBF4 related distant region	chr7:90929660	chr7:90929889
Pyrosequencing Regions	**From (5' to 3')**	**To (5' to 3')**
IL1RN promoter	chr2:113885083	chr2:113885112
ITGAX promoter	chr16:31366405	chr16:31366459
RHOG related distant region	chr11:9661726	chr11:9661761
CCR1 related distant region	chr3:46136912	chr3:46136958
CXCL8 related distant region	chr4:77140639	chr4:77140687
CHML related distant region	chr1:223349092	chr1:223349138
DBF4 related distant region	chr7:9092983	chr7:90929881

PCR conditions for RT-qPCR, BSP and Pyrosequencing

RT-qPCR conditions (10 µL/well)						
Hold Stage		**PCR Stage (40 cycles)**		**Melting Curve Stage**		
50 °C 2 min	95 °C 10 min	95 °C 15 sec	60 °C 1 min	95 °C 15 sec	60 °C 1 min	95 °C 15 sec

BSP conditions (for 100 ng DNA)					
Hold Stage	**PCR Stage (40 cycles)**			**Resting Stage**	
98 °C 1 min	98 °C 10 sec	57 °C 45 sec	72 °C 1 min	72 °C 7 min	4 °C ∞

Pyrosequencing PCR conditions (for 10 ng DNA)					
Hold Stage	**PCR Stage (48 cycles)**			**Resting Stage**	
96 °C 10 min	96 °C 30 sec	58 °C 30 sec	72 °C 30 sec	72 °C 10 min	15 °C ∞

ANNEXES

Table A-1. Cellular markers for the distinct stages of human B cell development. Grey cells depict represent markers that are not interrogated for a particular B cell differentiation stage. Surface cellular markers (starting with "CD": "Cluster of Differentiation") are usually interrogated by flow cytometry, while internal cellular markers (like PAX5, FOXO1, etc.) are usually analyzed by RT-qPCR.

Cell Markers	LT-HSC	ST-HSC	MPP	LMPP	CLP	Pre-Pro-B	Pro-B	Early-Pre-B	Late-Pre-B	Immature B cell	Mature B cell	T1 B cell	T2 B cell	MZ cell	FO cell	Centroblast	Centrocyte	Memory B cell	ST Plasma cell	LT Plasma cell
CD34	+	+	+	+	+	+	+	-	-	-	-	-	-	-	-	-	-	-	-	-
CD45RA	-	-	-	+ (Low)	+															
CD49f	+	-	-	-	-															
Thy1 (CD90)	+	-	-	+ (Low)	-															
Lin	-	-	-	-	-															
CD127					+	+	+	+	+	+	-									
CD133	+																			
CD201	+																			
GPI-80	+																			
CD38	-			-	+ (Low)	+	+	+	+	+ (High)	+ (High)	+ (Int)	+ (Int)	+ (Low)	+ (Low)	+ (Low)	+ (Low)	-	+ (High)	+ (High)
CD10				-	+	+	+	+	+	+	+	+ (Low)	+ (Low)	-	-	+	+	-	+ (Low)	+ (Low)
CD135 (Flt3)					+	+	-													
PAX5	-	-	-	-	-	+	+	+	+	+	+	+	+	+	+	+	+	-	-	-
FOXO1					+															
EBF						+	+	+	+	+	+	+	+	+		+	+			
E2A						+	+	+	+	+	+	+	+	+						
PU.1						+														
OCT2								+	+	+	+	+	+	+						
CD45							+													
CD43							+													
CD117 (c-Kit)	+				+	+ (Low)	+ (Low)	-	-											
ΨLC						-	-	+	+	-	-	-	-	-	-	-	-	-	-	-
CD19						+ (Low)	+	+	+	+	+	+	+	+	+	+	+	+	-	-
CD20						-	+	+	+	+	+	+	+	+	+	+	+	+	-	-
CD24						-	+	+	+	+ (High)	+ (High)	+ (Int)	+ (Low)	+ (Low)	-	-	-	-	-	-
CD28												+	+							
CD93 (C1qR1)						-	+	+							-					
IL3R						-	+	+												
IL7RA						-	+	+												
IL4RA						-	-	+												
CD79A								+	+											
CD79B								+	+											
CD179B					+	+	+	-												
TdT						+	+	-												
CD21						+ (Low)	+ (Low)	+ (Low)	+ (Low)	+ (Low)	+	+	+	+	+	+	+	+	-	-
CD27						-	-	-	-	-	-	-	-	+	-	+	+	+	+ (High)	+ (High)
CD40								+	+	+					-	+	+	+ (Low)	-	-
CD23															+					
TACI																			+	+
CD1c														+						
FCRL3														+						
CD22															+					
MHC-II															+ (High)	+	+	+	+ (Low)	+ (low)
BLIMP1																			+	+
IRF4																			+	+
XBP1																			+	+
OBF1																		+		
SPI-B																		+		
CD138																			+	+
CD83																-	+			
CD86																-	+			
CXCR4																+	-	-	+	+
BCL2																		+	+	+
BCl6																+	+	-	+	+
CD1D														+						
R123										+	+	+	+ (Low)	-	-					
IgA						-	-	-	-	-	-	-	-	-	-	+ (Variable)	+ (Variable)	+ (Variable)	-	-
IgD						-	-	-	-	-	-	-	-	-	-	+ (Variable)	+ (Variable)	+ (Variable)	-	-
IgG						-	-	-	-	-	-	-	-	-	-	+ (Variable)	+ (Variable)	+ (Variable)	-	-
IgM						-	-	-	-	+	+	+	+	+ (High)	+ (Low)	-	-	+ (Variable)	-	-
IgD						-	-	-	-	-	+	+	+	+ (Low)	+ (Low)	-	-	+ (Variable)	-	-

Table A-2. Cellular markers for the distinct stages of human macrophage development. Grey cells depict represent markers that are not interrogated for a particular B cell differentiation stage. Surface cellular markers (starting with “CD”: “Cluster of Differentiation”) are usually interrogated by flow cytometry, while internal cellular markers (like PAX5, FOXO1, etc.) are usually analyzed by RT-qPCR.

Cell Markers	LT-HSC	ST-HSC	MPP	CMP	GMP	NMP	MDP	cMoP	Monocyte	Int. Monocyte	Pat. Monocyte	M0 Mac.	M1 Mac.	M2 Mac.
CD34	+	+	+	+	+	+	+	+	-	-	-	-	-	-
CD45RA	-	-	-	-	+									
CD49f	+	-	-											
Thy1 (CD90)	+	-	-											
Lin	-	-	-	-	-	-	-	-						
CD117 (c-Kit)	+			+	+	+	+	+	-	-	-			
CD133	+													
CD201	+													
GPI-80	+													
CD38	-			+	+									
CD123				+	+									
Ly6A (Sca1)				-	-	-	-							
CD16/CD32				+ (Low)	+ (High)	+	+ (Low)	+ (High)	+	+	+			
CD115				+ (Low)	+ (Low)	+	+ (High)	+ (High)	+	+	+			
Flt3				+ (Low)	-		+	-	-	-	-			
CD11b						-	-	-	+	+	+	+	+	+
Ly6C				-	-	+	-	+	+ (High)	+ (Int)	-			
CX3CR1				-	+ (Low)		+ (High)	+ (High)	+ (Low)	+ (Int)	+ (High)			
CD62L									+		-			
CCR2								+ (Low)	+		-			
CD43								-	-	+ (Low)	+			
CXCR4								+ (High)	+ (Low)	+ (Low)	+			
CD31								+	-	-	-			
CD274											+			
CD14									+	+	+	+	+	+
CCR5												+	+	+
CD11c (ITGAX)												+	+	+
MHC-II												+	+	+
CD80													+	
CD86													+	
TLR2													+	
TLR4													+	
iNOS													+	
CD163														+
CD206														+
CD209														+
FIZZ1														+
Ym1/2														+
C/EBPα				+	+	+		+	+					
GATA-1				+										
GATA-2				+										
NF-E2				+										
PU.1				+	+	+		+						
TAL-1					+									
Gfi-1					+	+								
C/EBPε					+									
KLF4						+	+	+	+					
IRF8							+	+	+					
TFEC								+						
ZEB2									+					
IRF5									+					
NR4A1										+	+			
C/EBPβ									+	+	+			

Table A-3. List of references for each clinical case of lymphoid-to-myeloid transdifferentiation depicted in table I-3.

First Author	Journal/Book	Publication Year	Number of patients	Type
Cheng F et al	Int J Surg Pathol	2021	2	1 CLL/SLL to HS + 1 DLBCL to HS
Sabatini PJB et al	Br J Haematol	2021	1	1 MZL to HS
Tashakori M et al	Ann Diagn Pathol	2021	1	1 FL to Langerhans cell Sarcoma (LCS)
Andersen KF et al	Diagnostics (Basel)	2021	0	1 Pure HS, well treated, INCIDENCE
Egan C et al	Mod Pathol	2021	16	6 FL to HS + 2 CLL/SLL to HS + 3 B-ALL to HS + 4 T-ALL to HS + 1 T-ALL to Indet. Dendritic cell tumor
Okada K et al	Pathol Int	2021	2	15 Pure HS + 2 HS with IGH rearrang, indet. Origin
Zhang Q et al	Blood	2020	1	1 MCL to HS (response to CART-19)
Péricart S et al	Virchows Arch	2020	1	1 FL to HS synchronous. Mean 62 years (59-81 years, male predominance), 75% B metachrounous (after) to HS, 25% B synchronous (with) HS
Rassidakis GZ et al	Ann Hematol	2020	1	1 CLL to DLBCL to HS
Frauenfeld L et al	Virchows Arch	2019	1	1 CLL to LCH
Skala SL et al	Clin Pathol	2019	3	2 CLL/SLL to HS + 1 FL to LCS
Farris M et al	Clin Lymphoma Myeloma Leuk	2019	1	1 FL to HS (Bendamustine and Rituximab worked)
Skala SL et al	Arch Pathol Lab Med	2018	0	All types of B-to-Myeloid cancerous transformations (2-8% CLL/SLL cases transform to HS) (59-81 years, male predominance)
Choi SM et al	Diagn Pathol	2018	1	1 FL to LCS (KRAS mutation in post-transdifferentiation)
Kosmidis P et al	Diagn Pathol	2018	0	15 FL and 7 ISFN, nothing detected with FICTION. t(14;18)(q32;q21), is a B-cell FL only marker... thus transdifferentiation surrogate as IGH
Abid MB et al	Leuk Res Rep	2017	1	1 pre-B-ALL to Secondary Malignant Histiocytosis (SMH = Indet DCT) (Alemtuzumab treated, then sibling allogenic transplant)
Thakral B et al	Blood	2016	1	1 B-ALL to HS
Steussy B et al	Lab Med	2016	1	1 FL to AHL (Steussy)
Das DK et al	Diagn Cytopathol	2016	1	1 HL to LCH
Nakamine H et al	J Clin Exp Hematop	2016	0	LCH and LCS Incidence and Histologic findings
Verma A et al	Indian J Pathol Microbiol	2015	1	1 FL to HS
Ambrosio MR et al	Virchows Arch	2015	1	1 MZL to LCS
Alten J et al	Pediatr Blood Cancer	2015	2	2 T-ALL to HS (children, fulminant)
Mehrotra S et al	Diagn Cytopathol	2015	1	1 FL to HS
O'Malley DP et al	Ann Diagn Pathol	2015	2	1 AITL to Interdigitating dendritic cell sarcoma (IDCS) + 1 B-cell rearranged (indet) to IDCS
O'Malley DP et al	Ann Diagn Pathol	2014	1	3 pure IDCS + 1 CLL to IDCS
Buser L et al	Pathobiology	2014	1	1 Pro-T-ALL to Indeterminate dendritic cell tumor
Feldman AL et al	Surg Pathol Clin	2013	0	The Blue review (3 hypothesis and example table) - Andrew L Feldman
Subbiah V et al	Ann Hematol	2013	0	TO THE EDITOR --> LCH usually harbor BRAF V600E mutation (usually found in Hairy Cell Leukemia)
West DS et al	Am J Surg Pathol	2013	2	1 FL to LCS + 1 FL to LCH
Chen W et al	N Am J Med Sci	2013	1	1 CLL/SLL to LCS (Synchronous with BRAF V600E mutations)
Stoecker MM et al	Arch Pathol Lab Med	2013	0	The Classical Review 22 B-cell to H/DS (dismal prognosis)
Takahashi E et al	J Clin Exp Hematop	2013	0	The WHO review (HS is rare but very aggressive) - more related to mature leukemia than early leukemia
Llamas-Velasco M et al	J Cutan Pathol	2012	1	1 MZL to HS
Muslimani A et al	Ann Hematol	2012	1	1 HCL to LCS
Zeng W et al	J Cutan Pathol	2011	1	1 FL to HS
Shao H et al	Mod Pathol	2011	7	4 CLL/SLL to IDCS + 1 CLL/SLL to LCS + 1 CLL/SLL to HS + 1 CLL/SLL to Indet. Dendritic cell tumor (preferential usage of IGHV4-39 by the V–D–J gene rearrangement and Chr 17p abnormalities)
Wang E et al	Am J Surg Pathol	2011	1	1 FL to HS (17 years after FL diagnosis) and then to DLBCL
Congyang L et al	Int J Hematol	2011	1	1 DLBCL to HS (Syncrhonous)
Tucci M et al	Oncologist	2011	0	MM and DCs in the bone microenvironment (nothing to do with us)
Ratei R et al	Haematologica	2010	1	1 B-ALL to LCS
Chen W et al	Am J Surg Pathol	2010	18	4 LCH cases with IGH clonal rearrangements (no pre-cancer) + 5 IGK rear + 9 TRG rear + 32 pure LCH
Zhang D et al	Leuk Lymphoma	2010	0	Commentary to: Histiocytic sarcoma arising in indolent small B-cell lymphoma: report of two cases
Wang E et al	Leuk Lymphoma	2010	2	1 MZL to HS + 1 FL to HS
Castro EC et al	Pediatr Dev Pathol	2010	15	1 T-ALL to LCH + 2 T-ALL to HS + 1 T-ALL to LCS + 2 B-ALL to HS + 3 B-ALL Indet Dendritic cell tumor + 3 T-ALL Indet + 3 B-ALL to Xanthomatome
Fraser CR et al	Am J Clin Pathol	2009	1	1 CLL/SLL to IDCS
Chen W et al	Am J Surg Pathol	2009	11	9 IGH rearranged sporadic HS + 2 IGK rearranged sporadic HS
Bassarova A et al	J Hematop	2009	2	1 FL to HS + 1 DLBCL to HS
Zhang D et al	Int J Hematol	2009	1	1 FL to HS
Feldman AL et al	Blood	2008	8	7 FL to HS + 1 FL to IDCS

REFERENCES

REFERENCES

1. Bianconi, E., Piovesan, A., Facchin, F., Beraudi, A., Casadei, R., Frabetti, F., Vitale, L., Pelleri, M.C., Tassani, S., Piva, F., Perez-Amodio, S., Strippoli, P., Canaider, S.: An estimation of the number of cells in the human body. Ann Hum Biol. 40, 463–471 (2013). https://doi.org/10.3109/03014460.2013.807878
2. Newman, S.A.: Cell differentiation: What have we learned in 50 years? J Theor Biol. 485, (2020). https://doi.org/10.1016/j.jtbi.2019.110031
3. Xia, H., Li, X., Gao, W., Fu, X., Fang, R.H., Zhang, L., Zhang, K.: Tissue repair and regeneration with endogenous stem cells, (2018)
4. Anthony, B.A., Link, D.C.: Regulation of hematopoietic stem cells by bone marrow stromal cells, (2014)
5. Ronald Hoffman et al. - Hematology_ Basic Principles and Practice (2017, Elsevier).
6. Lee, Y., Decker, M., Lee, H., Ding, L.: Extrinsic regulation of hematopoietic stem cells in development, homeostasis and diseases, (2017)
7. Eibel, H., Kraus, H., Sic, H., Kienzler, A.K., Rizzi, M.: B cell biology: An overview topical collection on basic and applied science. Curr Allergy Asthma Rep. 14, (2014). https://doi.org/10.1007/s11882-014-0434-8
8. Schroeder, H.W., Radbruch, A., Berek, C.: B-Cell Development and Differentiation. In: Clinical Immunology: Principles and Practice. pp. 107-118.e1. Elsevier (2019)
9. Pieper, K., Grimbacher, B., Eibel, H.: B-cell biology and development, (2013)
10. Wang, J.-Y.: B Cells in Immunity and Tolerance. (1254)
11. Cobaleda, C., Jochum, W., Busslinger, M.: Conversion of mature B cells into T cells by dedifferentiation to uncommitted progenitors. Nature. 449, 473–477 (2007). https://doi.org/10.1038/nature06159
12. Epelman, S., Lavine, K.J., Randolph, G.J.: Origin and Functions of Tissue Macrophages, (2014)
13. Varol, C., Mildner, A., Jung, S.: Macrophages: Development and tissue specialization, (2015)
14. Gomez Perdiguero, E., Klapproth, K., Schulz, C., Busch, K., Azzoni, E., Crozet, L., Garner, H., Trouillet, C., de Bruijn, M.F., Geissmann, F., Rodewald, H.R.: Tissue-resident macrophages originate from yolk-sac-derived erythro-myeloid progenitors. Nature. 518, 547–551 (2015). https://doi.org/10.1038/nature13989

15. Hettinger, J., Richards, D.M., Hansson, J., Barra, M.M., Joschko, A.C., Krijgsveld, J., Feuerer, M.: Origin of monocytes and macrophages in a committed progenitor. Nat Immunol. 14, 821–830 (2013). https://doi.org/10.1038/ni.2638
16. Trzebanski, S., Jung, S.: Plasticity of monocyte development and monocyte fates, (2020)
17. Stepwise Reprogramming of B Cells into Macrophages.
18. Zhu, Y.P., Thomas, G.D., Hedrick, C.C.: Transcriptional Control of Monocyte Development. https://doi.org/10.1161/ATVBAHA
19. Iwasaki, H., Akashi, K.: Myeloid Lineage Commitment from the Hematopoietic Stem Cell, (2007)
20. Pillai, S., Cariappa, A.: The follicular versus marginal zone B lymphocyte cell fate decision, (2009)
21. Takahashi, K., Yamanaka, S.: Induction of Pluripotent Stem Cells from Mouse Embryonic and Adult Fibroblast Cultures by Defined Factors. Cell. 126, 663–676 (2006). https://doi.org/10.1016/j.cell.2006.07.024
22. Yao, Y., Wang, C.: Dedifferentiation: inspiration for devising engineering strategies for regenerative medicine, (2020)
23. Jessen, K.R., Mirsky, R.: Negative regulation of myelination: Relevance for development, injury, and demyelinating disease. Glia. 56, 1552–1565 (2008). https://doi.org/10.1002/glia.20761
24. Corti, S., Nizzardo, M., Simone, C., Falcone, M., Donadoni, C., Salani, S., Rizzo, F., Nardini, M., Riboldi, G., Magri, F., Zanetta, C., Faravelli, I., Bresolin, N., Comi, G.P.: Direct reprogramming of human astrocytes into neural stem cells and neurons. Exp Cell Res. 318, 1528–1541 (2012). https://doi.org/10.1016/j.yexcr.2012.02.040
25. Yang, H., Ling, W., Vitale, A., Olivera, C., Min, Y., You, S.: ErbB2 activation contributes to de-differentiation of astrocytes into radial glial cells following induction of scratch-insulted astrocyte conditioned medium. Neurochem Int. 59, 1010–1018 (2011). https://doi.org/10.1016/j.neuint.2011.08.021
26. Sher, F., Boddeke, E., Copray, S.: Ezh2 expression in astrocytes induces their dedifferentiation toward neural stem cells. Cell Reprogram. 13, 1–6 (2011). https://doi.org/10.1089/cell.2010.0052

27. Eguizabal, C., Montserrat, N., Veiga, A., Belmonte, J.I.: Dedifferentiation, transdifferentiation, and reprogramming: Future directions in regenerative medicine. Semin Reprod Med. 31, 82–94 (2013). https://doi.org/10.1055/s-0032-1331802
28. Porrello, E.R., Mahmoud, A.I., Simpson, E., Johnson, B.A., Grinsfelder, D., Canseco, D., Mammen, P.P., Rothermel, B.A., Olson, E.N., Sadek, H.A.: Regulation of neonatal and adult mammalian heart regeneration by the miR-15 family. Proc Natl Acad Sci U S A. 110, 187–192 (2013). https://doi.org/10.1073/pnas.1208863110
29. Jopling, C., Boue, S., Belmonte, J.C.I.: Dedifferentiation, transdifferentiation and reprogramming: Three routes to regeneration, (2011)
30. Wodarz, D.: Effect of cellular de-differentiation on the dynamics and evolution of tissue and tumor cells in mathematical models with feedback regulation. J Theor Biol. 448, 86–93 (2018). https://doi.org/10.1016/j.jtbi.2018.03.036
31. Gutierrez-Aranda, I., Ramos-Mejia, V., Bueno, C., Munoz-Lopez, M., Real, P.J., Mácia, A., Sanchez, L., Ligero, G., Garcia-Parez, J.L., Menendez, P.: Human induced pluripotent stem cells develop teratoma more efficiently and faster than human embryonic stem cells regardless the site of injection, (2010)
32. Yamada, Y., Haga, H., Yamada, Y.: Concise Review: Dedifferentiation Meets Cancer Development: Proof of Concept for Epigenetic Cancer. Stem Cells Transl Med. 3, 1182–1187 (2014). https://doi.org/10.5966/sctm.2014-0090
33. Friedmann-Morvinski, D., Verma, I.M.: Dedifferentiation and reprogramming: Origins of cancer stem cells, (2014)
34. Morris, S.A.: Direct lineage reprogramming via pioneer factors; a detour through developmental gene regulatory networks. Development (Cambridge). 143, 2696–2705 (2016). https://doi.org/10.1242/dev.138263
35. Davis, R.L., Weintraub, H., Lassar, A.B.: Expression of a Single Transfected cDNA Converts Fibmblasts to Myoblasts. (1987)
36. Huang, P., He, Z., Ji, S., Sun, H., Xiang, D., Liu, C., Hu, Y., Wang, X., Hui, L.: Induction of functional hepatocyte-like cells from mouse fibroblasts by defined factors. Nature. 475, 386–391 (2011). https://doi.org/10.1038/nature10116
37. Sekiya, S., Suzuki, A.: Direct conversion of mouse fibroblasts to hepatocyte-like cells by defined factors. Nature. 475, 390–395 (2011). https://doi.org/10.1038/nature10263

38. Zhu, S., Rezvani, M., Harbell, J., Mattis, A.N., Wolfe, A.R., Benet, L.Z., Willenbring, H., Ding, S.: Mouse liver repopulation with hepatocytes generated from human fibroblasts. Nature. 508, 93–97 (2014). https://doi.org/10.1038/nature13020
39. Ambasudhan, R., Talantova, M., Coleman, R., Yuan, X., Zhu, S., Lipton, S.A., Ding, S.: Direct reprogramming of adult human fibroblasts to functional neurons under defined conditions. Cell Stem Cell. 9, 113–118 (2011). https://doi.org/10.1016/j.stem.2011.07.002
40. Pang, Z.P., Yang, N., Vierbuchen, T., Ostermeier, A., Fuentes, D.R., Yang, T.Q., Citri, A., Sebastiano, V., Marro, S., Südhof, T.C., Wernig, M.: Induction of human neuronal cells by defined transcription factors, (2011)
41. Vierbuchen, T., Ostermeier, A., Pang, Z.P., Kokubu, Y., Südhof, T.C., Wernig, M.: Direct conversion of fibroblasts to functional neurons by defined factors. Nature. 463, 1035–1041 (2010). https://doi.org/10.1038/nature08797
42. Yoo, A.S., Sun, A.X., Li, L., Shcheglovitov, A., Portmann, T., Li, Y., Lee-Messer, C., Dolmetsch, R.E., Tsien, R.W., Crabtree, G.R.: MicroRNA-mediated conversion of human fibroblasts to neurons, (2011)
43. Caiazzo, M., Dell'Anno, M.T., Dvoretskova, E., Lazarevic, D., Taverna, S., Leo, D., Sotnikova, T.D., Menegon, A., Roncaglia, P., Colciago, G., Russo, G., Carninci, P., Pezzoli, G., Gainetdinov, R.R., Gustincich, S., Dityatev, A., Broccoli, V.: Direct generation of functional dopaminergic neurons from mouse and human fibroblasts, (2011)
44. Pfisterer, U., Kirkeby, A., Torper, O., Wood, J., Nelander, J., Dufour, A., Björklund, A., Lindvall, O., Jakobsson, J., Parmar, M.: Direct conversion of human fibroblasts to dopaminergic neurons. Proc Natl Acad Sci U S A. 108, 10343–10348 (2011). https://doi.org/10.1073/pnas.1105135108
45. Son, E.Y., Ichida, J.K., Wainger, B.J., Toma, J.S., Rafuse, V.F., Woolf, C.J., Eggan, K.: Conversion of mouse and human fibroblasts into functional spinal motor neurons. Cell Stem Cell. 9, 205–218 (2011). https://doi.org/10.1016/j.stem.2011.07.014
46. Pereira, C.F., Chang, B., Qiu, J., Niu, X., Papatsenko, D., Hendry, C.E., Clark, N.R., Nomura-Kitabayashi, A., Kovacic, J.C., Ma'Ayan, A., Schaniel, C., Lemischka, I.R., Moore, K.: Induction of a hemogenic program in mouse fibroblasts. Cell Stem Cell. 13, 205–218 (2013). https://doi.org/10.1016/j.stem.2013.05.024

47. Szabo, E., Rampalli, S., Risueño, R.M., Schnerch, A., Mitchell, R., Fiebig-Comyn, A., Levadoux-Martin, M., Bhatia, M.: Direct conversion of human fibroblasts to multilineage blood progenitors. Nature. 468, 521–526 (2010). https://doi.org/10.1038/nature09591
48. Lujan, E., Chanda, S., Ahlenius, H., Südhof, T.C., Wernig, M.: Direct conversion of mouse fibroblasts to self-renewing, tripotent neural precursor cells. Proc Natl Acad Sci U S A. 109, 2527–2532 (2012). https://doi.org/10.1073/pnas.1121003109
49. Thier, M., Wörsdörfer, P., Lakes, Y.B., Gorris, R., Herms, S., Opitz, T., Seiferling, D., Quandel, T., Hoffmann, P., Nöthen, M.M., Brüstle, O., Edenhofer, F.: Direct conversion of fibroblasts into stably expandable neural stem cells. Cell Stem Cell. 10, 473–479 (2012). https://doi.org/10.1016/j.stem.2012.03.003
50. Yu, B., He, Z.Y., You, P., Han, Q.W., Xiang, D., Chen, F., Wang, M.J., Liu, C.C., Lin, X.W., Borjigin, U., Zi, X.Y., Li, J.X., Zhu, H.Y., Li, W.L., Han, C.S., Wangensteen, K.J., Shi, Y., Hui, L.J., Wang, X., Hu, Y.P.: Reprogramming fibroblasts into bipotential hepatic stem cells by defined factors. Cell Stem Cell. 13, 328–340 (2013). https://doi.org/10.1016/j.stem.2013.06.017
51. Kurian, L., Sancho-Martinez, I., Nivet, E., Aguirre, A., Moon, K., Pendaries, C., Volle-Challier, C., Bono, F., Herbert, J.M., Pulecio, J., Xia, Y., Li, M., Montserrat, N., Ruiz, S., Dubova, I., Rodriguez, C., Denli, A.M., Boscolo, F.S., Thiagarajan, R.D., Gage, F.H., Loring, J.F., Laurent, L.C., Izpisua Belmonte, J.C.: Conversion of human fibroblasts to angioblast-like progenitor cells. Nat Methods. 10, 77–83 (2013). https://doi.org/10.1038/nmeth.2255
52. Yamamoto, K., Kishida, T., Sato, Y., Nishioka, K., Ejima, A., Fujiwara, H., Kubo, T., Yamamoto, T., Kanamura, N., Mazda, O.: Direct conversion of human fibroblasts into functional osteoblasts by defined factors. Proc Natl Acad Sci U S A. 112, 6152–6157 (2015). https://doi.org/10.1073/pnas.1420713112
53. Marro, S., Pang, Z.P., Yang, N., Tsai, M.C., Qu, K., Chang, H.Y., Südhof, T.C., Wernig, M.: Direct lineage conversion of terminally differentiated hepatocytes to functional neurons. Cell Stem Cell. 9, 374–382 (2011). https://doi.org/10.1016/j.stem.2011.09.002
54. Heinrich, C., Blum, R., Gascón, S., Masserdotti, G., Tripathi, P., Sánchez, R., Tiedt, S., Schroeder, T., Götz, M., Berninger, B.: Directing astroglia from the cerebral

cortex into subtype specific functional neurons. PLoS Biol. 8, (2010). https://doi.org/10.1371/journal.pbio.1000373

55. Berninger, B., Costa, M.R., Koch, U., Schroeder, T., Sutor, B., Grothe, B., Götz, M.: Functional properties of neurons derived from in vitro reprogrammed postnatal astroglia. Journal of Neuroscience. 27, 8654–8664 (2007). https://doi.org/10.1523/JNEUROSCI.1615-07.2007
56. Stepwise Reprogramming of B Cells into Macrophages.
57. Bussmann, L.H., Schubert, A., Vu Manh, T.P., de Andres, L., Desbordes, S.C., Parra, M., Zimmermann, T., Rapino, F., Rodriguez-Ubreva, J., Ballestar, E., Graf, T.: A Robust and Highly Efficient Immune Cell Reprogramming System. Cell Stem Cell. 5, 554–566 (2009). https://doi.org/10.1016/j.stem.2009.10.004
58. Rapino, F., Robles, E.F., Richter-Larrea, J.A., Kallin, E.M., Martinez-Climent, J.A., Graf, T.: C/EBPα Induces Highly Efficient Macrophage Transdifferentiation of B Lymphoma and Leukemia Cell Lines and Impairs Their Tumorigenicity. Cell Rep. 3, 1153–1163 (2013). https://doi.org/10.1016/j.celrep.2013.03.003
59. Li, P., Burke, S., Wang, J., Chen, X., Ortiz, M., Lee, S.C., Lu, D., Campos, L., Goulding, D., Ng, B.L., Dougan, G., Huntly, B., Gottgens, B., Jenkins, N.A., Copeland, N.G., Colucci, F., Liu, P.: Reprogramming of T cells to natural killer-like cells upon Bcl11b deletion. Science (1979). 329, 85–89 (2010). https://doi.org/10.1126/SCIENCE.1188063/SUPPL_FILE/LI.SOM.PDF
60. Noguchi, H., Kaneto, H., Weir, G.C., Bonner-Weir, S.: PDX-1 Protein Containing Its Own Antennapedia-Like Protein Transduction Domain Can Transduce Pancreatic Duct and Islet Cells. (2003)
61. Zhou, Q., Brown, J., Kanarek, A., Rajagopal, J., Melton, D.A.: In vivo reprogramming of adult pancreatic exocrine cells to β-cells. Nature. 455, 627–632 (2008). https://doi.org/10.1038/nature07314
62. Aviv, V., Meivar-Levy, I., Rachmut, I.H., Rubinek, T., Mor, E., Ferber, S.: Exendin-4 promotes liver cell proliferation and enhances the PDX-1-induced liver to pancreas transdifferentiation process. Journal of Biological Chemistry. 284, 33509–33520 (2009). https://doi.org/10.1074/jbc.M109.017608
63. Berninger, B., Costa, M.R., Koch, U., Schroeder, T., Sutor, B., Grothe, B., Götz, M.: Functional properties of neurons derived from in vitro reprogrammed postnatal

astroglia. Journal of Neuroscience. 27, 8654–8664 (2007). https://doi.org/10.1523/JNEUROSCI.1615-07.2007

64. Merrell, A.J., Stanger, B.Z.: Adult cell plasticity in vivo: De-differentiation and transdifferentiation are back in style, (2016)
65. Thorel, F., Népote, V., Avril, I., Kohno, K., Desgraz, R., Chera, S., Herrera, P.L.: Conversion of adult pancreatic α-cells to B-cells after extreme B-cell loss. Nature. 464, 1149–1154 (2010). https://doi.org/10.1038/nature08894
66. Yanger, K., Zong, Y., Maggs, L.R., Shapira, S.N., Maddipati, R., Aiello, N.M., Thung, S.N., Wells, R.G., Greenbaum, L.E., Stanger, B.Z.: Robust cellular reprogramming occurs spontaneously during liver regeneration. Genes Dev. 27, 719–724 (2013). https://doi.org/10.1101/gad.207803.112
67. Bell, J.J., Bhandoola, A.: The earliest thymic progenitors for T cells possess myeloid lineage potential. Nature. 452, 764–767 (2008). https://doi.org/10.1038/nature06840
68. Hvid-Jensen, F., Pedersen, L., Drewes, M., Sci, M., Sørensen, H.T., Funch-Jensen, P.: Incidence of Adenocarcinoma among Patients with Barrett's Esophagus A bs t r ac t. (2011)
69. Sekiya, S., Suzuki, A.: Intrahepatic cholangiocarcinoma can arise from Notch-mediated conversion of hepatocytes. Journal of Clinical Investigation. 122, 3914–3918 (2012). https://doi.org/10.1172/JCI63065
70. Fan, B., Malato, Y., Calvisi, D.F., Naqvi, S., Razumilava, N., Ribback, S., Gores, G.J., Dombrowski, F., Evert, M., Chen, X., Willenbring, H.: Cholangiocarcinomas can originate from hepatocytes in mice. Journal of Clinical Investigation. 122, 2911–2915 (2012). https://doi.org/10.1172/JCI63212
71. Kopp, J.L., von Figura, G., Mayes, E., Liu, F.F., Dubois, C.L., Morris, J.P., Pan, F.C., Akiyama, H., Wright, C.V.E., Jensen, K., Hebrok, M., Sander, M.: Identification of Sox9-Dependent Acinar-to-Ductal Reprogramming as the Principal Mechanism for Initiation of Pancreatic Ductal Adenocarcinoma. Cancer Cell. 22, 737–750 (2012). https://doi.org/10.1016/j.ccr.2012.10.025
72. Carriè re, C., Seeley, E.S., Goetze, T., Longnecker, D.S., Korc, M.: The Nestin progenitor lineage is the compartment of origin for pancreatic intraepithelial neoplasia. (2007)

73. Khan, M.S., Thornhill, J.A., Gaffney, E., Loftus, B., Butler, M.R.: Keratinising Squamous Metaplasia of the Bladder: Natural History and Rationalization of Management Based on Review of 54 Years Experience. (2002)
74. de Vries, A.C., Kuipers, E.J.: Epidemiology of premalignant gastric lesions: Implications for the development of screening and surveillance strategies, (2007)
75. Elson, D.A., Riley, R.R., Lacey, A., Thordarson, G., Talamantes, F.J., Arbeit, J.M.: Sensitivity of the cervical transformation zone to estrogen-induced squamous carcinogenesis. Cancer Res. 60, 1267–75 (2000)
76. Daniels, J.M.A., Sutedja, T.G.: Detection and minimally invasive treatment of early squamous lung cancer, (2013)
77. Dong, H.H., Xiang, S., Chen, X.P., Liang, H.F., Zhang, W., Jing, K., Zhang, W.G., Chen, L.: The epithelial-mesenchymal transition promotes transdifferentiation of subcutaneously implanted hepatic oval cells into mesenchymal tumor tissue. Stem Cells Dev. 18, 1293–1298 (2009). https://doi.org/10.1089/scd.2008.0321
78. Bakir, B., Chiarella, A.M., Pitarresi, J.R., Rustgi, A.K.: EMT, MET, Plasticity, and Tumor Metastasis, (2020)
79. Sinha, S., Nelson, P.S.: The path of most resistance: Transdifferentiation underlies exceptional nonresponses to androgen receptor pathway inhibition in prostate cancer. Cancer Discov. 7, 673–674 (2017). https://doi.org/10.1158/2159-8290.CD-17-0481
80. Feldman, A.L.: Clonal relationships between malignant lymphomas and histiocytic/dendritic cell tumors, (2013)
81. Emile, J.F., Cohen-Aubart, F., Collin, M., Fraitag, S., Idbaih, A., Abdel-Wahab, O., Rollins, B.J., Donadieu, J., Haroche, J.: Histiocytosis, (2021)
82. Andersen, K.F., Sjö, L.D., Kampmann, P., Pedersen, T.B.: Histiocytic sarcoma: Challenging course, dismal outcome. Diagnostics. 11, (2021). https://doi.org/10.3390/diagnostics11020310
83. Zhang, Q., Orlando, E.J., Wang, H.Y., Bogusz, A.M., Liu, X., Lacey, S.F., Strauser, H.T., Nunez-Cruz, S., Nejati, R., Zhang, P., Brooks, S., Watt, C., Melenhorst, J.J., June, C.H., Schuster, S.J., Wasik, M.A.: Letters to Blood Transdifferentiation of lymphoma into sarcoma associated with profound reprogramming of the epigenome.

84. Steussy, B., Lekostaj, J., Qian, Q., Rosenthal, N., Holman, C.J., Syrbu, S., Darbro, B., Bossler, A., Karandikar, N.J.: Leukemic transdifferentiation of follicular lymphoma into an acute histiocytic leukemia in a 52-year-old Caucasian woman. Lab Medicine. 47, 155–157 (2016). https://doi.org/10.1093/labmed/lmw011
85. Kosmidis, P., Mankel, B., Fend, F., Adam, P.: The t(14;18) translocation is absent from endothelial and follicular dendritic cells of follicular lymphoma (FL) and shows heterogeneous presence in preserved FL mantle zones. Diagn Pathol. 13, (2018). https://doi.org/10.1186/s13000-018-0703-2
86. Shao, H., Xi, L., Raffeld, M., Feldman, A.L., Ketterling, R.P., Knudson, R., Rodriguez-Canales, J., Hanson, J., Pittaluga, S., Jaffe, E.S.: Clonally related histiocytic/dendritic cell sarcoma and chronic lymphocytic leukemia/small lymphocytic lymphoma: A study of seven cases. Modern Pathology. 24, 1421–1432 (2011). https://doi.org/10.1038/modpathol.2011.102
87. Feldman, A.L., Arber, D.A., Pittaluga, S., Martinez, A., Burke, J.S., Raffeld, M., Camos, M., Warnke, R., Jaffe, E.S.: Clonally related follicular lymphomas and histiocytic/dendritic cell sarcomas: Evidence for transdifferentiation of the follicular lymphoma clone. Blood. 111, 5433–5439 (2008). https://doi.org/10.1182/blood-2007-11-124792
88. Stepwise Reprogramming of B Cells into Macrophages.
89. Wang, E., Papalas, J., Hutchinson, C.B., Kulbacki, E., Huang, Q., Sebastian, S., Rehder, C., Silbermins, D., Moore, J., Datto, M.: Sequential Development of Histiocytic Sarcoma and Diffuse Large B-cell Lymphoma in a Patient With a Remote History of Follicular Lymphoma With Genotypic Evidence of a Clonal Relationship: A Divergent (Bilineal) Neoplastic Transformation of an Indolent B-cell Lymphoma in a Single Individual. (2011)
90. Shao, H., Xi, L., Raffeld, M., Feldman, A.L., Ketterling, R.P., Knudson, R., Rodriguez-Canales, J., Hanson, J., Pittaluga, S., Jaffe, E.S.: Clonally related histiocytic/dendritic cell sarcoma and chronic lymphocytic leukemia/small lymphocytic lymphoma: A study of seven cases. Modern Pathology. 24, 1421–1432 (2011). https://doi.org/10.1038/modpathol.2011.102
91. Fraser, C.R., Wang, W., Gomez, M., Zhang, T., Mathew, S., Furman, R.R., Knowles, D.M., Orazi, A., Tam, W.: Transformation of chronic lymphocytic leukemia/small lymphocytic lymphoma to interdigitating dendritic cell sarcoma:

Evidence for transdifferentiation of the lymphoma clone. Am J Clin Pathol. 132, 928–939 (2009). https://doi.org/10.1309/AJCPWQ0I0DGXBMHO

92. Piechowski, J.: Hypothesis about transdifferentiation as backbone of malignancy. Front Oncol. 7, (2017). https://doi.org/10.3389/fonc.2017.00126
93. Waddington, C.H.: The epigenotype. 1942. Int J Epidemiol. 41, 10–13 (2012). https://doi.org/10.1093/ije/dyr184
94. Allis, C.D., Jenuwein, T.: The molecular hallmarks of epigenetic control, (2016)
95. Greenberg, M.V.C., Bourc'his, D.: The diverse roles of DNA methylation in mammalian development and disease, (2019)
96. Lyko, F.: The DNA methyltransferase family: A versatile toolkit for epigenetic regulation, (2018)
97. Li, D., Guo, B., Wu, H., Tan, L., Lu, Q.: TET Family of Dioxygenases: Crucial Roles and Underlying Mechanisms, (2015)
98. Spainhour, J.C.G., Lim, H.S., Yi, S. v., Qiu, P.: Correlation Patterns Between DNA Methylation and Gene Expression in The Cancer Genome Atlas. Cancer Inform. 18, (2019). https://doi.org/10.1177/1176935119828776
99. Cain, J.A., Montibus, B., Oakey, R.J.: Intragenic CpG Islands and Their Impact on Gene Regulation, (2022)
100. Cinghu, S., Yang, P., Kosak, J.P., Conway, A.E., Kumar, D., Oldfield, A.J., Adelman, K., Jothi, R.: Intragenic Enhancers Attenuate Host Gene Expression. Mol Cell. 68, 104-117.e6 (2017). https://doi.org/10.1016/j.molcel.2017.09.010
101. Claringbould, A., Zaugg, J.B.: Enhancers in disease: molecular basis and emerging treatment strategies, (2021)
102. Yin, Y., Morgunova, E., Jolma, A., Kaasinen, E., Sahu, B., Khund-Sayeed, S., Das, P.K., Kivioja, T., Dave, K., Zhong, F., Nitta, K.R., Taipale, M., Popov, A., Ginno, P.A., Domcke, S., Yan, J., Schübeler, D., Vinson, C., Taipale, J.: Impact of cytosine methylation on DNA binding specificities of human transcription factors. Science (1979). 356, (2017). https://doi.org/10.1126/science.aaj2239
103. Angeloni, A., Bogdanovic, O.: Enhancer DNA methylation: Implications for gene regulation, (2019)
104. Millán-Zambrano, G., Burton, A., Bannister, A.J., Schneider, R.: Histone post-translational modifications — cause and consequence of genome function, (2022)

105. Lawrence, M., Daujat, S., Schneider, R.: Lateral Thinking: How Histone Modifications Regulate Gene Expression, (2016)
106. Crusio, W.E., Dong, H., Radeke, H.H.: Volume 1283 Series Editors.
107. Audia, J.E., Campbell, R.M.: Histone modifications and cancer. Cold Spring Harb Perspect Biol. 8, (2016). https://doi.org/10.1101/cshperspect.a019521
108. Shvedunova, M., Akhtar, A.: Modulation of cellular processes by histone and non-histone protein acetylation, (2022)
109. Clapier, C.R., Iwasa, J., Cairns, B.R., Peterson, C.L.: Mechanisms of action and regulation of ATP-dependent chromatin-remodelling complexes, (2017)
110. Talbert, P.B., Henikoff, S.: Histone variants at a glance. J Cell Sci. 134, (2021). https://doi.org/10.1242/jcs.244749
111. Henikoff, S., Smith, M.M.: Histone variants and epigenetics. Cold Spring Harb Perspect Biol. 7, (2015). https://doi.org/10.1101/cshperspect.a019364
112. Rowley, M.J., Corces, V.G.: Organizational principles of 3D genome architecture. Nat Rev Genet. 19, 789–800 (2018). https://doi.org/10.1038/s41576-018-0060-8
113. Briand, N., Collas, P.: Lamina-associated domains: Peripheral matters and internal affairs, (2020)
114. Kempfer, R., Pombo, A.: Methods for mapping 3D chromosome architecture, (2020)
115. Esteller, M.: Non-coding RNAs in human disease, (2011)
116. O'Brien, J., Hayder, H., Zayed, Y., Peng, C.: Overview of microRNA biogenesis, mechanisms of actions, and circulation, (2018)
117. Kopp, F., Mendell, J.T.: Functional Classification and Experimental Dissection of Long Noncoding RNAs, (2018)
118. Jonkhout, N., Tran, J., Smith, M.A., Schonrock, N., Mattick, J.S., Novoa, E.M.: The RNA modification landscape in human disease. (2017). https://doi.org/10.1261/rna.063503
119. Cohn, W., Volkin, E.: Nucleoside-5′-Phosphates from Ribonucleic Acid. Nature. 167, 483–484 (1951). https://doi.org/10.1038/167483a0
120. Kierzek, E., Malgowska, M., Lisowiec, J., Turner, D.H., Gdaniec, Z., Kierzek, R.: The contribution of pseudouridine to stabilities and structure of RNAs. Nucleic Acids Res. 42, 3492–3501 (2014). https://doi.org/10.1093/nar/gkt1330
121. Walkley, C.R., Li, J.B.: Rewriting the transcriptome: Adenosine-to-inosine RNA editing by ADARs, (2017)

122. Dominissini, D., Moshitch-Moshkovitz, S., Amariglio, N., Rechavi, G.: Adenosine-to-inosine RNA editing meets cancer, (2011)
123. Desrosiers, R., Friderici, K., Rottman, F.: Identification of Methylated Nucleosides in Messenger RNA from Novikoff Hepatoma Cells (RNA methylation/RNA processing/methylnucleoside composition). (1974)
124. Zaccara, S., Ries, R.J., Jaffrey, S.R.: Reading, writing and erasing mRNA methylation, (2019)
125. Dominissini, D., Moshitch-Moshkovitz, S., Schwartz, S., Salmon-Divon, M., Ungar, L., Osenberg, S., Cesarkas, K., Jacob-Hirsch, J., Amariglio, N., Kupiec, M., Sorek, R., Rechavi, G.: Topology of the human and mouse m6A RNA methylomes revealed by m6A-seq. Nature. 485, 201–206 (2012). https://doi.org/10.1038/nature11112
126. Dominissini, D., Moshitch-Moshkovitz, S., Salmon-Divon, M., Amariglio, N., Rechavi, G.: Transcriptome-wide mapping of N6-methyladenosine by m 6A-seq based on immunocapturing and massively parallel sequencing. Nat Protoc. 8, 176–189 (2013). https://doi.org/10.1038/nprot.2012.148
127. He, P.C., He, C.: m 6 A RNA methylation: from mechanisms to therapeutic potential . EMBO J. 40, (2021). https://doi.org/10.15252/embj.2020105977
128. Fang, Z., Mei, W., Qu, C., Lu, J., Shang, L., Cao, F., Li, F.: Role of m6A writers, erasers and readers in cancer, (2022)
129. Murakami, S., Jaffrey, S.R.: Hidden codes in mRNA: Control of gene expression by m6A, (2022)
130. Ke, S., Pandya-Jones, A., Saito, Y., Fak, J.J., Vågbø, C.B., Geula, S., Hanna, J.H., Black, D.L., Darnell, J.E., Darnell, R.B.: m 6 A mRNA modifications are deposited in nascent pre-mRNA and are not required for splicing but do specify cytoplasmic turnover. (2017). https://doi.org/10.1101/gad.301036
131. Zhou, K.I., Shi, H., Lyu, R., Wylder, A.C., Matuszek, Ż., Pan, J.N., He, C., Parisien, M., Pan, T.: Regulation of Co-transcriptional Pre-mRNA Splicing by m6A through the Low-Complexity Protein hnRNPG. Mol Cell. 76, 70-81.e9 (2019). https://doi.org/10.1016/j.molcel.2019.07.005
132. Meyer, K.D., Saletore, Y., Zumbo, P., Elemento, O., Mason, C.E., Jaffrey, S.R.: Comprehensive analysis of mRNA methylation reveals enrichment in 3′ UTRs and

near stop codons. Cell. 149, 1635–1646 (2012). https://doi.org/10.1016/j.cell.2012.05.003

133. Wang, X., Lu, Z., Gomez, A., Hon, G.C., Yue, Y., Han, D., Fu, Y., Parisien, M., Dai, Q., Jia, G., Ren, B., Pan, T., He, C.: N 6-methyladenosine-dependent regulation of messenger RNA stability. Nature. 505, 117–120 (2014). https://doi.org/10.1038/nature12730

134. Bushkin, G.G., Pincus, D., Morgan, J.T., Richardson, K., Lewis, C., Chan, S.H., Bartel, D.P., Fink, G.R.: m6A modification of a 3′ UTR site reduces RME1 mRNA levels to promote meiosis. Nat Commun. 10, (2019). https://doi.org/10.1038/s41467-019-11232-7

135. Hsu, P.J., Zhu, Y., Ma, H., Guo, Y., Shi, X., Liu, Y., Qi, M., Lu, Z., Shi, H., Wang, J., Cheng, Y., Luo, G., Dai, Q., Liu, M., Guo, X., Sha, J., Shen, B., He, C.: Ythdc2 is an N6 -methyladenosine binding protein that regulates mammalian spermatogenesis. Cell Res. 27, 1115–1127 (2017). https://doi.org/10.1038/cr.2017.99

136. Huang, H., Weng, H., Sun, W., Qin, X., Shi, H., Wu, H., Zhao, B.S., Mesquita, A., Liu, C., Yuan, C.L., Hu, Y.C., Hüttelmaier, S., Skibbe, J.R., Su, R., Deng, X., Dong, L., Sun, M., Li, C., Nachtergaele, S., Wang, Y., Hu, C., Ferchen, K., Greis, K.D., Jiang, X., Wei, M., Qu, L., Guan, J.L., He, C., Yang, J., Chen, J.: Recognition of RNA N 6 -methyladenosine by IGF2BP proteins enhances mRNA stability and translation. Nat Cell Biol. 20, 285–295 (2018). https://doi.org/10.1038/s41556-018-0045-z

137. Wang, X., Zhao, B.S., Roundtree, I.A., Lu, Z., Han, D., Ma, H., Weng, X., Chen, K., Shi, H., He, C.: N6-methyladenosine modulates messenger RNA translation efficiency. Cell. 161, 1388–1399 (2015). https://doi.org/10.1016/j.cell.2015.05.014

138. Choe, J., Lin, S., Zhang, W., Liu, Q., Wang, L., Ramirez-Moya, J., Du, P., Kim, W., Tang, S., Sliz, P., Santisteban, P., George, R.E., Richards, W.G., Wong, K.K., Locker, N., Slack, F.J., Gregory, R.I.: mRNA circularization by METTL3–eIF3h enhances translation and promotes oncogenesis. Nature. 561, 556–560 (2018). https://doi.org/10.1038/s41586-018-0538-8

139. Meyer, K.D., Patil, D.P., Zhou, J., Zinoviev, A., Skabkin, M.A., Elemento, O., Pestova, T. v., Qian, S.B., Jaffrey, S.R.: 5′ UTR m6A Promotes Cap-Independent Translation. Cell. 163, 999–1010 (2015). https://doi.org/10.1016/j.cell.2015.10.012

140. Adhikari, S., Xiao, W., Zhao, Y.L., Yang, Y.G.: m6A: Signaling for mRNA splicing. RNA Biol. 13, 756–759 (2016). https://doi.org/10.1080/15476286.2016.1201628
141. Mendel, M., Delaney, K., Pandey, R.R., Chen, K.M., Wenda, J.M., Vågbø, C.B., Steiner, F.A., Homolka, D., Pillai, R.S.: Splice site m6A methylation prevents binding of U2AF35 to inhibit RNA splicing. Cell. 184, 3125-3142.e25 (2021). https://doi.org/10.1016/j.cell.2021.03.062
142. Zhou, K.I., Shi, H., Lyu, R., Wylder, A.C., Matuszek, Ż., Pan, J.N., He, C., Parisien, M., Pan, T.: Regulation of Co-transcriptional Pre-mRNA Splicing by m6A through the Low-Complexity Protein hnRNPG. Mol Cell. 76, 70-81.e9 (2019). https://doi.org/10.1016/j.molcel.2019.07.005
143. Xiao, W., Adhikari, S., Dahal, U., Chen, Y.S., Hao, Y.J., Sun, B.F., Sun, H.Y., Li, A., Ping, X.L., Lai, W.Y., Wang, X., Ma, H.L., Huang, C.M., Yang, Y., Huang, N., Jiang, G. bin, Wang, H.L., Zhou, Q., Wang, X.J., Zhao, Y.L., Yang, Y.G.: Nuclear m6A Reader YTHDC1 Regulates mRNA Splicing. Mol Cell. 61, 507–519 (2016). https://doi.org/10.1016/j.molcel.2016.01.012
144. Louloupi, A., Ntini, E., Conrad, T., Ørom, U.A.V.: Transient N-6-Methyladenosine Transcriptome Sequencing Reveals a Regulatory Role of m6A in Splicing Efficiency. Cell Rep. 23, 3429–3437 (2018). https://doi.org/10.1016/j.celrep.2018.05.077
145. Lesbirel, S., Viphakone, N., Parker, M., Parker, J., Heath, C., Sudbery, I., Wilson, S.A.: The m6A-methylase complex recruits TREX and regulates mRNA export. Sci Rep. 8, (2018). https://doi.org/10.1038/s41598-018-32310-8
146. Zheng, G., Dahl, J.A., Niu, Y., Fedorcsak, P., Huang, C.M., Li, C.J., Vågbø, C.B., Shi, Y., Wang, W.L., Song, S.H., Lu, Z., Bosmans, R.P.G., Dai, Q., Hao, Y.J., Yang, X., Zhao, W.M., Tong, W.M., Wang, X.J., Bogdan, F., Furu, K., Fu, Y., Jia, G., Zhao, X., Liu, J., Krokan, H.E., Klungland, A., Yang, Y.G., He, C.: ALKBH5 Is a Mammalian RNA Demethylase that Impacts RNA Metabolism and Mouse Fertility. Mol Cell. 49, 18–29 (2013). https://doi.org/10.1016/j.molcel.2012.10.015
147. Lesbirel, S., Wilson, S.A.: The m 6 A-methylase complex and mRNA export, (2019)
148. Sokpor, G., Xie, Y., Nguyen, H.P., Tuoc, T.: Emerging Role of m6 A Methylome in Brain Development: Implications for Neurological Disorders and Potential Treatment, (2021)
149. Jiang, X., Liu, B., Nie, Z., Duan, L., Xiong, Q., Jin, Z., Yang, C., Chen, Y.: The role of m6A modification in the biological functions and diseases, (2021)

150. Wang, P., Feng, M., Han, G., Yin, R., Li, Y., Yao, S., Lu, P., Wang, Y., Zhang, H.: RNA m6A Modification Plays a Key Role in Maintaining Stem Cell Function in Normal and Malignant Hematopoiesis, (2021)
151. Zhao, C., Xu, G., Zhang, X., Ye, Y., Cai, W., Shao, Q.: RNA m6A modification orchestrates the rhythm of immune cell development from hematopoietic stem cells to T and B cells, (2022)
152. Vu, L.P., Pickering, B.F., Cheng, Y., Zaccara, S., Nguyen, D., Minuesa, G., Chou, T., Chow, A., Saletore, Y., Mackay, M., Schulman, J., Famulare, C., Patel, M., Klimek, V.M., Garrett-Bakelman, F.E., Melnick, A., Carroll, M., Mason, C.E., Jaffrey, S.R., Kharas, M.G.: The N 6 -methyladenosine (m 6 A)-forming enzyme METTL3 controls myeloid differentiation of normal hematopoietic and leukemia cells. Nat Med. 23, 1369–1376 (2017). https://doi.org/10.1038/nm.4416
153. Lee, H., Bao, S., Qian, Y., Geula, S., Leslie, J., Zhang, C., Hanna, J.H., Ding, L.: Stage-specific requirement for Mettl3-dependent m6A mRNA methylation during haematopoietic stem cell differentiation. Nat Cell Biol. 21, 700–709 (2019). https://doi.org/10.1038/s41556-019-0318-1
154. Li, Z., Qian, P., Shao, W., Shi, H., He, X.C., Gogol, M., Yu, Z., Wang, Y., Qi, M., Zhu, Y., Perry, J.M., Zhang, K., Tao, F., Zhou, K., Hu, D., Han, Y., Zhao, C., Alexander, R., Xu, H., Chen, S., Peak, A., Hall, K., Peterson, M., Perera, A., Haug, J.S., Parmely, T., Li, H., Shen, B., Zeitlinger, J., He, C., Li, L.: Suppression of m6A reader Ythdf2 promotes hematopoietic stem cell expansion. Cell Res. 28, 904–917 (2018). https://doi.org/10.1038/s41422-018-0072-0
155. Yin, R., Chang, J., Li, Y., Gao, Z., Qiu, Q., Wang, Q., Han, G., Chai, J., Feng, M., Wang, P., Zhang, T., Xie, X., Hu, J., Cheng, Y., Guo, C., Wang, J., Gao, K., Cui, M., Li, S., Zheng, Y., Jiang, W., Hu, Y., Yang, Q. yong, Zhang, H.: Differential m6A RNA landscapes across hematopoiesis reveal a role for IGF2BP2 in preserving hematopoietic stem cell function. Cell Stem Cell. 29, 149-159.e7 (2022). https://doi.org/10.1016/j.stem.2021.09.014
156. Zheng, Z., Zhang, L., Cui, X.L., Yu, X., Hsu, P.J., Lyu, R., Tan, H., Mandal, M., Zhang, M., Sun, H.L., Sanchez Castillo, A., Peng, J., Clark, M.R., He, C., Huang, H.: Control of Early B Cell Development by the RNA N6-Methyladenosine Methylation. Cell Rep. 31, (2020). https://doi.org/10.1016/j.celrep.2020.107819

157. Huang, H., Zhang, G., Ruan, G.-X., Li, Y., Chen, W., Zou, J., Zhang, R., Wang, J., Ji, S.-J., Xu, S., Ou, X.: Mettl14-Mediated m6A Modification Is Essential for Germinal Center B Cell Response. The Journal of Immunology. 208, 1924–1936 (2022). https://doi.org/10.4049/jimmunol.2101071
158. Liu, Y., Liu, Z., Tang, H., Shen, Y., Gong, Z., Xie, N., Zhang, X., Wang, W., Kong, W., Zhou, Y., Fu, Y.: The N 6-methyladenosine (m 6 A)-forming enzyme METTL3 facilitates M1 macrophage polarization through the methylation of STAT1 mRNA. Am J Physiol Cell Physiol. 317, 762–775 (2019). https://doi.org/10.1152/ajpcell.00212.2019.-Compelling
159. Wang, X., Ji, Y., Feng, P., Liu, R., Li, G., Zheng, J., Xue, Y., Wei, Y., Ji, C., Chen, D., Li, J.: The m6A Reader IGF2BP2 Regulates Macrophage Phenotypic Activation and Inflammatory Diseases by Stabilizing TSC1 and PPARγ. Advanced Science. 8, (2021). https://doi.org/10.1002/advs.202100209
160. Gu, X., Zhang, Y., Li, D., Cai, H., Cai, L., Xu, Q.: N6-methyladenosine demethylase FTO promotes M1 and M2 macrophage activation. Cell Signal. 69, (2020). https://doi.org/10.1016/j.cellsig.2020.109553
161. Tong, J., Wang, X., Liu, Y., Ren, X., Wang, A., Chen, Z., Yao, J., Mao, K., Liu, T., Meng, F.-L., Pan, W., Zou, Q., Liu, J., Zhou, Y., Xia, Q., Flavell, R.A., Zhu, S., Li, H.-B.: Pooled CRISPR screening identifies m 6 A as a positive regulator of macrophage activation. (2021)
162. Gao, R., Ye, M., Liu, B., Wei, M., Ma, D., Dong, K.: m6A Modification: A Double-Edged Sword in Tumor Development, (2021)
163. Ianniello, Z., Paiardini, A., Fatica, A.: N6-Methyladenosine (M6A): A promising new molecular target in acute myeloid leukemia, (2019)
164. Yankova, E., Aspris, D., Tzelepis, K.: The N6-methyladenosine RNA modification in acute myeloid leukemia, (2021)
165. Weng, H., Huang, H., Wu, H., Qin, X., Zhao, B.S., Dong, L., Shi, H., Skibbe, J., Shen, C., Hu, C., Sheng, Y., Wang, Y., Wunderlich, M., Zhang, B., Dore, L.C., Su, R., Deng, X., Ferchen, K., Li, C., Sun, M., Lu, Z., Jiang, X., Marcucci, G., Mulloy, J.C., Yang, J., Qian, Z., Wei, M., He, C., Chen, J.: METTL14 Inhibits Hematopoietic Stem/Progenitor Differentiation and Promotes Leukemogenesis via mRNA m6A Modification. Cell Stem Cell. 22, 191-205.e9 (2018). https://doi.org/10.1016/j.stem.2017.11.016

166. Bansal, H., Yihua, Q., Iyer, S.P., Ganapathy, S., Proia, D., Penalva, L.O., Uren, P.J., Suresh, U., Carew, J.S., Karnad, A.B., Weitman, S., Tomlinson, G.E., Rao, M.K., Kornblau, S.M., Bansal, S.: WTAP is a novel oncogenic protein in acute myeloid leukemia, (2014)
167. Yankova, E., Blackaby, W., Albertella, M., Rak, J., de Braekeleer, E., Tsagkogeorga, G., Pilka, E.S., Aspris, D., Leggate, D., Hendrick, A.G., Webster, N.A., Andrews, B., Fosbeary, R., Guest, P., Irigoyen, N., Eleftheriou, M., Gozdecka, M., Dias, J.M.L., Bannister, A.J., Vick, B., Jeremias, I., Vassiliou, G.S., Rausch, O., Tzelepis, K., Kouzarides, T.: Small-molecule inhibition of METTL3 as a strategy against myeloid leukaemia. Nature. 593, 597–601 (2021). https://doi.org/10.1038/s41586-021-03536-w
168. Li, Z., Weng, H., Su, R., Weng, X., Zuo, Z., Li, C., Huang, H., Nachtergaele, S., Dong, L., Hu, C., Qin, X., Tang, L., Wang, Y., Hong, G.M., Huang, H., Wang, X., Chen, P., Gurbuxani, S., Arnovitz, S., Li, Y., Li, S., Strong, J., Neilly, M.B., Larson, R.A., Jiang, X., Zhang, P., Jin, J., He, C., Chen, J.: FTO Plays an Oncogenic Role in Acute Myeloid Leukemia as a N6-Methyladenosine RNA Demethylase. Cancer Cell. 31, 127–141 (2017). https://doi.org/10.1016/j.ccell.2016.11.017
169. Cheng, Y., Fu, Y., Wang, Y., Wang, J.: The m6A Methyltransferase METTL3 Is Functionally Implicated in DLBCL Development by Regulating m6A Modification in PEDF. Front Genet. 11, (2020). https://doi.org/10.3389/fgene.2020.00955
170. Han, H., Fan, G., Song, S., Jiang, Y., Ao Qian, C.', Zhang, W., Su, Q., Xue, X., Zhuang, W., Li, B.: piRNA-30473 contributes to tumorigenesis and poor prognosis by regulating m6A RNA methylation in DLBCL. (2021)
171. di Tullio, A., Graf, T.: C/EBPα bypasses cell cycle-dependency during immune cell transdifferentiation. Cell Cycle. 11, 2739–2746 (2012). https://doi.org/10.4161/cc.21119
172. Llinàs-Arias, P., Rosselló-Tortella, M., López-Serra, P., Pérez-Salvia, M., Setién, F., Marin, S., Muñoz, J.P., Junza, A., Capellades, J., Calleja-Cervantes, M.E., Ferreira, H.J., de Moura, M.C., Srbic, M., Martínez-Cardús, A., de La Torre, C., Villanueva, A., Cascante, M., Yanes, O., Zorzano, A., Moutinho, C., Esteller, M.: Epigenetic loss of the endoplasmic reticulum-associated degradation inhibitor SVIP induces cancer cell metabolic reprogramming. JCI Insight. 4, (2019). https://doi.org/10.1172/jci.insight.125888

173. Yin, Y., Morgunova, E., Jolma, A., Kaasinen, E., Sahu, B., Khund-Sayeed, S., Das, P.K., Kivioja, T., Dave, K., Zhong, F., Nitta, K.R., Taipale, M., Popov, A., Ginno, P.A., Domcke, S., Yan, J., Schübeler, D., Vinson, C., Taipale, J.: Impact of cytosine methylation on DNA binding specificities of human transcription factors. Science (1979). 356, (2017). https://doi.org/10.1126/science.aaj2239
174. Javierre, B.M., Sewitz, S., Cairns, J., Wingett, S.W., Várnai, C., Thiecke, M.J., Freire-Pritchett, P., Spivakov, M., Fraser, P., Burren, O.S., Cutler, A.J., Todd, J.A., Wallace, C., Wilder, S.P., Kreuzhuber, R., Kostadima, M., Zerbino, D.R., Stegle, O., Burden, F., Farrow, S., Rehnström, K., Downes, K., Grassi, L., Ouwehand, W.H., Frontini, M., Hill, S.M., Wang, F., Stunnenberg, H.G., Martens, J.H., Kim, B., Sharifi, N., Janssen-Megens, E.M., Yaspo, M.L., Linser, M., Kovacsovics, A., Clarke, L., Richardson, D., Datta, A., Flicek, P.: Lineage-Specific Genome Architecture Links Enhancers and Non-coding Disease Variants to Target Gene Promoters. Cell. 167, 1369-1384.e19 (2016). https://doi.org/10.1016/j.cell.2016.09.037
175. Ren, R., Horton, J.R., Zhang, X., Blumenthal, R.M., Cheng, X.: Detecting and interpreting DNA methylation marks, (2018)
176. Bueno-Costa, A., Piñeyro, D., Soler, M., Javierre, B.M., Raurell-Vila, H., Subirana-Granés, M., Pasquali, L., Martinez-Climent, J.A., Esteller, M.: B-cell leukemia transdifferentiation to macrophage involves reconfiguration of DNA methylation for long-range regulation. Leukemia. 34, 1158–1162 (2020). https://doi.org/10.1038/s41375-019-0643-1
177. Genuth, N.R., Barna, M.: The Discovery of Ribosome Heterogeneity and Its Implications for Gene Regulation and Organismal Life, (2018)
178. Bueno-Costa, A., Piñeyro, D., García-Prieto, C.A., Ortiz-Barahona, V., Martinez-Verbo, L., Webster, N.A., Andrews, B., Kol, N., Avrahami, C., Moshitch-Moshkovitz, S., Rechavi, G., Esteller, M.: Remodeling of the m6A RNA landscape in the conversion of acute lymphoblastic leukemia cells to macrophages. Leukemia. 36, 2121–2124 (2022). https://doi.org/10.1038/s41375-022-01621-1
179. Cho, Y.-D., Ryoo, H.-M.: Trans-differentiation via Epigenetics: A New Paradigm in the Bone Regeneration. J Bone Metab. 25, 9 (2018). https://doi.org/10.11005/jbm.2018.25.1.9
180. Xu, J., Du, Y., Deng, H.: Direct lineage reprogramming: Strategies, mechanisms, and applications, (2015)

181. Cho, Y.D., Yoon, W.J., Kim, W.J., Woo, K.M., Baek, J.H., Lee, G., Ku, Y., van Wijnen, A.J., Ryoo, H.M.: Epigenetic modifications and canonical wingless/int-1 class (WNT) signaling enable trans-differentiation of nonosteogenic cells into osteoblasts. Journal of Biological Chemistry. 289, 20120–20128 (2014). https://doi.org/10.1074/jbc.M114.558064
182. Har-Zahav, A., Lixandru, D., Cheishvili, D., Matei, I.V., Florea, I.R., Aspritoiu, V.M., Blus-Kadosh, I., Meivar-Levy, I., Serban, A.M., Popescu, I., Szyf, M., Ferber, S., Dima, S.O.: The role of DNA demethylation in liver to pancreas transdifferentiation. Stem Cell Res Ther. 13, (2022). https://doi.org/10.1186/s13287-022-03159-6
183. Rodríguez-Ubreva, J., Ciudad, L., Gómez-Cabrero, D., Parra, M., Bussmann, L.H., di Tullio, A., Kallin, E.M., Tegnér, J., Graf, T., Ballestar, E.: Pre-B cell to macrophage transdifferentiation without significant promoter DNA methylation changes. Nucleic Acids Res. 40, 1954–1968 (2012). https://doi.org/10.1093/nar/gkr1015
184. Tyler, J.K., Luo, C., Yi Lee, Q., Wapinski, O., Castanon, R., Nery, J.R., Mall, M., Kareta, M.S., Cullen, S.M., Goodell, M.A., Chang, H.Y., Wernig, M., Ecker, J.R.: Global DNA methylation remodeling during direct reprogramming of fibroblasts to neurons. https://doi.org/10.7554/eLife.40197.001
185. Argelaguet, R., Clark, S.J., Mohammed, H., Stapel, L.C., Krueger, C., Kapourani, C.A., Imaz-Rosshandler, I., Lohoff, T., Xiang, Y., Hanna, C.W., Smallwood, S., Ibarra-Soria, X., Buettner, F., Sanguinetti, G., Xie, W., Krueger, F., Göttgens, B., Rugg-Gunn, P.J., Kelsey, G., Dean, W., Nichols, J., Stegle, O., Marioni, J.C., Reik, W.: Multi-omics profiling of mouse gastrulation at single-cell resolution. Nature. 576, 487–491 (2019). https://doi.org/10.1038/s41586-019-1825-8
186. Weber, M., Hellmann, I., Stadler, M.B., Ramos, L., Pääbo, S., Rebhan, M., Schübeler, D.: Distribution, silencing potential and evolutionary impact of promoter DNA methylation in the human genome. Nat Genet. 39, 457–466 (2007). https://doi.org/10.1038/ng1990
187. Schmidt, C.S., Bultmann, S., Meilinger, D., Zacher, B., Tresch, A., Maier, K.C., Peter, C., Martin, D.E., Leonhardt, H., Spada, F.: Global DNA Hypomethylation Prevents Consolidation of Differentiation Programs and Allows Reversion to the Embryonic Stem Cell State. PLoS One. 7, (2012). https://doi.org/10.1371/journal.pone.0052629

188. Kaaij, L.T.J., van de Wetering, M., Fang, F., Decato, B., Molaro, A., van de Werken, H.J.G., van Es, J.H., Schuijers, J., de Wit, E., de Laat, W., Hannon, G.J., Clevers, H.C., Smith, A.D., Ketting, R.F.: DNA methylation dynamics during intestinal stem cell differentiation reveals enhancers driving gene expression in the villus. Genome Biol. 14, (2013). https://doi.org/10.1186/gb-2013-14-5-r50
189. Gu, H., Raman, A.T., Wang, X., Gaiti, F., Chaligne, R., Mohammad, A.W., Arczewska, A., Smith, Z.D., Landau, D.A., Aryee, M.J., Meissner, A., Gnirke, A.: Smart-RRBS for single-cell methylome and transcriptome analysis, (2021)
190. Neri, F., Rapelli, S., Krepelova, A., Incarnato, D., Parlato, C., Basile, G., Maldotti, M., Anselmi, F., Oliviero, S.: Intragenic DNA methylation prevents spurious transcription initiation. Nature. 543, 72–77 (2017). https://doi.org/10.1038/nature21373
191. Mittelstaedt, N.N., Becker, A.L., de Freitas, D.N., Zanin, R.F., Stein, R.T., de Souza, A.P.D.: Dna methylation and immune memory response, (2021)
192. Kallin, E.M., Rodríguez-Ubreva, J., Christensen, J., Cimmino, L., Aifantis, I., Helin, K., Ballestar, E., Graf, T.: Tet2 facilitates the derepression of myeloid target genes during CEBPα-Induced transdifferentiation of Pre-B cells. Mol Cell. 48, 266–276 (2012). https://doi.org/10.1016/j.molcel.2012.08.007
193. Sardina, J.L., Collombet, S., Tian, T. v., Gómez, A., di Stefano, B., Berenguer, C., Brumbaugh, J., Stadhouders, R., Segura-Morales, C., Gut, M., Gut, I.G., Heath, S., Aranda, S., di Croce, L., Hochedlinger, K., Thieffry, D., Graf, T.: Transcription Factors Drive Tet2-Mediated Enhancer Demethylation to Reprogram Cell Fate. Cell Stem Cell. 23, 727-741.e9 (2018). https://doi.org/10.1016/j.stem.2018.08.016
194. Moran, S., Arribas, C., Esteller, M.: Validation of a DNA methylation microarray for 850,000 CpG sites of the human genome enriched in enhancer sequences. Epigenomics. 8, 389–399 (2016). https://doi.org/10.2217/epi.15.114
195. Pidsley, R., Zotenko, E., Peters, T.J., Lawrence, M.G., Risbridger, G.P., Molloy, P., van Djik, S., Muhlhausler, B., Stirzaker, C., Clark, S.J.: Critical evaluation of the Illumina MethylationEPIC BeadChip microarray for whole-genome DNA methylation profiling. Genome Biol. 17, (2016). https://doi.org/10.1186/s13059-016-1066-1
196. Jeong, H., Mendizabal, I., Berto, S., Chatterjee, P., Layman, T., Usui, N., Toriumi, K., Douglas, C., Singh, D., Huh, I., Preuss, T.M., Konopka, G., Yi, S. v.: Evolution of

DNA methylation in the human brain. Nat Commun. 12, (2021). https://doi.org/10.1038/s41467-021-21917-7

197. Zhang, Y., Xiang, Y., Yin, Q., Du, Z., Peng, X., Wang, Q., Fidalgo, M., Xia, W., Li, Y., Zhao, Z.A., Zhang, W., Ma, J., Xu, F., Wang, J., Li, L., Xie, W.: Dynamic epigenomic landscapes during early lineage specification in mouse embryos. Nat Genet. 50, 96–105 (2018). https://doi.org/10.1038/s41588-017-0003-x
198. Menten, P., Wuyts, A., Damme, J. van: Macrophage inflammatory protein-1. (2002)
199. Schwartzman, O., Mukamel, Z., Oded-Elkayam, N., Olivares-Chauvet, P., Lubling, Y., Landan, G., Izraeli, S., Tanay, A.: UMI-4C for quantitative and targeted chromosomal contact profiling. Nat Methods. 13, 685–691 (2016). https://doi.org/10.1038/nmeth.3922
200. Li, G., Liu, Y., Zhang, Y., Kubo, N., Yu, M., Fang, R., Kellis, M., Ren, B.: Joint profiling of DNA methylation and chromatin architecture in single cells. Nat Methods. 16, 991–993 (2019). https://doi.org/10.1038/s41592-019-0502-z
201. Zhu, Z., Meng, W., Liu, P., Zhu, X., Liu, Y., Zou, H.: DNA hypomethylation of a transcription factor binding site within the promoter of a gout risk gene NRBP1 upregulates its expression by inhibition of TFAP2A binding. Clin Epigenetics. 9, (2017). https://doi.org/10.1186/s13148-017-0401-z
202. Moen, E.L., Mariani, C.J., Zullow, H., Jeff-Eke, M., Litwin, E., Nikitas, J.N., Godley, L.A.: New themes in the biological functions of 5-methylcytosine and 5-hydroxymethylcytosine. Immunol Rev. 263, 36–49 (2015). https://doi.org/10.1111/imr.12242
203. Paul, S., Zhang, X., He, J.Q.: Homeobox gene Meis1 modulates cardiovascular regeneration, (2020)
204. Xu, X., Tan, X., Tampe, B., Wilhelmi, T., Hulshoff, M.S., Saito, S., Moser, T., Kalluri, R., Hasenfuss, G., Zeisberg, E.M., Zeisberg, M.: High-fidelity CRISPR/Cas9- based gene-specific hydroxymethylation rescues gene expression and attenuates renal fibrosis. Nat Commun. 9, (2018). https://doi.org/10.1038/s41467-018-05766-5
205. Park, H., Shin, J., Kim, Y., Saito, T., Saido, T.C., Kim, J.: CRISPR/dCas9-Dnmt3a-mediated targeted DNA methylation of APP rescues brain pathology in a mouse model of Alzheimer's disease. Transl Neurodegener. 11, (2022). https://doi.org/10.1186/s40035-022-00314-0

206. Slamova, L., Starkova, J., Fronkova, E., Zaliova, M., Reznickova, L., van Delft, F.W., Vodickova, E., Volejnikova, J., Zemanova, Z., Polgarova, K., Cario, G., Figueroa, M., Kalina, T., Fiser, K., Bourquin, J.P., Bornhauser, B., Dworzak, M., Zuna, J., Trka, J., Stary, J., Hrusak, O., Mejstrikova, E.: CD2-positive B-cell precursor acute lymphoblastic leukemia with an early switch to the monocytic lineage. Leukemia. 28, 609–620 (2014). https://doi.org/10.1038/leu.2013.354
207. Britten, O., Ragusa, D., Tosi, S., Kamel, Y.M.: Mll-rearranged acute leukemia with t(4;11)(q21;q23)—current treatment options. is there a role for CAR-T cell therapy?, (2019)
208. Wu, B., Jug, R., Luedke, C., Su, P., Rehder, C., McCall, C., Lagoo, A.S., Wang, E.: Lineage Switch between B-Lymphoblastic Leukemia and Acute Myeloid Leukemia Intermediated by “occult” Myelodysplastic Neoplasm. In: American Journal of Clinical Pathology. pp. 136–147. Oxford University Press (2017)
209. Ohlsson, E., Hasemann, M.S., Willer, A., Lauridsen, F.K.B., Rapin, N., Jendholm, J., Porse, B.T.: Initiation of MLL-rearranged AML is dependent on C/EBPα. Journal of Experimental Medicine. 211, 5–13 (2014). https://doi.org/10.1084/jem.20130932
210. Thoennissen, N.H., Thoennissen, G.B., Abbassi, S., Nabavi-Nouis, S., Sauer, T., Doan, N.B., Gery, S., Müller-Tidow, C., Said, J.W., Koeffler, H.P.: Transcription factor CCAAT/enhancer-binding protein alpha and critical circadian clock downstream target gene PER2 are highly deregulated in diffuse large B-cell lymphoma. Leuk Lymphoma. 53, 1577–1585 (2012). https://doi.org/10.3109/10428194.2012.658792
211. Stoecker, M.M., Wang, E.: Histiocytic/dendritic cell transformation of B-Cell Neoplasms: Pathologic evidence of lineage conversion in differentiated hematolymphoid malignancies, (2013)
212. El-Sharkawi, D., Sproul, D., Allen, C.G., Feber, A., Wright, M., Hills, R.K., Linch, D.C., Gale, R.E.: Variable outcome and methylation status according to CEBPA mutant type in double-mutated acute myeloid leukemia patients and the possible implications for treatment. Haematologica. 103, 91–100 (2018). https://doi.org/10.3324/haematol.2017.173096
213. Wouters, B.J., Jordà, M.A., Keeshan, K., Louwers, I., Erpelinck-Verschueren, C.A.J., Tielemans, D., Langerak, A.W., He, Y., Yashiro-Ohtani, Y., Zhang, P., Hetherington, C.J., Verhaak, R.G.W., Valk, P.J.M., Löwenberg, B., Tenen, D.G.,

Pear, W.S., Delwel, R.: Distinct gene expression profiles of acute myeloid/T-lymphoid leukemia with silenced CEBPA and mutations in NOTCH1. Blood. 110, 3706–3714 (2007). https://doi.org/10.1182/blood-2007-02-073486

214. Hollink, I.H.I.M., van den Heuvel-Eibrink, M.M., Arentsen-Peters, S.T.C.J.M., Zimmermann, M., Peeters, J.K., Valk, P.J.M., Balgobind, B. v., Sonneveld, E., Kaspers, G.J.L., de Bont, E.S.J.M., Trka, J., Baruchel, A., Creutzig, U., Pieters, R., Reinhardt, D., Zwaan, C.M.: Characterization of CEBPA mutations and promoter hypermethylation in pediatric acute myeloid leukemia. Haematologica. 96, 384–392 (2011). https://doi.org/10.3324/haematol.2010.031336
215. Chen, X., Zhou, W., Song, R.-H., Liu, S., Wang, S., Chen, Y., Gao, C., He, C., Xiao, J., Zhang, L., Wang, T., Liu, P., Duan, K., Cheng, Z., Zhang, C., Zhang, J., Sun, Y., Jackson, F., Lan, F., Liu, Y., Xu, Y., Jong-Leong Wong, J., Wang, P., Yang, H., Xiong, Y., Chen, T., Li, Y., Ye, D.: Tumor suppressor CEBPA interacts with and inhibits DNMT3A activity. (2022)
216. Aivalioti, M.M., Bartholdy, B.A., Pradhan, K., Bhagat, T.D., Zintiridou, A., Jeong, J.J., Thiruthuvanathan, V.J., Pujato, M., Paranjpe, A., Zhang, C., Levine, R.L., Viny, A.D., Wickrema, A., Verma, A., Will, B.: PU.1-Dependent Enhancer Inhibition Separates Tet2 -Deficient Hematopoiesis from Malignant Transformation . Blood Cancer Discov. 3, 444–467 (2022). https://doi.org/10.1158/2643-3230.bcd-21-0226
217. de la Rica, L., Rodríguez-Ubreva, J., García, M., Islam, A.B.M.M.K., Urquiza, J.M., Hernando, H., Christensen, J., Helin, K., Gómez-Vaquero, C., Ballestar, E.: PU.1 target genes undergo Tet2-coupled demethylation and DNMT3b-mediated methylation in monocyte-to-osteoclast differentiation. Genome Biol. 14, (2013). https://doi.org/10.1186/gb-2013-14-9-r99
218. Tzircotis, G., Braga, V.M.M., Caron, E.: Rhog is required for both fccr- and cr3-mediated phagocytosis. J Cell Sci. 124, 2897–2902 (2011). https://doi.org/10.1242/jcs.084269
219. Hosono, M., Koma, Y.-I., Takase, N., Urakawa, N., Higashino, N., Suemune, K., Kodaira, H., Nishio, M., Shigeoka, M., Kakeji, Y., Yokozaki, H.: CXCL8 derived from tumor-associated macrophages and esophageal squamous cell carcinomas contributes to tumor progression by promoting migration and invasion of cancer cells. (2017)

220. Kaufmann, A., Salentin, R., Gemsa, D., Sprenger, H.: Increase of CCR1 and CCR5 expression and enhanced functional response to MIP-1α during differentiation of human monocytes to macrophages. J Leukoc Biol. 69, 248–252 (2001). https://doi.org/10.1189/jlb.69.2.248
221. Rosselló-Tortella, M., Ferrer, G., Esteller, M.: Epitranscriptomics in Hematopoiesis and Hematologic Malignancies. Blood Cancer Discov. 1, 26–31 (2020). https://doi.org/10.1158/2643-3249.bcd-20-0032
222. Minervini, C.F., Parciante, E., Impera, L., Anelli, L., Zagaria, A., Specchia, G., Musto, P., Albano, F.: Epitranscriptomics in normal and malignant hematopoiesis, (2020)
223. Ceci, M., Fazi, F., Romano, N.: The role of RNA-binding and ribosomal proteins as specific RNA translation regulators in cellular differentiation and carcinogenesis, (2021)
224. Shi, Z., Fujii, K., Kovary, K.M., Genuth, N.R., Röst, H.L., Teruel, M.N., Barna, M.: Heterogeneous Ribosomes Preferentially Translate Distinct Subpools of mRNAs Genome-wide. Mol Cell. 67, 71-83.e7 (2017). https://doi.org/10.1016/j.molcel.2017.05.021
225. Xiao, Y., Wang, Y., Tang, Q., Wei, L., Zhang, X., Jia, G.: An Elongation- and Ligation-Based qPCR Amplification Method for the Radiolabeling-Free Detection of Locus-Specific N 6 -Methyladenosine Modification . Angewandte Chemie. 130, 16227–16232 (2018). https://doi.org/10.1002/ange.201807942
226. Körtel, N., Rücklé, C., Zhou, Y., Busch, A., Hoch-Kraft, P., Sutandy, F.X.R., Haase, J., Pradhan, M., Musheev, M., Ostareck, D., Ostareck-Lederer, A., Dieterich, C., Hüttelmaier, S., Niehrs, C., Rausch, O., Dominissini, D., König, J., Zarnack, K.: Deep and accurate detection of m6A RNA modifications using miCLIP2 and m6Aboost machine learning. Nucleic Acids Res. 49, (2021). https://doi.org/10.1093/nar/gkab485
227. Moerke, N.J., Aktas, H., Chen, H., Cantel, S., Reibarkh, M.Y., Fahmy, A., Gross, J.D.D., Degterev, A., Yuan, J., Chorev, M., Halperin, J.A., Wagner, G.: Small-Molecule Inhibition of the Interaction between the Translation Initiation Factors eIF4E and eIF4G. Cell. 128, 257–267 (2007). https://doi.org/10.1016/j.cell.2006.11.046

228. Jin, X., Kruth, H.S.: Culture of macrophage colony-stimulating factor differentiated human monocyte-derived macrophages. Journal of Visualized Experiments. 2016, (2016). https://doi.org/10.3791/54244
229. Rodríguez-Ubreva, J., Català-Moll, F., Obermajer, N., Álvarez-Errico, D., Ramirez, R.N., Company, C., Vento-Tormo, R., Moreno-Bueno, G., Edwards, R.P., Mortazavi, A., Kalinski, P., Ballestar, E.: Prostaglandin E2 Leads to the Acquisition of DNMT3A-Dependent Tolerogenic Functions in Human Myeloid-Derived Suppressor Cells. Cell Rep. 21, 154–167 (2017). https://doi.org/10.1016/j.celrep.2017.09.018
230. R Core Team: R: A language and environment for statistical computing. . R Foundation for Statistical Computing, Vienna, Austria.
231. Aryee, M.J., Jaffe, A.E., Corrada-Bravo, H., Ladd-Acosta, C., Feinberg, A.P., Hansen, K.D., Irizarry, R.A.: Minfi: A flexible and comprehensive Bioconductor package for the analysis of Infinium DNA methylation microarrays. Bioinformatics. 30, 1363–1369 (2014). https://doi.org/10.1093/bioinformatics/btu049
232. Fortin, J.P., Triche, T.J., Hansen, K.D.: Preprocessing, normalization and integration of the Illumina HumanMethylationEPIC array with minfi. Bioinformatics. 33, 558–560 (2017). https://doi.org/10.1093/bioinformatics/btw691
233. Pidsley, R., Zotenko, E., Peters, T.J., Lawrence, M.G., Risbridger, G.P., Molloy, P., van Djik, S., Muhlhausler, B., Stirzaker, C., Clark, S.J.: Critical evaluation of the Illumina MethylationEPIC BeadChip microarray for whole-genome DNA methylation profiling. Genome Biol. 17, (2016). https://doi.org/10.1186/s13059-016-1066-1
234. Du, P., Zhang, X., Huang, C.C., Jafari, N., Kibbe, W.A., Hou, L., Lin, S.M.: Comparison of Beta-value and M-value methods for quantifying methylation levels by microarray analysis. BMC Bioinformatics. 11, (2010). https://doi.org/10.1186/1471-2105-11-587
235. Chain B: agilp: Agilent expression array processing package
236. Szczesna, K., de La Caridad, O., Petazzi, P., Soler, M., Roa, L., Saez, M.A., Fourcade, S., Pujol, A., Artuch-Iriberri, R., Molero-Luis, M., Vidal, A., Huertas, D., Esteller, M.: Improvement of the rett syndrome phenotype in a mecp2 mouse model upon treatment with levodopa and a dopa-decarboxylase inhibitor. Neuropsychopharmacology. 39, 2846–2856 (2014). https://doi.org/10.1038/npp.2014.136

237. Azagra, A., Román-gonzález, L., Collazo, O., Rodríguez-ubreva, J., de Yébenes, V.G., Barneda-zahonero, B., Rodríguez, J., de Moura, M.C., Grego-Bessa, J., Fernández-duran, I., Islam, A.B.M.M.K., Esteller, M., Ramiro, A.R., Ballestar, E., Parra, M.: In vivo conditional deletion of hdac7 reveals its requirement to establish proper b lymphocyte identity and development. Journal of Experimental Medicine. 213, 2591–2601 (2016). https://doi.org/10.1084/jem.20150821

238. Janin, M., Ortiz-Barahona, V., de Moura, M.C., Martínez-Cardús, A., Llinàs-Arias, P., Soler, M., Nachmani, D., Pelletier, J., Schumann, U., Calleja-Cervantes, M.E., Moran, S., Guil, S., Bueno-Costa, A., Piñeyro, D., Perez-Salvia, M., Rosselló-Tortella, M., Piqué, L., Bech-Serra, J.J., de La Torre, C., Vidal, A., Martínez-Iniesta, M., Martín-Tejera, J.F., Villanueva, A., Arias, A., Cuartas, I., Aransay, A.M., la Madrid, A.M., Carcaboso, A.M., Santa-Maria, V., Mora, J., Fernandez, A.F., Fraga, M.F., Aldecoa, I., Pedrosa, L., Graus, F., Vidal, N., Martínez-Soler, F., Tortosa, A., Carrato, C., Balañá, C., Boudreau, M.W., Hergenrother, P.J., Kötter, P., Entian, K.D., Hench, J., Frank, S., Mansouri, S., Zadeh, G., Dans, P.D., Orozco, M., Thomas, G., Blanco, S., Seoane, J., Preiss, T., Pandolfi, P.P., Esteller, M.: Epigenetic loss of RNA-methyltransferase NSUN5 in glioma targets ribosomes to drive a stress adaptive translational program. Acta Neuropathol. 138, 1053–1074 (2019). https://doi.org/10.1007/s00401-019-02062-4

239. Schwartzman, O., Mukamel, Z., Oded-Elkayam, N., Olivares-Chauvet, P., Lubling, Y., Landan, G., Izraeli, S., Tanay, A.: UMI-4C for quantitative and targeted chromosomal contact profiling. Nat Methods. 13, 685–691 (2016). https://doi.org/10.1038/nmeth.3922

240. Ramos-Rodríguez, M., Subirana-Granés, M., Pasquali, L.: UMI4Cats: an R package to analyze chromatin contact profiles obtained by UMI-4C. Bioinformatics. 37, 4240–4242 (2021). https://doi.org/10.1093/bioinformatics/btab392

241. Quinlan, A.R., Hall, I.M.: BEDTools: A flexible suite of utilities for comparing genomic features. Bioinformatics. 26, 841–842 (2010). https://doi.org/10.1093/bioinformatics/btq033

242. Tan, G., Lenhard, B.: TFBSTools: An R/bioconductor package for transcription factor binding site analysis. Bioinformatics. 32, 1555–1556 (2016). https://doi.org/10.1093/bioinformatics/btw024

243. Khan, A., Fornes, O., Stigliani, A., Gheorghe, M., Castro-Mondragon, J.A., van der Lee, R., Bessy, A., Chèneby, J., Kulkarni, S.R., Tan, G., Baranasic, D., Arenillas, D.J., Sandelin, A., Vandepoele, K., Lenhard, B., Ballester, B., Wasserman, W.W., Parcy, F., Mathelier, A.: JASPAR 2018: Update of the open-access database of transcription factor binding profiles and its web framework. Nucleic Acids Res. 46, D260–D266 (2018). https://doi.org/10.1093/nar/gkx1126
244. Ziebarth, J.D., Bhattacharya, A., Cui, Y.: CTCFBSDB 2.0: A database for CTCF-binding sites and genome organization. Nucleic Acids Res. 41, (2013). https://doi.org/10.1093/nar/gks1165
245. Schones, D.E., Smith, A.D., Zhang, M.Q.: Statistical significance of cis-regulatory modules. BMC Bioinformatics. 8, (2007). https://doi.org/10.1186/1471-2105-8-19
246. Bolger, A.M., Lohse, M., Usadel, B.: Trimmomatic: A flexible trimmer for Illumina sequence data. Bioinformatics. 30, 2114–2120 (2014). https://doi.org/10.1093/bioinformatics/btu170
247. Dobin, A., Davis, C.A., Schlesinger, F., Drenkow, J., Zaleski, C., Jha, S., Batut, P., Chaisson, M., Gingeras, T.R.: STAR: Ultrafast universal RNA-seq aligner. Bioinformatics. 29, 15–21 (2013). https://doi.org/10.1093/bioinformatics/bts635
248. Li, H., Handsaker, B., Wysoker, A., Fennell, T., Ruan, J., Homer, N., Marth, G., Abecasis, G., Durbin, R.: The Sequence Alignment/Map format and SAMtools. Bioinformatics. 25, 2078–2079 (2009). https://doi.org/10.1093/bioinformatics/btp352
249. Broad Institute, G.R.: Picard Toolkit.
250. Antanaviciute, A., Baquero-Perez, B., Watson, C.M., Harrison, S.M., Lascelles, C., Crinnion, L., Markham, A.F., Bonthron, D.T., Whitehouse, A., Carr, I.M.: m6aViewer: software for the detection, analysis, and visualization of N 6-methyladenosine peaks from m 6 A-seq/ME-RIP sequencing data. (2017). https://doi.org/10.1261/rna
251. Heinz, S., Benner, C., Spann, N., Bertolino, E., Lin, Y.C., Laslo, P., Cheng, J.X., Murre, C., Singh, H., Glass, C.K.: Simple Combinations of Lineage-Determining Transcription Factors Prime cis-Regulatory Elements Required for Macrophage and B Cell Identities. Mol Cell. 38, 576–589 (2010). https://doi.org/10.1016/j.molcel.2010.05.004
252. Hahne, F., Ivanek, R.: Visualizing genomic data using Gviz and bioconductor. In: Methods in Molecular Biology. pp. 335–351. Humana Press Inc. (2016)
253. Wickham, H.: ggplot2. Springer New York (2009)

254. Ritchie, M.E., Phipson, B., Wu, D., Hu, Y., Law, C.W., Shi, W., Smyth, G.K.: Limma powers differential expression analyses for RNA-sequencing and microarray studies. Nucleic Acids Res. 43, e47 (2015). https://doi.org/10.1093/nar/gkv007

It ain't about how hard you hit.
It's about how hard you can get hit
and keep moving forward.

R.B.